Modulation of neuronal function and redox homeostasis by Sulfiredoxin-1

Timothy Johnston

PhD

University of York

Department of Biology

September 2024

Abstract

Neurons are metabolically-demanding cells, producing reactive oxygen species (ROS) primarily as a by-product of aerobic respiration. ROS serve an important physiological role to modulate signalling pathways, gene expression, and cell function. However, unregulated levels of ROS can cause cellular damage and a state of oxidative stress (OS), which is a pathological hallmark of many neurodegenerative conditions. A better understanding of how ROS are controlled could elucidate therapeutic strategies for such conditions. My research sought to elucidate the physiological relevance of the antioxidant enzyme Sulfiredoxin-1 (Srx), which resolves Peroxiredoxins and additional putative substrates to maintain ROS homeostasis.

To investigate the role of Srx, I generated *Drosophila melanogaster Srx* mutants, which exhibited mild increases in sensitivity to OS. Redox-sensitive signalling pathways in *Drosophila Srx* mutants were differentially perturbed, and ROS levels in tissue homogenates were not significantly affected. These modest changes to redox homeostasis were contrasted by pronounced changes to fly behaviour and physiology, which include enhanced negative geotaxis responses and diminished neurotransmission in the visual system. Physiological changes to *Drosophila Srx* mutants were accompanied by enhanced neuron growth *in vivo* and *in vitro*, a morphological feature that is well-established to be regulated by redox signalling. Rat primary hippocampal neurons also exhibited enhanced growth following loss of Srx, demonstrating that Srx-regulated neuron growth is conserved across species.

Collectively, my work indicates that Srx modulates signalling pathways involved in neuronal growth and function, rather than conferring widespread defence against OS. My work has opened up avenues for further research into the identity of Srx-regulated signalling events and pathways and adds to a growing body of work that highlights ROS as being a critical modulators of nervous system development and function.

Table of Contents

List of Figures

List of Tables

Acknowledgements

Firstly, thank you to Dr Sangeeta Chawla for being a terrific PhD supervisor. I have learned a great deal under her mentorship and am extremely grateful for the support, generosity, and patience that she has shown me throughout my time at York.

I would like to thank my secondary supervisor Professor Sean Sweeney for his support and insights into *Drosophila*, which have helped my research enormously. Also thank you to Professor William Brackenbury, my thesis advisory panel member, for his advice and helpful comments throughout my PhD.

Thank you to my funders, BBSRC, and members of the University of York Technology Facility for supporting my research. Particularly Dr Grant Calder and Dr Jared Cartwright for their help with confocal microscopy and protein synthesis, respectively.

I have had the privilege to work alongside some brilliant people at York, to whom I need to express a great deal of gratitude. This includes Dr Egle Beigate, Dr Chris Ugbode, Alison Fellgett, Dr Annabel Smith, Lubna Nuhu-Soso, Nicholas West, Katy Hyde, Dr Savvas Ioannou, Alex Roof, Diogo Candeias, Rakshana Ramachandran, Robert Allen, Molly Margarotto, Gabriele Vilkaite, and all the D1 PIs.

Thanks to my housemate and friend of four years, Ben Fletcher, for his good company and always reminding me of life outside science. Thanks also to my friends from Gravesend (I look forward to frequenting The Robert Pocock soon), and my friends from my days at Cardiff University.

My time at York would not be the same without representing the Biology Football team on Fridays. I made many friends through playing for the team and enjoyed winning the league on multiple occasions - *UP THE YELLOWS*!

Thank you to my wonderful family for their support and encouragement: Mum, Dad, Heather, Cameron, Grandma J, Darren, Rosie, Jess, Grandma T, and Grandad T.

Lastly, a special thank you to Emily for all your support and being an absolute *superstar*.

Declaration

I declare that this thesis is a presentation of original work and I am the sole author. This work has not previously been presented for an award at this, or any other, University. All sources are acknowledged as References.

1. Introduction

1.1. Rationale

The high metabolic demands of neurons generates reactive oxygen species (ROS), primarily as a product of aerobic respiration at the mitochondria. ROS control signalling pathways to regulate gene expression and, in turn, synaptic plasticity and neuron function (Kamsler and Segal, 2003; Lennicke and Cochemé, 2021; Milton and Sweeney, 2012). Enzymatic antioxidant systems function to help maintain ROS homeostasis, preventing high levels and a state of 'oxidative stress' (OS) that is a pathological hallmark of many neurodegenerative conditions (Singh et al., 2019). A better understanding of how homeostasis is maintained could help to generate therapeutic strategies for such diseases and help prepare for a forecasted ageing population (Mitchell and Walker, 2020). This thesis aimed to elucidate the contribution of Sulfiredoxin-1 (Srx) in regulating ROS homeostasis and neuron function.

1.2. ROS in the cellular environment

1.2.1. Overview of ROS

Reactive Oxygen Species (ROS) are radical and non-radical-containing oxygen species that are formed via the partial reduction of oxygen atoms (Ray et al., 2012). Oxygen has an electron configuration of $1S^2 2S^2 2P^4$ (Figure 1.1.A). The two unpaired P-orbital electrons mean that electrons are readily accepted and oxygen atoms are reduced. This also renders oxygen susceptible to radical production, in which there are lone unpaired electrons.

ROS include superoxide anions ($O_2^{\cdot -}$), hydroxyl radicals ($HO\cdot$), and Hydrogen Peroxide (H_2O_2). The free radical ROS variants ($O_2^{\cdot -}$ and $HO\cdot$) can react with organic substrates in the cellular environment to propagate radical production (Figure 1.1.B). Although H_2O_2 is less reactive, it acts as a source of hydroxyl radicals via the Fenton reaction in the presence of divalent metal ions (Figure 1.1.C) and the Haber-Weiss reaction (Figure 1.1.D) (Haber and Weiss, 1934). ROS can interact with nitrogen-containing species to propagate reactive nitrogen species

production (RNS). For instance, superoxide anions can interact with nitric oxide to produce peroxynitrite (ONOO·).

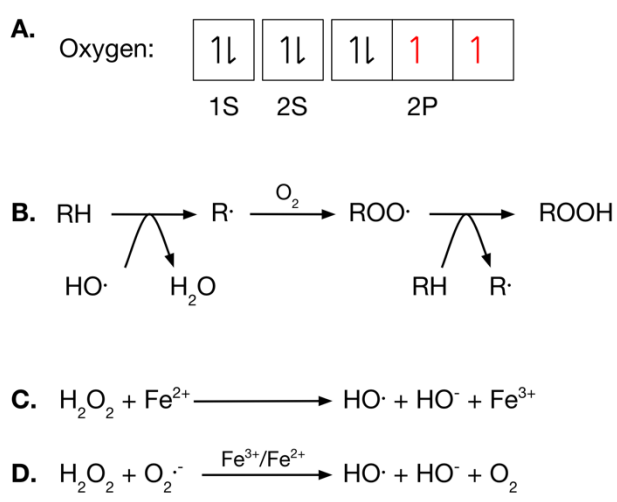

Figure 1.1. Oxygen acts as a source of radicals in the cellular environment.

A. Oxygen has two unpaired p-orbital electrons (highlighted in red) that enable free radical formation. **B.** ROS propagate via interactions with organic molecules. H_2O_2 is a source of radicals via the Fenton (**C**) and Haber-Weiss reactions (**D**).

1.2.2. Redox-sensitive organic molecules

ROS can cause widespread damage in the cellular environment by interacting with a variety of macromolecules. Hydroxyl radicals can interact with DNA directly to cause strand scission (Brawn and Fridovich, 1981; Lesko et al., 1980). Although superoxide ions and hydrogen peroxide cannot induce such changes directly, they are proposed to indirectly contribute to DNA damage. Superoxide ions can reduce DNA-bound iron, which in turn participates in the Fenton reaction to generate hydroxyl radicals from hydrogen peroxide (Brawn and Fridovich, 1981; Keyer and Imlay, 1996; Lesko et al., 1980). Cells have no enzymatic mechanism to eradicate hydroxyl radicals (Mitra et al., 2019), whereas they have enzymatic mechanisms to reduce superoxide dismutase (see Chapter 1.2.6.1) and hydrogen peroxide (see Chapter 1.2.6.2-4). Therefore, an excess of hydroxyl radicals can lead to widespread DNA damage and cell death.

ROS can interact with lipids to cause lipid peroxidation and compromise membrane integrity and permeability (Ayala et al., 2014). ROS also regulate the oxidation state of thiol-containing cysteine groups in proteins (Figure 1.2). Oxidation of these residues can generate intra- and intermolecular disulphide bonds to alter the secondary and tertiary structure of proteins (Baba

and Bhatnagar, 2018). Under conditions of OS, redox modifications could irreversibly denature proteins to inhibit their function.

Some redox modifications also serve to protect cysteine residues from oxidation. S-glutathionylation, whereby glutathione tripeptides are conjugated to these residues, protects cysteine residues from oxidation (Forman et al., 2009). S-glutathionylation of histones also induces epigenetic changes (De Luca et al., 2011), demonstrating the far-reaching physiological functions of ROS.

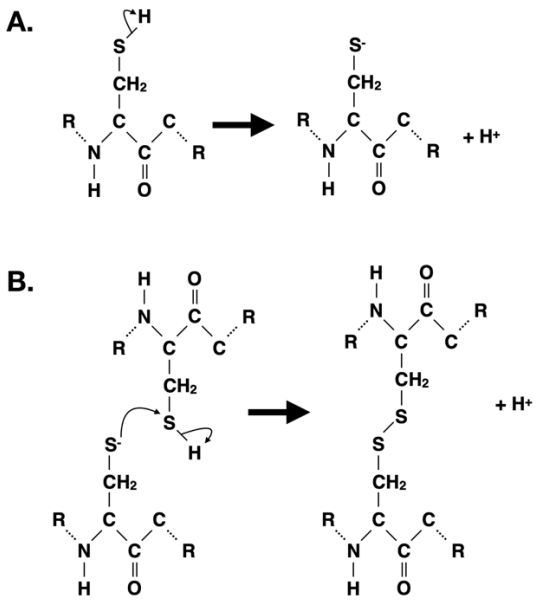

Figure 1.2. Redox-sensitive cysteine residues regulate protein tertiary and quaternary structures.
A. Cysteine residue thiol groups are readily de-protonated in cells, depending on the pH of the protein microenvironment. **B.** The resulting thiolate ion can initiate nucleophilic attacks on other cysteine residue thiol groups to generate intra- or intermolecular disulphide bonds. This can regulate protein structure and function.

1.2.3. ROS modulate signalling pathways and gene expression

Despite the potential for OS to damage cellular components, ROS also serve an important physiological role in controlling signalling pathways. Redox-mediated modifications to transcription factor proteins and their upstream cytosolic pathway components controls gene expression and cell activity. In this manner, ROS function as second messengers.

1.2.3.1 MAPK signalling

Mitogen-activated protein kinase (MAPK) signalling pathways are redox-sensitive. MAPKs are a large family of proline-directed, serine/threonine kinases that are the terminal kinases in three-tiered kinase signalling cascades, also referred to as modules. Within each module is a MAPK, a MAPK kinase (MAPKK), and a MAPKK kinase (MAPKK). For activation,

MAPKKKs phosphorylate and activate MAPKKs, which in turn phosphorylate and activate MAPKs at conserved TxY motifs. MAPKKKs are activated by a variety of sources, often through phosphorylation and interactions with small GTP-binding proteins of the Ras/Rho family (Cargnello and Roux, 2011).

Seven modules of MAPKs have been identified, which are classed as either conventional or atypical. The latter possess non-conforming particularities, such a lack of the three-tiered cascade structure (Coulombe and Meloche, 2007). Irrespective of activation, all MAPKs phosphorylate target serine or threonine residues that are followed by proline residues immediately afterwards, rendering them 'proline-directed' (Cargnello and Roux, 2011). The MAPK substrates are diverse. Examples include cytoskeletal proteins, kinases, and transcription factors. Phosphorylation of transcription factors by MAPKs can influence gene expression and are sensitive to OS. An example of a redox-sensitive MAPK signalling cascade is JNK/AP-1 signalling.

The transcription factor Activator Protein 1 (AP-1) exists as dimers of Jun, Fos, MAF, and ATF proteins (Johnson and Nakamura, 2007). Jun and Fos proteins are the most extensively researched AP-1 components, with prototypical AP-1 entities consisting as heterodimers of a Fos family component (c-fos FosB, Fra-1, Fra-2) complexed with a Jun family component (c-jun, JunB and JunD). DNA binding assays indicate that human c-Jun/c-Fos heterodimers are more stable and bind to DNA with more affinity compared to c-Jun homodimers, which in turn are more stable and bind to DNA more readily than c-Fos homodimers (Halazonetis et al., 1988). However, the large range of potential dimer combinations has made it difficult to characterise the DNA-binding affinity of all Jun/Fos family members in response to specific cellular stimuli. Conversely, *Drosophila melanogaster* exhibit a single homologue for Jun and Fos proteins (Ciapponi and Bohmann, 2002).

AP-1 components have highly conserved basic-leucine zipper domains (bZIP) domains. Leucine zippers allow dimerisation, whereas basic regions facilitate DNA binding (Bejjani et al., 2019). The composition of the dimers affects their affinity for different types of palindromic DNA sequences. Fos/Jun heterodimers and Jun/Jun homodimers bind to 12-O-tetradecanoylphorbol-13-acetate (TPA)-responsive element (TRE), for which the consensus sequence is 5'-TGA(C/G)TCA motifs (Angel et al., 1987). Fos/Jun heterodimers and Jun/Jun homodimers are also able to bind cAMP-responsive elements (CRE) with less affinity. The mechanisms by which AP-1 control transcription are still poorly understood, but AP-1 is likely to bind to distal enhancer sequences, rather than promoters, to exert transcription-regulatory actions (Bejjani et al., 2019).

OS causes increased activation of the MAPK JNK, which phosphorylates and enhances the transcriptional activity of c-Jun and ATF2 (Karin, 1995). This pathway has been shown to regulate apoptosis (Behrens et al., 1999). OS-induced activation of JNK/AP-1 signalling also promotes neuron growth in *Drosophila*, with sources of ROS differentially activating AP-1 components to induce overgrowths as the *Drosophila* third instar larval neuromuscular junction (NMJ) (Collins et al., 2006; Milton et al., 2011). For instance, *sod2* mutations induce overgrowths that can be rescued by the expression of dominant-negative *Fos* and *Jun* transgenes, whereas *sod1* mutations induce overgrowths that can be rescued by the expression of dominant-negative *Fos* transgenes only (Milton et al., 2011). As sod2 is a mitochondrial matrix protein, whereas sod1 is broadly distributed amongst the cytosol and alternative organelles, this may suggest that the cellular source of ROS may determine the manner of JNK/AP-1 activation. Further research is required to explore whether Jun localisation to mitochondria could underly the specific activation of JNK/AP-1 signalling components in response to mitochondrial ROS.

JNK also phosphorylates the transcription factor Forkhead box O (FOXO) to increase nuclear translocation and the transcription of target genes (Brunet et al., 2004; Essers et al., 2004). OS also promotes this nuclear import via the dimerisation of FOXO with transportin (TNPO) at redox-sensitive cysteine residues (Putker et al., 2013). Conversely, insulin signalling promotes Akt phosphorylation of FOXO at alternative sites to prevent nuclear import (Brunet et al., 1999; Jacobs et al., 2003; Kops et al., 1999). Therefore, FOXO integrates antagonistic signalling from OS-induced c-Jun N-terminal kinase (JNK) and nutrient-dependent insulin signalling pathways (Yen et al., 2011).

1.2.3.2. PI3K/Akt signalling

Phosphoinositide 3-kinase (PI3K)/Protein kinase B (Akt) signalling regulates cell growth and survival. This pathway is typically activated by the phosphorylation of PI3K by receptor tyrosine kinases (RTKs). This kinase, in turn, phosphorylates the lipid phosphatidylinositol-4,5-biphosphate (PIP_2) to phosphatidylinositol-4,5-triphosphate (PIP_3), a potent activator of Akt. Akt can phosphorylate many targets to have a stimulatory or inhibitory effect (Hemmings and Restuccia, 2012). One such target is mammalian target of Rapamycin (mTOR), a kinase that interacts with other proteins to form one of two complexes: mTORC1 and mTORC2. These complexes phosphorylate a myriad of targets, including transcriptional and translational regulators, to facilitate cell growth, proliferation, and survival (reviewed in Laplante and Sabatini, 2012).

PI3K/Akt signalling is inhibited by the actions of Phosphatase and tensin homologs deleted on chromosome 10 (PTEN). This plasma-membrane lipid phosphatase dephosphorylates PIP_3 to PIP_2 to antagonise PI3K/Akt signalling and, therefore, cell growth and proliferation (Zhang et al., 2020). PTEN activity is sensitive to OS. Exposure to H_2O_2 generates intramolecular disulphide bonds that form between two cysteine residues, one of which is in the active site. This inhibits PTEN (Lee et al., 2002). Therefore, OS regulates downstream PI3K/AKT signalling also. The redox state of PTEN is also controlled by antioxidant enzymes (see Chapter 1.2.6.4). Additionally, Akt phosphorylates and negatively regulates the MAPKKK ASK1 (Kim et al., 2001), as well as FOXO4 (Brownawell et al., 2001). This demonstrates the complexity and cross-talk between redox-sensitive signalling pathways.

1.2.3.3. Nrf2 signalling

The transcription factor Nuclear factor erythroid 2-related factor 2 (Nrf2) is also modulated by the oxidative state of cells. Nrf2 signalling upregulates many antioxidant enzymes, such as glutathione S-transferase, Thioredoxin-1, Peroxiredoxin-1, and Sulfiredoxin-1, which are detailed in Chapter 1.2.6 (Hayes and Dinkova-Kostova, 2014). Under unstressed conditions, Kelch-like ECH-associated protein 1 (KEAP1) binds to Nrf2, leading to its ubiquitination and degradation. KEAP1 forms intramolecular disulphide bonds when exposed to OS, which liberates Nrf2 and permits nuclear import (Fourquet et al., 2010; Kobayashi et al., 2004).

Nrf2 is also regulated by the redox-sensitive kinase Glycogen synthase kinase-3 beta (GSK-3β). GSK-3β phosphorylates Nrf2 to promote its nuclear exclusion and attenuate the transcription of target genes (Rojo et al., 2008; Salazar et al., 2006). Under acute bouts of OS, GSK-3β is phosphorylated and inactivated by Akt at Ser9, which promotes increased Nrf2 signalling and correlates with the general increase in PI3K/Akt signalling associated with OS. Chronic OS promotes Akt dephosphorylation, leading to decreased GSK-3β phosphorylation that promotes the nuclear exclusion of Nrf2 (Martín et al., 2002; Rojo et al., 2008; Salazar et al., 2006). The interaction between PI3K and Nrf2 signalling further demonstrates the large degree of cross-talk between redox-sensitive signalling pathways.

1.2.4. Mitochondria as a source of ROS

Mitochondria are organelles responsible for ATP production under aerobic conditions. Energy is primarily sourced from glucose that is converted to pyruvate in glycolysis in the cytosol, which is then transported into mitochondria. Mitochondria possess an outer and an inner membrane, the latter of which is highly folded to form cristae, and within this is the mitochondrial matrix. Here, pyruvate is converted to acetyl coenzyme A (Acetyl CoA) for processing in the Krebs cycle. The mitochondrial inner membrane houses protein complexes that participate in redox reactions, known as the 'electron transport chain' (ETC), which sources electrons from the products of glycolysis and the Krebs cycle. The resulting redox reactions, depicted in Figure 1.3, generate a proton gradient across the inner mitochondrial membrane that drives ATP production. The ETC and proton-driven ATP synthesis are collectively referred to as oxidative phosphorylation (Zhao et al., 2019).

NADH, sourced from glycolysis and the Krebs cycle, is the principal electron donor for complex I, from which electrons are passed to Coenzyme Q (CoQ). Similarly, FADH2, sourced from the Krebs cycle, is the principal electron donor for complex II, which also passes electrons to CoQ. Electrons are shuttled from CoQ to complex III, Cytochrome C (Cyt C), and complex IV, respectively. Complexes I, III, and IV transport protons across the mitochondrial membrane as they receive electrons and acquire a 'supercharged' state. The resulting proton gradient is used by ATP synthase to convert ADP to ATP (Zhao et al., 2019).

ROS are primarily produced in cells from mitochondria as a product of the ETC. ROS have been directly measured from isolated mitochondria (Loschen and Flohé, 1971) and the isolated mitochondrial complexes that facilitate oxidative phosphorylation and ATP production (Cadenas et al., 1977; Kussmaul and Hirst, 2006). Both complex I and complex III have been observed to be a source of ROS.

Isolated complex I has been induced to produce $O_2\bullet^-$ in multiple ways. Flavin mono nucleotide (FMN) is the principal electron acceptor for complex I, and the proportion of FMN that is reduced is determined by the ratio of NADH to NAD+. High NADH/NAD+ ratios have been shown to increase $O_2\bullet^-$ production, likely due to the transfer of electrons from reduced FMN to oxygen molecules (Kussmaul and Hirst, 2006). This production is enhanced by the use of rotenone, which binds to the CoQ binding site to impede the passage of electrons from complex I to CoQ (Cadenas et al., 1977). It is also proposed that complex I can produce $O_2\bullet^-$ from an unspecified site when the CoQ pool is highly reduced, which induces reverse electron transport chain (RET) (Chance and Hollunger, 1961). The energetic demands of cells will

influence the extent to which mitochondria are actively generating ATP. During periods of high activity mitochondria *in vivo* are more likely to be in a state where they are synthesising ATP. Some postulate that in such states, it is likely that complex III is actually the major source of $O_2^{\bullet -}$ as the reduction of CoQ produces ubisemiquinone free radicals that can react with molecular oxygen (Turrens et al., 1985). These sources of ROS are depicted in Figure 1.3.

Mitochondrial toxins impede the function of protein complexes in the ETC, resulting in increased ROS production. Rotenone is an insecticide and herbicide that impedes the movement of electrons from iron-sulphur centres in complex I to ubiquinone (Heinz et al., 2017). Paraquat, another pesticide, also induces ROS production from complex I (Cochemé and Murphy, 2008). Due to their toxicity, the commercial availability and use of these substances is now restricted in many countries. However, researchers commonly use these compounds to generate OS in model organisms under tightly-regulated experimental conditions.

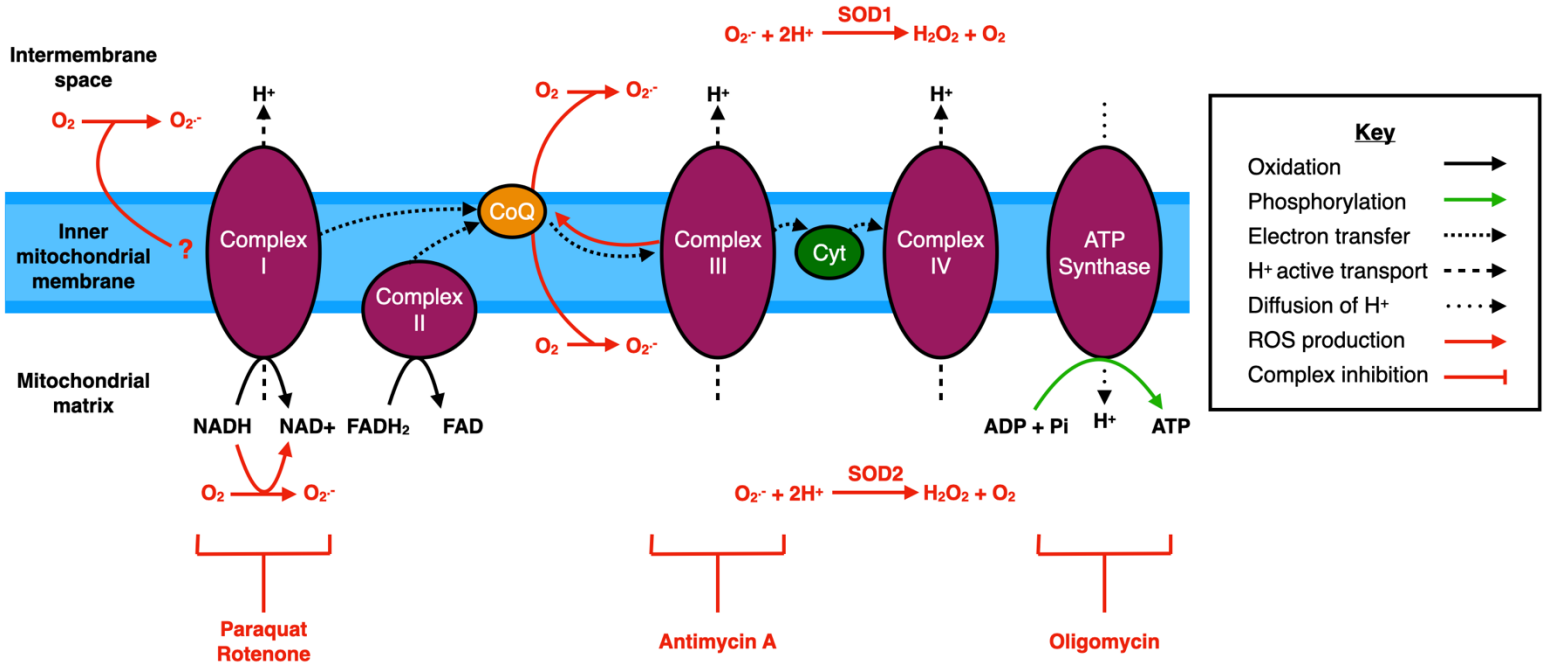

Figure 1.3. ROS are a product of aerobic respiration at mitochondria.

Redox reactions between protein complexes at the inner mitochondrial membrane create a proton gradient that drives ATP production. Complex I produces ROS under conditions that produce high ratios of NADH to NAD+, where the former donates electrons to oxygen molecules. ROS can also be produced from this complex due to a high proportion of ubiquinol (QH_2) that leads to the reverse electron transport chain (RET) and the release of electrons from an unspecified site. Complex III can be induced to produce ROS when the movement of electrons to the Q_i site is inhibited. Ubisemiquinone acts as an electron donor on both sides of the inner mitochondrial membrane. Commonly known inhibitors of protein complex function are indicated at the bottom of the diagram.

1.2.5. Non-mitochondrial sources of ROS

Along with the mitochondrial respiratory chain, the other major source of ROS in cells is considered to be NADPH oxidase (NOX) enzymes (Holmström and Finkel, 2014). This class of transmembrane enzyme complexes carries electrons across membranes to reduce diatomic oxygen to superoxide radicals ($O_2^{\bullet -}$). As their name suggests, the electrons are sourced from the oxidation of NADPH at their cytosolic domain, which is then passed along redox centres in the complex (Panday et al., 2015). The localisation of these enzymes varies from plasma membranes to intracellular compartments like the membranes of the endoplasmic reticulum (Buul et al., 2005) and mitochondria (Graham et al., 2010).

ROS are also a product of golgi-derived organelles such as peroxisomes. These are single-membraned organelles containing H_2O_2-producing oxidases and catalase, which catalyses the breakdown of H_2O_2 to oxygen and water (De Duve and Baudhuin, 1966). Peroxisomes have many metabolic roles, such as fatty acid oxidation and polyamine oxidation. They contain many enzymes that produce ROS as a natural product of these processes, such as polyamine oxidase, which catalyses the breakdown of polyamines and produces H_2O_2. Peroxisomes contain antioxidant enzymes to defend against OS, such as catalase and peroxiredoxin 5 (Fransen et al., 2012).

Lysosomes can also act as a source of ROS. These organelles are responsible for autophagy: the breakdown of cellular components to remove biological waste. Lysosomal dysfunction can result in the accumulation of this waste to form lipofuscin, an intracellular, non-degradable deposit of lipids and proteins. Lipofuscin accumulates with age, and is common in ageing post-mitotic cells like neurons (Różanowska, 2023). Lysosomal dysfunction causes increased oxidative damage (Donida et al., 2017; Milton et al., 2011). This is thought to stem from the accumulation of senescent mitochondria and lysosomal iron (Fe^{2+}), with the latter producing ROS via the Fenton reaction (Terman et al., 2006).

1.2.6. Cellular mechanisms to maintain ROS homeostasis

ROS homeostasis is maintained in cells using a plethora of antioxidant defence mechanisms. This includes molecular antioxidants like ascorbic acid and tocopherols, which directly neutralise ROS and can be exogenously sourced from our diets (Behl, 2000; May, 2012). There are also endogenous enzymatic defences that neutralise ROS and ROS-induced modifications.

1.2.6.1. Superoxide Dismutase Enzymes

The principal form of ROS generated in cells is superoxide anions ($O_2^{\bullet -}$). These radicals are produced via the reduction of diatomic oxygen. To prevent this interacting with macromolecules in the cellular environment, as well as prevent radical propagation, superoxide dismutase (SOD) enzymes catalyse the conversion of superoxide to hydrogen peroxide (H_2O_2). There are three isoforms of this enzyme, named SOD1-3. SOD1 uses Cu^{2+} ions as a cofactor and is present in the mitochondrial intermembrane space, cytoplasm, and endoplasmic reticulum amongst other organelles (Crapo et al., 1992; Okado-Matsumoto and Fridovich, 2001). SOD2 uses Mn^{2+} ions as a cofactor and is localised to the mitochondrial matrix (Okado-Matsumoto and Fridovich, 2001). Lastly, SOD3 uses Cu^{2+} ions as a cofactor and is transported to the extracellular space (Folz and Crapo, 1994).

1.2.6.2. Catalase

Although hydrogen peroxide is more stable than superoxide anions, it can be readily reduced in the Fenton reaction to generate hydroxyl radicals (see Chapter 1.2.1). To remove this potential source of radicals, hydrogen peroxide is further reduced by the actions of multiple enzymes. This includes catalase, glutathione peroxidase, and peroxiredoxins. Catalase catalyses the breakdown of two hydrogen peroxide molecules into one molecule of oxygen and two molecules of water in a two-step reaction (Deisseroth and Dounce, 1970). Catalase is primarily located in the peroxisomes of mammalian cells. However, some specific cell types exhibit catalase in other organelles. For instance, catalase has been observed in the mitochondria of rat cardiomycytes (Radi et al., 1991). Cell senescence also appears to compromise import of catalase to peroxisomes, increasing cytosolic levels of this enzyme (Legakis et al., 2002).

1.2.6.3. The Glutathione system

The most abundant mammalian antioxidant is glutathione (Dringen, 2000). This tripeptide is the eponymous feature of the glutathione system. It is comprised of a glutamate, cysteine, and glycine amino acid with an atypical peptide bond between the γ-carboxyl group of glutamate and the cysteine. Glutathione is present in many organelles including the cytoplasm, endoplasmic reticulum, and mitochondria. Similarly, the enzymes that use it as a substrate exhibit a broad distribution. Glutathione peroxidases (Gpxs) catalyse the reduction

of peroxides to oxidise glutathione, forming a disulphide bond between two tripeptides. This can then be reduced by the actions of glutathione reductases, which use NADPH as an electron donor to remove this bond and recycle the glutathione (Santacroce et al., 2023). Glutathione-S-transferase (GST) enzymes conjugate glutathione to cysteine residues directly to protect them from oxidation, known as S-glutathionylation (Forman et al., 2009).

1.2.6.4. The Peroxiredoxin system

Peroxiredoxins (Prdxs) are another family of antioxidant enzymes that reduce hydrogen peroxide and alkyl hydroperoxides. There are multiple classes of this enzyme that all undergo three common mechanistic steps (Figure 1.4). This mechanism involves a 'peroxidatic' and a 'resolving' cysteine residue, denoted C_P and C_R, respectively (reviewed in Hall et al., 2009). Firstly, Prdxs undergo 'peroxidation' in which a C_P residue is deprotonated to a thiolate ion to induce a nucleophilic attack on peroxides. Secondly, the now-oxidised C_P residue undergoes 'resolution' whereby a deprotonated C_R residue thiolate ion initiates a nucleophilic attack to form a disulphide bond (Chae et al., 1994b). Finally, 'recycling' of the enzymes occurs when the free thiols of the C_P and C_R residues are regenerated by thioredoxin (Trx). Trx is reduced via the actions of thioredoxin reductase (TrxR) that uses NADPH as an electron donor (Chae et al., 1994a; Hall et al., 2009). Thioredoxin is known to reduce a multitude of other enzymes, including PTEN (Lee et al., 2002).

The classes of Prdx enzymes differ according to where the C_R residue is derived for the C_P resolution (Table 1.1). Typical 2-Cys Prdxs possess N-terminal C_P residues that interact with C-terminal C_R residues on other Prdx enzymes, forming intermolecular disulphide bonds to function as obligate homodimers (Hall et al., 2009). They are broadly distributed throughout many cellular organelles. Prdx1 and 2 are located in the nucleus and cytosol, Prdx3 is mitochondrial, and Prdx4 is found in the endoplasmic reticulum (Rhee et al., 2012). The specific types of Prdx also seem to have differing functions as well as locations. Prdx1 can bind to PTEN to form intermolecular heterodimers and protect against OS-induced inactivation of this phosphatase. Prdx2 cannot, however (Cao et al., 2009).

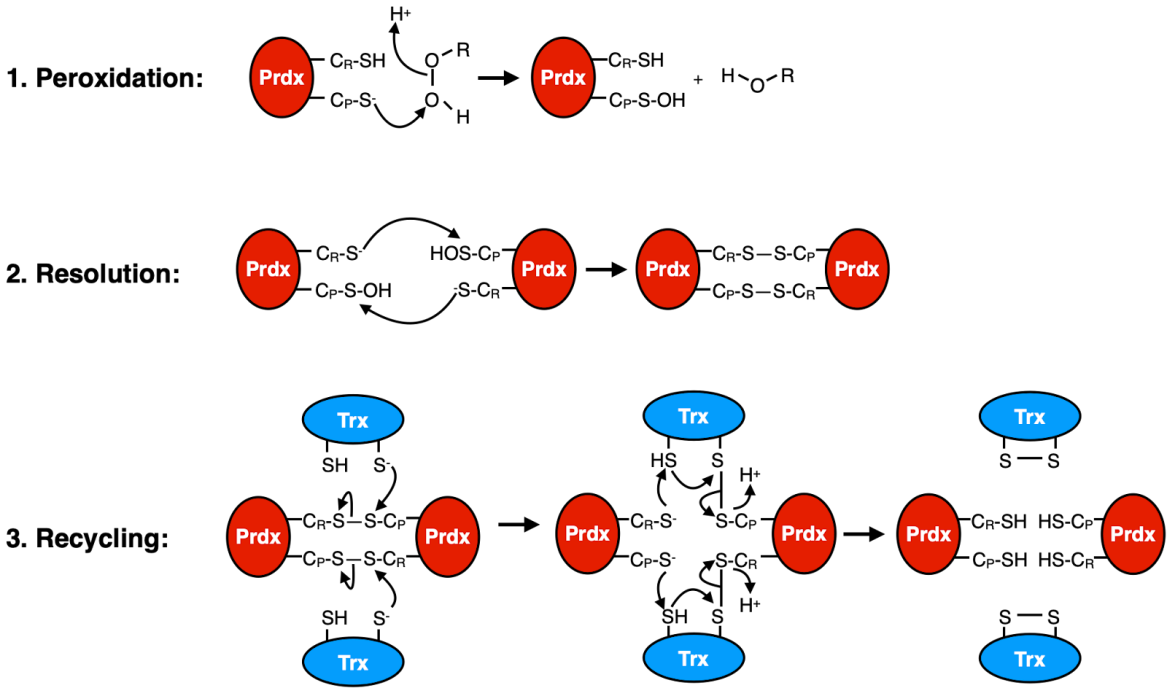

Figure 1.4. Mechanism of Prdx-mediated reduction of peroxides.

Prdx enzymes reduce peroxides and hydroperoxides via disulphide bonds at catalytic cysteine residues. All Prdx enzymes follow the same three catalytic stages. In 'peroxidation,' Peroxidatic cysteine residue (C_P) thiolate ions attack peroxides to become oxidised. Oxidised C_P residues are then attacked by resolving cysteine residue (C_R) thiolate ions to form disulphide bonds in 'resolution.' Prdxs undergo 'recycling,' whereby Trx resolves the disulphide bonds. Here the mechanism has been shown for Typical 2-Cys Prdxs (see Table 1.1).

Table 1.1. Prdx classes have different resolving mechanisms.

Prdx classes differ according to how their peroxidatic cysteine residues (C_P) are resolved and reduced via interactions with resolving cysteine residues (C_R) to form disulphide bonds (green lines).

Class	C_P	C_R	C_P - C_R Interaction	Graphical Interaction
Typical 2-Cys Prdxs	Yes	Yes	Intermolecular - enzymes function as obligate homodimers, with disuphide bonds forming between the C_P residue of one Prdx and the C_R residue of another (and vice versa).	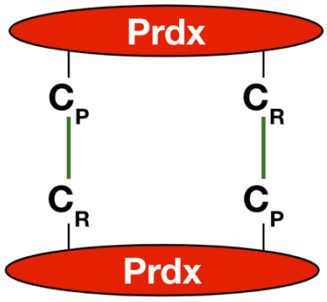
Atypical 2-Cys Prdxs	Yes	Yes	Intramolecular - enzymes form disulphide bonds between the C_P and C_R residues within the same enzyme.	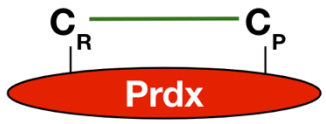
1-Cys Prdxs	Yes	No	Intermolecular - C_R residue is sourced from an alternative thiol group (not a Prdx enzyme).	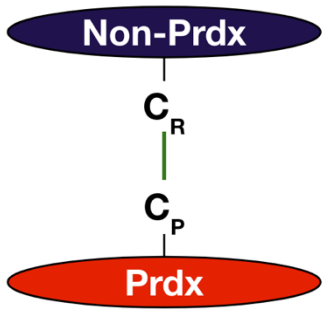

The oxidation state of C_P residues on typical 2-Cys Prdxs determines the manner in which they are reduced and recycled. If they are partially oxidised to sulfenic acid functional groups (SOH), these residues are readily attacked by C_R residue thiolate ions to form intermolecular disulphide bonds that can then be reduced by Trx (see Figure 1.5.A). However, hyperoxidation of C_P residues to sulfinic acid (SOOH) or sulfonic acid (SOOOH) functional groups prevents such interactions.

1.2.6.5. Sulfiredoxin-1

Although once thought to be irreversible, sulfinic acid functional groups on 2-Cys Prdxs are reduced by Sulfiredoxin-1 (Srx) (Biteau et al., 2003; Chang et al., 2004; Woo et al., 2005). This process is ATP- and Mg^{2+}-dependent and requires a thiol as an electron donor. The catalytic mechanism has been elucidated through mutating specific amino acid (AA) residues in rat Srx (Jeong et al., 2006). Co-immunoprecipitation experiments demonstrate that mutating the charged AA residues Arg^{50}, Asp^{57}, and Asp^{79} inhibits 26dimerisation with rat Prdx1. Mutation of these residues also inhibits the ATPase activity of Srx, as do mutations to the positively charged residues Lys^{60}, His^{99}, Arg^{100}, and the catalytic cysteine residue Cys^{98}. Mutations to each of the aforementioned residues prevents the reduction of Prdx1.

Combining these findings with the proposed structure by (Jönsson et al., 2005), Jeong et al. (2006) suggest a catalytic mechanism in which Srx binds to Prdx via residues Arg^{50}, Asp^{57}, and Asp^{79}. Binding to ATP phosphate groups happens independently of Prdx-binding and is facilitated by Lys^{60}, His^{99}, Arg^{100}. The catalytic Cys^{98} residue is deprotonated via interactions with the neighbouring Asp^{79} residue, creating a thiolate ion that initiates a nucleophilic attack on the γ-phosphate of ATP to hydrolyse it. This is transferred to the sulfinic acid moiety of hyperoxidised Prdx to form a sulfinic acid phosphoryl ester that is reductively cleaved by thiols, such as glutathione and Trx. The mechanism is depicted in Figure 1.5.B.

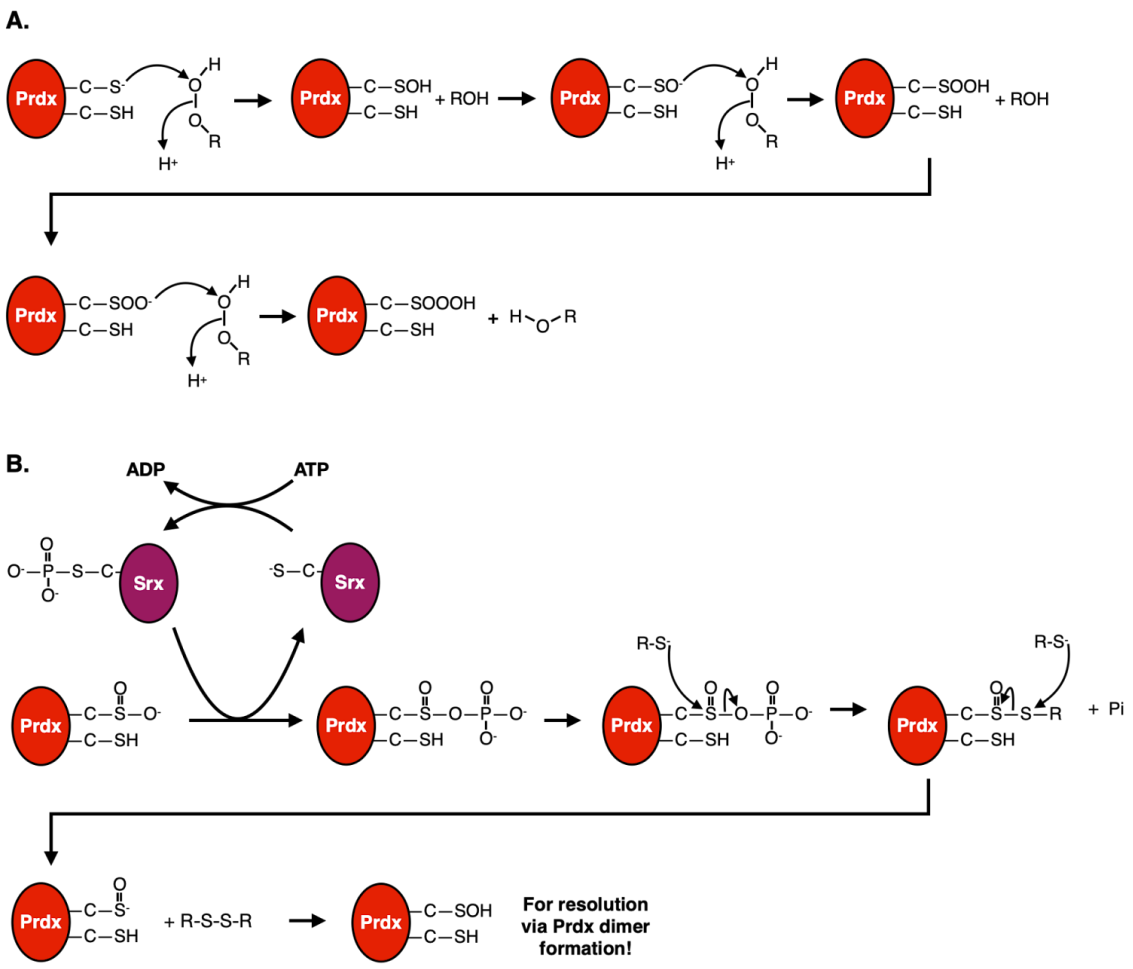

Figure 1.5. The recycling mechanism for typical 2-Cys Prdx enzymes is dependent on their oxidation state.

A. Peroxiredoxin C_P residues can be partially oxidised to sulfenic acid functional groups (SOH), or hyperoxidised to sulfinic (SOOH) and sulfonic acids (SOOOH). Partial oxidation allows typical 2-Cys-Prdx enzymes to be resolved by intermolecular disulphide bonds to form homodimers. These cannot form if C_P residues are hyperoxidised. **B.** Srx can reduce hyperoxidised typical 2-Cys Prdx C_P residues with sulfinic acid functional groups. This process requires ATP and Mg^{2+}. A sulfinic acid phosphoryl ester intermediate is formed that can then be reductively cleaved by thiols.

H_2O_2 alone is not sufficient to induce the hyperoxidation of 2-Cys Prdx enzymes, as ATP and Mg^{2+} are also required for H_2O_2-induced hyperoxidation (Yang et al., 2002). This indicates that the hyperoxidation only occurs when the enzymes are engaged in the catalytic cycle and the C_P residue is exposed. Eukaryotic 2-Cys Prdx enzymes possess a conserved C-terminus motif (Gly-Gly-Leu-Gly) that is lacking in prokaryotic Prdx. The latter is not susceptible to hyperoxidation and suggests that Srx has developed as an evolutionary adaptation to a change in the structure of eukaryotic 2-Cys Prdxs (Wood et al., 2003). The unusual situation, whereby 2-Cys-Prdx enzymes are inactivated by their own substrates (hydrogen peroxide and alkyl hydroperoxides), has led researchers to postulate that this system acts as a "floodgate" to prevent a pathological build-up of peroxides, whilst still permitting levels sufficient to regulate peroxide signalling (Wood et al., 2003). Kil et al. (2015) found that hyperoxidised Prdx3 and Srx undergo anti-phasic circadian oscillations in the mitochondria of various mouse tissues. Srx is cytosolic but it is imported into mitochondria to reduce hyperoxidised Prdx3 via a non-canonical N-terminal mitochondrial targeting sequence. This 'floodgate' system therefore permits an oscillatory release of H_2O_2 from mitochondria.

An alternative hypothesis is that Prdx hyperoxidation reduces interactions with Trx enzymes and permits them to be redirected towards other substrates. In fission yeast the hyperoxidation of Tpx1, which is the only typical 2-Cys Prdx in this organism, inhibits its thioredoxin peroxidase activity, enabling Trx to reduce alternative substrates that improve cell viability under conditions of OS (Day et al., 2012). This model may be more plausible than the 'floodgate' hypothesis as the latter assumes that high ROS levels may be produced in young, healthy cells. Typically, one might not expect such cells to generate such conditions.

Multiple studies suggest that Srx confers protection against OS within mammalian neurons. Srx is localised to synaptic terminals, and protects against OS-induced neurite retractions in rat primary neuron cultures (Ugbode et al., 2020). Knockdown of Srx using short interfering RNAs (siRNAs) increases lipid peroxidation in ischaemic rat cortices, which correlates with increased levels of hyperoxidised Prdx enzymes (Wu et al., 2017). Conversely, over-expressing Srx in rat spinal cord cultures deprived of oxygen and glucose rescues the increased MDA levels and apoptosis associated with this treatment (Lan et al., 2021). Loss of Srx also reduces the viability of rat cortical astrocyte cultures, which is also observed under conditions of OS and oxygen-glucose deprivation (Zhou et al., 2015).

Within neurons, Srx is upregulated in response to both synaptic activity and OS via JNK/AP-1 signalling (Papadia et al., 2008; Ugbode et al., 2020). This happens via distinct signalling cascades. OS recruits c-Jun homodimers, whereas synaptic activity recruits c-Jun/c-Fos heterodimers. It is also a transcriptional target of Nrf2 (Hayes and Dinkova-Kostova, 2014). Increased Srx transcript levels are observed in the blood of patients with mild cognitive impairment and hippocampal atrophy (Cucos et al., 2022).

Collectively, this evidence suggests that Srx may have an important protective role against OS. However, *Drosophila Srx* hypomorphs fail to exhibit sensitivity to food containing H_2O_2 (McGinnis et al., 2021). Therefore, this thesis sought to address the contradictory evidence and elucidate whether Srx primarily serves to protect against OS.

Srx regulates the chaperone activity of typical 2-Cys Prdx enzymes. Once dimerised, these can oligomerise to higher-order decamers (Gourlay et al., 2003; Lee et al., 2007; Wood et al., 2002) that are associated with chaperone behaviour in yeast and mammalian cells (Jang et al., 2004; Moon et al., 2005). This oligomerisation is irreversible in *Srx* mutant yeast, meaning that they are stuck in their HMW form that assumes chaperone holdase function (Noichri et al., 2015). The physiological relevance of these decamers and the potential chaperone functions remains unclear (Perkins et al., 2015).

Srx regulates the oxidation state of Prdx3 in the mitochondria of adrenal cortex cells to control circadian oscillations in the production of corticosteroid hormones in mammals. Corticosteroids have wide ranging functions such as the regulation of immune function and blood sugar levels. Corticotropin-releasing hormone and arginine vasopressin released from the hypothalamus stimulate adrenocorticosteroid hormone (ACTH) release from the anterior pituitary gland into the bloodstream in a circadian manner. ACTH stimulates glucocorticoid synthesis in the adrenal cortex that is released into the bloodstream to exert influence over the activity of multiple organs (process reviewed in Gjerstad et al., 2018). In humans, this glucocorticoid is cortisol, whereas this is corticosterone (CS) in murinae (Kil et al., 2012). At the adrenal cortex cells, ACTH stimulates glucocorticoid synthesis in mitochondria via the oxidation of cholesterol by cytochrome P450 enzymes. This process produces H_2O_2, which is subsequently reduced by Prdx3. Hyperoxidation and inactivation of Prdx3 leads to H_2O_2 release from the mitochondria, which activates p38 mitogen-activated protein kinase signalling to inhibit CS synthesis through the inhibition of steroidogenic acute regulatory protein. The H_2O_2 release also promotes the mitochondrial import of Srx via disulphide bonds with HSP90. Once inside mitochondria, Srx reduces Prdx3 and is then degraded by Lon protease in a manner dependent on Prdx3 oxidation state. Srx degradation completes a

negative feedback cycle to help control circadian oscillation of H_2O_2 release and steroidogenesis. Ablation of Srx prevents the circadian oscillation of Prdx3 oxidation state H_2O_2 release from mitochondria, and CS (Kil et al., 2015, 2012). It is unknown whether Prdx3 and Srx perform a similar role in neurons.

Additional, putative Srx substrates besides Prdx enzymes were identified by (Akter et al., 2018). A sulfinic acid probe was combined with proteomic analyses in mouse embryonic fibroblast cells (MEFs) to identify 55 proteins that exhibited increased amounts of sulfinic acid groups in the absence of Srx. This highlights the fact that Srx may reduce additional substrates. Many of the putative Srx substrates identified by Akter et al. (2018) are implicated in neuron function. This includes DJ-1/PARK7, a multifunctional protein that acts as a critical sensor for ROS in neurons to induce homeostatic adaptions (Oswald et al., 2018). Mutations to this gene cause rare, familial forms of Parkinson's disease (Repici and Giorgini, 2019).

Another Srx substrate identified by Akter et al. (2018) is Rab10. This mediates membrane-specific tethering between vesicles and targets to facilitate the movement of vesicles between the Golgi and plasma membrane (Hutagalung and Novick, 2011). Rab10 facilitates many of the phenotypes present in a *Drosophila* model of Parkinson's Disease, as induced by ectopic expression of the human *LRRK2-G2019S* mutation in dopaminergic neurons (Fellgett et al., 2021). Further work is required to validate and elucidate the physiological relevance of such interactions between Srx and its putative substrates.

1.3 ROS regulation and function in the nervous system

Neurons are metabolically-demanding cells due to the energy requirements of synaptic transmission and maintaining membrane potentials. The large energy requirements, polarised structures, and terminally-differentiated nature of neurons means that ROS regulation is critical for their function and long-term viability.

1.3.1. Neuron metabolism and energy production

The energy requirements of neurons are principally met by oxidative phosphorylation (Hall et al., 2012). The manner in which respiratory substrates fuel neuronal oxidative phosphorylation is contested, with some evidence suggesting that it is predominantly fuelled by glucose derivatives sourced from glia. This theory postulates that glycolysis in astrocytes synthesises pyruvate from glucose, which is converted to lactate by lactate dehydrogenase (LDH). Lactate can then be shuttled from the glia to neighbouring neurons, where it is re-converted to pyruvate to power aerobic respiration. This hypothesis is named the 'astrocyte-neuron lactate shuttle' (ANLS), and is speculated to be conserved across many model organisms (Pellerin and Magistretti, 2012, 1994; Volkenhoff et al., 2015). The ANLS is triggered by astrocytic uptake of glutamate from the synaptic cleft, an energy-consuming process that triggers glycolysis in glia and lactate production. Alanine, another glucose derivative produced in glycolysis, is also reported to be shuttled from glia to neurons (Rabah et al., 2023; Volkenhoff et al., 2015).

Alternative studies find that glycolysis in neurons is not dispensable for oxidative phosphorylation, and has a key role in maintaining long-term neuron function. Li et al. (2023) observed that mice with postnatal knockout of the predominant neuronal glucose transporter (GLUT3) in hippocampal cells exhibit sex-specific and age-dependent spatial learning and memory deficits that correlate with diminished hippocampal and total brain volume. Postnatal knockout mutations of the neuron-enriched pyruvate kinase isoform (PKM1), which catalyses the final rate-limiting step of glycolysis, also produced these age- and sex-dependent learning and memory deficits. GLUT3-knockout mice demonstrate diminished ATP levels at synaptic boutons, but not in the cell bodies, which suggests that glucose-fuelled oxidative phosphorylation is important for ATP production within specific cellular locations.

1.3.2. ROS regulation in neurons

Neurons have a much lower antioxidant capacity than glia, which they rely on to maintain ROS homeostasis. Nrf2, which modulates the expression of some enzymes that synthesise glutathione, amongst other antioxidant enzymes, is epigenetically repressed in neurons (see Chapter 1.2.3.3) (Bell et al., 2015). Without Nrf2, neurons are heavily reliant on glia synthesising glutathione and exporting it to neurons to maintain ROS homeostasis (Shih et al., 2003). Consequently, the concentration of glutathione in neurons is less than the surrounding astrocytes (Sagara et al., 1993).

The dependency of neurons on glia for respiratory substrates is also hypothesised to aid defence against OS. Despite fuelling oxidative phosphorylation with glia-sourced glucose derivatives, neurons have transporters in their plasma membrane to import glucose (Vannucci et al., 1997; Volkenhoff et al., 2018). It is hypothesised that neurons uptake glucose to fuel the pentose phosphate pathway (PPP), rather than glycolysis (Herrero-Mendez et al., 2009). The PPP generates NADPH, which reduces and replenishes antioxidants such as glutathione. This suggests that the decreased levels of glutathione in neurons are compensated by an increased capacity to replenish and regenerate this antioxidant (Bolaños and Almeida, 2010; Sagara et al., 1993).

1.3.3. Physiological functions of ROS signalling

ROS are emerging as a key regulator of neuron morphology and synaptic plasticity, regulating synaptogenesis. Neurons are highly polarised cells and exhibit a major presynaptic axonal neurite and postsynaptic dendritic neurites in the somatodendritic compartment. Redox signalling controls the generation of these polarised structures, particularly the enhanced elongation of developing axons at growth cones. ROS-generating NOX enzymes are reported to modulate axon outgrowth. Over-expressing the $p47^{phox}$ subunit of NOX2 facilitates axonal outgrowth in mouse hippocampal neuron cultures (Wilson et al., 2016), whereas expressing a dominant-negative form of $p47^{phox}$ inhibits axon elongation (Wilson et al., 2015). These changes appear to be facilitated by the release of Ca^{2+} from intracellular stores via redox-modifications of ryanodine receptors and inositol-3-phosphate receptors (Wilson et al., 2016). Calcium released from ER intracellular stores regulates cytoskeleton organisation and dynamics (Akiyama and Kamiguchi, 2015) and also promotes expression of Rac1, a potent activator of NOX2 (Wilson et al., 2016), to generate a positive feedback loop that sustains high levels of ROS at axon terminals to promote axon elongation. In the adult mammalian CNS, growth cones at axon terminals axons have generally reached their target location, collapse, and axon lose their ability to grow. Subsequently, they will not change length in response to elevated ROS levels that are observed with ageing ROS levels (Chen and Tonegawa, 1998).

The neuronal cytoskeleton is directly modulated through changes to the redox state of cysteine residues in cytoskeletal proteins. For example, actin polymerisation and dynamics are modulated by glutathionylation of cysteine residues (Dalle-Donne, 2001; Dalle-Donne et al., 2003). ROS indirectly affect cytoskeletal architecture through modulating components of signalling pathways. Ectopic expression of the transcriptional regulator Nrf2 in mouse cortical

neuron cultures inhibits neurite outgrowths and arborisation, through inhibition of the redox-sensitive JNK and Wnt pathways (Bell et al., 2015).

During *Drosophila* larval development, NMJs exhibit synaptic plasticity to allow structural and functional changes to occur. ROS-induced JNK/AP-1 signalling is a critical regulator of adaptive neuron growth at the *Drosophila* larval NMJ. ROS-generating pharmacological agents and antioxidant gene mutations differentially activate AP-1 components to increase neuron growth, which is accompanied by functional synaptic changes. Mutations to the endosomal protein *spinster* cause *Fos*-dependent overgrowths and diminished synaptic transmission following repeated presynaptic stimulation (Milton et al., 2011).

PI3K signalling also facilitates neuron growth at the *Drosophila* larval NMJ induced by both ROS-generating pharmacological agents and enhanced neuron activity. The latter can be achieved via the expression of temperature-sensitive TRP channels in motor neurons. ROS-induced, PI3K-mediated neuron growth at the *Drosophila* NMJ is dependent on DJ-1β, suggesting this protein acts as a critical 'redox sensor' to regulate structural plasticity (Oswald et al., 2018). As a mediator of plasticity, ROS could modulate complex, high order neurological processes like learning and memory. In agreement with this theory, applications of H_2O_2 to rat hippocampal slices enhance LTP, which is widely assumed to underpin learning and memory (Kamsler and Segal, 2003).

ROS are also implicated in maintaining circadian rhythms in both neuronal and non-neuronal cells. Circadian rhythms are biological events that align with a period length of approximately 24 hours, which are driven by molecular 'clocks' or 'pacemakers.' These rhythms allow organisms to predict changes in their environment and adjust their activity accordingly (Tataroglu and Emery, 2014). The oxidation state of Prdx enzymes undergoes circadian oscillations, which is conserved across species (Edgar et al., 2012). The PPP, which uses glucose to regenerate NADPH, controls the circadian rhythms in Prdx oxidation, even in the absence of genetic negative feedback loops that also contribute to circadian oscillations (see Chapter 1.4.7). NADPH is the principal electron donor for reducing hyperoxidised enzymes. The application of 6-aminonicotinamide (6-AN), which is metabolised to a NADP+ orthologue and competitively inhibits NADPH synthesis, disrupts circadian rhythms in the oxidation state of Prdx enzymes in human U2OS cells, and disrupts the circadian rhythmicity in mammals and *Drosophila* (Rey et al., 2016).

1.3.4. OS and nervous system pathologies

OS is a pathological hallmark of many neurodegenerative conditions, such as Parkinson's Disease (PD). PD is characterised by a loss of dopaminergic neurons in the substantia nigra pars compacta (SNc) (Fahn and Sulzer, 2004). These neurons have a modulatory role within the basal ganglia to coordinate voluntary movements (Lanciego et al., 2012). Consequently, patients exhibit motor symptoms like tremors, dyskinesia, and rigidity. They may also exhibit cognitive symptoms such as anxiety. Surviving neurons in the SNc contain protein aggregates named Lewy bodies, which are primarily composed of alpha synuclein (Spillantini et al., 1997).

OS has been implicated in PD pathogenesis. Post-mortem analysis shows increased lipid peroxidation in the SNc of PD patients, as shown by increased levels of 4-hydroxyl-2-nonenal (4-HNE) (Yoritaka et al., 1996). Mitochondrial toxins that increase OS are also linked to PD, such as the pesticides Paraquat and Rotenone (Tanner et al., 2011). Mice exposed to these compounds exhibit a selective loss of dopaminergic SNc neurons (Inden et al., 2011; McCormack et al., 2002).

The susceptibility of SNc neurons to OS may be partially attributed to dopamine acting as a source of ROS. At cytosolic pH levels, it undergoes auto-oxidation to form quinones, as protons readily dissociate from the hydroxyl groups (Muñoz et al., 2012). It is typically sequestered into vesicles for release in synaptic transmission, facilitated by vesicular monoamine transporter 2 (VMAT2), which concurrently releases two protons (Chaudhry et al., 2008). Membrane-bound ATPase enzymes transport protons into the vesicles to provide a continual source of protons, which consequently lowers the pH to prevent the loss of dopamine protons and dopamine auto-oxidation (Muñoz et al., 2012). Defects in dopamine storage and turnover are suggested to render the SNc neurons vulnerable to OS (Dias et al., 2013).

The metabolism of dopamine also generates free radicals. Excess dopamine in the cytosol is degraded by monoamine oxidase (MAO) enzymes in the mitochondrial membrane that produce H_2O_2. There are two types of this enzyme: MAO-A and MAO-B. The former is predominantly found in the dopaminergic neurons in the SNc, whereas the latter is mainly found in glia (Riederer et al., 1987). Post-mortem tissue analysis and positron emission tomography (PET) have revealed age-related increases in MAO-B expression in human brains, but not increases in MAO-A (Fowler et al., 1997; Saura et al., 1997). This is hypothesised to increase H_2O_2 production in the glia of SNc, which are highly permeable and

could diffuse into local SNc neurons to induce oxidative damage and neurodegeneration (Kumar and Andersen, 2004). In support of this theory, inducible expression of human MAO-B in the astrocytes of adult mice causes the selective and progressive loss of SNc dopaminergic neurons (Mallajosyula et al., 2008).

Early-onset, familial forms of PD are caused by rare mutations, which may help provide insights into the aetiology of sporadic PD. This includes mutations to DJ-1, otherwise known as PARK7 (Bonifati et al., 2003; Repici and Giorgini, 2019). This protein confers resistance to oxidative stress in mice (Kim et al., 2005), *Drosophila* (Meulener et al., 2005), and cultured neuroblastoma cells (Taira et al., 2004). A conserved cysteine residue (Cys^{106}) facilitates its protective function in both mammals (Blackinton et al., 2009) and *Drosophila* (Meulener et al., 2006). Redox modifications at this residue promote the mitochondrial localisation of DJ-1 in response to OS, as C106A missense mutations fail to recapitulate the localisation seen in controls following Paraquat treatment (Canet-Avilés et al., 2004).

DJ-1 appears to protect against OS in multiple ways. It scavenges H_2O_2 to act as an atypical Prdx-like peroxidase (Andres-Mateos et al., 2007). It also binds to Ask1 via disulfide bonds at Cys106 to attenuate its dissociation from Trx and inhibit downstream JNK signalling and apoptosis (Im et al., 2010; Waak et al., 2009). Through redox modifications to this residue, DJ-1 is proposed to act as a critical sensor of ROS, initiating signalling events to mediate synaptic plasticity in *Drosophila* (Oswald et al., 2018).

OS is also associated with Amyotrophic Lateral Sclerosis (ALS). In this condition, there is degeneration of the upper motor neurons in the motor cortex and lower motor neurons in the brainstem that descend through the spinal cord to innervate voluntary muscles. With progressive degeneration of these neurons, there is an accompanying denervation of muscles that weaken and atrophy. Death from neuromuscular respiratory failure typically occurs within 2-5 years of disease onset (Masrori and Van Damme, 2020). Post-mortem examinations reveal higher protein carbonylation levels in ALS patient spinal cords (Shaw et al., 1995) and higher levels of lipid peroxidation (Shibata et al., 2001). It is not clear if OS drives the pathology or is a consequence of it (Parakh et al., 2013). However, many of the risk factors for the disease are associated with generating OS in cells. This includes exposure to agricultural chemicals, heavy metals, and intense exercise (D'Amico et al., 2013).

Familial, early-onset forms of ALS may provide insights into the aetiology of the sporadic, late-onset form of the disease. Mutations to Superoxide Dismutase 1 (SOD1) are associated with familial forms of ALS (Rosen et al., 1993). Transgenic mice expressing human SOD1 mutations (G39A) exhibit increased H_2O_2 levels, protein oxidation, and lipid peroxidation in the spinal cord tissue lysates (Liu et al., 1999). It is not yet resolved whether ALS-associated SOD1 mutations drive pathogenesis through LOF of this enzyme or the acquisition of toxic properties through protein misfolding and accumulation.

As OS is implicated in the pathogenesis of many neurodegenerative diseases, the potential therapeutic effects of dietary antioxidants on disease progression have been widely researched. Although many antioxidants show promise when tested on animal or *in vitro* models of diseases, these treatments do not necessarily translate to benefits for human patients in clinical trials. For example, Vitamin C has been found to delay locomotor defects in *Drosophila* models of PD, whereby human alpha-synuclein is ectopically expressed in neurons (Khan et al., 2012). However, meta-analysis has shown that Vitamin C is not effective in reducing the risk of PD in human patients (Etminan et al., 2005). A reason for this, as well as the failure of other water-soluble antioxidants, may be its bioavailability in the CNS. The neuroprotective potential of Vitamin C could be limited as it requires active transport at the Choroid Plexus to enter the CNS (Etminan et al., 2005).

1.3.5. OS, autophagy, and mitochondrial dynamics

Mitochondria are dynamic organelles that undergo a continuous cycle of fission and fusion, exhibiting a wide variety of shapes. It is proposed that various mitochondrial structures, such as fragmented or tubular shapes, may reflect different metabolic states. However, it is still not definitively established whether such differences produce changes in function (Willems et al., 2015).

Mitochondrial morphology and dynamics are influenced by the redox state of cells, largely due to the control OS exerts over autophagy. Autophagy, meaning ‘self-eating,’ is an intracellular degradation process in which components are digested by lysosomes and the macromolecular derivatives are released into the cytosol. There are three classes of autophagy: macroautophagy, microautophagy, and chaperone-mediated autophagy (reviewed in Lee et al., 2012). Macroautophagy is the process by which lysosomes fuse with double-membraned autophagosomes containing cargo to be degraded. Macroautophagy can occur in a selective manner, whereby the autophagy of specific cargo or organelles is

degraded. Microautophagy is the process by which lysosomes directly engulf and digest cytosolic constituents. Chaperone-mediated autophagy delivers cargo with KFERQ AA motifs to lysosomes via binding to lysosome-associated membrane protein 2A (LAMP2A) receptors on the lysosomal membrane (Bejarano and Cuervo, 2010).

OS stimulates macroautophagy and is indispensable for its induction. Antioxidant treatment of HeLa and CHO cells prevents the formation of starvation-induced autophagosomes (Scherz-Shouval et al., 2007). Mild OS induces mitophagy in a manner that is dependent on mitochondrial fission. Frank et al. (2012) demonstrated that treating HeLa and MEF cells with low concentrations of H_2O_2 or rotenone, which were insufficient to impair cell viability, induced mitochondrial fragmentation, increased the colocalisation of mitochondria with autophagic vesicles, and reduced the relative mitochondrial mass per cell. These changes appeared to be independent from non-selective autophagy, as increases in autophagolysosomes were not detected via electron microscopy. Frank et al. (2012) also found that expression of dominant-negative isoforms of Dynamin-related protein 1 (DRP1) in HeLa cells, which is critical for mitochondrial fission, suppressed mild OS-induced colocalisation of mitochondria with autophagic structures. It has been suggested that OS-induced mitophagy acts as a negative feedback mechanism to regulate mitochondrial ROS production (Kurihara et al., 2012).

1.4. *Drosophila melanogaster* as a tool to study redox biology in neurons

1.4.1. *Drosophila* as a model organism in neuroscience

Drosophila melanogaster, commonly known as fruit flies, are a well-established invertebrate model organism for researching genetics, cell biology, and physiology. Thomas Hunt Morgan used this model to prove the chromosomal theory of inheritance, whereby white eyes in *Drosophila* were associated with the inheritance of X chromosomes (Morgan, 1910). This seminal work established flies as a powerhouse for biological research.

Drosophila have short lifespans, high fecundity, and inexpensive maintenance requirements relative to many mammalian model organisms (Roote and Prokop, 2013). Transgenic flies can be readily produced and housed in segregated 'stocks.' A plethora of genetic tools available to researchers that use fruit flies, which afford spatio-temporal control of gene expression. Such techniques can be coupled with well-characterised behavioural, physiological, morphometric, and immunohistological paradigms to screen for phenotypic traits.

Approximately 75% of known human disease genes have homologues in the *Drosophila* genome, demonstrating their usefulness to model various pathologies (Ugur et al., 2016). This is particularly true for neurodegenerative conditions, as there are many common functional and regulatory features in the fly and human nervous system (Hirth and Reichert, 1999). Studies in *Drosophila* first proved genetic interactions between *PTEN-induced Kinase 1* (*Pink1*) and *parkin*, which coordinate mitochondrial quality control (Clark et al., 2006; Park et al., 2006; Pickrell and Youle, 2015). Mutations to these genes cause early-onset, hereditary forms of Parkinson's Disease in human patients who exhibit locomotive defects and decreased dopamine production, which are also observed in *Drosophila Pink1* and *parkin* mutants.

Many mammalian antioxidant enzymes and redox-sensitive signalling components are conserved in *Drosophila*, which have also been used to demonstrate the antioxidant potential of dietary supplements (reviewed in Yi et al., 2021). Likewise, the administration of dietary compounds to induce OS is common practice. This includes hydrogen peroxide (H_2O_2) and mitochondrial toxins like paraquat. Collectively, this shows that *Drosophila* are a useful model for studying redox biology and its relevance to neuron function and development.

1.4.2 The life cycle of *Drosophila*

Drosophila are a holometabolous insect with four distinct life stages: embryos, larvae, pupae, and adult flies (see Figure 1.6). Adult flies mate to fertilise embryos in females, which are laid onto a food source. Embryos develop into larvae, for which there are three instar stages. First instar larvae feed at the surface of a food source, second instar larvae burrow into the food, and third instar larvae exit the food source to pupate. Adult flies eclose from the pupae (process reviewed in Fernández-Moreno et al., 2007). The rate of the development can be controlled by changing the temperature of the environment, with cooler temperatures slowing

down the process. Temperatures of 25°C care typically used to rear experimental flies. This gives a total development period of approximately 10 days.

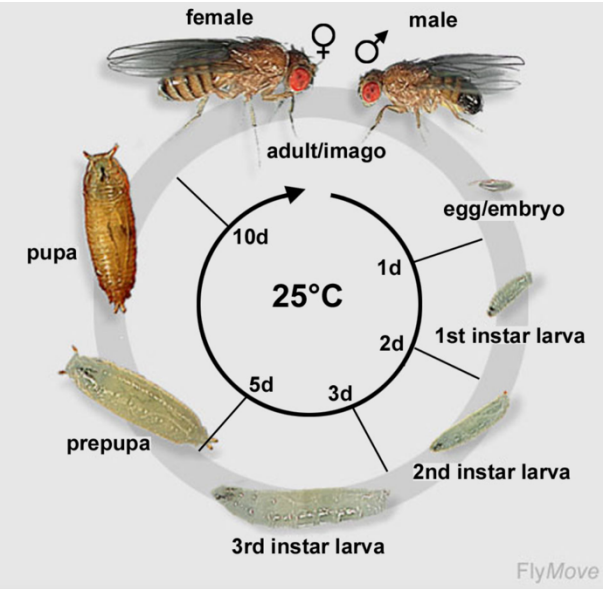

Figure 1.6. *Drosophila melanogaster* undergo metamorphosis.
Fertilised embryos develop into larvae. There are three larval stages, which precede pupa formation. Adult flies eclose from pupae, which mate to fertilise embryos and repeat the life cycle. Figure is adapted from (Weigmann et al., 2003).

1.4.3. Genetic tools in *Drosophila*

A plethora of genetic tools are available to researchers using *Drosophila*. Fruit flies have four pairs of chromosomes: one pair of heterosomes and three pairs of autosomes that encode approximately 13,600 genes (Adams et al., 2000). The *Drosophila* genome exhibits low redundancy, meaning that few genes encode proteins of the same class. Conversely, higher organisms like mammals have higher redundancy, whereby multiple genes encode protein classes with similar functions (Roote and Prokop, 2013). Using flies can reduce the complications of researching loss-of-function alleles, as it is often less likely that there will be multiple paralogous genes.

1.4.3.1. Balancer Chromosomes

A key genetic feature of *Drosophila* are balancer chromosomes, which allow for genes of interest to be maintained within fly stocks and tracked through mating schemes (reviewed in Miller et al., 2019). Balancer chromosomes contain multiple nested inversions that suppress synapsis and homologous recombination events. Any that do occur are likely to be lethal, as they can cause the deletion or duplication of chromosomal regions, causing them to be

'unbalanced.' Such events may occur in centromeric regions to create acentric or dicentric chromosomes, compromising their stability. Balancer chromosomes also contain recessive, homozygous lethal mutations and typically have dominant 'marker' genes that allow for easy identification. An example is the second chromosome balancer *CyO*, which carries the *Curly* gene mutation that causes curly wings. The combination of these features is particularly useful for maintaining alleles that are homozygous lethal.

1.4.3.2. *P-Elements* and the ΦC31 integrase system

Transgenic flies, which have exogenous DNA sequences inserted into their genome, form the bedrock of current research in *Drosophila*. These are mostly derived from the use of transposons, such as *P-Elements*, which are virus-like DNA fragments that stably insert into the host genome. They encode transposase enzymes that catalyse mobilisation of the sequence to other genomic locations. Transposons can be modified to introduce a gene of interest to the host genome, rather than a functional enzyme. The encoding DNA is injected into the posterior pole of *Drosophila* embryos with 'helper elements' that ensure integration into the genome of gamete progenitor cells (Bachmann and Knust, 2008).

P-Elements insert into the genome at random loci. These differing insertion sites affect their expression level due accessibility to transcriptional machinery. These 'position effects' can be overcome by using site-directed insertion using the ΦC31 integrase system, which promotes recombination between attP and attB motifs. DNA with flanking attB sites is injected into embryos expressing ΦC31 and attP sites at known loci (Bischof et al., 2007).

Existing *P-Element* insertions can be mobilised to new locations to disrupt gene expression in multiple ways (Hummel and Klämbt, 2008). Firstly, this process may create imprecise excisions and excise flanking regions of DNA. Secondly, this may cause insertion into coding sequences of genes to cause mutagenesis.

1.4.3.3. The Gal4/UAS system

P-Elements can be used to generate transgenes that allow for the spatial specificity of gene expression in *Drosophila* through the Gal4/UAS system. In this system, two separate transgenes are combined in the fruit fly genome through crossing schemes. One contains the exogenous, yeast-derived Gal4 transcription factor under the control of a tissue-specific promoter. The other contains a gene of interest downstream of the promoter sequence that

Gal4 binds to, named the 'upstream activation sequence,' or 'UAS' (Brand and Perrimon, 1993). The nature of this sequence can vary according to the needs of researchers. It could encode endogenous *Drosophila* genes to induce overexpression, dominant-negative genes, shRNA molecules to induce RNA interference, or biochemical tools and reporters. A temperature-sensitive Gal80 protein, which binds to Gal4 at temperatures below 29°C to inhibit Gal4-UAS binding, can confer additional temporal specificity of gene expression through rearing flies at specific temperatures at different timepoints (McGuire et al., 2004).

Whilst *Drosophila* offer a wealth of tools to manipulate gene expression, there are some features that differentiate them from working with mammalian systems. X chromosome dosage compensation in mammals is achieved through the epigenetic silencing of one X chromosome, whereas in *Drosophila*, this is achieved through upregulation of genes on the singular X chromosome (Lucchesi and Kuroda, 2015).

1.4.4. Limitations of *Drosophila* for neuroscience research

Despite the many useful features of *Drosophila* as a model organism for neuroscience research, several limitations render them unsuitable for specific research topics. *Drosophila* exhibit open circulation systems and are consequently inappropriate for modelling brain infarcts or haemorrhages (Jeibmann and Paulus, 2009).

Drosophila are inappropriate for modelling the glial ensheathment of neuron axons in vertebrates, which establishes distinct domains for saltatory conduction. In vertebrates, axons are encapsulated by multi-layered myelin membranes provided by oligodendrocytes and Schwann cells in the central and peripheral nervous system, respectively (Poliak and Peles, 2003). Conversely, invertebrates lack myelin and the *Drosophila* genome lacks most genes encoding homologues to the major myelin proteins (Banerjee and Bhat, 2008). *Drosophila* do, however, exhibit multi-layered glial membrane sheaths around neurons that perform a similar function. For instance, ensheathing glia processes in the peripheral nervous system encapsulate individual axons or axon fascicles (Leiserson et al., 2000).

1.4.5. The *Drosophila* third instar larvae neuromuscular junction

Drosophila third instar larvae can be dissected to observe neuromuscular junctions (NMJs) using immunohistological staining techniques, providing information on neuron development. NMJs in *Drosophila* larvae differ from those found in vertebrates as they are predominantly glutamatergic, rather than cholinergic, with ionotropic postsynaptic receptors (GluR) homologous to mammalian AMPA receptors (Menon et al., 2013). This renders NMJs useful for modelling the excitatory synapses found in the mammalian central nervous system (CNS). This paradigm is powerful as it can be complemented by additional experiments to investigate the functional consequences of changes to neuron morphology. Crawling assays can assess locomotor output and coordination (Nichols et al., 2012), and excitatory junction potentials (EJPs) can be recorded to identify changes in synaptic transmission (Imlach and McCabe, 2009).

1.4.5.1. Anatomy of the *Drosophila* third instar neuromuscular junction

Larval dissections along the anteroposterior axis unveil muscles attached to the body wall within the cuticle. Each muscle is a multinucleate cell derived from the fusion of myoblasts, which have been annotated and are readily identifiable by their shape and relative positions (Keshishian et al., 1996). Abdominal hemisegments A2-A7 have 30 muscles that are innervated by motor neurons derived from peripheral nerves. Typically, the NMJs at muscle 6/7 in hemisegment A3 are used to study factors affecting neuron development. Neurons at these synapses are glutamatergic and have short, localised branches with large, varicose presynaptic structures called boutons (Johansen et al., 1989). The anatomy of the *Drosophila* third instar NMJ can be observed in in Figure 1.7. Each bouton contains multiple active sites, from which neurotransmitter is released. They can be large or small, referred to as type Ib and type Is boutons, respectively (Atwood et al., 1993). The number of boutons is used as a measure of synapse growth, which is assumed to be coupled to the size of the muscle (Sweeney and Davis, 2002). Consequently, values are often normalised to the surface area of muscle 6/7. Henceforth, the term NMJ will refer to these specific synapses.

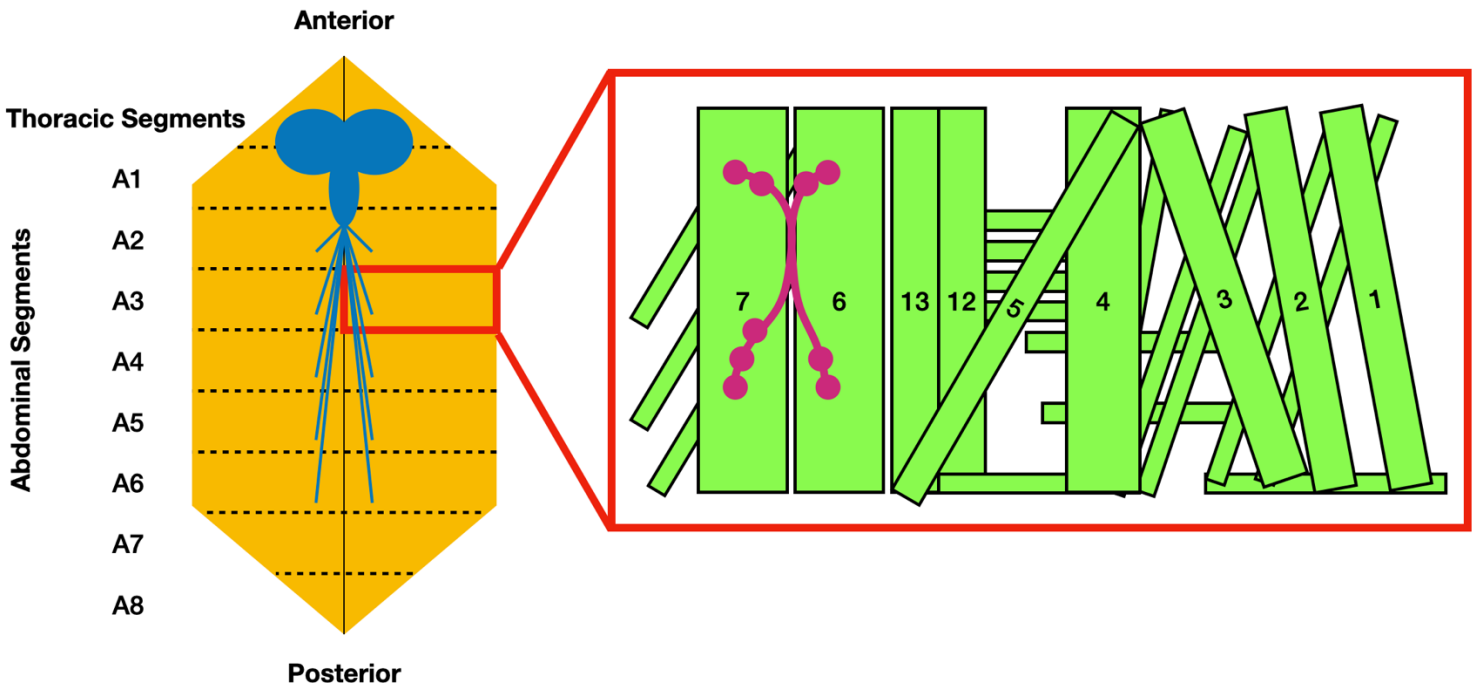

Figure 1.7. Anatomy of the *Drosophila* NMJ.

Schematic of a third instar *Drosophila* larvae dissected along the anteroposterior axis, whereby the body wall (yellow) is pinned back. Nerves descending from brain via the ventral nerve cord innervate muscles in the body wall (collectively shown in blue). The body wall exhibits eight abdominal segments that can be further divided into symmetrical hemisegments. Abdominal segments A2-6 have identical innervation and muscle patterns. The neuron (magenta) lying against muscle 6/7 (green) in segment A3 is commonly used as a model for studying neurodevelopment, with the number of synaptic boutons used as a measure of growth. Due to the symmetrical nature of the muscle wall, two such neurons can be observed per larvae.

1.4.5.2. Development of the *Drosophila* third instar larvae NMJ

Drosophila NMJ synaptogenesis occurs in embryos, approximately 12 hours after egg-laying, when the growth cones of neurons contact myoblasts, triggering differentiation into presynaptic terminals (Broadie and Bate, 1995). Many genes are required for synapse formation at this stage. Bruchpilot (Brp) is needed in neurons for the formation and organisation of various presynaptic components. It is required for the formation of T Bars, the T-shaped structures in active sites thought to promote vesicle fusion, and the clustering of Ca^{2+} channels (Kittel et al., 2006). GluRs and Discs large (Dlg), the *Drosophila* orthologue to postsynaptic density 95 (PSD-95), cluster at the postsynaptic contact sites (Chen and Featherstone, 2005). A functional synapse is formed in embryos approximately 20 hours after egg-laying.

Post-embryonic growth of the larval NMJ is facilitated by many complex signalling pathways, including bidirectional morphogenic signalling between the developing presynaptic neuron terminals and postsynaptic muscles (see Figure 1.8). Wingless (wg) signalling, which is homologous to Wnt signalling in vertebrates, positively regulates synapse formation. Wingless is secreted from neurons to promote the formation of boutons, active zones, and postsynaptic structures (Packard et al., 2002). It binds to the postsynaptic G protein-coupled receptor (GPCR) *Drosophila* Frizzled2 (Dfz2) on muscles to function as an anterograde signal. This causes the receptors to be endocytosed, where the C-terminus is then cleaved and translocates into the nucleus. This is presumed to initiate transcriptional changes in the muscle that regulate synapse development (Mathew et al., 2005). Wingless also binds to presynaptic Dfz2 receptors to function as an autocrine signal. This activates the phosphoprotein dishevelled (dsh) to inhibit the glycogen synthase kinase (GSK) shaggy (sgg). This prevents phosphorylation of the microtubule-associated protein futsch, which binds microtubules to promote the formation of microtubule loops and stable boutons (Miech et al., 2008).

Retrograde transforming growth factor β (TGF-β) signalling positively regulates NMJ growth. The morphogen Glass bottom boat (Gbb) is released from postsynaptic muscle cells to act as a retrograde signal and promote TGF-β signalling in the presynaptic neuron (Marqués, 2005). Mutations to the presynaptic type II TGF-β receptor wishful thinking (*wit*), as well as mutations to the type I TGF-β receptors *thick veins* (*tkv*) and *saxophone* (*sax*) diminish synapse growth (Sweeney and Davis, 2002).

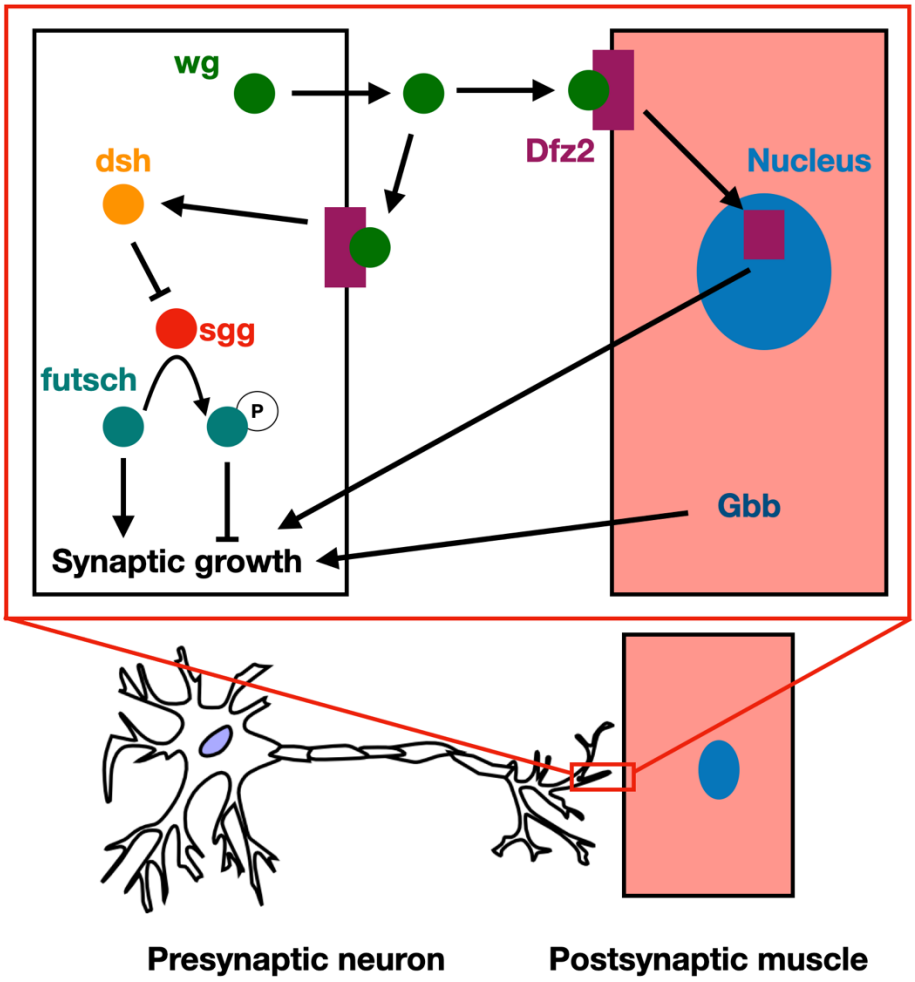

Figure 1.8. Morphogenic signalling pathways regulate *Drosophila* NMJ growth.
Retrograde TGF-β signalling promotes synapse growth when Glass bottom boat (Gbb) is released from postsynaptic muscle cells and binds to presynaptic neuron receptors including thick veins (tkv), saxophone (sax) and wishful thinking (wit). Wingless (wg) signalling, which is homologous to vertebrate Wnt signalling, is released from presynaptic neurons. It binds to pre- and postsynaptic *Drosophila* frizzled 2 (Dfz2) receptors to enhance synapse growth. Binding of wg to postsynaptic receptors causes the nuclear localisation of the Dfz2 C-terminus to initiate transcriptional changes. Binding of wg to presynaptic receptors activates dishevelled (dsh), which in turn inhibits shaggy (sgg). Inhibition of sgg prevents futsch phosphorylation and promotes futsch binding to microtubules and synapse growth.

1.4.5.3. OS, MAPK signalling, and *Drosophila* NMJ development

OS enhances *Drosophila* NMJ growth. This is evident through administering pharmacological agents in larval food to induce OS. Examples include Diethyl maleate (DEM), a compound that conjugates to glutathione tripeptides to inhibit the glutathione system, and the mitochondrial toxin Paraquat (Oswald et al., 2018; Ugbode et al., 2020). Genetic manipulation techniques to modulate ROS production and resolution also generate overgrown synapses. This has been achieved through mutations to the antioxidant genes *sod1*, *sod2*, and *spinster*, which encodes an endosomal protein needed for lysosome function (Milton et al., 2011). Similarly, ectopic expression of the NADPH oxidase Duox in motor neurons increases synapse growth (Oswald et al., 2018).

OS enhances *Drosophila* NMJ growth through redox-sensitive MAPK signalling (see Figure 1.9). This mechanism was originally discovered when dominant-negative isoforms of *Highwire* (*Hiw*), an E3 ubiquitin ligase, increased bouton counts (Wan et al., 2000). These mutants have unrestrained activity of Wallenda, a JNK Kinase Kinase (JNKKK) that activates JNK/AP-1 signalling (Collins et al., 2006). Ectopic neural expression of *fos* and *jun*, which constitute AP-1 heterodimers, increase bouton counts, whereas expression of dominant-negative isoforms decreases growth (Sanyal et al., 2003, 2002). Mutations to *Puckered* (*puc*), a phosphatase that mediates a JNK/AP-1 negative feedback loop, similarly increases bouton counts (Martin-Blanco et al., 1998; Ugbode et al., 2020).

Interestingly, differential JNK/AP-1 signalling appears to integrate synapse growth from different sources of OS. Neural expression of dominant-negative isoforms of Fos, but not Jun, rescues overgrowths induced by mutations to *Hiw* (Collins et al., 2006) and *spinster* (Milton et al., 2011). However, expression of both dominant negative Fos and Jun isoforms can rescue overgrowths induced by *sod1* mutations (Milton et al., 2011) and the administration of DEM in fly food (Ugbode et al., 2020). Collectively, these findings suggest that specific sources of OS differentially activate JNK/AP-1, whereby Jun/Jun homodimers or Jun/Fos heterodimers facilitate transcriptional changes and synapse growth.

Oswald et al. (2018) identified DJ-1β as being critical to facilitating ROS-induced changes to NMJ growth (see Figure 1.9). Mutating the *DJ-1β* gene, or expressing dominant negative isoforms, blocks OS-induced and neuronal activity-induced increases in NMJ growth. DJ-1β is oxidised by ROS to inhibit PTEN and increase PI3K signalling, causing enhanced bouton numbers via an unidentified downstream factor. This mechanism appears to have a direct impact on the plasticity of neural networks governing larval locomotion. Wild type larvae

adapt their crawling speed to chronic changes in temperature so that a constant speed is maintained. *DJ-1β* mutants do not exhibit this adaptation, suggesting that this gene gates OS-mediated changes to both neuron structure and network plasticity. Interestingly, *DJ-1β* mutations do not exhibit other ROS-induced changes to NMJs, such as numbers of active zone at the boutons. However, these changes are not modulated via PTEN/PI3K signalling.

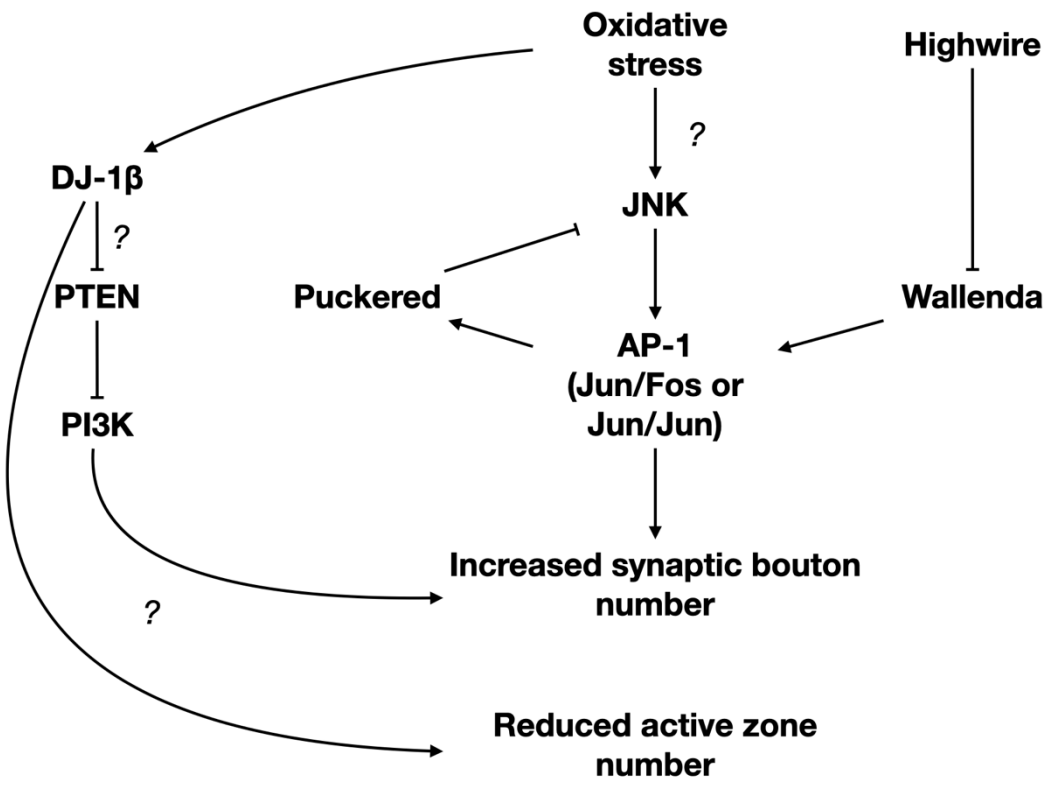

Figure 1.9. Redox-sensitive MAPK signalling regulates *Drosophila* NMJ growth.
Oxidative stress stimulates JNK/AP-1 signalling and synapse growth at the *Drosophila* NMJ, with different sources of ROS differentially recruiting AP-1 components. How different sources activate this pathway remains to be fully characterised. Puckered is an AP-1 target that represses AP-1 activity, forming a negative feedback loop. Wallenda is a JNKKK that stimulates AP-1. The E3 ubiquitin ligase Highwire targets Wallenda for degradation and, as such, mutations to Highwire stimulate AP-1 signalling. DJ-1β also enhances NMJ growth via PTEN/PI3K signalling. The mechanism of PTEN antagonism by DJ-1β and the downstream effectors of this pathway are yet to be elucidated.

1.4.6. The *Drosophila* visual system

The *Drosophila* visual system is well-characterised and frequently used in electrophysiological assays to screen for aberrant neuron function and synaptic transmission (Afsari et al., 2014; Vilinsky and Johnson, 2012). The morphology of *Drosophila* eyes is also used to observe neurodevelopmental defects, as small changes to the highly-ordered eye structure have profound effects on its appearance (Iyer et al., 2016).

The *Drosophila* visual system is composed of two compound eyes with approximately 800 functional units, called ommatidia, in each (reviewed by Ranganathan et al., 1995; Wang and Montell, 2007). Within each ommatidium are 8 rhabdomeric photoreceptors, denoted R1-8, and glia that provide structural and metabolic support. R1-R6 exhibit Rhodopsin (Rh) 1 (Rh1), a pigment that is most sensitive to blue wavelengths of light. In response to blue light activation, Rh1 changes conformation to activate the G-protein isoform Gq, which in turn activates phospholipase C (PLC). PLC catalyses the breakdown of phosphatidylinositol 4,5-biphosphate (PIP_2) to Inositol-1,4,5-triphosphate (IP_3) and diacyl glycerol. This leads to the opening of transient receptor potential (TRP) and TRP-like channels, with the subsequent sodium and calcium ion influx causing depolarisation of the neurons. These photoreceptors are histaminergic and project onto neurons in the lamina. Photoreceptor depolarisation causes synaptic histamine release and the hyperpolarisation of the postsynaptic lamina neurons. R7 photoreceptors exhibit UV-sensitive rhodopsins, whereas R8 photoreceptors exhibit blue or green-sensitive rhodopsins. Both R7 and R8 photoreceptors are also histaminergic, but project through the lamina targets in the medulla of the optic lobe of the *Drosophila* brain.

1.4.7. Circadian regulation in *Drosophila melanogaster*

Transcription-translation feedback loops (TTFLs) maintain circadian rhythms in all *Drosophila* cells, as well as all other organisms. In TTFLs there is rhythmic transcription of genes, whose protein products feedback to inhibit their own transcription (reviewed by Tataroglu and Emery, 2014). Briefly, the transcription factors CLOCK and CYCLE promote the transcription of the genes *period* (*per*) and *timeless* (*tim*), which are transcribed to form heterodimeric complexes that accumulate during night time. Phosphorylation of PER/TIM complexes by kinases promotes nuclear entry and the phosphorylation of CLOCK/CYCLE to inhibit their affinity for DNA and suppress transcription of *period* and *timeless*, completing a negative

feedback loop. During the day, the phosphorylated PER/TIM heterodimer is bound by E3 ubiquitin ligases for degradation. This transcriptional clock can be entrained to light stimuli by cryptochrome (CRY). CRY absorbs blue light to undergo a conformational change, allowing it to bind TIM to promote its ubiquitination and degradation. Photoreceptors in the *Drosophila* eye receive light information to entrain locomotor behaviour via pathways that are yet to be fully elucidated (Helfrich-Förster et al., 2001).

1.5. Project aims and objectives

As detailed in this chapter, there are multiple cellular sources of ROS, and a plethora of mechanisms that neutralise ROS and maintain redox homeostasis. The relative contribution of Srx to ROS homeostasis is unclear.

The work described in this thesis aimed to elucidate the role of Srx using *Drosophila melanogaster* and mammalian cell culture techniques. I hypothesised that Srx would significantly contribute to defence against OS in *Drosophila*, modulate neuron development, and impact physiological features that could be further validated using rat primary neuron cultures.

The specific aims of this study were:

- To generate *Drosophila Srx* null mutants and investigate the contribution of Srx to the maintenance of redox homeostasis in *Drosophila melanogaster*.
- To determine whether *Drosophila Srx* mutations impact behavioural and physiological traits that reflect perturbed neuron function *in vivo*.
- To investigate whether loss of Srx affects neuron morphology in both *Drosophila* and rat primary neuron cultures, which may underlie physiological abnormalities identified whilst addressing Aim 2.

2. Methods and materials

2.1. *In silico* techniques

2.1.1. *Sulfiredoxin-1* homologue search in the *Drosophila melanogaster* genome

When this research commenced, *Drosophila* Sulfiredoxin-1 was yet to be characterised by McGinnis et al. (2021). To probe the *Drosophila melanogaster* genome for a *Srx* homologue, a blastp search was conducted (NCBI, 2024). The AA sequence derived from human *Srx* (Uniprot code Q9BYN0) was used as the search term and results were limited to the *Drosophila melanogaster* taxid (no. 7227). The search parameters were adjusted to exclude sequences that were not derived from expressed sequence tags (ESTs) generated from cDNA libraries and were instead predicted from genomic sequences without verification of expression at the transcript level. Such sequences were annotated with the prefix XM, XR, or XP. All other standard parameters from the search tool were conserved. Identified orthologous sequences were used to probe for human Srx.

2.1.2. Identification of the putative *Sulfiredoxin-1* homologue in *Drosophila*

To identify the putative *Srx* homologues in *Drosophila*, a multiple sequence alignment was performed using the Clustal Omega multiple sequence alignment tool with default settings (Madeira et al., 2024). Included in this alignment were Srx protein derived from humans, mice (*Mus musculus*), rats (*Rattus norvegicus*), and the putative *Drosophila* Srx isoforms identified from the blastp search. The key residues critical for Srx function, identified by (Jeong et al., 2006), were manually identified and highlighted to detect conservation amongst the isoforms from all the species.

2.1.3. Mitochondrial localisation prediction

Sulfiredoxin-1 in mammals localises to mitochondria, which allows it to recycle and resolve Prdx3 (Noh et al., 2009). This function is likely to be conserved in valid *Drosophila* isoforms, so MitoFates software was used to detect the presence of N-terminal mitochondrial targeting motifs in the polypeptide structure (Fukasawa et al., 2015). This tool identifies sequences with hydrophobic and basic residues that facilitate the creation of amphipathic alpha helices and binding to Translocase of Outer Mitochondrial Membrane 20 (TOM20) for mitochondrial import. Additionally, helical wheel plots were generated using the online Netwheels application to demonstrate the amphipathicity of the N-terminal regions in the Srx isoforms detailed in Chapter 2.1.2 (Mól et al., 2018).

2.2. *Drosophila* techniques and husbandry

2.2.1. *Drosophila* stocks and handling

During this research, stocks were incubated at room temperature in polystyrene 25 cm^3 vials (Flystuff) or polyethylene bottles (Flystuff) containing 'stock food' composed of 10 g/l Agar, 39.12 g/l maize flour, 37 g/l yeast, 93.75 g/l sucrose, and 6.75 ml/l propionic acid. Flies were housed in vials/bottles that were plugged with cotton wool to prevent the escape of flies, whilst allowing the passage of air. They were transferred to fresh vials/bottles every 3-4 weeks.

Experimental flies were bred and housed in vials containing approximately 7 ml of 'instant food' comprised of instant *Drosophila* medium (Carolina Biological Supply Company) with added solution of 5% w/v inactivated yeast with 10% w/v Sucrose in dH_2O. To generate this solution, yeast was repeatedly boiled in dH_2O using a microwave to inactivate it. Sucrose was added and the solution was made up to the appropriate volume, then autoclaved. 20 g of medium was used per 100 ml of yeast-sucrose solution. Unless otherwise stated, all experimental flies were bred and reared on this food and kept in 25°C incubators with a 12-hour light-dark cycle.

Unless otherwise stated, all experimental flies used in this research were males. *Srx* mutant virgins were backcrossed to w^{1118} males to reduce the effect of background mutations in experimental flies. To observe and sort flies, of a particular sex or genotype, flies were

anaesthetised on perforated plates that supplied CO_2 from a compressed gas cylinder. Flies were sorted using a paintbrush, which was performed under a dissection microscope to observe the sex or morphological features of flies (Stemi 2000, Zeiss). A full list detailing the stocks used in this study can be observed in Table 2.1.

Table 2.1. *Drosophila* stocks used in this research.			
Stock	**Source**	**Genotype**	**Description**
Wild type stocks			
Canton S	O'Kane lab, Cambridge (UK)	+/+ ; +/+ ; +/+	Wild type with red eyes.
w^{1118} (*w-*)	Simon lab, Stanford	*w-*/*w-* ;;	Wild type with white eyes.
***Srx* mutant generation and transgenic stocks**			
P{EP}CG6762^{G1102}	Bloomington *Drosophila* Stock Centre	*P{EP}CG6762*^{G1102}/ *P{EP}CG6762*^{G1102} ;;	Stock containing a *P-Element* insertion into the *Srx* locus (*CG6762*), on the *Drosophila* X chromosome.
Srx$^{\Delta 1\text{-}2}$	Made as part of this study	*Srx*$^{\Delta 1\text{-}2}$/*Srx*$^{\Delta 1\text{-}2}$; +/+ ; +/+	Flies generated from the *P{EP}CG6762*^{G1102} stock with the first two exons of *Srx* excised via imprecise *P-Element* transposition. First two exons of *Srx* have been excised.
Srx$^{\Delta 3}$	Made as part of this study	*Srx*$^{\Delta 3}$/*Srx*$^{\Delta 3}$; +/+ ; +/+	Flies generated from the *P{EP}CG6762*^{G1102} stock with the third exon of *Srx* excised via imprecise *P-Element* transposition. Third exon of *Srx* has been excised.
UAS-Srx.FLAG	Made as part of this study	; *UAS-Srx.FLAG* / *UAS-Srx.FLAG* ;	Flies generated from the injection of *Drosophila* embryos with a pUAST plasmid that allows for Srx with a C-terminal FLAG tag to be expressed in a tissue-specific manner using the Gal4/UAS system.

Δ2-3 Transposase	Bloomington *Drosophila* Stock Centre	;; *P{Δ2-3}99B*/TM6B	Functional but non-excisable transposase enzyme that excises and transposes *P-Element* insertions.
Balancer Chromosomes			
FM7h/C(1)DX	Bloomington *Drosophila* Stock Centre	*FM7h/C(1)DX,y,f* ;;	X chromosome balancer stock with an attached-X chromosome, which is two X chromosomes attached at the centromere, so that they are always inherited together. This means virgins for *C(1)DX;;* can be bred with males containing an X chromosome of interest to form a stable stock.
CyO-GFP/Sco	Davis lab, San Francisco	*w-/w-* ; *CyO-GFP/Sco* ; +/+	Second chromosome balancer stock.
TM3/TM6b	O'Kane lab, Cambridge (UK)	*w-/w-* ; +/+ ; *TM3,Sb/TM6b,Tb,Hu*	Third chromosome balancer stock.
Gal4 stocks			
Act5C-Gal4	O'Kane lab, Cambridge (UK)	; *Act5C-Gal4/Cyo-GFP* ;	Promotes ubiquitous Gal4 expression using an *Act5C* promoter.

nSyb-Gal4	Goodwin lab, Oxford (UK)	*; nSyb-Gal4 / CyO-GFP ;*	Promotes pan-neuronal Gal4 expression using an *n-Syb* promoter.
OK6-Gal4	O'Kane lab, Cambridge (UK)	*; OK6-Gal4 / CyO-GFP ;*	Promotes Gal4 expression in *Drosophila* motor neurons using an *OK6* promoter. Also promotes Gal4 expression in the precursors of the adult fat body.
TH-Gal4	Birman lab, Marseille	*;; TH-Gal4 / TH-Gal4*	Promotes Gal4 expression in Dopaminergic neurons using a *TH* promoter.
MHC-Gal4	Goodman lab, Washington	*;; MHC-Gal4 / MHC-Gal4*	Promotes Gal4 expression in muscles using an *MHC* promoter.
Miscellaneous transgenes and mutants			
gstD1-GFP	(Sykiotis and Bohmann, 2008)	*; gstD1-GFP / CyO-GFP ;*	GFP reporter of glutathione S-transferase D1 expression levels (induced by Nrf2 signalling).
TRE-dsRed.T4	(Chatterjee and Bohmann, 2012)	*; TRE-dsRed.T4 / TRE-dsRed.T4;*	dsRed.T4 reporter of AP-1 signalling.
Jafrac1	(Bellen et al., 2004)	*P{SUPor-P}Prdx2^{KG05372}/P{SUPor-P}Prdx2^{KG05372} ;;*	Loss of function *Jafrac1* mutant (cytosolic 2-Cys Prdx) validated by DeGennaro et al. (2011).
EV	Bloomington (stock no. 36303)	*;; EV/EV*	Control line with an empty *P-Element* insertion

2.2.2. *Drosophila* crossing schemes

Flies were bred in crossing schemes to combine mutations, transgenes, and balancer chromosomes in a variety of experiments. Per 25 cm^3 vial, 6-8 virgin female flies were housed with 3-5 male flies. Offspring would eclose from pupae approximately 10 days later. Crosses were typically transferred to fresh vials every 1-3 days to prevent overcrowding amongst the larvae.

The use of virgin female flies in these crosses is essential because females can store sperm from previous male copulations. Virgin flies can be identified and retrieved for crosses via one of two methods. Firstly, they can be identified by morphological traits as they possess a swollen body, folded wings, and an abdominal spot called a meconium that is caused by faecal matter. Secondly, they can be retrieved by emptying vials/bottles of flies and collecting female flies for up to five hours afterwards. For the first 5 or so hours of their lives, male flies remain sterile and will not fertilise females during this period (Roote and Prokop, 2013).

For the experiments detailed in this report, the *Srx* mutant fly stocks were out-crossed to diminish the effects of background mutations that may have arisen. Virgin *Srx* mutant flies were bred with w^{1118} males to achieve this, with male offspring used as experimental flies. Control flies for the experiments were the white-eyed w^{1118} mutant males.

2.2.3. *Drosophila Srx* mutant generation

To investigate the biological relevance of Srx in *Drosophila*, *P-Element* transposition was used to generate *Srx* knockout mutants. This strategy was preferred to RNAi and CRISPR-Cas9 techniques to avoid off-target effects, whereby the short interfering RNA (siRNA) or single guide RNA (sgRNA) sequences bind to unintended targets (Guo et al., 2023; Sudbery et al., 2010). Knockout mutations also allow for rescue transgenes to be easily expressed in the background for rescue experiments. The creation of *Srx* mutants would also establish that *Srx* was not an essential gene in *Drosophila*.

Previous work has generated public collections of mutant strains that contain single *P-Element* (*PE)* insertions into the *Drosophila* genome (Bellen et al., 2011). *PE* insertions at a locus of interest may be mobilised to generate imprecise excision events with the removal of flanking DNA regions. Removal of regions that contain the CDS of a particular gene can

generate null mutant stocks (Figure 2.1.A). To generate *Drosophila Srx* mutants, *PE* insertions into the *Srx* locus (FlyBase gene annotation ID *CG6762*) were mobilised (Figure 2.1.B).

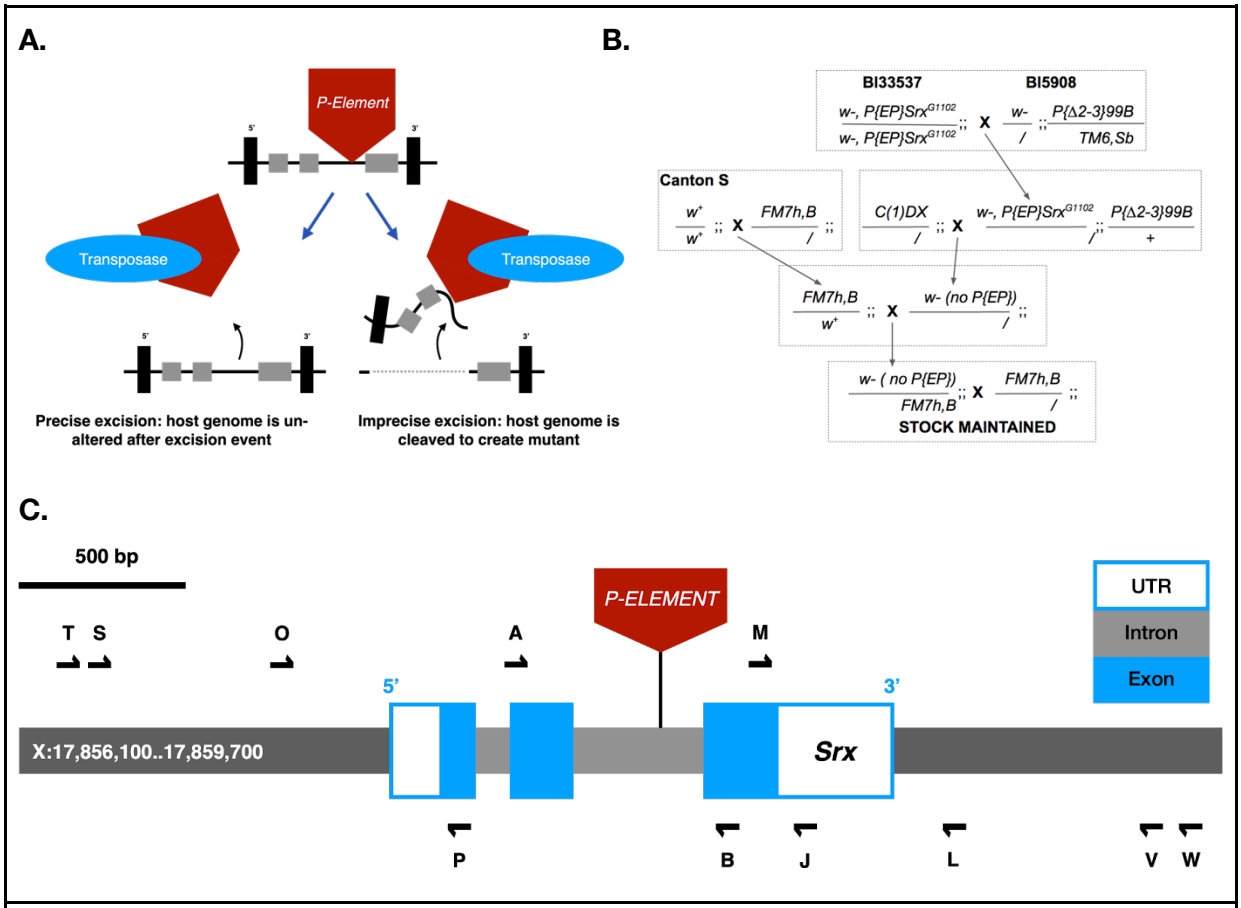

Figure 2.1. *P-Element* transposition to generate *Drosophila Srx* mutant stocks.
A. Graphical depiction of the precise and imprecise excision events that can result from *P-Element* transposition. **B.** The crossing scheme used to generate imprecise excisions of *Srx* and mutant stocks. **C.** Location of the primer annealing sites within the *Drosophila Srx* locus, which were used to screen for mutations and to characterise them. The *P-Element* insertion and the primers widths are not to scale.

Flies containing a *PE* insertion in the second intron of the *Srx* gene (*P{EP}Srx*^{G1102}) were crossed with flies containing a functional, but non-excisable transposase (*P{Δ2-3}99B*). This generated excision events in the sperm of the male offspring, which could be bred with females carrying attached-X balancer chromosomes. Male progeny from this cross were screened for the loss of eye pigment, which indicated transposition events and the removal of a mini-white gene construct (w^+) that was contained within the *PE*. Once these males were

isolated and bred with virgin flies carrying X chromosome balancers, balanced stocks were established, and the males could be retrieved for genomic DNA extraction (see Chapter 2.5.2). The extracted DNA was used as a template for PCR reactions to screen for mutant stocks with imprecise excision events (see Chapter 2.5.1). The PCR used combinations of primers targeting the *Srx* locus (Figure 2.1.C and Table 2.4). An absence of PCR product indicated that primer annealing sites had been excised, whereas truncated PCR product suggested that intervening DNA regions had been excised. Truncated PCR product could be further analysed using sanger sequencing techniques to accurately map the regions of the *Srx* locus that were removed (see Chapter 2.5.6).

2.2.4. *Drosophila UAS-Srx.FLAG* transgenic fly generation

For rescue experiments, whereby Srx could be expressed in specific tissues in the background of *Srx* mutant flies, *Drosophila* with a *UAS-Srx.FLAG* transgene were generated. This was achieved via the injection of *Drosophila* embryos with a construct containing the *Drosophila Srx* CDS derived from reverse transcription polymerase chain reaction (RT-PCR).

2.2.4.1. RNA extraction

To isolate RNA from *Drosophila*, 20 w^{1118} males were homogenised in 50 µl TRIzol reagent (Thermo Scientific,15596018) with a plastic pestle, before an additional 450 µl TRIzol reagent was added. Samples were incubated at room temperature for 5 minutes and then centrifuged for 15 minutes at 4°C and 13,000 RPM to remove insoluble debris. Supernatant was transferred to a new 1.5 ml tube and 100 µl of Chloroform was added. Tubes were shaken vigorously by hand and incubated at room temperature for 3 minutes. Samples were centrifuged at 13,000 RPM for 15 minutes at 4°C and the aqueous upper phase was transferred to a new 1.5 ml tube and 250 µl isopropanol was added. Samples were mixed by vortexing and incubated at -20°C for 2 hours. Afterwards, samples were centrifuged for 30 minutes at 4°C and 13,000 RPM to pellet the RNA. Supernatant was removed and the pellet was washed via the addition of 1 ml 75% ethanol with centrifugation for 5 minutes at 4°C and 13,000 RPM. This step was repeated, and supernatant was removed to air-dry the pellet for 10 minutes. The RNA was resuspended in 50 µl of Diethyl pyrocarbonate (DEPC)-treated water. For quantification, RNA was diluted in DEPC-treated water and quantified using an Ultrospec 2100 pro (Amersham Biosciences).

To destroy residual DNA that may remain in the samples, 10 µg of the RNA samples underwent DNase treatment with the DNase I RNase-free kit (Thermo Scientific, EN0521). RNA was added to 5 µl 10X DNase buffer, 2 µl DNAse, 1 µl RiboLock RNase inhibitor (Thermo Fisher, EO0381) then made up to 50 µl in DEPC-treated water and incubated at 37°C for 1 hour. To inactivate the DNase, 6 µl of 25 mM Ethylenediaminetetraacetic acid (EDTA) was added to the samples, which were then heated to 65°C for 10 minutes prior to storage at -70°C.

2.2.4.2. cDNA synthesis

Complementary DNA (cDNA) was generated from *Drosophila* RNA by adding 5 µg of RNA to a 20 µl mix containing 2.5 µM oligo$(dT)_{18}$ primer (Thermo Scientific, SO131) and 0.5 mM deoxyribonucleotide triphosphates (Thermo Scientific, R0192). This mixture was heated to 65°C for 5 minutes to destroy secondary structures, before being incubated on ice for 5 minutes. To synthesise cDNA, the SuperScript IV reverse transcriptase kit was used (Thermo Scientific, 18090050). Briefly, 1 µl 0.1 M DTT, 1 µl 40 U/µl RiboLock RNase inhibitor (Thermo Fisher, EO0381), 1 µl 200 U/µl Superscript IV reverse transcriptase and 4 µl of the associated 5X first strand buffer was added to this mix. Samples were Incubated at 50°C for 15 minutes, room temperature for 15 minutes, then 70°C for 15 minutes to inactivate the enzyme.

2.2.4.3. Generation of a *UAS-Srx.FLAG* construct

A *UAS-Srx.FLAG* transgene was made via the insertion of the *Drosophila* dSrx-RA coding sequence to pUAST plasmid (depicted in Figure 2.2). Primers were designed to amplify cDNA derived from dSrx-RA mRNA sequences. The forward primer targeted the 5' portion of the cDNA and was designed to attach a EcoRI endonuclease restriction site. The reverse primer targeted the 3' portion of the cDNA and was designed to attach a XhoI endonuclease restriction site and a FLAG tag. The resulting PCR product, as well as a pUAST vector, were digested with the aforementioned enzymes and ligated together (see Chapter 2.5.7-8). This plasmid was then amplified using molecular cloning techniques (see Chapter 2.5.9).

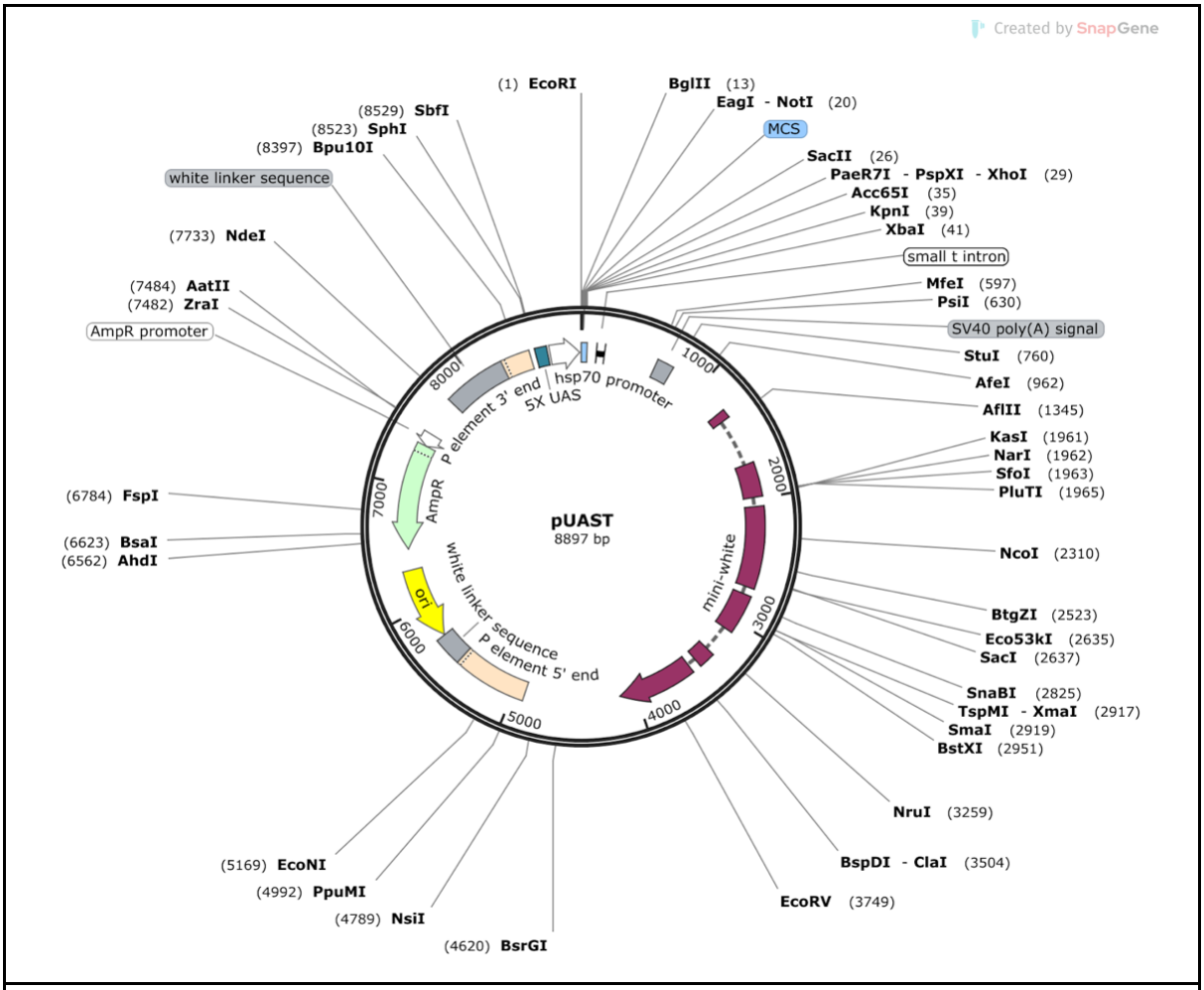

Figure 2.2. The pUAST plasmid map.

The *Drosophila Srx* CDS was amplified using PCR with primers that adhered a FLAG tag and EcoRI/XhoI digestion sites. A recombinant plasmid was generated by restriction digest of both the plasmid and PCR product with the aforementioned enzymes, followed by ligation and molecular cloning techniques. The resulting plasmid was inserted into the *Drosophila* genome via the ϕC31 integrase system to generate *UAS-Srx.FLAG* transgenic flies. The image of this plasmid was generated using Snapgene software (www.snapgene.com).

2.2.4.4. *Drosophila* embryo injection and stock formation

To generate the transgenic *Drosophila* stock, this study recruited the services of FlyORF *Drosophila* Injection service (FlyORF, Zurich). The assembled pUAST plasmid was prepared using a Qiagen HiSpeed Midiprep kit (see Chapter 2.5.9.3) and injected into *Drosophila* embryos. The pUAST plasmid contained attB sites for site-directed recombination with attP

sites in the *Drosophila* genome using the ϕC31 integrase system (see Chapter 1.4.3.2). The plasmid was injected into the embryos of stock 'P40' and flies were screened for insertion into the 2nd chromosome at cytological location 25C7. Flies were on a *yw* background so successful recombination events could be identified by the expression of the *mini-white* gene (w^{+mc}) encoded by the plasmid. The integrase was removed and successful lines were balanced prior to being returned.

2.3. Cell culture techniques

All cell culture techniques in this study were conducted using proper aseptic technique, performing experiments within tissue culture hoods. Unless otherwise stated, all cultures were maintained in a humidified CO_2 incubator at 37°C and 5% CO_2.

2.3.1. HEK293t cell cultures

Human embryonic kidney cells (HEK293t) cells were cultured in Dulbecco's modified Eagle Medium (DMEM) (Gibco, 41966029) containing 10% Fetal Bovine Serum (HyClone, SV30160.03) and 1% Penicillin-Streptomycin (Gibco, 15140122). Cells were maintained in T75 flasks (BioLite, Thermo, 130190) and passaged at a 1:5 ratio every 3-5 days after dissociating in 0.05% Trypsin-EDTA (Gibco, 15140122) in PBS.

2.3.2. Rat primary neuron cultures

Timed-mated female Wistar Rats (Charles River UK) were purchased from Charles River (UK). All procedures were conducted in accordance with the regulations detailed in the UK Animals (Scientific Procedures) Act, 1986. All appropriate project and personal licences (to the Chawla lab) were granted by the UK Home Office. Hippocampi were dissected from postnatal day 1 (P1) mixed sex rat pups. The animals were euthanised via pentobarbital injection, followed by cervical dislocation, according to Home Office guidelines.

Cultures were generated as previously described by Suman et al. (2016). Dissections were carried out in a solution comprised of Dissociation Media (81.8 mM Na_2SO_4, 30 mM K_2SO_4, 5.8 mM $MgCl_2$, 252 µM $CaCl_2$, 1 mM HEPES, 20 mM Glucose, Phenol Red 1000X) and Kynurenate-Magnesium Solution (9.98 mM $C_{10}H_7NO_3$, 100 mM $MgCl_2$, 200X Phenol Red, 5 mM HEPES, 1M NaOH added until Kynurenic acid dissolves). To form the working solution,

63 ml of Dissociation Media was added to 7 ml of Kynurenate-Magnesium Solution. Henceforth, this solution is referred to as DM/KY.

Dissected hippocampi/cortices were incubated in 3 ml Papain solution (DM/KY with 3.71 mM Cysteine, 1 U/µl Papain Latex, pH 7-7.4) at 37°C for 20 minutes, mixing every 5 minutes. The solution was removed and this incubation was repeated. Papain solution was then removed and the samples were washed in 2-3 ml of DM/KY 3 times. The solution was removed and 2 ml Trypsin Inhibitor (DM/KY with 0.1 g/ml Trypsin) was added and samples were incubated at 37°C for 5 minutes. This solution was removed and the process was repeated 2 times. Trypsin Inhibitor was removed and washed 3 times with warm Growth Medium (2% B27, 35 mm Glucose, 1 mm L-Glutamine, 5% Foetal Bovine Serum, 0.5% Penicillin-Streptomycin).

Samples were triturated, then the wash buffer removed and replaced with 2 ml fresh Growth Medium. This was gently triturated with a 5 ml pipette until cloudy. A pellet was allowed to form and the media was removed so as to not disturb the process. Fresh Growth Medium was added and the trituration process was repeated a further 2 times. Cells were diluted to the appropriate concentration and plated. For 35 mm dishes, 2 ml media was plated containing 0.4 hippocampi/ml.

After two hours cells would adhere to the surface of the culture vessel and media was aspirated and replaced with fresh Growth Medium. After 1 day *in vitro* (DIV), cultures were treated with cytosine arabinoside (AraC, 2.4 µM final concentration) to inhibit the proliferation of glial cells.

For the generation of protein lysates, cultures were performed in 6-well plates. For immunocytochemistry experiments, cultures were conducted in 35 mm dishes containing 4 13 mm glass coverslips that had been coated in Poly-D-Lysine to facilitate cell adherence. Coverslips were coated in 0.1 mg/ml Poly-D-Lysine solution overnight, rinsed in dH_2O, then allowed to dry prior to plating the cells.

2.3.3. *Drosophila* embryonic neuron cultures

Drosophila embryonic neuron cultures were conducted according to Voelzmann and Sanchez-Soriano (2022). Experimental fly stocks were kept on ‘stock food’ overnight at 25°C to lay embryos. The following day, embryos were dechlorinated with 50% bleach for 90 seconds and washed in a sieve with water. The embryos were collected with a paint brush and placed onto a 1% agar plate. Using a microscope, stage 11-12 embryos were identified

by their autofluorescence pattern in blue light and collected in groups of 30, detailed by Campos-Ortega and Hartenstein (1997).

The embryos were briefly washed in 70% ethanol solution in 1.5 ml tubes, which was then removed and replaced with supplemented Schneider's medium (20% heat-inactivated Foetal Bovine Serum, 2 µg/ml insulin, 0.1% (w/w) Penicillin-Streptomycin, pH 6.8-7). Schneider's medium was replaced with 100 µl Hank's Balanced Salt Solution (HBSS)-based dispersion media, comprised of 1% (w/w) Penicillin-Streptomycin, 0.25% (w/v) Dispase II (Sigma, D4693), and 0.05% (w/v) Collagenase type V (Worthington, LS004214). Embryos were ground using a pestle, then incubated at 37°C for 4 minutes. The dispersion reaction was terminated by the addition of 200 µl supplemented Scheider's medium and cells were pelleted by centrifugation at 3000 RPM for 4 minutes. The supernatant was discarded and the pellet was resuspended in 90 µl of supplemented Schneider's medium.

Glass bottom dishes, which were cleaned with acetone, were filled with 30 µl of medium containing the resuspended cells. Dishes were covered by concanavalin A (conA)-coated coverslips and sealed by a ring of petroleum jelly. The dishes were inverted to allow the cells to adhere to the conA-treated surface for 2 hours at 26°C, before being inverted for the neurons to develop as hanging drop cultures. The conA-coated coverslips were generated in advance by applying 150 µl of 20 µg/ml conA in dH_2O to square coverslips and incubating them at 37°C for 60-90 minutes. Coverslips were rinsed with dH_2O before being dried at 50°C overnight and stored at room temperature.

2.3.4. Transfection techniques

As part of this study, mammalian cells *in vitro* underwent cationic lipid-mediated transfection to transiently express transgenes. Full details of the plasmids used can be found in Table 2.5, which also denotes the antibacterial selection agents used for the molecular cloning techniques.

2.3.4.1. Transfection of HEK293t cells

Transient transfection of HEK293t cells was performed at least 24 hours after plating cells into a 6-well plate at a confluency of 50-70%, with identical confluences used for the same experiment. The medium of HEK293t cells was aspirated and replaced with fresh, serum-containing DMEM an hour prior to the transfection process. PolyJet transfection reagent

(SignaGen) was used to transfect these cells, with 6 µl made up to 50 µl in serum-free DMEM and added to 50 µl serum-free media containing 2 µg of plasmid DNA. This mixture was incubated at room temperature for 10-20 minutes and then added dropwise to wells. Cells were left in this transfection mixture for 9-12 hours, which was then aspirated and replaced with fresh, serum-containing DMEM. Transfected HEK293t cells were not used for experiments until 36-48 hours post-transfection to afford high levels of expression of the genes being transiently transfected. Typically, transfection rates of 70-80% could be observed.

2.3.4.2. Transfection of Rat primary neurons

Rat primary neurons were transfected in Transfection Medium composed of 90% CO_2-dependent Salt-Glucose-Glycine (114 mM NaCl, 26.1 mM $NaHCO_3$, 5.3 mM KCl, 1 mM $MgCl_2$, 2 mM $CaCl_2$, 10 mM HEPES, 1 mM Glycine, 0.5 mM Sodium Pyruvate, Phenol Red 0.001%), 10% Minimal Essential Medium (Gibco, 21090022), 1% Insulin/Transferrin/Selenium (Gibco, 41400045), 0.5% Penicillin-Streptomycin (Gibco, 15140122).

5 µl of Lipofectamine 2000 (Thermo, 11668019) was made up to 100 µl of Transfection Medium and added to 2 µg of plasmid made up to 100 µl of Transfection Media. This mixture was incubated at room temperature in the hood for 30 minutes, then made up to 1 ml with Transfection Medium and added to 35 mm dishes of cells. Cells were incubated for 4-6 hours, before the medium was aspirated and fresh Transfection Medium was added. These transfections were performed at 2-4 DIV and experiments were performed 3 days post-transfection.

2.3.5. Srx shRNA construct generation

To investigate the effect of reduced Srx expression, shRNA constructs were created to induce RNA interference (RNAi) of both the human and rat isoforms of the protein using the pSuper RNAi system (Oligoengine, VEC-PBS-0006). Constructs are designed to express shRNA molecules under the control of a polymerase-III H1-RNA promoter, with transcription terminated by a signal of 5 consecutive thymidine residues with 2 3’ overlapping Uracil residues. shRNA molecules are processed by Dicer and R2D2 proteins to short interfering RNAs (siRNAs). The siRNA antisense strands are recruited into RNA-induced silencer

complexes (RISC) with Argonaute proteins. The RISC complexes can then bind and degrade homologous mRNA sequences to inhibit translation (Iwasaki et al., 2010).

Plasmids were generated according to the manufacturer's instructions. Briefly, inserts to the pSuper.neo+GFP backbone (Figure 2.3.A) were generated by designing complementary oligos containing a 19 nt sequence to the target mRNA in both the sense and antisense direction (see Figure 2.3.B). Target sequences for each plasmid are shown in Table 2.2. A control plasmid was also synthesised with a non-targeting shRNA (Keenan et al., 2017). The oligos (see Table 2.4) were annealed by resuspending 3 µg of each primer in 50 µl of annealing buffer (100 mM NaCl, 50 mM HEPES pH 7.4) and heating to 90°C for 4 minutes. The mixture was gradually cooled in a stepwise fashion through 10-minute incubations at 80°C, 70°C, 60°C, 50°C, and 37°C. Annealing these oligos generated overhangs that afforded ligation into the pSuper.neo+GFP plasmid digested with BglII and HindIII restriction endonucleases (see Chapter 2.5.7-8). Plasmids could then be amplified using molecular cloning techniques (see Chapter 2.5.9). Colony screening was performed using primers that spanned the insertion site in the pSuper.neo+GFP plasmid to identify the successful recombinant plasmids (see Table 2.4).

Table 2.2. Amino acid sequences targeted as part of shRNA construct design.

Plasmid name	**Target**	**Target sequence (sense strand)**
shRNA control	N/A	GCGCGATAGCGCTAATAAT
H1	Human Srx	GACTACTTCTACTCCTTTG
H2	Human Srx	GGAGCATCCACACCAGACT
H3	Human Srx	AGCATCCACACCAGACTTG
R1	Rat Srx	GCCAAGGAAGCAATATGGG
R2	Rat Srx	GCGGTGACTACTACTACTC
R3	Rat Srx	GACCATTCCTGCCAAGCTC

A.

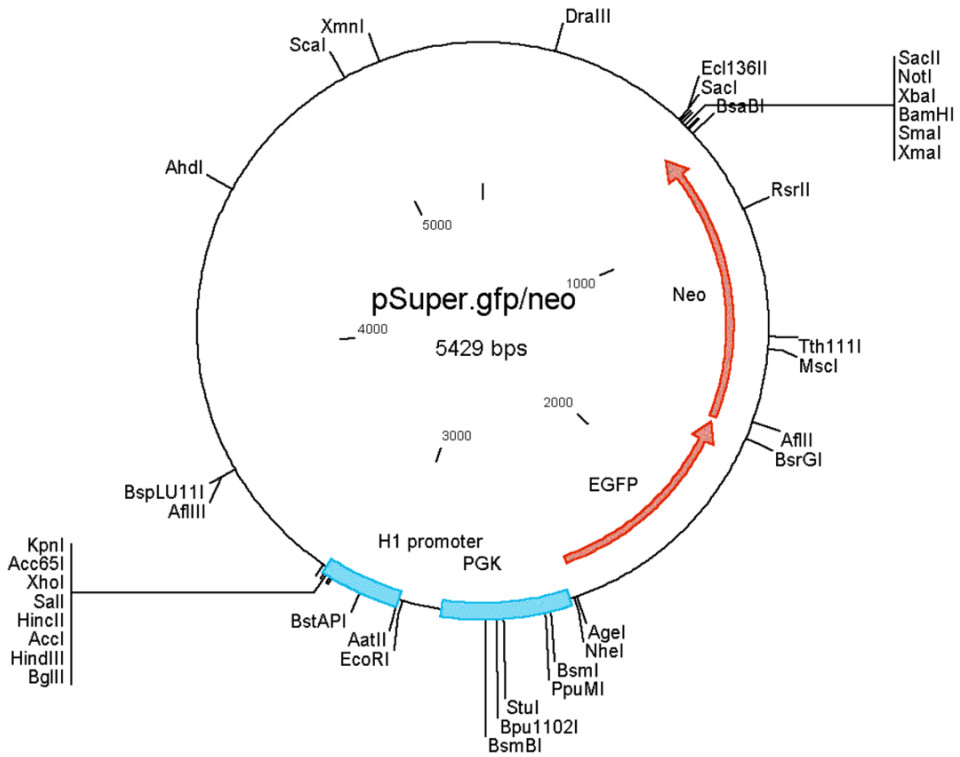

B.

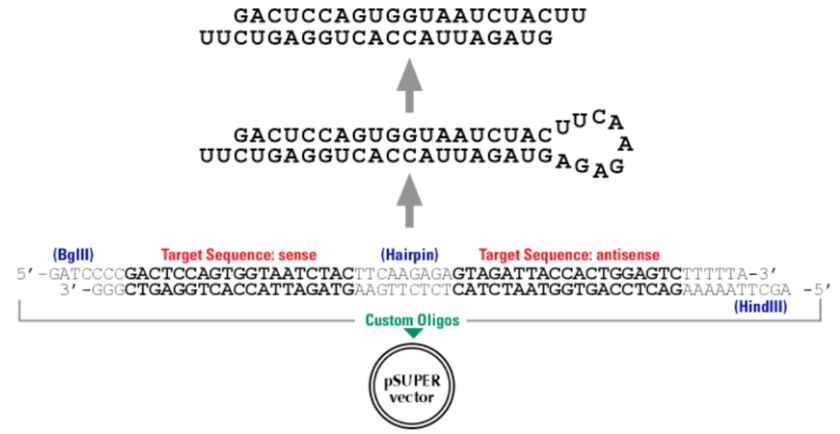

Figure 2.3. The pSuper system expresses shRNAs to induce RNAi.

A. The pSuper.neo+GFP plasmid map. **B.** pSuper construct assembly. Inserts to the pSuper.neo+GFP plasmid backbone were generated by annealing complementary oligos. The resulting DNA fragment exhibited 3' and 5' overhangs to enable ligation into a pSuper.neo+GFP plasmid digested using BglII and HindIII. The resulting plasmid encoded a hairpin molecule, which is further processed to an siRNA duplex. Antisense strands of the duplex hybridise to human/rat Srx mRNA to mediate cleavage and repress translation.

Validation of these plasmids was achieved by co-transfecting HEK293t cells with the shRNA constructs and constructs encoding Myc-tagged human Srx (Origene, RC207654) or rat Srx (Origene, RR209543). High transfection rates can be achieved using this cell line, which are readily observable as the pSuper plasmids encode GFP. Protein lysates were generated, and the relative amounts of Myc-tagged protein were observed using western blots (see Chapter 2.6.3). Successful shRNA constructs repressed the Myc-tagged protein expression.

2.4. Immunohistochemistry and microscopy techniques

Unless otherwise stated, the imaging experiments in this thesis were conducted in a blinded fashion to ensure objectivity. This was achieved using the 'Blind Analysis Tools' plugin (Jaiswal and Lorenz, 2019). Antibodies used the following assays are presented at the end of Chapter 2.4 in Table 2.3.

2.4.1. *Drosophila* NMJ dissection fixation, staining, and imaging

The morphological characteristics of neurons at the *Drosophila* neuromuscular junction (NMJ) are controlled by redox-sensitive signalling pathways (Milton et al., 2011; Ugbode et al., 2020). Therefore, this can be used as a physiological marker of OS. We sought to find out whether *Srx* mutants had altered neuron morphology at the NMJ.

Third instar wandering larvae, which had climbed out of the food and up the vial, were collected. Male larvae of the correct genotype were selected and transferred to a Sylgard dish (Silicone elastromere kit, Dow Corning). Dissections were performed in PBS, with minuten pins (Austerlitz Insect Pins 0.1 mm diameter, Fine Science Tools) applied to the posterior and anterior ends of the larvae to immobilise them. Scissors were used to cut the larvae along their antero-lateral axis, then the guts (amongst other internal organs) were removed using forceps and the muscle walls pinned back using minuten pins.

The larvae were fixed for 7 minutes in PBS with 4% (w/v) Formaldehyde, then transferred to a 2 ml tube with PBT (PBS with 0.05% Triton X-100). Larvae were washed in PBT 3 times, before 1 ml fresh PBT was added containing primary antibodies at the desired concentration. Samples were incubated overnight at 4°C, whilst left on a rotary shaker. The next day,

samples were washed in PBT 3 times for 10 minutes, before 1 ml PBT was added with secondary antibodies at the relevant concentration. Samples were left to incubate at room temperature for 2 hours on a nutator before being washed in PBT 3 times for 10 minutes. PBT was removed and 1 ml of 70 % Glycerol in PBS was added. Larvae were left in this solution for at least 30 minutes (until they sank) and then mounted onto microscopy slides of 0.8-1.0 mm (Fisher) with the muscle wall facing away from the slide. A suitable amount of Fluoromount (Thermo) was applied to samples and coverslips were placed onto the preparations and sealed with nail vanish. The concentrations of antibodies used is detailed in Table 2.3. Anti-HRP-Cy3 was used to visualise neurons, which binds to neuronal membranes in *Drosophila* and acts as a specific neuronal marker (Jan and Jan, 1982). Anti-Syn1 was used to label boutons.

A Carl Zeiss LSM880 confocal AiryScan microscope was used to take z-stack images of the neuron located at muscle 6/7 at abdominal hemisegment A3. The 40X oil-immersion lens was used. The same pixel resolution and distance between z-stack planes was used for all images. For larger neurons, image tiling and stitching was required. In the central plane of the z-stack image, a 3X3 tiling image with 10% overlap was created for muscle 6/7 in this muscle segment, for the purpose of normalising bouton counts to the muscle surface area (MSA). Z-stacks images were assembled in Fiji and the bouton counts were recorded using the 'Cell Counter' analysis feature (Schindelin et al., 2012). The surface area of the muscles was also recorded by drawing lines across the length and width of the muscle (Figure 2.4). Bouton counts were normalised to the muscle surface area (MSA). This was done by dividing the surface area of the muscle by the control group average, then multiplying by the bouton count number. Sample sizes were based on those used in previous published work, with at least 10 NMJs analysed per group (see Sweeney and Davis, 2002).

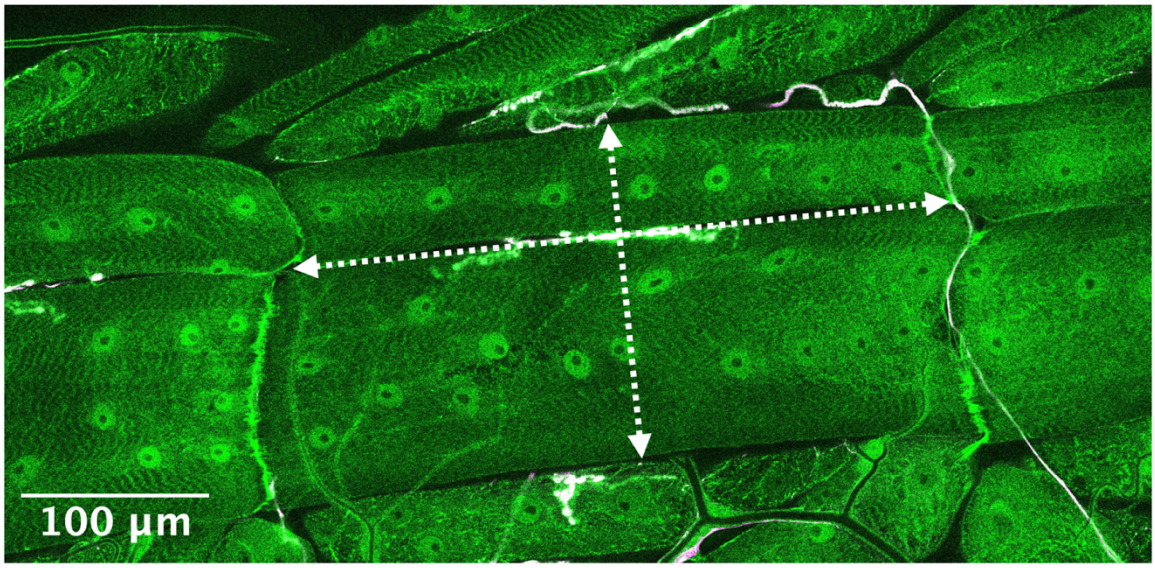

Figure 2.4. Quantification of *Drosophila* third instar larvae MSA.
The length and the width of muscles were measured to calculate MSA for the normalisation of bouton numbers at the NMJ.

2.4.2. Rat primary neuron fixation, staining, and imaging

Cells in 32 mm dishes were washed in PBS before being fixed in 1 ml of PBS with 3% (w/v) Paraformaldehyde (PFA), 4% (w/v) Sucrose for 20 minutes. Cells were washed twice in PBS and permeabilised in PBS with 0.5% (w/w) NP-40 for 5 minutes and washed in PBS again. Primary antibodies were made up to the desired concentration in PBS and 50-70 µl droplets were applied to a sheet of Parafilm. Individual coverslips were removed from the 35 mm dishes, inverted and placed onto these droplets and incubated overnight at 4°C in a humidified chamber.

The next day, cover slips were retrieved and washed twice with PBS. Secondary antibodies were made up to the appropriate concentration in PBS and applied to the coverslips for an hour. These steps were either achieved by placing the inverted coverslips onto PBS droplets, as was done for the primary antibody incubation, or by un-inverting them and placing them into a 12-well plate to apply 500 µl PBS. Afterwards, two washes in PBS were performed, followed by a 5-minute incubation in PBS with Hoechst 33342, trihydrochloride trihydrate (Molecular Probes, 10 µg/ml). Two washes in PBS were performed and coverslips were mounted in Fluoromount Aqueous Mounting Medium (Sigma, F4680). In the experiments

detailed in this study, neurons transfected with GFP-encoding shRNA constructs were imaged using anti-GFP.

A Carl Zeiss LSM880 confocal AiryScan microscope was used to take images of the fixed and stained neurons. The 20X air lens was used with the same pixel resolution and pinhole size for experiments. The Images were analysed in Fiji, with neurite tracings performed using the plugin package (Meijering et al., 2004; Schindelin et al., 2012). This enabled neurite lengths to be quantified, or for sholl analysis to be performed using the Neuroanatomy plugin to quantify neurite growth and branching (Ferreira et al., 2014). The 63X oil-immersion lens was used to image DsRed-labelled mitochondria within primary neurites within a 150 µm radius of the soma. Z-stack images were converted to 2D images using maximum intensity projections. The same pixel resolution and distance between z-stack planes was used for all images. Images were individually thresholded, and analysed using the 'mitochondrial analyzer' plugin (Chaudhry et al., 2020). Sample sizes for these imaging experiments were based on those used in previous published work (see West et al., 2018). For each group, approximately 50 neurons were imaged and analysed from 3 independent cultures.

2.4.3. *Drosophila* embryonic neuron fixation, staining, and imaging

Drosophila embryonic neuron cultures were fixed at 1 DIV. Cells were fixed by applying 200 µl droplets of PBS with 4% (w/v) PFA and 0.02% (w/w) Glutaraldehyde to the coverslip surface and incubating them at room temperature for 30 minutes. Afterwards, cells were permeabilised via the application of 200 µl PBT (PBS with 0.3% Triton X-100) for 20 minutes. Cells were washed with 200 µl of PBS 3 times and then 200 µl of PBS with primary antibodies at the relevant concentration were applied. Cells were incubated overnight at 4°C in a humidified chamber. The next day, cells were washed in PBS twice and then PBS with secondary antibodies at the relevant concentration were applied for two hours. Cells were washed in PBS twice and then mounted in ProLong Gold Antifade Reagent with DAPI (Invitrogen, P36931). Cells were imaged using an inverted fluorescence LED microscope (Leice, DM IL) with a 100X oil immersion lens and associated USB microscope camera (Leica, DFC3000G). Images were analysed in Fiji, with neurites traced and quantified using the NeuronJ plugin (Meijering et al., 2004; Schindelin et al., 2012). Neurons were stained with anti-HRP-Cy3. For each group, approximately 30 neurons were imaged and analysed from multiple independent cultures.

Table 2.3. Antibodies used for immunohistological and immunocytochemical experiments in this research.

Antibody	Type	Experiment	Source	Host	Concentration
Anti- GFP	Primary (monoclonal)	Rat primary neuron cultures	Life Technologies, RRID: AB_221568, Ref: A11120	Mouse	1:500
Anti- Ms-Alexa 488	Secondary	Rat primary neuron cultures	Invitrogen, RRID: AB_2534088, Ref: A11029	Goat	1:500
Anti- HRP (Cy3 conjugated)	Primary (polyclonal)	*Drosophila* NMJs and embryonic neuron cultures	Jackson ImmunoResearch labs, RRID: AB_2338959	Goat	1:200
Anti- Syn1	Primary (polyclonal)	*Drosophila* NMJs	Sweeney lab, York (West et al., 2015), RRID: AB_2713991	Rabbit	1:1000
Anti- Rb-Alexa 488	Secondary	*Drosophila* NMJs	Jackson ImmunoResearch labs, RRID: AB_2338046, Ref: 111-545-003	Goat	1:200
Anti- GP-FITC	Secondary	*Drosophila* NMJs	Jackson ImmunoResearch labs, RRID: AB_2337415	Goat	1:200
Anti-Srx	Primary (polyclonal)	*Drosophila* NMJs	Made in this project (Final bleed, SCK018)	Guinea Pig	A range tested
Anti-Srx	Primary (polyclonal)	*Drosophila* NMJs	Made in this project (Final bleed, SCK017)	Guinea Pig	A range tested
Anti-FLAG M2	Primary (monoclonal)	*Drosophila* NMJs	Sigma, F3165	Mouse	A range tested
Anti-FLAG	Primary (polyclonal)	Rat primary neuron cultures *Drosophila* NMJs	Cell Signalling, RRID: AB_2217020	Rabbit	1:200 for primary neuron cultures

2.5. Molecular Biology

2.5.1. PCR and agarose gel electrophoresis

To conduct Polymerase Chain Reaction (PCR) for the amplification of DNA, optimal primer design is required. This research adhered to the general principles of primer design for effective amplification (reviewed by Álvarez-Fernández, 2013). Primers were designed using NCBI's Primer-BLAST tool (Ye et al., 2012) and melting temperatures (Tm) for the specific PCR conditions were estimated using the New England Biolabs Tm calculator ("NEB Tm Calculator," 2024). Primers were synthesised by Sigma Aldrich (UK).

PCR reactions conducted for the purpose of validating DNA ligations and *P-Element* imprecise excision events were performed as 20 µl reactions containing 2X taq polymerase mastermix (Thermo Fisher, K0171), 250 nM of both forward and reverse primers, plus <500 ng of template DNA. Samples were initially exposed to 95°C for 2 minutes to denature DNA and activate the polymerase. This was followed by iterative cycles of exposure to 95°C for 30 seconds to denature DNA, the appropriate DNA reannealing temperature for 30 seconds, and then 72°C for elongation of PCR product. This elongation time was adjusted according to the size of the desired product, with each minute facilitating the creation of DNA up to 1 kb. After 30-35 cycles, a final extension period of 10 minutes at 72°C was performed and samples were cooled to 4°C to prevent decomposition.

PCR reactions conducted for molecular cloning purposes were performed using Phusion High Fidelity Polymerase (NEB, M0530S). Reactions were assembled in a 20 µl volume containing 0.2 µl Phusion DNA polymerase, 4 µl 5X Phusion HF buffer, 500 nM forward and reverse primers, plus 0.6 µl DMSO and <500 ng of template DNA. Samples were initially exposed to 98°C for 30 seconds to denature DNA and activate the polymerase. This was followed by iterative cycles of exposure to 98°C for 10 seconds for DNA denaturation, the appropriate annealing temperature for 30 seconds for DNA reannealing, and then 72°C for elongation of PCR product. This elongation time was adjusted according to the size of the desired product, with 30 seconds facilitating the creation of DNA up to 1 kb. After 30-35 cycles, a final extension period of 10 minutes at 72°C was performed and samples were cooled to 4°C to prevent decomposition.

PCR product was analysed using gel electrophoresis. The appropriate volume of 6X TriTrack loading dye (Thermo Fisher, R1161) was added to samples before loading into the well of a 1.5% (w/v) agarose gel in Tris Acetate-EDTA (TAE) buffer (Sigma, T4038) with 0.01% (v/v) SYBR safe (Invitrogen, S33102) to visualise DNA bands. Gels were submerged in TAE buffer prior to the loading of wells with samples, which were run alongside GeneRuler 1 kb DNA ladder (Thermo Fisher, SM0311) or HyperLadder 1kb (Bioline, 33025) to determine PCR product size. Gels were typically run at 70-90 V for 30-60 minutes. Gels were imaged using a blue-light box or a Bio-Rad Gel Doc EZ gel imaging system.

Table 2.4. Primer sequences used in this research project and their associated melting-point temperatures (Tm).			
Primer	**Sequence (5'->3')**	**Tm (°C)**	**Experiment**
A	ATGGACACCACCGTTCACTC	60	*Drosophila Srx* mutagenesis detection (chapter 2.2.3)
B	ATCCACAGCAGGTCGATGGG	63	*Drosophila Srx* mutagenesis detection (chapter 2.2.3)
J	TCCAGCGATCACGACATTCT	59	*Drosophila Srx* mutagenesis detection (chapter 2.2.3)
L	TGAGGTGATGAGATGGTCGC	60	*Drosophila Srx* mutagenesis detection (chapter 2.2.3)
M	TGGCCTGATCTTTGTCGCTG	61	*Drosophila Srx* mutagenesis detection (chapter 2.2.3)
O	ATAGGGCGATGGGAATTGGG	60	*Drosophila Srx* mutagenesis detection (chapter 2.2.3)
P	CTCGTCGCTCGCAAGAAATG	59	*Drosophila Srx* mutagenesis detection (chapter 2.2.3)

S	ATGCCGATTACTGACGCACA	59	*Drosophila Srx* mutagenesis detection (chapter 2.2.3)
T	TTACCCGGAATCGGTTGCTT	59	*Drosophila Srx* mutagenesis detection (chapter 2.2.3)
V	CAGGACCAATACGACTGCGA	60	*Drosophila Srx* mutagenesis detection (chapter 2.2.3)
W	CTGCGCTACACCATACAGGT	60	*Drosophila Srx* mutagenesis detection (chapter 2.2.3)
Drosophila Srx CDS FWRD (plus EcoRI digest site)	GCGGAATTCATGGAGTTCATTAGCCATTTC	66	*Drosophila UAS-Srx.FLAG* transgene generation (chapter 2.2.4)
Drosophila Srx CDS RVRS (plus FLAG-tag and XhoI digest site)	GCGCTCGAGCTACTTGTCGTCATCGTCTTT-GTAGTCGGCCAGGTACTTGGGC	81	*Drosophila UAS-Srx.FLAG* transgene generation (chapter 2.2.4)
pUAST sequencing primer	AGCGCAGCTGAACAAGCTA	N/A	Sequencing primer to validate plasmid synthesis for the *UAS-Srx.FLAG* transgene generation (chapter 2.2.4)
pSuper shRNA control FWRD	GATCCCCGCGCGATAGCGCTAATAATTTCA-AGAGAATTATTAGCGCTATCGCGCTTTTTA	N/A	Control shRNA construct generation for Srx knockdown experiments (see Chapter 2.3.5)

pSuper shRNA control RVRS	AGCTTAAAAAGCGCGATAGCGCTAATAATT-CTCTTGAAATTATTAGCGCTATCGCGCGGG	N/A	Control shRNA construct generation for Srx knockdown experiments (see Chapter 2.3.5)
pSuper shRNA human Srx FWRD (H1)	GATCCCCGACTACTTCTACTCCTTTGTTCA-AGAGACAAAGGAGTAGAAGTAGTCTTTTTA	N/A	shRNA construct generation for human Srx knockdown (see Chapter 2.3.5)
pSuper shRNA human Srx RVRS (H1)	AGCTTAAAAAGACTACTTCTACTCCTTTGT-CTCTTGAACAAAGGAGTAGAAGTAGTCGGG	N/A	shRNA construct generation for human Srx knockdown (see Chapter 2.3.5)
pSuper shRNA human Srx FWRD (H2)	GATCCCCGGAGCATCCACACCAGACTTTCA-AGAGAAGTCTGGTGTGGATGCTCCTTTTTA	N/A	shRNA construct generation for human Srx knockdown (see Chapter 2.3.5)
pSuper shRNA human Srx RVRS (H2)	AGCTTAAAAAGGAGCATCCACACCAGACTT-CTCTTGAAAGTCTGGTGTGGATGCTCCGGG	N/A	shRNA construct generation for human Srx knockdown (see Chapter 2.3.5)
pSuper shRNA human Srx FWRD (H3)	GATCCCCAGCATCCACACCAGACTTGTTCA-AGAGACAAGTCTGGTGTGGATGCTTTTTTA	N/A	shRNA construct generation for human Srx knockdown (see Chapter 2.3.5)
pSuper shRNA human Srx RVRS (H3)	AGCTTAAAAAAGCATCCACACCAGACTTGT-CTCTTGAACAAGTCTGGTGTGGATGCTGGG	N/A	shRNA construct generation for human Srx knockdown (see Chapter 2.3.5)
pSuper shRNA rat Srx FWRD (R1)	GATCCCCGCCAAGGAAGCAATATGGGTTCA-AGAGACCCATATTGCTTCCTTGGCTTTTTA	N/A	shRNA construct generation for human Srx knockdown (see Chapter 2.3.5)

pSuper shRNA rat Srx RVRS (R1)	AGCTTAAAAAGCCAAGGAAGCAATATGGGT-CTCTTGAACCCATATTGCTTCCTTGGCGGG	N/A	shRNA construct generation for human Srx knockdown (see Chapter 2.3.5)
pSuper shRNA rat Srx FWRD (R2)	GATCCCCGCGGTGACTACTACTACTCTTCA-AGAGAGAGTAGTAGTAGTCACCGCTTTTTA	N/A	shRNA construct generation for human Srx knockdown (see Chapter 2.3.5)
pSuper shRNA rat Srx RVRS (R2)	AGCTTAAAAAGCGGTGACTACTACTACTCT-CTCTTGAAGAGTAGTAGTAGTCACCGCGGG	N/A	shRNA construct generation for human Srx knockdown (see Chapter 2.3.5)
pSuper shRNA rat Srx FWRD (R3)	GATCCCCGACCATTCCTGCCAAGCTCTTCA-AGAGAGAGCTTGGCAGGAATGGTCTTTTTA	N/A	shRNA construct generation for human Srx knockdown (see Chapter 2.3.5)
pSuper shRNA rat Srx RVRS (R3)	AGCTTAAAAAGACCATTCCTGCCAAGCTCT-CTCTTGAAGAGCTTGGCAGGAATGGTCGGG	N/A	shRNA construct generation for human Srx knockdown (see Chapter 2.3.5)
pSuper colony screening FWRD	AGGAAGATGGCTGTGAGGGA	60	Positive clone identification for Srx shRNA constructs (see Chapter 2.3.5)
pSuper colony screening RVRS	ACTTTATGCTTCCGGCTCGT	59	Positive clone identification for Srx shRNA constructs (see Chapter 2.3.5)
H1 sequencing primer	TCGCTATGTGTTCTGGGAAA	N/A	Sequencing primer to validate Srx shRNA construct generation (see Chapter 2.3.5)

2.5.2. Genomic DNA extraction from *Drosophila*

To extract genomic DNA from *Drosophila*, a single fly was collected in a 1.5 ml tube and homogenised in 50 µl lysis buffer (10 mM Tris pH 8.2, 1 mM EDTA, 25 mM NaCl, 200 µg/ml proteinase K) using a pipette tip. After a 45-minute incubation at 37°C, samples were placed at 95°C to inactivate the proteinase K. These samples could then be frozen at -20°C for storage. For PCR experiments using *Drosophila* genomic DNA as a template, 1-2 µl of this solution was used.

2.5.3. Gel extraction of DNA

DNA bands within gels were visualised using a blue-light box and excised using a scalpel. These bands were placed into a 2 ml tube and silica membrane-based extraction of DNA was performed using the QIAquick gel extraction kit (Qiagen, 28704) protocol. Briefly, 1 volume of gel was dissolved in 3 volumes of buffer QG at 50°C, then 1 volume of isopropanol was added. This mixture was transferred to a QIAquick spin column and centrifuged to facilitate DNA binding to the column. The column was washed with 750 µl buffer PE (with ethanol added) to remove salts and eluted into a fresh 1.5 ml tube using 20-50 µl buffer EB at 50°C or nuclease-free water.

2.5.4. Nucleic acid quantification

To calculate the DNA or RNA concentration of samples, either a NanoDrop (Thermo Scientific, ND-1000) or a Ultrospec 2100 *pro* (Amersham Biosciences) was used.

2.5.5. DNA precipitation

To increase the concentration of DNA samples, ethanol precipitation was performed and DNA was resuspended in a smaller quantity of solution. This was achieved by adding 0.1 volumes of 3 M Sodium Acetate pH 5.2 to 1 volume of DNA sample, followed by two volumes of ethanol. This mixture was incubated at -20°C for 1-2 hours and then centrifuged at 13,000 RPM at 4°C for 30 minutes. The resulting pellets of DNA were washed with 70% ethanol in ddH_2O twice before being allowed to air-dry for 10 minutes and re-suspended in the appropriate amount of nuclease-free water or relevant buffer.

2.5.6. DNA Sequencing

DNA samples were sequenced using the LightRun sequencing service (eurofins genomics). Sanger sequencing was performed on pre-assembled 1.5 ml tubes containing a 10 µl sample with 400-500 ng plasmid DNA, or 100-400 ng PCR product, and 2.5 µM of the sequencing primer.

2.5.7. Restriction endonuclease digestion

As part of this study, recombinant plasmids were generated via the insertion of specific DNA fragments into vector backbones at multiple cloning sites. To achieve this, plasmids and insert sequences were digested with restriction endonucleases to generate 'sticky ends' that can be ligated (see Chapter 2.5.8). The digests could either be performed simultaneously, known as double digestion, or sequentially.

Prior to the creation of *UAS-Srx.FLAG* transgenic flies, the coding sequence for *Drosophila* Srx (Srx-PA) was inserted into a pUAST plasmid. *Drosophila Srx* was amplified from cDNA using primers designed to adhere EcoRI and XhoI restriction sites, as well as a nucleotide sequence encoding a FLAG tag. Double digestion of the PCR product and pUAST vector was achieved using EcoRI-HF (New England Biolabs, R3101) and XhoI (New England Biolabs, R0146) in either rCutSmart (New England Biolabs B6004S) or r2.1 (New England Biolabs, B6002S) buffer according to the manufacturer's instructions.

For the shRNA construct, pSuper.neo+GFP plasmids were double digested with BglII (Thermo Scientific, ER0081) and HindIII (Thermo Scientific, ER0501) in buffer R (Thermo Scientific, BR5) according to the manufacturer's instructions. Alternatively, sequential digest of BglII in buffer R and HindIII in buffer O (Thermo Scientific, BO5) was performed. After ligation into pSuper.neo+GFP plasmids and prior to transformations, 5 µl from ligation reactions were digested using BglII in buffer O to reduce the occurrence of unwanted cloned, as this site is destroyed upon ligation and such treatment will reduce the number of unwanted unsuccessful transformants.

2.5.8. DNA ligation

Sticky-end DNA ligation was performed using T4 Ligase (New England Biolab, M0202S). The reaction was assembled as a 20 µl mix containing 2 µl 10X T4 DNA Ligase buffer and 1 µl T4 ligase. The appropriate insert:vector molar ratios were calculated using NEBioCalculator ("NEBioCalculator," 2024). Ligation reactions were typically left at room temperature for at least 10 minutes. The enzyme was inactivated by incubation at 65°C for 10 minutes and 1-5 µl of this reaction could be used in bacterial transformation experiments. In some instances, 10 µl reactions were performed by adjusting the proportions of the reagents by a factor of 2.

2.5.9. Molecular cloning techniques

2.5.9.1. Bacterial transformation and culture

Molecular cloning experiments were performed to generate a pUAST plasmid containing a *UAS-Srx.FLAG* sequence for the creation of transgenic *Drosophila*. All bacterial cultures in this research were performed using DH5α e coli bacteria. Heat shock transformation of cells was performed after 50 µl of bacteria (BL21 DH5α) was incubated with 1-5 µl of plasmid for 30 minutes. Heat shock at 42°C for 45 seconds was performed and samples were incubated on ice for 5 minutes. 500 µl of Luria-Bertani (LB) medium (1% (w/v) Tryptone, 0.5% (w/v) Yeast extract, 1% (w/v) NaCl) was added and the samples were incubated at in a shaker-incubator at 37°C with a rotation speed of 210 RPM. Samples were then centrifuged at 5000 RCF to pellet the bacteria, which were resuspended in 50-150 µl LB and spread onto prewarmed LB Agar plates (LB plus 1.5 % (w/v) Agar) with the relevant antibacterial agent for selection, which are presented in Table 2.5. Working concentrations for Ampicillin were 50 µg/ml, whereas working concentrations for Kanamycin were 30 µg/ml. Plates were incubated in an inverted fashion at 37°C overnight to allow colonies to grow.

Table 2.5. Plasmids used in this study.			
Plasmid	**Source**	**Bacterial resistance**	**Experiment**
pSuper.neo+GFP	Evans lab, University of York	Ampicillin	Srx shRNA production for use in in mammalian cells *in vitro*
Mito-DSred	Chawla lab, University of York	Kanamycin	Mitochondrial labelling in mammalian cells *in vitro*
Human Srx-Myc-DDK	Origene (Cat no. RC207654)	Kanamycin	Expression of human Srx in mammalian cells *in vitro*
Rat Srx-Myc-DDK	Origene (Cat no. RR209543)	Kanamycin	Expression of rat Srx in mammalian cells *in vitro*
pUAST	Sweeney lab, University of York	Ampicillin	Generation of a *UAS-Srx.FLAG* transgene

The next day, individual colonies were picked and grown in 10-12 ml of LB with the relevant antibacterial agent (at the same concentration used for the LB-Agar plates). Cultures were grown overnight in a shaker-incubator at 37°C with a rotation speed of 210 RPM. Glycerol stocks could be made for individual cultures by mixing 500 µl of the LB culture with 500 µl 50% (v/v) Glycerol solution and storage at -70°C. Cultures underwent centrifugation at 5000 RPM for 10 minutes at 4°C and the subsequent pellets were frozen at -20°C. Pellets could be stored in this manner until plasmid extraction was performed (see Chapter 2.5.9.3).

2.5.9.3. Plasmid extraction

LB cultures of 10-12 ml were developed for the purification of up to 20 µg of plasmid DNA using the QIAprep Spin Miniprep Kit (Qiagen, 27104). Plasmid DNA was purified in this manner for the generation of all the recombinant plasmids synthesised in this study. Greater yields of up to 200 µg of plasmid DNA could be produced using the QIAGEN HiSpeed Midi Kit (Qiagen, 12643), which was performed to generate the plasmid used for *Drosophila* embryo injection (see Chapter 2.2.4.4) as well as to generate larger quantities of plasmids used for *in vitro* experiments. Smaller cultures of 10 µl were used to inoculate a larger 100 ml culture.

2.6. Biochemical assays

2.6.1. *Drosophila* Srx antibody generation

Polyclonal antibodies were generated via the immunisation of Guinea Pigs using HIS-MBP-tagged *Drosophila* Srx protein (Srx-PA). The CDS of *Drosophila Srx* was used to generate a soluble HIS-MBP-tagged Srx protein by the Technology Facility Protein Production Lab (Biology, University of York), which were used to inoculate 2 Guinea Pigs over a three-month immunisation scheme (Eurogentec, Belgium). Each animal received 4 injections of 30 µg of protein in up to 250 µl PBS.

2.6.2. BCA assay

Protein concentrations were routinely calculated throughout this research using the BCA assay (Thermo Fisher, Cat No. 23225). The BCA assay was performed to ensure that equal protein levels were loaded into wells during western blot experiments, as well as to normalise the results of fluorescence or absorbance assays using tissue homogenates. A 2X series dilution of 2-0.0625 µg/µl BSA (Thermo) in the relevant lysis buffer/solution was used as a reference standard curve. 10 µl of protein/standard solutions were added to 200 µl of the BCA reagent in a clear 96-well plate (BioLite, Thermo). Duplicates were run for samples and standards. The 96-well plate was placed into a 37°C incubator for 30-45 minutes, then allowed to cool at room temperature for 10 minutes. Absorbance at 562 nm was recorded for each well using a Multiskan GO Microplate Reader (Thermo). A custom-built R script was used to quantify the protein levels, which generated a linear model using the standard curve absorbances. The average absorbances for samples were plugged into the resulting model to estimate protein concentration.

2.6.3. Western blotting

Western blots samples were prepared from *Drosophila* heads. Flies were collected in 1.5 ml tubes and snap-frozen on dry ice. To dissociate the heads, a falcon tube could be filled with 2-3 of these tubes and several pieces of dry ice, then vortexed at high speeds for at least a minute. To collect the heads using a paintbrush, the contents of the tubes could be emptied onto a petri dish covered in filter paper, which was kept on dry ice. For individual samples, 30-60 heads were ground on dry ice using a pestle, with similar numbers used for separate

experiments. Radioimmunoprecipitation assay (RIPA) buffer (10 mM Tris, 30 mM NaCl, 0.2% v/v Triton X-100, 0.1% w/v Sodium Deoxycholate, 0.02% w/v Sodium dodecyl sulphate, 0.2 mM EDTA, 0.2 mM Sodium Orthovanadate, pH 8) was added to the heads at a range of 1-2 µl per head. RIPA was supplemented with 0.5% v/v Phenylmethylsulfonyl fluoride (PMSF) and 1% v/v protease inhibitor (Sigma, P8340) to prevent protein degradation in samples. The BCA assay was used to adjust the concentration of *Drosophila* samples to 2 µg/µl.

Samples were incubated on ice for 30 minutes and centrifuged at 13,000 RPM and 4°C for 20 minutes to remove insoluble debris. The supernatant was added to 2X Sodium dodecyl sulphate (SDS) loading buffer (30% (v/v) Glycerol, 4% (w/v) SDS, 160 mM Tris-HCl pH 6.8, 0.1% (w/v) Bromophenol blue) and heated to 70-80°C for 10 minutes to denature proteins. DTT was omitted from the 2X SDS loading buffer to avoid oxidation of disulphide bonds that may be of interest to this research. Pre-cast gels (NuPAGE, 4–12% Bis-Tris Gels, Thermo) were loaded with 20 µl to ensure that each sample had 20 µg of protein loaded. Samples were run in MOPS buffer (20X Bolt, Invitrogen) at 150 V for 1-1.25 hours. A protein ladder (Thermo Fisher, PageRuler Plus Prestained) was used to track migration during the electrophoresis and observe the approximate molecular weight of proteins during imaging in kilodaltons (kDa).

Wet transfer to PVDF membranes was performed in transfer buffer (25 mM Tris, 192 mM Glycine 20% Methanol, plus 500 µl 10% SDS per litre) at 30 V overnight at 4°C or at 70 V for 4 hours. Blots were blocked in 5% (w/v) skimmed milk powder in TBS-T for 2 hours at room temperature under gentle agitation. This was followed by overnight incubation in the primary antibody-containing solutions of 5% (w/v) milk in TBS-T at 4°C under gentle agitation. Aliquots of the primary antibody were frozen and reused up to 5 times. Blots underwent 10-minute washes in TBS-T 3 times, before secondary HRP-conjugated antibodies in 5% (w/v) milk in TBS-T were applied and incubated under gentle agitation for 2 hours at room temperature. After 3X 10-minute washes in TBS-T, approximately 1 ml of chemiluminescent HRP substrate (Immobilon, Millipore) was added and chemiluminescence was recorded using an IBright (Thermo). The concentrations of the primary and secondary antibodies used are detailed in Table 2.6.

For HEK293t and rat primary neurons, protein lysates were generated using cells derived from the individual wells of a 6-well plate at 80-90% confluency. Media was aspirated from the cells, which were washed in 2 ml PBS. 200 µl of RIPA buffer was added to each well and cell scrapers used to help harvest the cells and collect them in 1.5 ml tubes. Protein

concentration was not calculated using the BCA assay due to low levels of variation amongst samples, but lysates were then processed in an identical process to those from *Drosophila*.

Table 2.6. Antibodies used for Western Blot experiments in this research.					
Antibody	**Type**	**Target species/size**	**Source**	**Host**	**Concentration**
Anti- Beta Actin	Primary (monoclonal)	*Drosophila*/~42 kDa	Proteintech (60008, RRID:AB_2289225)	Mouse	1:5000- 1:100,000
Anti- GAPDH	Primary (monoclonal)	Rat/~38 kDa	Millipore (MAB374)	Mouse	1:15,000-1:50,000
Anti- c-Myc (9E10)	Primary (monoclonal)	N/A	DSHB (RRID:AB_2266850)	Mouse	1:1000
Anti- Srx	Primary (polyclonal)	*Drosophila*	Made in this project (Final bleed, SCK018)	Guinea Pig	1:600
Anti- Srx	Primary (polyclonal)	Human/Rat	Proteintech (14273-1-AP)	Rabbit	1:1000
Anti- DJ-1β	Primary (polyclonal)	*Drosophila*	Sweeney lab, York	Guinea Pig	1:3000
Anti- Mouse IgG, HRP-linked	Secondary	N/A	Cell Signalling (7076, RRID:AB_330924)	Horse	1:5000
Anti- Rabbit IgG, HRP-linked	Secondary	N/A	Cell Signalling (3678, RRID:AB_1549606)	Mouse	1:5000
Anti- Guinea Pig IgG, HRP-linked	Secondary	N/A	Sigma (A5545)	Rabbit	1:5000

2.6.4. Amplex Red assay

To see if manipulating *Srx* expression affected levels of ROS in *Srx* mutant flies, the Amplex Red assay was performed to quantify H_2O_2 levels in tissue homogenates. This is a relatively easy and cost-effective method to address whether Srx affects H_2O_2 levels in *Drosophila* tissue. Horseradish Peroxidase (HRP) in the presence of H_2O_2 converts Amplex red reagent to the fluorescent pigment Resorufin, to indirectly quantify ROS levels in biological samples. Cohorts of 10 3-4 day old flies were homogenised in 1.5 ml tubes in 500 µl of HL3 solution (128 mM NaCl, 2 mM KCl, 1.8 mM $CaCl_2.2H_2O$, 4 mM $MgCl_2.6H_2O$, 5 mM HEPES, 35.5 mM Sucrose at pH7.2) containing 0.5 µl HRP at 100 u/ml (Thermo Scientific, 31490) and 2.5 µl of Amplex Red at 10 mM (Invitrogen, A12222) in DMSO per ml. The samples were incubated for 1 hour in the dark. Afterwards, they were spun down for 1 minute on a table-top centrifuge, and additional debris was removed from the supernatant via centrifugation through Spin-X columns (Corning 8160). 100 µl duplicates from each sample were aliquoted into a clear 96 well plate (Thermo Scientific, 130188) and absorbance at 560 nm was recorded using a Multiskan GO Microplate Reader (Thermo). Once the absorbances were recorded, 10 µl from each sample duplicate were retrieved and protein concentration was calculated using the BCA assay to normalise absorbance readings (AU) to protein levels.

For experiments using HEK293t cells, cells were split into 6-well plates to generate confluencies of approximately 50%. The dishes had been coated in poly-D-lysine prior to plating. After 24 hours the cells in each well were transfected with either shRNA control plasmids or shRNA-encoding plasmids targeting human Srx. 48 hours post-transfection, cells were carefully washed and incubated in 1.5 ml of HBSS supplemented with 1 mM Sodium Pyruvate, D-4500 mg/ml D-Glucose, 1 mM L-glutamine, 1.5 µl HRP at 100 u/ml (Thermo Scientific, 31490) and 7.5 µl of Amplex Red at 10 mM (Invitrogen, A12222) in DMSO per ml. After 1 hour, 500 µl of medium was retrieved from each well, spun through Spin-X columns (Corning 8160), and 100 µl duplicates from each sample were aliquoted into a clear 96 well plate (Thermo Scientific, 130188). Absorbance at 560 nm was recorded using a Multiskan GO Microplate Reader (Thermo). Alongside the samples, a standard curve was generated using the modified HBSS solution supplemented with H_2O_2. A 2X dilution series from 100 µM - 3.125 µM H_2O_2 generated a standard curve to ascertain the H_2O_2 concentrations in the samples.

2.6.5. Nrf2 and AP-1 signalling assays

To determine whether *Drosophila Srx* mutant flies exhibited increased Nrf2 signalling, this research used a transgene that expressed GFP under the control of a glutathione S-transferase D1 (*gstD1*) promoter sequence (Sykiotis and Bohmann, 2008). Nrf2 signalling is enhanced under conditions of oxidative stress and binds to antioxidant response element (ARE) sequences within the promoter regions of genes like *gstD1*. Quantification of green fluorescence in tissue homogenates derived from flies with this transgene can be used to observe activation of this pathway and the redox state in cells. Similarly, to determine whether *Drosophila Srx* mutant flies exhibited increased Nrf2 signalling, this research used a transgene that expressed DsRed.T4 under the control of a *TRE* promoter sequence.

Cohorts of 10 flies, which carried this transgene in a heterozygous fashion, were homogenised in 150 µl of lysis buffer in a 1.5 ml tube. This buffer consisted of 150 mM NaCl, 20 mM Tris-HCl, pH 8.0, 2 mM EDTA with 100X protease inhibitor added (Sigma, F4680). Samples were left on ice for 30 minutes, before being centrifuged at 13000 g for 30 minutes at 4°C. 120 µl of the supernatant was transferred to a new vial and the centrifugation step was repeated. 100 µl of this supernatant was then added to 300 µl ice-cold PBS and mixed. 2 aliquots of 100 µl were pipetted into a black 96-well plate (Costar) and fluorescence was measured using a CLARIOstar Plus Microplate Reader (BMG Labtech). A matrix scan of 3X3 was used for each well with a scan width of 6 mm. For the Nrf2 signalling assays, GFP fluorescence was measured using an excitation/emission range of 470-15/515-20 nm was used, along with a gain of 1970 and adjustment for a focal height of 5.6 mm. For AP-1 signalling assays, DSRed.T4 fluorescence was measured using an excitation/emission range of 570-20/630-40 nm, along with a gain of 2462 and adjustment for a focal height of 6.2 mm. Expression of both fluorophores was normalised to protein content in the sample, measured using the BCA assay.

These experiments were conducted using 3-7 day old flies that were either reared under standard conditions, or placed onto food made using sucrose-yeast solution supplemented with 10 mM DEM. This treatment was performed 72 hours prior to the experiment to see if OS elicited differences between the genotypes. Three groups of 10 flies for each genotype and condition were used.

2.7. *Drosophila* physiological assays

2.7.1. H_2O_2 survival assays

Cohorts of 20 flies aged 0-1 days were collected and housed in vials containing 2-3 ml of 1% (w/v) Agar and a 1.5 cm^2 piece of thick filter paper soaked in 5% (w/v) Sucrose, 5% H_2O_2 (w/v) solution in dH_2O. This setup ensured that the filter paper did not dry out. The survival of the flies was recorded twice a day, and flies were transferred to new tubes with fresh H_2O_2-supplemented sucrose solution every day. At least 8 vials were established for each genotype.

2.7.2. Climbing assay

The effect of a loss of Srx function on the locomotor activity of flies was determined by performing the climbing assay. Freshly-eclosed male offspring were collected and aged for 4-7 days prior to experiments. The assay was performed using cohorts of 20 flies at ZT3.5-6.5 to avoid differences being induced by the circadian rhythms of the flies.

Cohorts were placed into a 100 ml measuring cylinder, which had a line drawn onto it 10 cm from the bottom. A light source was positioned above this apparatus and flies were allowed to adjust for at least one minute, before being knocked to the bottom of the cylinder by tapping it 10 times against the work surface. The process was recorded using a Samsung Galaxy A21S in FHD mode and videos were analysed manually. The number of flies to climb to or past the 10 cm mark after 5 seconds was recorded and expressed as a percentage of the total flies tested. Each cohort was tested three times and the average number of flies to reach 10 cm, referred to as the 'success rate,' was recorded and compared amongst experimental groups.

2.7.3. Larval crawling assay

Third instar larvae were placed onto the centre of a 150x25mm plate filled with 50 ml of 1% Agar solution. The plate was inserted into a box that was illuminated so that a light intensity of 20 lux was recorded on a photometer (Fisher Scientific, 11784196). Larvae were briefly washed in dH_2O, placed onto the plate and allowed to adjust for 15 seconds. The larvae were recorded for 1 minute on a mobile phone (Samsung Galaxy A21s). Videos were recorded at

Full HD, before being converted to 720p and from an alternating frame rate to a constant frame rate of 5 frames per second (Handbrake). The videos were then converted to an AVI format and limited to 300 frames, representative of the 1-minute recording time (FFMPEG). The resulting videos were processed in Fiji using a median filter, with all files having the colour threshold adjusted to the same degree. The Mtrack2 plug-in was used to trace the path of crawling larvae and the number of millimetres moved per second was calculated.

2.7.4. Steady-state visually evoked potentials

To assess the functioning of neurons in the *Drosophila* visual system, steady-state visually evoked potential (SSVEP) assays were performed. These measure the response of different components of the visual system to flickering light stimuli (Figure 2.5). Seven-day old males were used for the control group and outcrossed mutants. Flies were immobilised in shortened 200 µl micropipette tips and secured in position using nail vanish. Reference electrodes were placed against the mouthpiece and recording electrodes were placed against one of the compound eyes. These electrodes were filled with simple *Drosophila* Saline solution (128 mM NaCl, 4.70 mM KCl, 1.82 mM $CaCl_2.2H_2O$). Initially, electroretinograms (ERGs) were performed to check that the electrodes were suitably positioned, as evidenced by the production of a typical trace with an on- and off-transients (Vilinsky and Johnson, 2012). Experiments were performed at ZT5.5-8.5.

SSVEPs were performed as previously described by (Afsari et al., 2014). Flies are presented with light stimuli produced by blue light-emitting diodes (LEDs). This stimulus was the sum of 2 square waves that had frequencies of 12 and 15 Hertz that flickered about the mean illumination. The intensity was controlled by a sequence generator encoded in MATLAB. Some parts of this sequence contained only the 12 Hertz stimulus 'probe,' whereas in other parts this was accompanied by a 15 Hertz 'mask.' The amplitude of each component was determined randomly. This generated response traces that underwent Fast Fourier transform analysis, which produced peaks at the input frequency (1F1) and twice the input frequency (2F1), as well as intermodulation terms (1F1+1F2, 1F2-1F1 and 2F1+2F2). Manipulating the expression of genes crucial to the *Drosophila* visual system has demonstrated that the harmonics, 1F1 and 2F1, correspond to the activity of photoreceptors in the compound eye and second order neurons in the lamina of the optic lobe of the brain, respectively. 2F1+2F2 intermodulation terms correspond to medulla neuron activity (Afsari et al., 2014). The 1F2 and 2F1 amplitudes of the flies were compared via one-way ANOVAs.

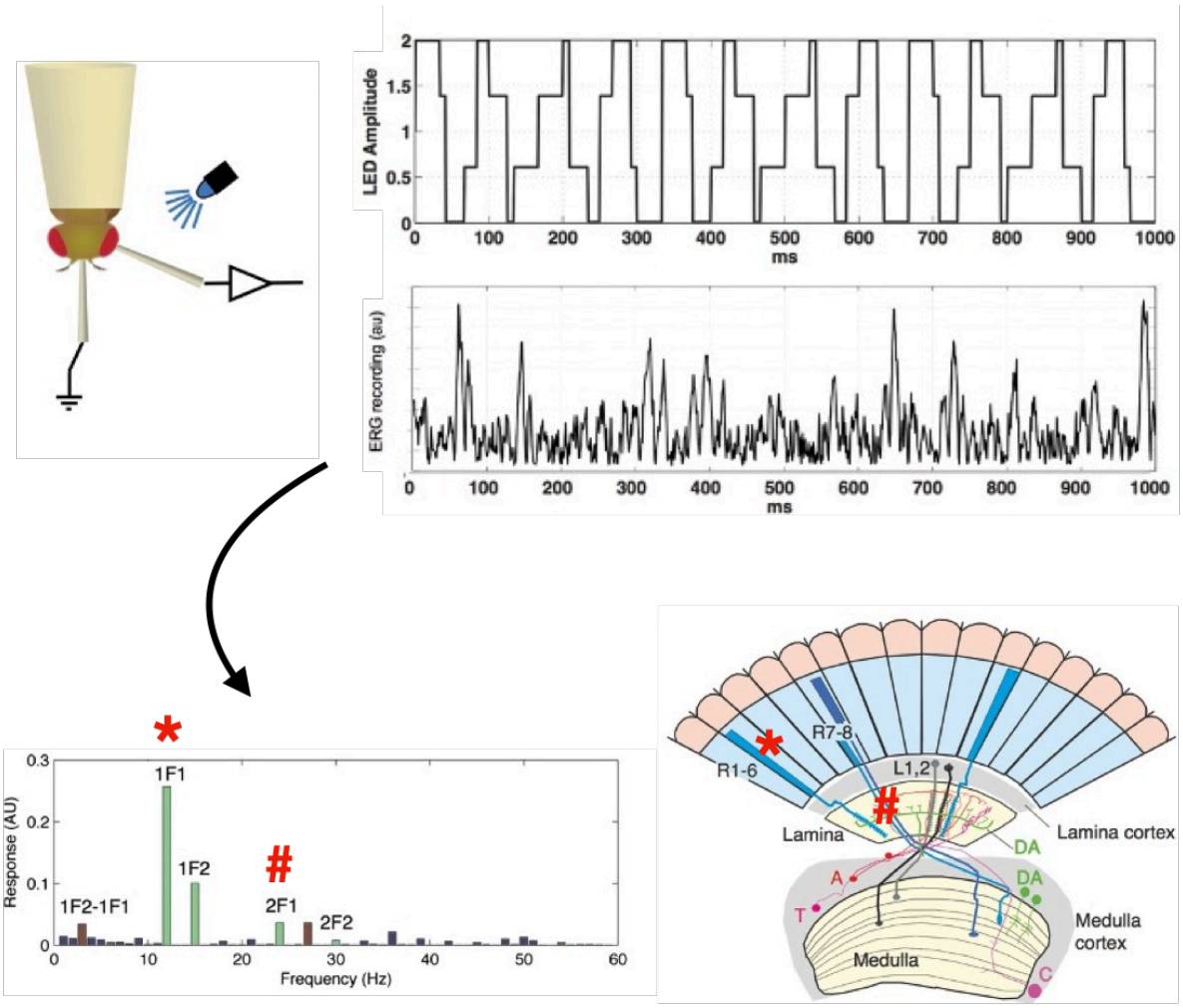

Figure 2.5. Recording and analysing *Drosophila* visual responses with SSVEPs.

Drosophila are immobilised in a shortened pipette tip using nail varnish. Reference electrodes are placed against the mouthpiece of flies, whereas recording electrodes are placed against the compound eye. Harmonic light stimuli, generated by blue LEDs, are presented to the flies and the response traces are recorded. Fast-fourier transform (FFT) breaks down response traces into specific components that reflect the activity of specific neuron populations within the *Drosophila* visual system as determined by using genetic tools to silence the activity of specific neuron types (Afsari et al., 2014). The amplitude of 1F1 peaks corresponds to the activity of first-order photoreceptors in the *Drosophila* compound eyes (*), whereas 2F1 peaks correspond to the activity of second-order neurons within the lamina of the optic lobe (#). This figure is adapted from (Afsari et al., 2014).

2.7.5. Circadian rhythms

The DAM2 *Drosophila* activity monitor system (Trikinetics Inc. Massachusetts) was used to record locomotor activity in 1 minute bins. Age-matched males were collected and loaded into activity tubes containing 1% w/v Agar 5% sucrose at one end. Flies were entrained to 12h:12h light:dark (LD) cycles for 4 days and activity was monitored for a further 7 days in constant darkness (DD). Activity records were analysed and actograms were produced using ShinyR-DAM web-based analysis software (Cichewicz and Hirsh, 2018). A chi-sq period testing range of 18-30 hours and a chi-sq period testing resolution of up to 0.2 hours was used. The period strength was calculated using Qp.act/Qp.sig ratios.

2.8. Statistical analysis

All statistical analysis and data presentation was performed using R 4.2.2 (R Core Team, 2022). This included the use of the following packages: RColorBrewer (Neuwirth, 2014), ggpubr (Kassambara, 2023), ggplot2 (Wickham, 2016), dplyr (Wickham et al., 2023), car (Fox and Weisberg, 2019), agricolae (de Mendiburu, 2023), tidyverse (Wickham et al., 2019), survival (Therneau, 2023), survminer (Kassambara et al., 2021), and plotrix (Lemon, 2006). Where possible, sample sizes for each experiment were based on those used in previous published studies.

Experiments with one measurement variable and one nominal variable, in which the nominal variable only had two values, were primarily analysed using a two-sample t-test. The two-sample t-test was conducted under the assumption that data from the two groups exhibited a normal distribution and a homogeneity of variances. The former was checked using the Shapiro-Wilk test, whereas the latter was checked using Bartlett's test. If both groups did not exhibit normal distributions, homogeneity of variance was re-tested using Levene's test, which is less sensitive to departures from normality. Experiments with equal variance, but non-normal distributions were instead analysed via the Wilcoxon test. Experiments with normal distributions, but unequal variance were analysed via the Welch two-sample t-test. Experiments with neither normal distributions, nor equal variance, were analysed via the Kolmogorov-Smirnov test.

Experiments with one measurement variable and one nominal variable, in which the nominal variable had more than two values, were primarily analysed using a one-way ANOVA. The one-way ANOVA test was conducted under the assumption that the groups exhibited normal distributions and a homogeneity of variances using the previously described tests. Post-hoc Tukey's HSD test comparisons or Dunnett's test could be used to identify groups that were significantly different from one another. Experiments with equal variance, but non-normal distributions were analysed via the Kruskal-Wallis test followed by Dunn's post-hoc test.

Experiments with one measurement variable and two nominal variables were analysed using a two-way ANOVA, permitted the groups exhibited normal distributions and a homogeneity of variances. Post-hoc comparison between the groups was conducted with Tukey's HSD test. The Scheirer-Ray-Hare test was used as a non-parametric alternative to the two-way ANOVA.

Pearson's Chi-square test was used for categorical data (see Chapter 5.2.5) to determine whether data was significantly different from the expected results. Log-rank analysis was used to compare survival amongst fly populations for longevity assays (see Chapter 3.2.6).

3. Identification and mutagenesis of the *Drosophila Sulfiredoxin-1* locus: implications for redox homeostasis

This chapter describes work that examines the utility of *Drosophila* to understand the function of Srx from the cellular to the organismal level. I first used *in silico* approaches, whereby the *Drosophila Srx* gene was identified and compared to mammalian orthologues to see if the key amino acids to Srx function were conserved. *Drosophila Srx* was also analysed using *in silico* tools to identify whether mitochondrial targeting motifs were conserved. I then developed genetic tools to manipulate expression of Srx in *Drosophila* so that its biological function may be investigated. To this end, I generated *Drosophila Srx* mutants, the creation of which provides evidence for the notion that *Srx* is not an essential gene in *Drosophila*. I also generated transgenic stocks to express Srx using the *Gal4/UAS* binary expression system. The newly generated *Drosophila Srx* mutants were screened for changes to redox homeostasis and tolerance to OS to characterise its relevance as an antioxidant enzyme.

3.1. Introduction

Several lines of evidence, reviewed in the introduction, indicate that Srx-mediated ROS homeostasis is important for neuronal viability (Lan et al., 2021; Ugbode et al., 2020; Wu et al., 2017). Previous research has predominantly used mammalian cell cultures. A limited number of studies have used null mutant organisms and *in vivo* techniques, which afford cell biology to be studied in a natural physiological context. However, *Srx* null mutant mice have been generated and display increased mortality in response to lipopolysaccharide-induced endotoxemia (Planson et al., 2011). Although *Srx* null mice do not exhibit any obvious abnormalities under standard laboratory conditions, they have not been comprehensively screened for neurological defects and, as such, the neurophysiological roles for *Srx* remain unclear.

Here, I sought to exploit the well-characterised electrophysiological, biochemical, and behavioural assays used to study neuron function in *Drosophila*. The short generation times and wealth of genetic tools render *Drosophila* a practical alternative to murine models for *in vivo* research. Generating *Drosophila Srx* mutant stocks would allow for the role of Srx to be researched and establish whether *Srx* is an essential gene for *Drosophila* survival.

This chapter details the generation of *Drosophila Srx* null mutant stocks via *P-Element* transposition. Transgenic fly strains were created to allow for the expression of Srx in a tissue-specific fashion. This allowed for the rescue of null mutant-associated phenotypes, as well as the exploration of effects when *Srx* was over-expressed. An antibody was also generated to monitor *Srx* expression levels in *Drosophila* via Western blotting.

3.2. Results

3.2.1. Srx conservation in *Drosophila*

There are many practical advantages to using *Drosophila* to study neuron function (discussed in Chapter 1.4). To capitalise on these, I first sought to create null mutant stocks to investigate Srx function. There is a limited body of work investigating Srx in *Drosophila*. To this end, gene conservation is paramount. The *Drosophila Srx* locus has previously been identified by (Jönsson et al., 2005). In the present study, this process was repeated to confirm the result and account for updated cDNA libraries. A basic local alignment search tool (BLAST) was used to identify similar protein sequences derived from *Drosophila* cDNA libraries (NCBI, 2024). The results of this BLAST are based on an annotated *Drosophila* transcriptome derived from a multitude of cDNA libraries. These are generated via RNA extraction, cDNA synthesis, and cloning into sequencing vectors. Sequencing these generates a collection of expressed sequences derived from regions of the genome that are transcribed, known as expressed sequence tags (ESTs). These have been collated and annotated by the FlyBase consortium (FlyBase, 2024).

The blastp search of human Srx (hSrx) (Uniprot code Q9BYN0) identified three homologous isoforms in *Drosophila*. All three were produced from transcripts derived from the same gene, *sulfiredoxin/CG6762* (Srx-PA, blast E value 1e-42; Srx-PB, blast E value 1e-42; Srx-PD, blast E value 1e-42). The *Drosophila* Srx locus is located on the X chromosome at cytogenetic band 16E2. The human *sulfiredoxin-1* product was also identified when *Drosophila* Srx-PA

was used as the search term in blastp (blast E value 1e-41). Similar results are observed when the search term is changed to Srx-PB (blast E value 8e-42) and Srx-PD (blast E value 1e-41).

The Srx-PA isoform is 162 amino acids (AA) in length and encoded by the *CG6762-RA* transcript of 984 bp, translated in reading frame (RF) 3. Srx-PB is 112 AA long with a truncated N-terminus, encoded by the 921 bp transcript *CG6762-RB* in RF3. Srx-PD is 152 AA long, exhibiting an N-terminal extension that misses 10 AA residues relative to Srx-PA. This is encoded by the 787 bp *CG6762-RD* transcript.

```
hSrx      --------------------------MGLRAGGTLGRAGAGRGAPEGPGPSGGAQGGSIH 34
mSrx      --------------------------MGLRAGGALRRAGAGPGAPEGQGPG-GAQGGSIH 33
rSrx      -------MVQPGRVKRPGGAVRQGSNMGLRAGGALRRASAGPGAPDGQGPS-GAQGGSIH 52
dSrx-PA   MEFISHFLRATSRRTAALGPILQRNRSEIIQKQSL----TNRQAFRRYRSSCSTMDTTVH 56
dSrx-PB   ------------------------------------------------------MDTTVH 6
dSrx-PD   MEFISHFLRATSRRTAALGPILQRNRSEIIQK--------------QYRSSCSTMDTTVH 46
                                                                . ::*
hSrx      SGRIAAVHNVPLSVLIRPLPSVLDPAKVQSLVDTIRED--PDSVPPIDVLWIKGAQGGDY 92
mSrx      SGCIATVHNVPIAVLIRPLPSVLDPAKVQSLVDTILAD--PDSVPPIDVLWIKGAQGGDY 91
rSrx      SGCIDTVHNVPIAVLIRPLPSVLDPVKVQSLVDTILED--PDSVPPIDVLWIKGAQGGDY 110
dSrx-PA   SAGIDETHLVPMSVIQRPIPSVLDEQKVQSLMETIKNETSEDEVPPIDLLWISGSEGGDY 116
dSrx-PB   SAGIDETHLVPMSVIQRPIPSVLDEQKVQSLMETIKNETSEDEVPPIDLLWISGSEGGDY 66
dSrx-PD   SAGIDETHLVPMSVIQRPIPSVLDEQKVQSLMETIKNETSEDEVPPIDLLWISGSEGGDY 106
          *. *  .* **::*: **:*****  *****::**  :   *.*****:***.*::****

hSrx      FYSFGGCHRYAAYQQLQRETIPAKLVQSTLSDLRVYLGASTPDLQ- 137
mSrx      YYSFGGCHRYAAYQQLQRETIPAKLVRSTLSDLRMYLGASTPDLQ- 136
rSrx      YYSFGGCHRYAAYQQLQRETIPAKLVRSTLSDLRMYLGASTPDLQ- 155
dSrx-PA   YFSFGGCHRFEAYKRLQRPTIKAKLVKSTLGDLYHYMGSSAPKYLA 162
dSrx-PB   YFSFGGCHRFEAYKRLQRPTIKAKLVKSTLGDLYHYMGSSAPKYLA 112
dSrx-PD   YFSFGGCHRFEAYKRLQRPTIKAKLVKSTLGDLYHYMGSSAPKYLA 152
          ::*******: **::*** ** ****:***.**  *:*:*:*.
```

Figure 3.1. BLAST followed by multiple sequence alignment indicates that Sulfiredoxin-1 is conserved in *Drosophila*.

Relative to hSrx, the sequence similarities were 50.38% (dSrx-PA), 57.80% (dSrx-PB), and 52.03% (dSrx-PD). Relative to rSrx, sequence similarities were 46.36% (dSrx-PA), 58.72% (dSrx-PB), and 48.23% (dSrx-PD). The crucial residues required for Srx function are conserved across species. Charged AA residues required for Prdx binding are highlighted in pink, whereas those needed for ATP phosphate group binding are highlighted in yellow. The conserved catalytic cysteine residue is highlighted in green. Residues are annotated according to whether the AA residues completely match (*), show high similarity (:), low similarity (.), or no similarity (unannotated).

Crucially, all the *Drosophila* Srx isoforms possess the AA residues that are critical for Srx function and are highly conserved. This is demonstrated through a multiple sequence alignment of the *Drosophila* Srx isoforms with hSrx, *Mus musculus* (Mouse) Srx (mSrx), and *Rattus norvegicus* (Rat) Srx (rSrx) using the Clustal Omega online tool (Madeira et al., 2024). All of the charged AAs that facilitate Prdx dimerisation and ATP-binding are conserved (Figure 3.1). It should be noted that the AA residue numbers for rSrx differ to those detailed in Chapter 1.2.6.5 because the sequence has been updated on the NIH Genbank database since the seminal work of Jeong et al. (2006), which originally characterised the function of specific AA residues, was published.

3.2.2. Are all the *Drosophila* Srx isoforms valid?

The cDNA libraries used to elucidate the *Drosophila* transcriptome have been generated from distinct tissue types. which have produced ESTs corresponding to different *Drosophila* Srx isoforms. Srx-PA ESTs were generated from *Drosophila* head extracts, which contain a large proportion of neurons, whereas Srx-PB was generated from larvae and early stage pupae (Rubin et al., 2000). This may indicate that the Srx-PA isoform, with an N-terminal extension, is more relevant to neuron function. However, this does not necessarily render the alternative isoforms as invalid and irrelevant to this investigation. This may instead be resolved by a comparison of the conserved AA motifs in each isoform.

Mammalian Srx translocates into the mitochondrial matrix, where it can recycle Prdx3 (Noh et al., 2009). Mitochondrial import of Srx is protective against OS and appears to regulate oscillatory H_2O_2 release (Kil et al., 2015). Mitochondrial import of proteins is typically facilitated by translocase of outer mitochondrial membrane 20 (TOM20), a component of the TOM complexes in the outer mitochondrial membrane. TOM20 can interact with the N-terminal sequences of proteins targeted for the mitochondrial matrix and inner membrane, which are typically cleaved upon import, although not always (Chacinska et al., 2009). These sequences are composed of 15-40 AA residues with an abundance of positively charged residues that tend to form an amphipathic α-helix (von Heijne, 1986).

The N-terminus of mSrx has been found to contain an unorthodox, non-cleavable mitochondrial-targeting sequence, which is conserved in hSrx and rSrx too. Mutating the first 10 or 20 AA residues of the mSrx N-terminus, or the Arginine residues at position 4 and 11, prevents mitochondrial localisation in human-derived HeLa cells (Kil et al., 2015). It also prevents TOM20-binding, as shown through co-immunoprecipitation experiments.

Therefore, these residues and the neighbouring hydrophobic residues likely generate the amphipathic helical structure that can interact with TOM20. HSP90 chaperones Srx to the TOM complex via disulphide bonds at the catalytic cysteine residue of Srx, along with the co-chaperone FK506-binding protein (FKBP). This presequence is not cleaved, unlike motifs in other proteins (Kil et al., 2015).

The *Drosophila* genome also encodes Prdx3, a mitochondrial typical 2-Cys Prdx enzyme that is important for conferring resistance to OS (Kayashima and Yamakawa-Kobayashi, 2012; Radyuk et al., 2001). Therefore, valid dSrx isoforms are likely to encode an analogous N-terminus sequence to facilitate amphipathic α-helix formation, TOM20 binding, and mitochondrial import. Analysis of the first 18 AA residues in dSrx isoforms, using MitoFates prediction tool, revealed TOM20 recognition motifs in Srx-PA and Srx-PD, but not Srx-PB, as shown in Figure 3.2.A (Fukasawa et al., 2015). The motif is composed of 5 AA residues (φχβφφ, where φ is hydrophobic, β is basic and χ is any residue). This sequence, and the mammalian N-termini, are likely to generate amphipathic α-helices, as demonstrated through helical wheel plots, generated using NetWheels application (Mól et al., 2018). These are presented in Figure 3.2.B-E. Srx-PB lacks this motif and does not appear to have amphipathic sequences organised in a manner that permits TOM20 binding (Figure 3.2.F).

Collectively, this evidence suggests that dSrx-PA may be the valid orthologue to mammalian Srx. It possesses a predicted TOM20 recognition motif for localisation into mitochondria, which is required to reduce mitochondrial typical 2-Cys Prdx enzymes (Prdx3). It has also been identified from the neuron-rich adult head cDNA libraries, suggesting it is the predominant isoform in neurons. However, one cannot conclusively dispel the notion that the other isoforms perform Srx function in non-mitochondrial organelles and other tissue types.

A.

```
hSrx      -------------------------MGLRAGGTLGRAGAGRGAPEGPGPSGGAQGGSIH  34
mSrx      -------------------------MGLRAGGALRRAGAGPGAPEGQGPG-GAQGGSIH  33
rSrx      -------MVQPGRVKRPGGAVRQGSNMGLRAGGALRRASAGPGAPDGQGPSG-AQGGSIH  52
dSrx-PA   MEFISHFLRATSRRTAALGPILQRNRSEIIQKQSL----TNRQAFRRYRSSCSTMDTTVH  56
dSrx-PB   ------------------------------------------------------MDTTVH  6
dSrx-PD   MEFISHFLRATSRRTAALGPILQRNRSEIIQK--------------QYRSSCSTMDTTVH  46
                                                                . ::*
```

B.

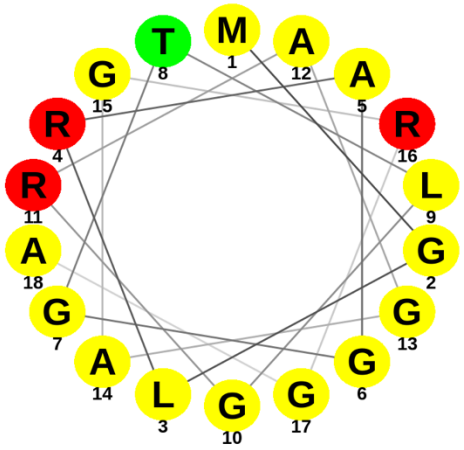

C.

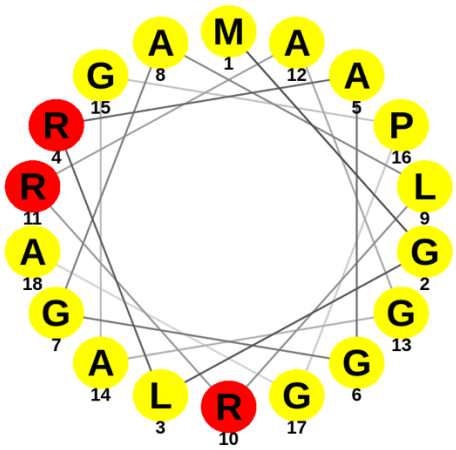

D.

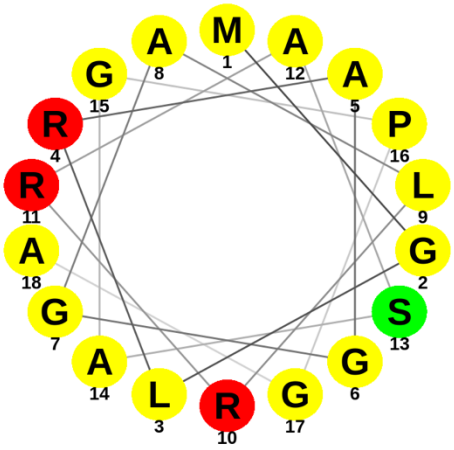

E.

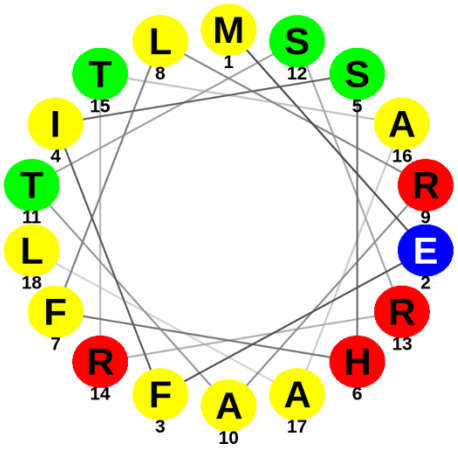

F.

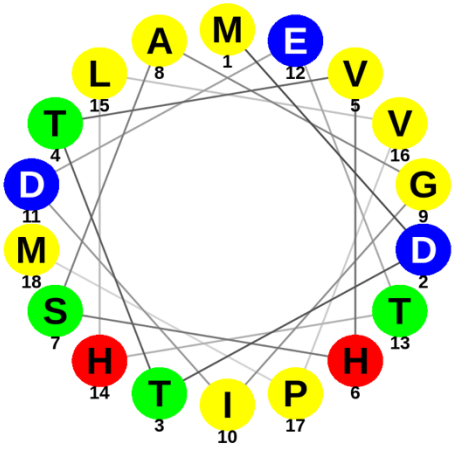

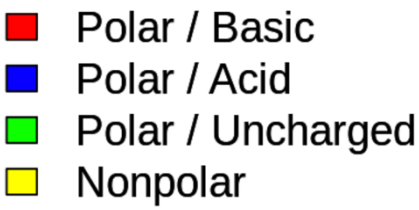

Figure 3.2. Mammalian Srx and two *Drosophila* Srx isoforms contain predicted mitochondrial targeting sequences at the N-terminus.

A. In mammals, basic AA (Arginine) residues at position 4 and 11 facilitate the creation of amphipathic α-helices, TOM20 binding, and mitochondrial localisation (Kil et al., 2015). This sequence is not conserved in dSrx isoforms. However, dSrx-PA and dSrx-PD are predicted to contain alternative TOM20 recognition motifs in the N-terminus region, as predicted using the MitoFates online tool (Fukasawa et al., 2015). This motif is composed of φχβφφ AA residues, where φ is hydrophobic (highlighted in yellow), β is basic (highlighted in red) and χ is any residue (highlighted in grey). Predicted MPP cleavage sites are highlighted in pink. A TOM20 recognition motif is not predicted for dSrx-PB. **B.** Helical wheel plots of the 18 AA residues at the hSrx N-terminus demonstrates that polar residues are localised on one side of the helix, with hydrophobic residues on the other side. These have the potential to form amphipathic α-helices consistent with structures that bind TOM20. The first 18 AA residues of mSrx (**C**), rSrx (**D**), dSrx-PA, and dSrx-PD (**E**) also exhibit this pattern. dSrx-PB does not exhibit such a motif in the first 18 AA residues, with hydrophobic and hydrophilic uniformly expressed across the helix (**F**).

3.2.3. Generation of *Drosophila Srx* null mutant stocks

Drosophila Srx (*CG6762*) null mutants were produced via *P-Element* transposition, as identified by a PCR screen using carefully designed primers (Figure 3.3.A). A crossing scheme was employed to co-express a functional, non-excisable transposon and a non-functional, excisable transposable *P-Element* in the germline cells of flies. This generated either precise excision events, in which the *Srx* gene was undisturbed, or imprecise excision events that excised adjacent DNA regions to create deletion mutations. Such events could be screened for using PCR (Figure 3.3.B).

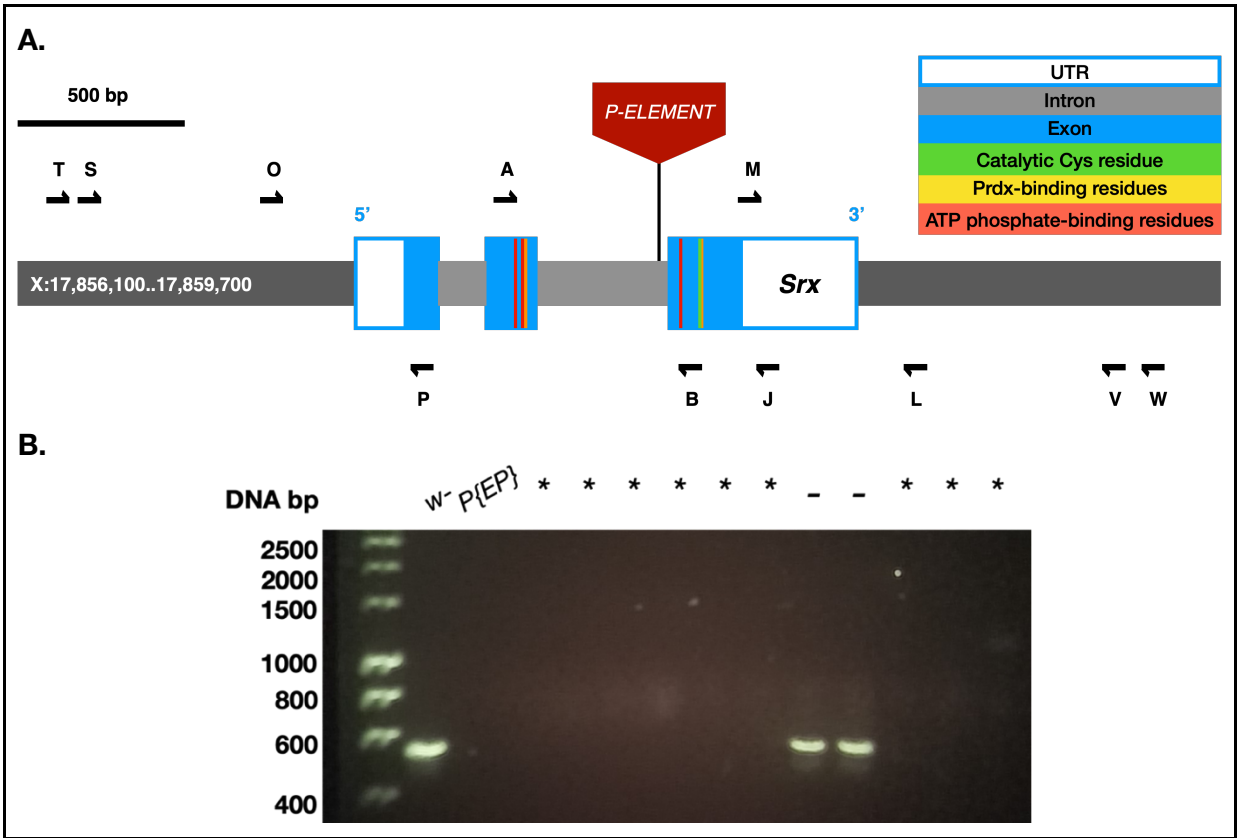

Figure 3.3. Single fly PCR screen for potential *Srx* mutants.

A. PCR using carefully designed primer pairs detected imprecise excision events and *Srx* mutant generation. With the exception of the primers and *P{EP}* insertion, the diagram is to scale. Genomic regions mapping to the amino acid residues critical for Srx function are indicated. **B.** Exemplary gel image demonstrating the first stage of the PCR screen using primers A and B. Control flies (*w-*) generated fragments of 574 bp, whereas *P{EP}Srx*^{G1102} (*P{EP}*) acted as a negative control as the PCR extension time only permitted products of up to 1 kb (the *P{EP}* insertion was approximately 8 kb). Precise excision events, in which the product size recapitulates that of *w-*, are indicated (-), as are imprecise excision events where there is no product (*). These excisions could be further characterised by primer pairs targeting the flanking regions, such as M and L.

Two *Srx* mutant stocks were identified in this PCR screen (Figure 3.4). The first, *Srx*$^{\Delta 1\text{-}2}$, had genomic DNA encoding the first two exons excised (Figure 3.4.A). This was apparent from a lack of PCR product using primers O and P, as well as a smaller PCR product when primers S and J were used. The second, *Srx*$^{\Delta 3}$, had genomic DNA encoding the third exon excised (Figure 3.4.B). This was evident from a lack of PCR product using primers M and L, as well as smaller PCR product when primers A and L were used. Sanger sequencing revealed the

precise nature of these excisions (Figure 3.4.C). *Srx*$^{\Delta 1\text{-}2}$ mutants had 1221 bp of genomic DNA excised, which was determined by the creation of PCR product using primers T and J, then sequencing with Primer S. *Srx*$^{\Delta 3}$ mutants had 718 bp of DNA excised, shown by the creation of PCR product with A and W, then sequencing using primer V.

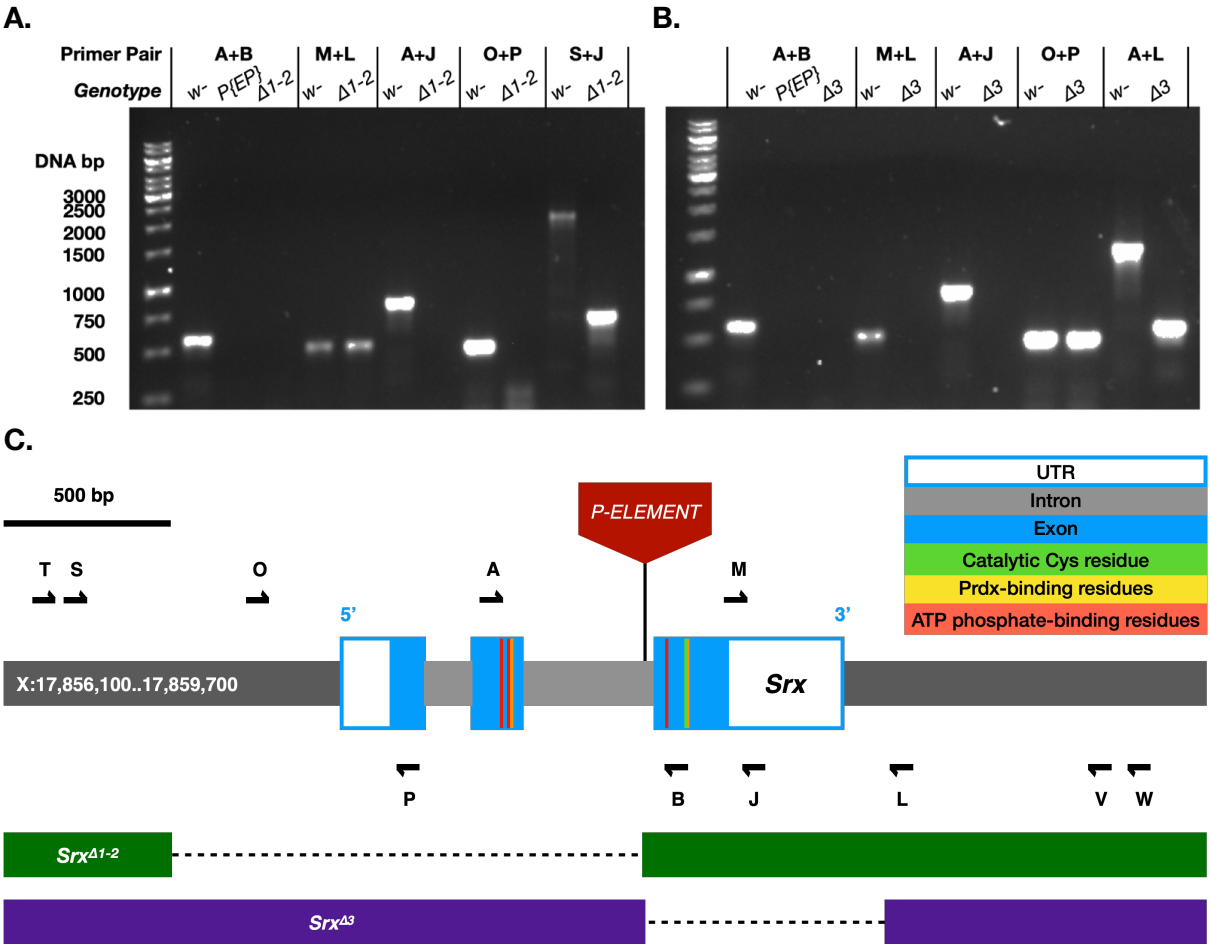

Figure 3.4. Imprecise *P-Element* excision generated *Srx* mutant fly strains.

A. *Srx*$^{\Delta 1\text{-}2}$ could be identified using primer combinations targeting genomic regions upstream of the *P{EP}Srx*^{G1102} site, such as primers O and P. **B.** *Srx*$^{\Delta 1\text{-}2}$ could be identified using primer combinations targeting regions downstream of this site, such as M and L. PCR screens highlighted the regions of DNA excised following a *P-Element* transposition event. **C.** Sanger sequencing revealed the exact regions of DNA that had been cleaved in the mutant stocks (dotted lines). This diagram is to scale, excluding the *P-Element* insertion and primer lengths. Both *Srx*$^{\Delta 1\text{-}2}$ and *Srx*$^{\Delta 3}$ excisions cause a loss of DNA encoding amino acid residues that are critical for Srx function. The *Srx*$^{\Delta 3}$ mutants lack the DNA encoding the catalytic cysteine residue of Srx, whereas the *Srx*$^{\Delta 1\text{-}2}$ stock lacks the DNA encoding amino acid residues that confer Prdx association and the deprotonation of the catalytic cysteine residue.

3.2.4. Generation of a *UAS-Srx.FLAG* transgene

To express Srx in a tissue-specific manner, a *UAS-Srx.FLAG* transgene was generated via molecular cloning techniques and *Drosophila* embryo injection. RNA was extracted from *w-* male flies and RT-PCR was performed to produce complementary DNA (cDNA). This was used as a template to generate PCR product encoding *Drosophila* dSrx-PA with EcoRI and XhoI restriction enzyme sites attached. This fragment was then digested and ligated into a *pUAST* vector for injection into *Drosophila* embryos. This produced stocks stably expressing the *UAS-Srx.FLAG* transgene.

This stock permitted over-expression of Srx using the *Gal4-UAS* binary expression system. Yeast-derived Gal4 transcription factors are expressed using tissue specific promoters, which can be combined with transgenes containing *Gal4*-binding UAS promoter sequences conjugated to a gene of interest (Brand and Perrimon, 1993). This allowed for overexpression of Srx in specific cell types, as well as the rescue of null-mutant phenotypes in a tissue-specific manner. The functionality of the *UAS-Srx.FLAG* construct was validated via western blot analysis (see Figure 3.5).

3.2.5. Generation of a *Drosophila* Srx antibody

To monitor expression levels of Srx, polyclonal antibodies were generated via the immunisation of guinea pigs using the full-length *Drosophila* Srx protein (Srx-PA) with an N-terminal HIS-MBP tag. Final bleed serum from one animal proved effective at detecting Srx via western blotting using *Drosophila* head lysates (Figure 3.5). Although non-specific bands are visible between 20 and 35 kDa, Srx is readily detectable at 16 kDa in *w-* (control) lysates, but not in lysates derived from $Srx^{\Delta 1\text{-}2}$ and $Srx^{\Delta 3}$ mutants. Lysates made from flies over-expressing Srx in neurons, via use of the *nSyb-Gal4* and *UAS-Srx.FLAG* transgenes, exhibit increased levels of Srx. Together, these findings validate the affinity of this polyclonal antibody for Srx.

Figure 3.5. Immunisation of a guinea pig generated a polyclonal antibody for Srx.

Western blotting validated the antibody, with Srx detected at 16 kDa in *w- Drosophila* brain lysates, but not in the *Srx* mutants, $Srx^{\Delta 1-2}$ and $Srx^{\Delta 3}$ (see Chapter 3.2.3). Similarly, increased luminescence is seen when Srx is overexpressed in brain lysates using the *nSyb-Gal4* and *UAS-Srx.FLAG* transgenes. Non-specific bands are visible between 20 and 35 kDa. Staining for β-actin demonstrated equal loading of samples in the lanes of the polyacrylamide gel.

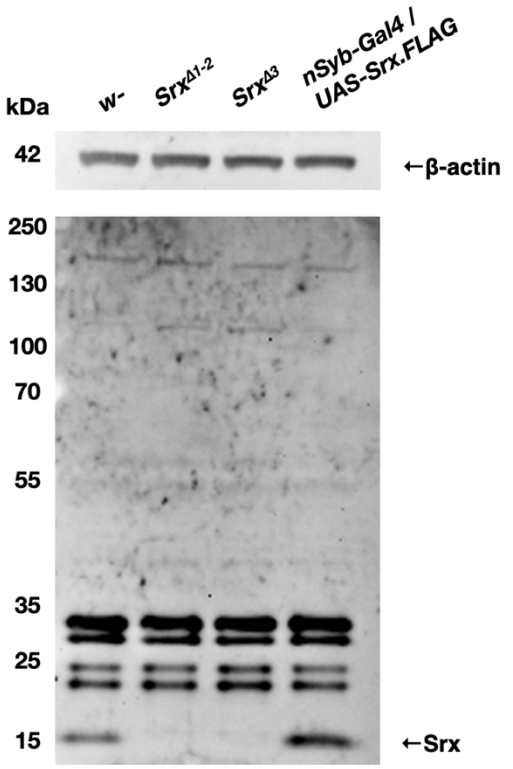

3.2.6. *Drosophila Srx* mutants are sensitive to dietary H_2O_2

As Srx functions as an antioxidant protein in yeast and mammals, I hypothesised that *Drosophila Srx* mutant males would exhibit a diminished ability to resolve ROS, compromising defence against OS. To test this hypothesis, I compared the survival of wild type (WT) and *Srx* mutant flies fed with sucrose solution supplemented with 5% w/v H_2O_2. H_2O_2 is routinely used to induce OS and reduce longevity (Tuxworth et al., 2011). $Srx^{\Delta 1-2}$ and $Srx^{\Delta 3}$ mutants exhibited a small, but significant reduction in survival rates compared to WT flies (Figure 3.6.A). The median time of death was after 111 hours for WT flies, whereas both *Srx* mutations reduced this by 13.5% to 96 hours.

A.

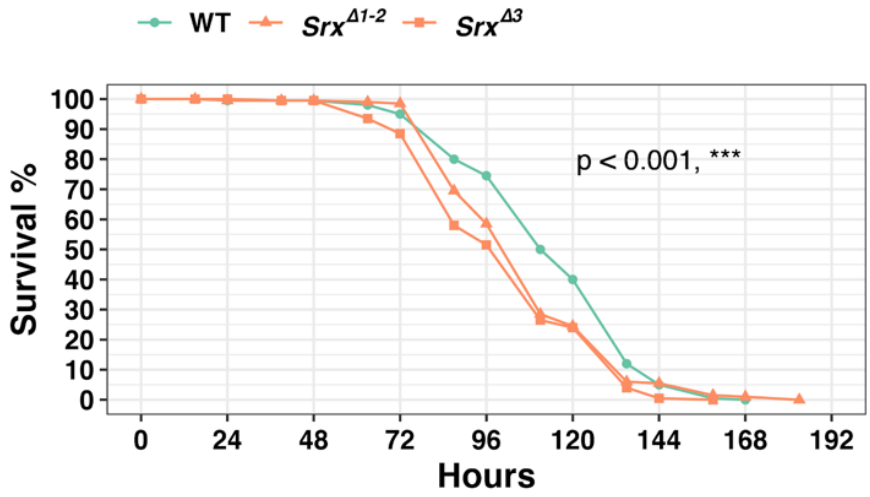
WT
Srx^Δ1-2
Srx^Δ3
Survival %
100
90
80
70
60
50
40
30
20
10
0
p < 0.001, ***
0
24
48
72
96
120
144
168
192
Hours

B.

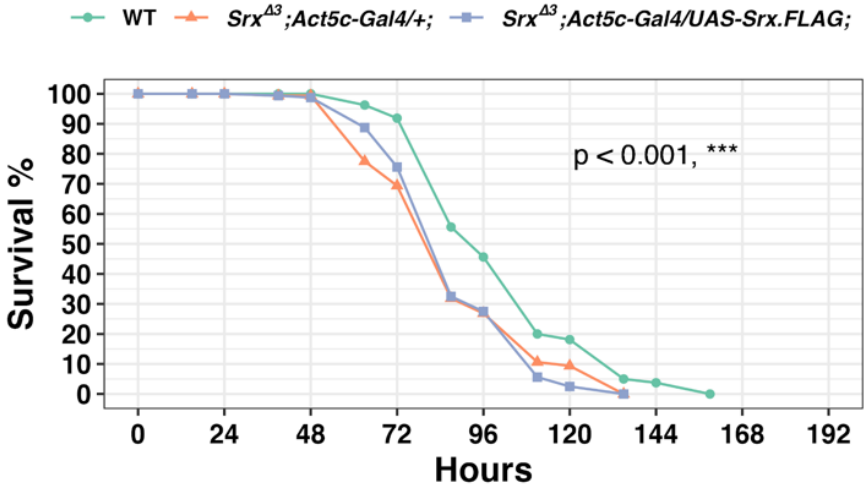
WT
Srx^Δ3;Act5c-Gal4/+;
Srx^Δ3;Act5c-Gal4/UAS-Srx.FLAG;
Survival %
100
90
80
70
60
50
40
30
20
10
0
p < 0.001, ***
0
24
48
72
96
120
144
168
192
Hours

C.

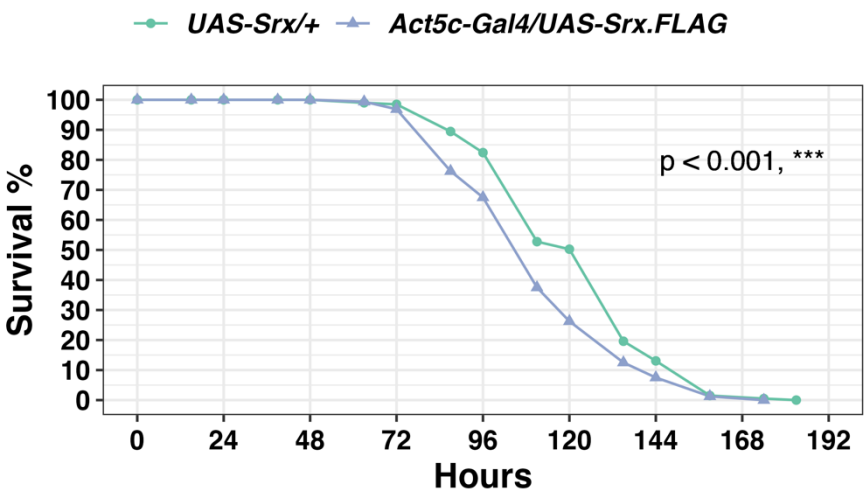
UAS-Srx/+
Act5c-Gal4/UAS-Srx.FLAG
Survival %
100
90
80
70
60
50
40
30
20
10
0
p < 0.001, ***
0
24
48
72
96
120
144
168
192
Hours

Figure 3.6. *Srx* mutations and *Srx* overexpression reduce *Drosophila* survival on H_2O_2-supplemented food.

A. *Drosophila Srx* mutants exhibit reduced longevity on sucrose solution containing 5% w/v H_2O_2 (log-rank analysis, p<0.001***, multiple pairwise comparisons to WT with BH adjustment: $Srx^{\Delta 1\text{-}2}$ p<0.01**, $Srx^{\Delta 3}$ p<0.001***). **B.** Ubiquitous expression of Srx in the *Srx* mutant background, using the *Act5c-Gal4* and *UAS-Srx.FLAG* transgenes, does not rescue diminished survival on food containing H_2O_2 (log-rank analysis, p<0.001***, multiple pairwise comparisons to WT with BH adjustment: $Srx^{\Delta 1\text{-}2}$*;Act5c-Gal4/+;* p<0.001***, $Srx^{\Delta 3}$*;Act5c-Gal4/UAS-Srx.FLAG;,* p<0.001***). **C.** Ubiquitous over-expression of Srx diminishes longevity on food containing H_2O_2 (log-rank analysis, p<0.001***). For all experiments, at least 160 flies were analysed (in cohorts of 20).

To validate that loss of Srx conferred sensitivity to H_2O_2, I attempted to rescue the H_2O_2 sensitivity phenotype by ubiquitously re-expressing Srx in the background of the $Srx^{\Delta 3}$ mutant stock using the *Act5c-Gal4* and *UAS-Srx.FLAG* transgenes. This failed to rescue the phenotype (Figure 3.6.B). To ensure similar genetic backgrounds, all experimental flies possessed the *Act5c-Gal4* transgene. Both the $Srx^{\Delta 3}$ mutants with and without the *UAS-Srx.FLAG* transgene exhibited a median time of death after 72 hours. WT flies had a median time of death after 87 hours.

The failure to rescue the H_2O_2 sensitivity phenotype using the *UAS-Srx.FLAG* transgene raised the possibility that the global over-expression of Srx may itself confer sensitivity to OS. In support of this notion, I found that ubiquitous over-expression of *Srx* using the *Act5c-Gal4* and *UAS-Srx.FLAG* transgenes decreased survival of flies exposed to H_2O_2. Flies over-expressing Srx had a median death time after 96 hours, whereas the median death time was after 120 hours for WT flies. Collectively, this data suggests that both the decreased and increased expression of *Srx* conferred sensitivity to H_2O_2 in *Drosophila*. An optimal level of Srx expression may be required for defence against OS. Low expression may result in increased Prdx hyperoxidation and peroxide levels. High Srx expression may conversely decrease Prdx hyperoxidation, allowing it to interact with Trx to oxidise it and prevent it from interacting with alternative substrates (discussed in Chapter 3.3.3). High or low levels may instead alter the chaperone function of Prdx. Differences in longevity could also be attributed to variations in the genetic background of flies.

3.2.7. *Drosophila Srx* mutants do not exhibit elevated levels of ROS or redox-sensitive Nrf2 signalling

The decreased survival of *Drosophila Srx* mutants on food containing H_2O_2 suggests that they possess a diminished ability to resolve ROS and prevent OS. This could lead to constitutively elevated levels of ROS and activation of redox-sensitive signalling pathways. To address whether *Drosophila Srx* mutants exhibited elevated H_2O_2 levels in tissue homogenates, the Amplex Red assay was performed. In this technique, Horseradish Peroxidase (HRP) enzyme is incubated with Amplex Red reagent in the presence of *Drosophila* tissue homogenates. Tissue-derived H_2O_2 acts as a co-factor for HRP to convert the Amplex Red substrate to the red dye resorufin, which can be measured via fluorimetry to indirectly quantify H_2O_2 concentration (Chávez et al., 2007; Mohanty et al., 1997). Recordings can be normalised to protein levels using the Bicinchoninic Acid (BCA) assay to account for differences in the degree of tissue homogenisation (Smith et al., 1985).

The Amplex Red assay did not reveal significant differences in *Drosophila* tissue H_2O_2 levels following the loss of Srx (Figure 3.7.A). However, a trend was observed whereby *Srx* mutants exhibited lower H_2O_2 levels. This could reflect a homeostatic adaption in the flies, whereby there is upregulation of other antioxidant enzymes that scavenge peroxides, such as glutathione peroxidase. WT flies exhibited a mean fluorescence of 0.130 AU/mg of protein (±0.005 AU/mg), whereas $Srx^{\Delta 1\text{-}2}$ and $Srx^{\Delta 3}$ flies had mean scores of 0.111 AU/mg (±0.006 AU/mg) and 0.114 AU/mg (±0.001 AU/mg) of protein, respectively.

To assess whether Srx can regulate redox-sensitive signalling pathways, I next examined the effect of *Drosophila Srx* mutations on Nrf2 signalling. The transcriptional regulator Nrf2 accumulates in the nucleus under conditions of OS and binds to antioxidant response element (ARE) sequences within promoters to upregulate the expression of specific target genes (see Chapter 1.2.3.3). Glutathione S-transferase D1 (*gstD1*) is one such Nrf2 target gene. A transgenic reporter gene that contains the GFP coding sequence under the control of the promoter sequence for *gstD1* allows researchers to observe the activation of Nrf2 signalling via the quantification of green fluorescence (Sykiotis and Bohmann, 2008). I therefore bred flies to carry the *gstD1-GFP* transgene heterozygously in the WT or *Srx* mutant backgrounds and measured green fluorescence in tissue homogenates in a fluorescence plate reader. Flies were either reared under standard conditions or placed onto food made with 10 mM DEM sucrose-yeast solution for 72 hours to induce OS. Administering

DEM allowed an assessment of transgene expression in response to sustained OS and allowed me to see if OS differentially elicited Nrf2 signalling in the WT and *Srx* mutant flies.

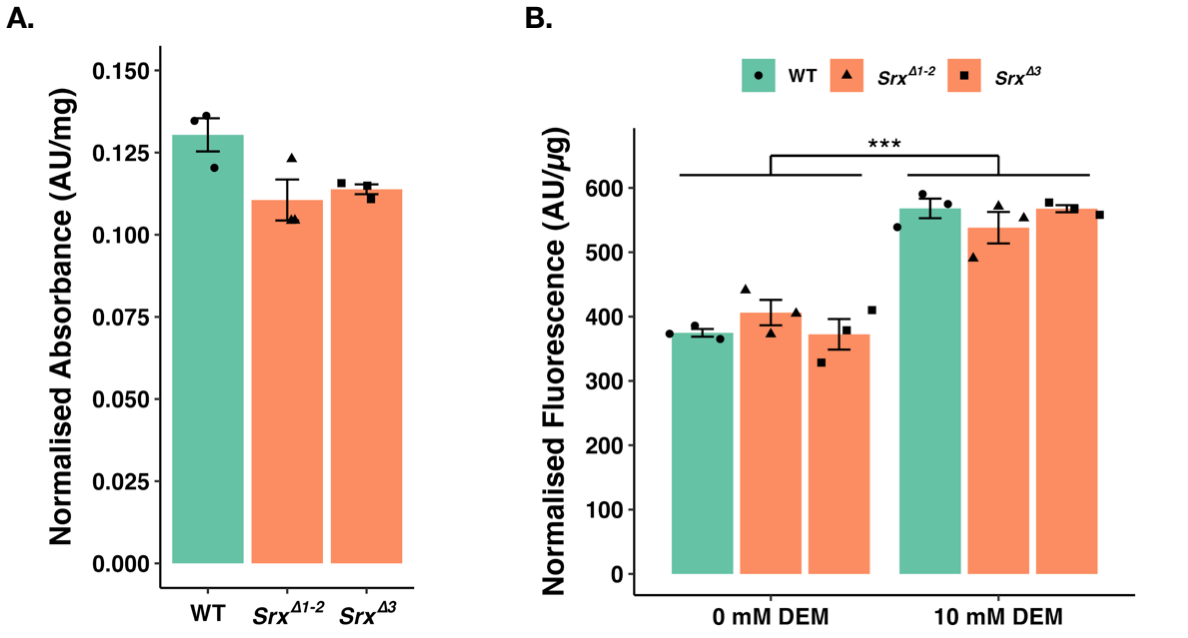

Figure 3.7. Loss of *Drosophila Srx* does not increase ROS levels or activation of redox-sensitive Nrf2 signalling.

A. Loss of Srx does not increase H_2O_2 levels, as measured via the Amplex Red assay in *Drosophila Srx* mutant tissue lysates (Kruskal-wallis, df=3, χ^2=4.36, p=0.113, ns). **B.** Loss of Srx does not affect Nrf2 signalling in *Drosophila*, as shown through expression of the *gstD1-GFP* transgene and tissue homogenate analysis. A two-way ANOVA revealed significantly increased fluorescence in the lysates generated from flies fed DEM-supplemented food (p<0.001***). No significant differences existed between the genotypes (p=0.993, ns) and there was no significant interaction between the genotype and food (p=0.165, ns). For both experiments, absorbance and fluorescence values were normalised to the protein concentration in each tissue homogenate, as measured by the BCA assay, to account for differences in the extent of sample homogenisation or tissue mass. For all of the graphs, bars represent mean ± SEM and n=3 for each group.

Feeding flies DEM-containing food increased green fluorescence in the homogenates, with the mean score increasing by 45.1% from 384.447 AU/µg (±10.590 AU/µg) to 558.009 AU/µg (±9.811 AU/µg) of protein (Figure 3.7.B). However, there were no significant differences between the genotypes, or the interaction term. Under standard conditions, WT flies

exhibited a mean score of 374.749 AU/µg of protein (±6.032 AU/µg), $Srx^{\Delta 1\text{-}2}$ mutants exhibited a mean score of 406.165 AU/µg of protein (±19.724 AU/µg), and $Srx^{\Delta 3}$ mutants exhibited a score of 372.428 AU/µg of protein (±23.774 AU/µg). After rearing with a DEM-supplemented diet, WT flies exhibited a mean score of 568.114 AU/µg of protein (±15.238 AU/µg), $Srx^{\Delta 1\text{-}2}$ mutants exhibited a mean score of 538.197 AU/µg of protein (±24.452 AU/µg), and $Srx^{\Delta 3}$ mutants exhibited a score of 567.717 AU/µg of protein (±5.518 AU/µg).

Collectively, these results indicate that Srx is not critical for redox homeostasis under standard conditions as levels of H_2O_2 are not significantly affected. In response to imposed stress, there are no differences in the activation of redox-sensitive Nrf2 signalling, suggesting that the redox state of cells is largely unperturbed in *Srx* mutants.

3.2.8. *Drosophila Srx* mutations attenuate AP-1 signalling

The lack of any changes in Nrf2 signalling in *Drosophila Srx* mutants prompted an investigation into whether other OS-induced signalling pathways were affected by loss of Srx. Redox-sensitive JNK/AP-1 signalling is a crucial pathway for the upregulation of antioxidant gene expression, including transcriptional upregulation of Srx itself (Papadia et al., 2008; Ugbode et al., 2020) and regulates synapse growth at the *Drosophila* NMJ (Martin-Blanco et al., 1998; Milton et al., 2011). Therefore, I tested whether *Srx* mutations affected AP-1 signalling using a transgene expressing DsRed.T4 fluorescent protein under the control of a palindromic tetradecanoylphorbol acetate response element (TRE) sequence, which AP-1 dimers bind to upregulate target genes (Chatterjee and Bohmann, 2012). This transgene was expressed heterozygously in the WT or *Srx* mutant background, and lysates were generated from multiple flies prior to fluorimetry experiments being conducted. Fluorescence readings were normalised to protein content, as measured by the BCA assay. Flies were reared under standard conditions or placed on food composed of sucrose-yeast solution with 10 mM DEM for 72 hours to induce OS.

Under standard conditions, WT flies had an average normalised reading of 605.6 AU/µg of protein (±16.9 AU/µg). For $Srx^{\Delta 1\text{-}2}$ mutants, the normalised reading was 17.8% lower at 497.8 AU/µg of protein (±3.6 AU/µg), and the $Srx^{\Delta 3}$ reading was 30.5% lower at 420.8 AU/µg of protein (±28.8 AU/µg). DEM treatment increased the average WT normalised reading by 11.2% to 673.5 AU/µg of protein (±11.6 AU/µg). Similarly, the $Srx^{\Delta 1\text{-}2}$ and $Srx^{\Delta 3}$ mutant normalised readings increased by 5.4% and 26.5%, respectively. Despite the treatment, the $Srx^{\Delta 1\text{-}2}$ and $Srx^{\Delta 3}$ mutant normalised readings were 22.1% and 20.9% lower than that of WT

flies, respectively. These results demonstrate that AP-1 signalling is enhanced by OS and that *Srx* mutations attenuate this increase in AP-1 signalling under both standard conditions and conditions of OS. *Srx* mutants exhibit more modest increases in AP-1 signalling following DEM feeding and are comparable to those observed under standard conditions. These results are depicted in Figure 3.8.

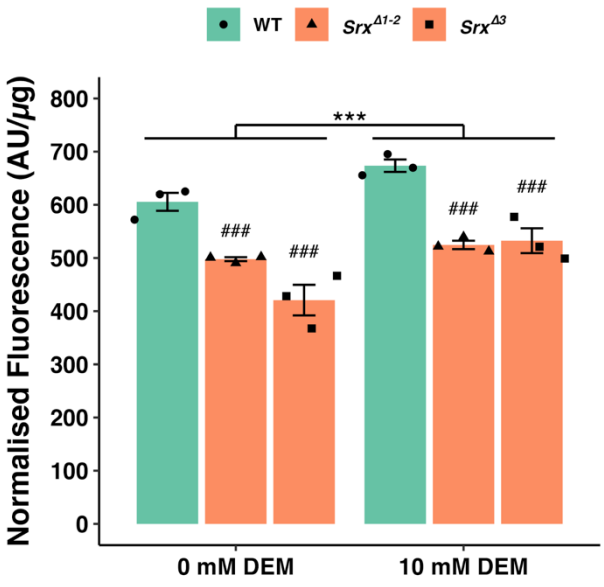

Figure 3.8. *Srx* mutations attenuate AP-1 signalling in *Drosophila* and repress OS-induced increases in AP-1 signalling.

Expression of a *TRE-DsRed.T4* transgene in the WT and *Srx* mutant backgrounds allowed for the extent of AP-1 signalling to be quantified in *Drosophila* homogenates. *Drosophila* were either reared under standard conditions or reared on food made with sucrose-yeast solution containing 10 mM DEM to induce OS. DEM feeding enhanced DsRed.T4 production (Two-way ANOVA, F=22.8, df=1, p<0.001***, with Tukey's HSD test for multiple comparisons, p<0.001***), whereas both $Srx^{\Delta 1-2}$ and $Srx^{\Delta 3}$ mutations attenuated DSRed.T4 production (Two-way ANOVA, F=47.3, df=2, p<0.001***, with Tukey's HSD test for multiple comparisons, p<0.001###). No interaction effect was observed (Two-way ANOVA, F=2.89, df=2, p=0.09, ns). Fluorescence values were normalised to the protein concentration in each tissue homogenate, as measured by the BCA assay, to account for differences in the extent of sample homogenisation or tissue mass. Bars represent mean ± SEM and n=3 for each group.

3.3. Discussion

3.3.1. *Drosophila* Srx is structurally related to mammalian Srx

To identify homologous Srx loci in the *Drosophila* genome, BLAST analysis of the *Drosophila* transcriptome revealed three cDNA sequences with a high degree of similarity to hSrx. One of these, dSrx-PA, was identified from cDNA libraries generated using adult heads, which are rich in neurons. It also contains an N-terminal sequence predicted to bind to TOM20 to facilitate mitochondrial import.

In mammals, Srx is important for regulating the redox state of Prdx enzymes, which confers defence against OS. This process is facilitated by a catalytic cysteine residue and charged AA residues that bind to Prdx enzymes and ATP phosphate groups. All of these are conserved in the dSrx isoforms, meaning it is likely to perform a similar function and recycle Prdx. In support of this notion, McGinnis et al. (2021) found that Srx hypomorphs exhibited increased amounts of hyperoxidised Prdx enzymes, as determined by western blots using antibodies targeting hyperoxidised Prdx isoforms.

Another important feature of mammalian Srx is that it localises to mitochondria where it can reduce Prdx3 and exert an anti-apoptotic effect (Noh et al., 2009). This localisation is facilitated by TOM20 binding to an N-terminal sequence. Yeast Srx lacks such a motif and likely does not translocate into mitochondria (Kil et al., 2015). The valid Srx isoform in *Drosophila* is likely to encode a similar mitochondrial-targeting sequence. Analysis of the N-terminal sequences of these isoforms reveals dSrx-PA and dSrx-PD to contain predicted TOM20 recognition motifs. Collectively, this evidence suggests that dSrx-PA is the closest orthologue of mammalian Srx in *Drosophila*.

A limitation of my *in silico* work is that it has not experimentally determined whether the proposed TOM20 recognition motif is crucial for mitochondrial import. Future work should produce *Srx* transgenes with mutations to the proposed TOM20 N-terminal targeting motif. Mutating the basic Histidine residue in this motif would compromise the amphipathicity of the helix that is proposed to be important for TOM20 binding. Immunofluorescence techniques could be employed to see if Srx co-localisation with mitochondria is observed following these mutations. This work attempted to address this matter by generating an antibody against *Drosophila* Srx using a guinea pig immunisation programme (see Figure 3.5). Unfortunately, the antibody derived from the final bleeds of both animals was ineffective at

labelling Srx in immunohistochemical assays. WT and *Srx* mutant third instar larvae were dissected and incubated with the antibodies at a range of concentrations, followed by incubation with the relevant secondary antibodies (data not shown). Similarly, I was unable to detect Srx using anti-FLAG antibodies following expression of the *UAS-Srx.FLAG* transgene in the neurons of third instar larvae (data not shown). This tag may be cleaved by post-translational modifications to Srx.

3.3.2. *Drosophila Srx* mutations confer mild sensitivity to dietary H_2O_2 but do not affect levels of ROS in tissue or Nrf2 signalling

I found that *Drosophila Srx* mutants exhibit slightly increased sensitivity to dietary H_2O_2. They have a small but significant reduction in survival when fed H_2O_2-containing sucrose solution. Ubiquitous over-expression of Srx similarly reduced lifespan in this paradigm. Although I hypothesised that increased sensitivity could be caused by constitutively higher levels of ROS, I did not observe higher H_2O_2 levels in *Drosophila Srx* mutant tissue. Similarly, the redox-sensitive Nrf2 signalling pathway was unperturbed in *Srx* mutants, whose response to DEM was indistinguishable from that of WT flies.

The increased H_2O_2 sensitivity of *Srx* mutants in my work is in contrast with the findings of McGinnis et al. (2021), who found that *Drosophila Srx* mutants exhibited slightly enhanced survival when fed H_2O_2-supplemented sucrose solution. McGinnis et al. (2021) used the *P-Element* insertion stock from which the $Srx^{\Delta 1\text{-}2}$ and $Srx^{\Delta 3}$ mutants were generated, and showed that the *P-Element* insertion reduced Srx mRNA levels via RT-PCR. McGinnis et al. (2021) also observed that *Drosophila Srx* mutations did not shorten lifespan under standard conditions in which no drug was administered to induce OS. The differences between the results of the present study and those of McGinnis et al. (2021) may be reconciled by the fact that different concentrations of H_2O_2 were administered. a high concentration of 1.632 M (5% w/v) H_2O_2 was administered to flies in this research, whereas McGinnis et al. (2021) used a more modest concentration of 0.5 M. The contribution of Srx to the OS response may be redundant or minor given the glutathione system and other antioxidant defence mechanisms. Extreme conditions of OS may be required for a loss of Srx to have cellular consequences. The duration of OS exposure and the source of OS may determine the extent to which Srx is recruited as part of the antioxidant response. Another possibility is that drugs such as H_2O_2 may predominantly affect the digestive organs, where Srx does not play a major role in defence against OS. To address whether other tissues are adversely affected by *Srx*

mutations, tissue specific expression of NOX enzymes could be performed in the background of WT and *Srx* mutant flies, followed by the appropriate assays to look for diminished function and increased OS.

The subtle sensitivity of *Drosophila Srx* mutants to H_2O_2 contrasts the sensitivity of specific *Drosophila Prdx* mutants. Downregulation of *Drosophila Prdx2*, *Prdx3*, and *Prdx4* using RNAi techniques causes reductions in longevity and sensitivity to OS (Kayashima and Yamakawa-Kobayashi, 2012; McGinnis et al., 2021; Radyuk et al., 2010, 2001). Conversely, downregulation of *Prdx1* does not induce such phenotypes (McGinnis et al., 2021). Srx may preferentially reduce Prdx1 as hyperoxidized, inactivated Prdx2-4 enzymes are likely to produce more severe phenotypes. Alternatively, it may be that the transcription and translation of Prdx isoforms in general is sufficient to regenerate reduced Prdx enzymes and maintain antioxidant defences. In this instance, Srx may play more of a regulatory role to affect the chaperone function of these enzymes, rather than a protective role against ROS.

The reduced longevity of *Srx* mutants fed H_2O_2-containing sucrose solution could be attributable to the altered redox status of substrates other than Prdx, given that Akter et al., (2018) identified several novel putative substrates. This notion is supported by the reduced longevity of flies that ubiquitously overexpress *Srx*, which should theoretically promote the reduced state of Prdx enzymes to assist in their antioxidant role. Srx substrates such as DJ-1 are known to confer resistance to OS. *Drosophila* possess two orthologous genes for mammalian DJ-1: *DJ-1α* and *DJ-1β*. DJ-1β is ubiquitously expressed in flies, and *DJ-1β* knockout mutations display sensitivity to Paraquat (Meulener et al., 2005). Srx could regulate the redox state and function of DJ-1β to influence sensitivity to OS.

The evidence presented in this chapter seems to suggest that Srx is dispensable for regulating the overall redox state of cells in *Drosophila*. H_2O_2 levels and redox-sensitive Nrf2 signalling are unaffected by *Srx* mutations. The literature around this subject provides mixed support for these ideas. In agreement with my findings, *Srx* mutant mice do not exhibit any obvious abnormalities under standard laboratory conditions (Planson et al., 2011). However, multiple mammalian *in vitro* studies have shown Srx to play an important role in defending against OS in both neural and non-neural tissue (see Chapter 1.2.6.5). It may be that Srx has different roles in mammalian and invertebrate cells or different cell types.

Future experiments should determine whether *Srx* mutations affect NADPH concentrations in cells or tissue homogenates. Higher ROS levels will result in more antioxidant enzymes requiring reduction, for which NADPH is the principal electron donor. This will promote the formation of intracellular NADP+. Commercially available kits, such as the NADP/NADPH Glo Assay (Promega, G9081), could be used to observe whether NADPH levels are perturbed in *Srx* mutant homogenates. In this paradigm, the amount of NADPH is indirectly measured through incubating lysates with proluciferin reductase enzymes and the associated substrate. The reductase enzymes reduce the substrate to luciferin in the presence of lysate-sourced NADPH. Luciferin can then be quantified using luciferase enzymes, with the light production proportional to the amount of NADPH in the lysate.

Future research should also observe whether alternative OS-inducing pharmacological agents, such as DEM and Paraquat, generate similar phenotypes as H_2O_2. Experiments should also be repeated with extensive backcrossing of *Srx* mutant and *UAS-Srx.FLAG* transgenic flies to determine whether differing genetic backgrounds are responsible for the differences in longevity.

3.3.3. *Drosophila Srx* mutations attenuate AP-1 signalling

I found that *Srx* mutations decreased DsRed.T4 fluorescence in homogenates derived from flies expressing a *TRE-DsRed.T4* transgene, indicating that AP-1 signalling was attenuated. AP-1 signalling is redox-sensitive and receives modulatory input from a variety of converging signalling pathways. JNK, a MAPK, phosphorylates and activates AP-1 components such as jun and fos to promote synapse growth at the *Drosophila* NMJ (Milton et al., 2011; Sanyal et al., 2003, 2002; Ugbode et al., 2020). I did not observe elevated ROS levels or activation of Nrf2 signalling in *Srx* mutant flies, so the diminished AP-1 signalling likely does not relate to increased ROS in cells as a whole. Instead, hyperoxidation of yet to be identified Srx substrates could account for decreased AP-1 activity.

The *Srx* mutations may decrease AP-1 signalling through modulating the oxidation state of Prdx, Trx, and AP-1, which has been observed in Schizosaccharomyces pombe (Fission yeast). Fission yeast possess a singular cytosolic typical 2-Cys Prdx enzyme named Tpx1, a Trx orthologue named Trx1, and a Srx orthologue named Srx1. Day et al. (2012) observed that H_2O_2-induced oxidation of Trx1 was suppressed by Tpx1 mutations, suggesting that Tpx1 directly oxidises Trx1. Oxidised Trx1 is unable to reduce alternative substrates like Mxr1, a mitochondrial peptide methionine sulfoxide reductase (Msra) orthologue. Mxr1

reduces methionine sulfoxide in mitochondria to enhance cell survival under conditions of OS. In this manner, Tpx1 hyperoxidation is crucial for redirecting Trx1 to substrates critical for protection against extreme OS. Yeast Trx1 was found to regulate the oxidation state and nuclear localisation of a bZIP protein analogous to AP-1 constituents, named Pap1 (pombe AP-1). Intramolecular disulphide bonds in Pap1 obstruct nuclear export signals to prevent Exportin-1 binding, which promotes nuclear aggregation (Castillo et al., 2002). It is not clear whether Trx1 reduces Pap1 directly in yeast, as co-immunoprecipitation experiments and *in vitro* biochemical assays have not been conducted to definitively prove a catalytic interaction.

Day et al. (2012) also characterised the contribution of Srx1 to controlling Trx1 activity. Constitutive overexpression of Srx1 diminishes hyperoxidised Tpx1 to promote dimer formation and diminish the survival of yeast exposed to H_2O_2. The formation of such Tpx1 dimers facilitates Trx1 oxidation and Pap1 oxidation. *Drosophila Srx* mutations may decrease AP-1 signalling via a similar mechanism, promoting hyperoxidised Prdx enzymes, as reported by McGinnis et al. (2021), that cannot oxidise Trx. Trx would then be redirected towards other substrates to promote AP-1 reduction and attenuate AP-1 signalling (see Figure 3.9). It is unclear whether OS induces disulphide bonds in AP-1 components to inhibit nuclear export and enhance nuclear localisation in *Drosophila* or mammals, which has been demonstrated in fission yeast.

Overall, the model proposed by Day et al. (2012) reinforces the importance of ROS as a signalling molecule in controlling the transcription of AP-1 targets. Moderate ROS enhances AP-1 signalling and the transcription of targets like *Srx* (Papadia et al., 2008). Conversely, severely high ROS levels, which exceed the reductive capacity of the Srx-Prdx axis, hyperoxidise Prdx, diminish Prdx-Trx interactions, and then attenuate AP-1 signalling.

As such, the Srx-Prdx-Trx axis may function to complete a negative feedback loop, limiting the duration of AP-1 signalling and enhancing cell survival by the reduction of critical Trx substrates. Given that many antioxidant proteins are AP-1 targets, this system may exist to avoid quenching ROS levels to such an extent that their function as signalling molecules is repressed. ROS homeostasis is maintained by such a system. Srx functions in this system as a 'gate-keeper,' whereby it's reductive capacity determines the threshold for the repression of the AP-1 signalling and the reduction of critical substrates for cell survival. Future research should determine if this system is relevant to specific cell types that exhibit different metabolic profiles and antioxidant protein expression.

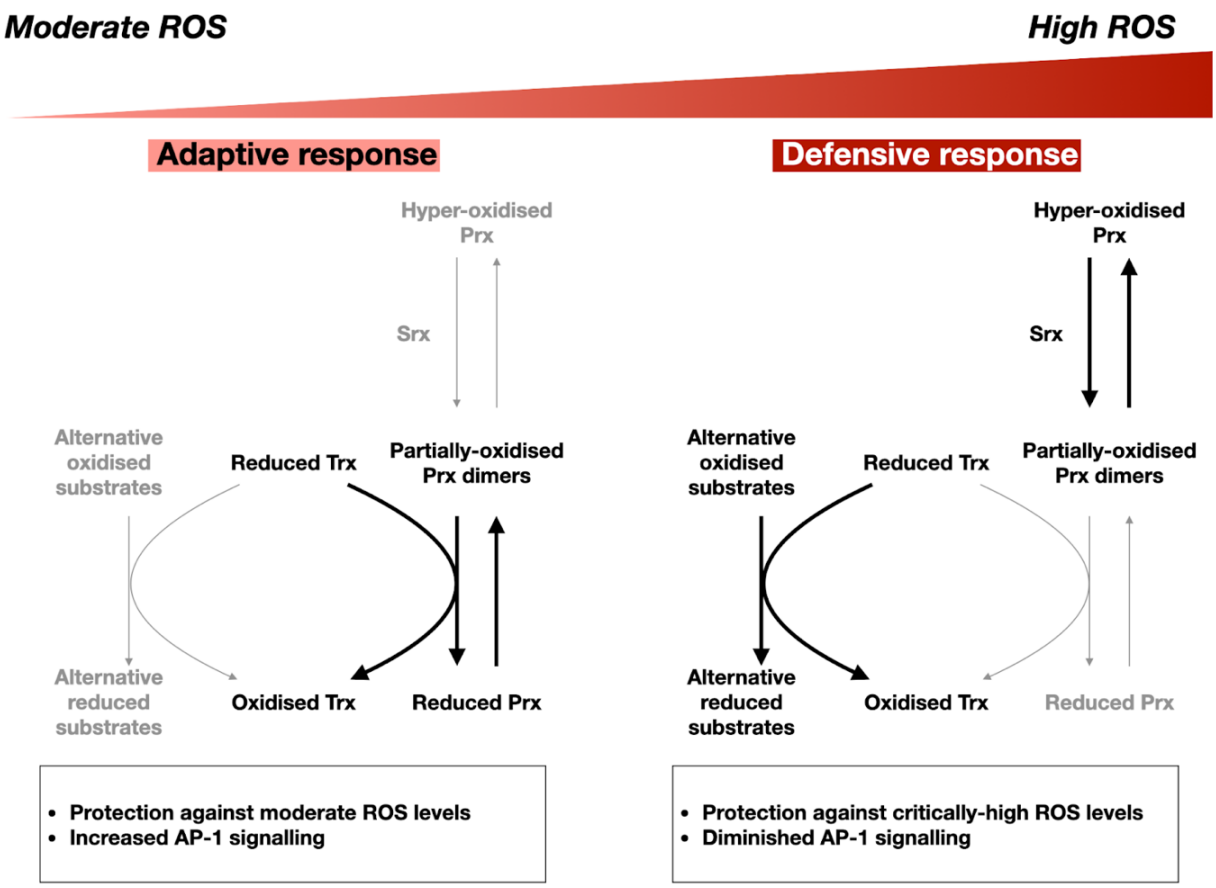

Figure 3.9. Proposed model of AP-1 signalling regulation by the Srx-Prdx-Trx axis.

Under moderate ROS levels, Prdx enzymes undergo partial oxidation as part of an adaptive response, forming dimers that are readily reduced by Trx. Under conditions of OS, hyperoxidation of Prdx reduces the proportion of Prdx dimers. Thus, Trx engages with alternative substrates to reduce them, many of which are critical for cell survival under extreme OS, such as Msra. This also appears to diminish AP-1 signalling, but it has not been conclusively resolved whether this is a consequence of Trx directly reducing AP-1 components. In this model, Srx exerts control over Prdx oxidation to modulate Trx activity, the defence state to OS in cells, and AP-1 signalling. Loss of Srx may increase the proportion of hyperoxidised Prdx enzymes, even under conditions with moderate ROS levels, to promote Trx redirection to alternative substrates and diminish AP-1 signalling. Figure is adapted from (Day et al., 2012).

The theory that Srx and Prdx function to redirect Trx activity to protect against OS, formulated by Day et al. (2012), differs from the 'floodgate hypothesis' proposed by Wood et al. (2003). Wood et al. (2003) postulated that hyperoxidation of Prdx allows H_2O_2 accumulation for modulation of signalling pathways, or to regulate the chaperone activity of Prdx enzymes. It is possible that Srx regulates both H_2O_2 signalling and directs the activity of Trx to modulate AP-1 signalling. The latter point could be tested experimentally by generating experimental flies that combine *Srx* mutations with mutations that induce OS and enhance JNK/AP-1 signalling to cause overgrowths at the *Drosophila* NMJ. Such mutations include those to the genes *spinster*, *sod1*, and *sod2* (Milton et al., 2011). If *Srx* mutations rescue the increased neuron growths, this indicates that Srx attenuates AP-1 signalling. The oxidation state of c-Jun and c-Fos components could then be investigated by incubating protein lysates derived from the aforementioned experimental flies with 4-acetamido-4′-maleimidylstilbene-2,2′-disulfonic acid (AMS). AMS conjugates to free thiols in protein lysates to increase the molecular weight of proteins by approximately 500 Da (Denoncin et al., 2013). Differences in the migration of the AP-1 components in western blots would demonstrate changes to protein oxidation state and could help to validate the model proposed Day et al. (2012), whereby the Srx-Prdx-Trx axis regulates AP-1 component oxidation states and signalling.

A weakness of this study is that it did not explore whether over-expression of Srx increases activation of AP-1 signalling in *Drosophila*. Overexpressing Srx should promote the reduced state of Prdx enzymes to indirectly promote the oxidation of Trx, and AP-1 signalling. In this scenario, AP-1 signalling would be enhanced. Day et al. (2012) found that Srx overexpression in yeast inhibited the H_2O_2-induced hyperoxidation of Tpx1 and had a detrimental effect on the survival of yeast cells treated with H_2O_2. However, Srx over-expression did not affect the viability of Tpx1 mutant cells. Similarly, my research found that overexpression of Srx diminished the survival of *Drosophila* fed sucrose solution containing H_2O_2. The expression of *Drosophila* AP-1 targets, such as the JNK phosphatase puckered, could be observed using qPCR or western blots to determine if there is increased AP-1 signalling following genetic manipulation of Srx levels. Validating these findings in a mammalian system would also elucidate whether this mechanism is conserved in mammalian organisms.

Future work should address whether the control of AP-1 signalling by *Srx* occurs in specific tissues and cell types, particularly in neurons. This may be achieved using the *TRE-DsRed.T4* transgene in the background of WT and *Srx* mutant flies. Brains could be dissected out of larval or adult flies and immunohistochemistry techniques could be used to observe the relative fluorescence levels. Signals may need to be potentiated using primary antibodies that

target the DSRed.T4 fluorescent protein. Similarly, such techniques could also be used with WT and *Srx* mutant flies carrying the *gstD1-GFP* transgene in the background to see if Srx controls Nrf2 signalling within certain tissues.

To conclude, the data presented here suggest that *Srx* mutations diminish AP-1 signalling in *Drosophila*. It is possible that Srx positively regulates AP-1 signalling through maintaining partially oxidised Prdx enzymes, which can oxidise Trx. The oxidation of Trx then prevents it from reducing alternative substrates that affect AP-1 signalling. Future research should determine whether Trx directly reduces AP-1 components in *Drosophila* and mammalian systems to fully characterise the contribution of Srx to regulating defence against OS.

4. Neurological and morphological phenotypes in *Drosophila Srx* mutants

The experimental findings of the previous chapter suggest that *Drosophila Srx* null mutants are sensitive to dietary H_2O_2 but do not exhibit differences in cellular H_2O_2 levels or OS-induced Nrf2 signalling. *Srx* mutants did, however, show attenuated activation of AP-1 signalling. Given the importance of AP-1 signalling in the nervous system, in this chapter I investigated the neurological phenotypes of *Srx* mutants by examining both behavioural and electrophysiological outputs of neuronal function.

4.1. Introduction

ROS and redox-sensitive signalling pathways regulate several aspects of neuron function, including synaptic plasticity. Application of small concentrations of H_2O_2 to rat hippocampal slices enhances long-term potentiation (LTP), which is thought to underpin learning and memory (Kamsler and Segal, 2003). JNK/AP-1 signalling regulates neurotransmission in *Drosophila*. The expression of a dominant-negative *fos* transgene, a component of AP-1 dimers, in neurons prevents OS-induced diminishments in neurotransmission at the *Drosophila* larval NMJ (Milton et al., 2011).

Srx null mutant mice do not exhibit any overt abnormalities under standard laboratory conditions (Planson et al., 2011). However, these mice have not been comprehensively screened for neurological defects and as such the neurophysiological roles for Srx remain unclear. Work described in this chapter sought to exploit the multitude of well-characterised electrophysiological and behavioural paradigms established to screen for neurological dysfunction in *Drosophila melanogaster*, to address whether Srx is important to the function of neurons or neural networks.

Drosophila locomotion is frequently used to screen for functional abnormalities following genetic manipulation techniques. Flies exhibit an innate escape response upon mechanical agitation, whereby they climb upwards. This is frequently used to observe age-related locomotive dysfunction, which is associated with Parkinson's Disease and ALS *Drosophila* models (Madabattula et al., 2015). Similarly, the crawling speed of larvae is used to observe

motor dysfunction too, although this is less useful for observing age-related changes (Kohsaka, 2023).

The visual system of *Drosophila* can be readily probed for changes in neuron function using electrophysiological recordings. Electroretinograms (ERGs) have previously been used to screen for changes in neuron excitability and synaptic transmission. Recording electrodes are placed against the compound eye of flies and the response to light stimuli is recorded. Response traces exhibit characteristic sustained depolarisation, corresponding to the activation of first-order photoreceptors, and on- and off-transients that correspond to the activation and de-activation of second-order lamina neurons, respectively (Vilinsky and Johnson, 2012). Whilst this technique is informative and able to detect major changes to neurotransmission, the technique can be prone to a large signal-to-noise ratio and artefacts.

Steady-state visually evoked potentials (SSVEPs) offer an alternative, more sophisticated approach to probing the electrophysiological properties of the *Drosophila* nervous system. In this technique, *Drosophila* are presented with a harmonic light stimulus composed of multiple wavelengths. Response traces are recorded and undergo a fast fourier transform (FFT) to break them down into their individual components. Via genetic silencing of specific neuron types, it has been established that the relative amplitude of the FFT peaks corresponds to the activity of specific neuron populations in the visual system. 1F1 peaks correspond to photoreceptor activity, whereas 2F1 peaks correspond to the response of second order lamina neurons (Afsari et al., 2014). Many hundreds of stimulus events are averaged together and out-of-band noise is eliminated from the analysis, rendering the technique more accurate than ERGs.

In this chapter I also investigate whether Srx has an important role in controlling the circadian rhythms of neurons in *Drosophila*, which can be observed through the locomotion activity of flies. Circadian rhythms are biological events that align with a period length of approximately 24 hours, which are driven by molecular ‘clocks’ or ‘pacemakers.’ These rhythms allow organisms to predict changes in their environment and adjust their activity accordingly. For instance, increasing activity at specific periods of the day may help to avoid predators (Tataroglu and Emery, 2014). A defined group of neurons control circadian locomotor behaviour in *Drosophila* that can be entrained to light stimuli detected by photoreceptors in the compound eye (Helfrich-Förster et al., 2001). Circadian locomotor activity of flies can be monitored using *Drosophila* activity monitors (DAMs, TriKinetics) that house flies in narrow tubes and record activity via the interception of infrared beams.

At the molecular and cellular level circadian rhythms are driven by transcription-translation feedback loops (TTFLs) that operate in all *Drosophila* cells (see Chapter 1.4.7). In addition, oscillations in metabolism, driven by the pentose phosphate pathway (PPP) also maintain oscillations in circadian rhythms independently of TTFLs. The PPP generates NADPH, the principal electron donor for reduction of antioxidant enzymes, that drives oscillations in oxidation state of Prdx enzymes (Edgar et al., 2012; Rey et al., 2016). As Srx regulates the oxidation state of Prdx enzymes, this may have implications for circadian rhythms, which this research sought to address. The role of Srx in maintaining cellular circadian oscillations has already been the subject of research. Kil et al. (2015) found that Srx and Prdx3 undergo antiphasic oscillations in the mitochondria of adrenal cortex cells, which is important for regulating the release of glucocorticoid hormone levels in the blood of mammals to prepare them to deal with and recover from stress (see Chapter 1.2.6.5). It is unknown whether Prdx3 and Srx perform a similar role in neurons and what consequences this would have for behavioural rhythms. I used the new *Srx* mutants that I generated to evaluate the role of Srx on *Drosophila* locomotion activity over circadian time.

Redox-sensitive signalling pathways regulate neuronal development and neuronal structural plasticity. Oswald et al. (2018) identified PI3K signalling downstream of the redox-sensor DJ-1β. PTEN, which antagonises PI3K signalling, is redox-sensitive and regulated by Prdxs (Nguyen Huu et al., 2021). One readout of the PI3K pathway activity is apparent at the *Drosophila* wing, the size of which is promoted by PI3K/AKT signalling (see Chapter 1.2.3.2). Overexpression of the PI3K catalytic subunit Dp110 increases wing size (Gao et al., 2000). Conversely, overexpression of PTEN, which antagonises PI3K signalling, or a dominant-negative Dp110 isoform, decreases wing size (Gao et al., 2000). These changes were also reflected in the size of the bristles that surround the wing perimeter. Mutations in *Dakt1*, the *Drosophila AKT* orthologue, suppress the increased bristle growth observed in PTEN mutants (Gao et al., 2000). PI3K/AKT/mTOR signalling has also been shown to increase growth and dendritic arborisation in rat hippocampal neuron cultures through increased protein synthesis (Jaworski et al., 2005). Therefore, altered wing morphology may reflect changes in signalling pathways that also affect neuron development.

The aforementioned paradigms were applied in this study to screen *Drosophila Srx* mutants for neurological and morphological abnormalities. This would provide a better understanding as to the significance of Srx for neuron function and elucidate its potential involvement in signalling pathways.

4.2. Results

4.2.1. *Srx* mutants have altered negative geotaxis response

Drosophila exhibit an innate escape response induced by mechanical stimulation, whereby they climb upwards. The negative geotaxis response can be used to observe differences in locomotion ability and coordination, which is largely controlled by dopaminergic and glutamatergic neural networks (Sun et al., 2018). Here, I assessed whether loss of Srx altered this response, which may suggest abnormal neuron function.

Loss of Srx enhanced the negative geotaxis response of *Drosophila* (Figure 4.1.A) with a much higher proportion of flies reaching the threshold distance (10 cm) within the stipulated time (5 seconds). Control flies had an average climb success rate of 50.3% (±4.74%). $Srx^{\Delta 1\text{-}2}$ and $Srx^{\Delta 3}$ mutants exhibited higher success rates of 78.6% (±2.5%) and 75.7% (±2.71%), respectively. This suggested Srx was important for locomotor function, which warranted further experiments to dissect the cell types responsible for the enhanced climbing phenotype.

Expressing various *Gal4* transgenes with *UAS-Srx.FLAG* in the *Srx* mutant background allowed for attempts to rescue this phenotype in a cell-specific manner (Figure 4.1.B). Similarly to the initial experiment, *Srx* mutants displayed enhanced climbing performance. 67.1% (±5.5%) of $Srx^{\Delta 1\text{-}2}$ flies and 63.8% (±5.0%) of $Srx^{\Delta 3}$ flies reached the 10 cm mark within 5 seconds. These scores were nearly double that of the 31.2% (±3.3%) average achieved by cohorts of WT flies.

These phenotypes were rescued by the pan-neuronal expression of *Srx* using the *nSyb-Gal4* and *UAS-Srx.FLAG* transgenes in mutant backgrounds. The average $Srx^{\Delta 1\text{-}2}$ and $Srx^{\Delta 3}$ scores decreased by 30.4% and 24.0%, respectively. Therefore, the altered negative geotaxis response relates to changes in nervous system function. Similar reductions were also seen with use of the *OK6-Gal4* transgene for expression in motor neurons. Average $Srx^{\Delta 1\text{-}2}$ mutant success scores decreased by 32.1%, whereas average $Srx^{\Delta 3}$ scores decreased by 22.6%.

Expression of the rescue construct in the mutant backgrounds without a functional Gal4, via co-expression of ‘empty vector’ (*EV*), resulted in higher success scores relative to WT flies. This validated that there was no ‘leakiness’ of the *UAS-Srx.FLAG* construct (Scialo et al., 2016). Although the *EV* insertion site is on the third chromosome, rather than the second

chromosome like the *UAS-Srx.FLAG* transgene, this still reinforces the findings made using the mutant stocks as it shows a functional Gal4 is needed to facilitate the rescue.

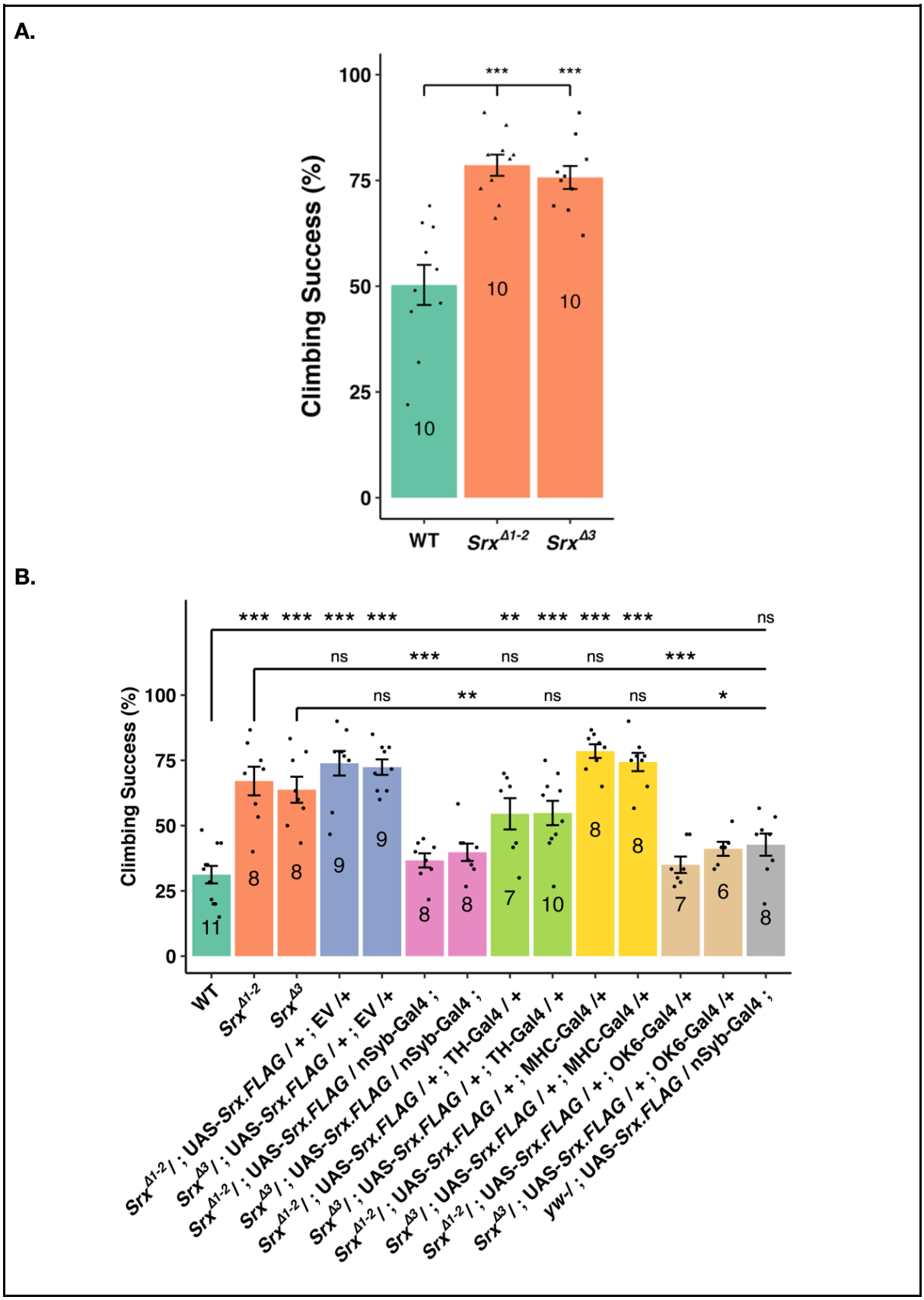

Figure 4.1. Aberrant motor neuron function enhances negative geotaxis response in *Srx* mutants.

A. *Srx* mutants exhibit enhanced negative geotaxis responses (One-way ANOVA, df=2, F=20.2, p<0.001***, with post-hoc Tukey's HSD test comparison to WT, p<0.001***). **B.** *Srx* mutants still exhibit increased climbing ability when the *UAS-Srx.FLAG* transgene is expressed in the background in the absence of a Gal4 driver, validating the phenotype and proving there is no UAS 'leakiness.' Pan-neuronal rescue using the *nSyb-Gal4* and *UAS-Srx.FLAG* transgenes rescues the enhanced performance in the climbing assay, as does use of *OK6-Gal4*. Use of *TH-Gal4* and *MHC-Gal4* for dopaminergic and muscular expression, respectively, did not rescue the phenotype. Collectively, this data shows the enhanced climbing phenotype is caused by changes in motor neuron function (One-way ANOVA df=13, F=18.91, p<0.001***, with posthoc Tukey's HSD test for multiple comparisons, p<0.05*, p<0.01**, p<0.001***). Sample sizes are presented, and bars represent mean ± SEM.

Two Gal4 drivers also failed to rescue this phenotype. Namely *TH-Gal4*, for dopaminergic expression of the rescue construct, and *MHC-Gal4*, for muscular expression. Therefore, the altered negative geotaxis response was not caused by aberrant dopaminergic neuron or muscle function. Over-expressing Srx in the neurons of flies, using *nSyb-Gal4*, did not significantly change climbing performance, with these flies displaying an average performance of 42.7% (±4.2%).

4.2.2. Larval crawling speed is not affected by *Srx* mutations

The crawling speed of third instar larvae was recorded to determine whether the enhanced locomotion of *Srx* mutants, which was observed in the negative geotaxis assay, was also observed at the larval stage. Larvae crawling tracks were recorded for 60 seconds and the speed was calculated accordingly (see Figure 4.2). There were no differences in the genotypes; control larvae exhibited a mean crawling speed of 0.412 mm/s (±0.035 mm/s). $Srx^{\Delta 1\text{-}2}$ and $Srx^{\Delta 3}$ mutants exhibited average crawling speeds of 0.544 (±0.044 mm/s) and 0.460 mm/s (±0.055 mm/s), respectively.

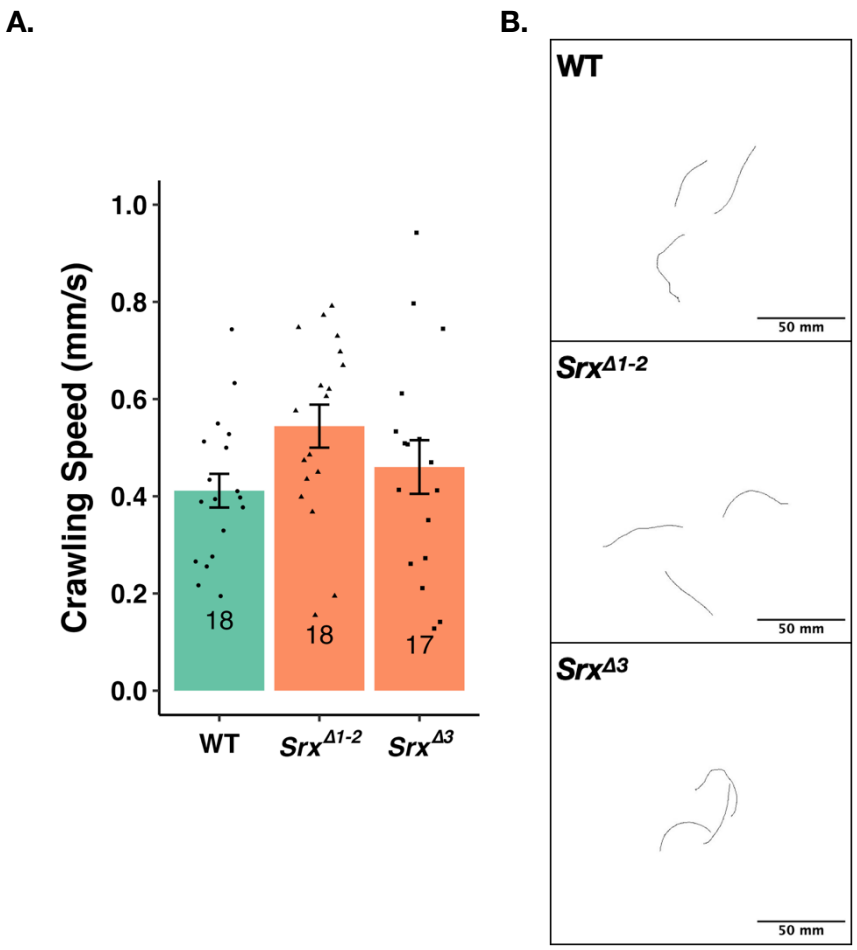

Figure 4.2. Third instar larvae crawling speed is unaffected by *Srx* mutations.
Srx mutants did not exhibit significantly different crawling speeds to WT larvae (one-way AVOVA, df=2, F=2.26, p=0.12, ns). **B.** Exemplar traces of larvae recorded for 60 seconds. Sample sizes are presented, and bars represent mean ± SEM.

4.2.3. *Srx* mutants have perturbed visual system function

The behaviour of the *Srx* mutant flies suggested altered neurological function in *Drosophila*. Therefore, neurotransmission was assessed in the visual system of flies. Steady-state visually evoked potentials (SSVEPs) were performed to assess the function of distinct neuron populations in the *Drosophila* visual system. In this assay FFT analysis at the input frequency (1F1) and twice the input frequency (2F1) identifies the response of photoreceptors and lamina neurons, respectively (Figure 4.3.A).

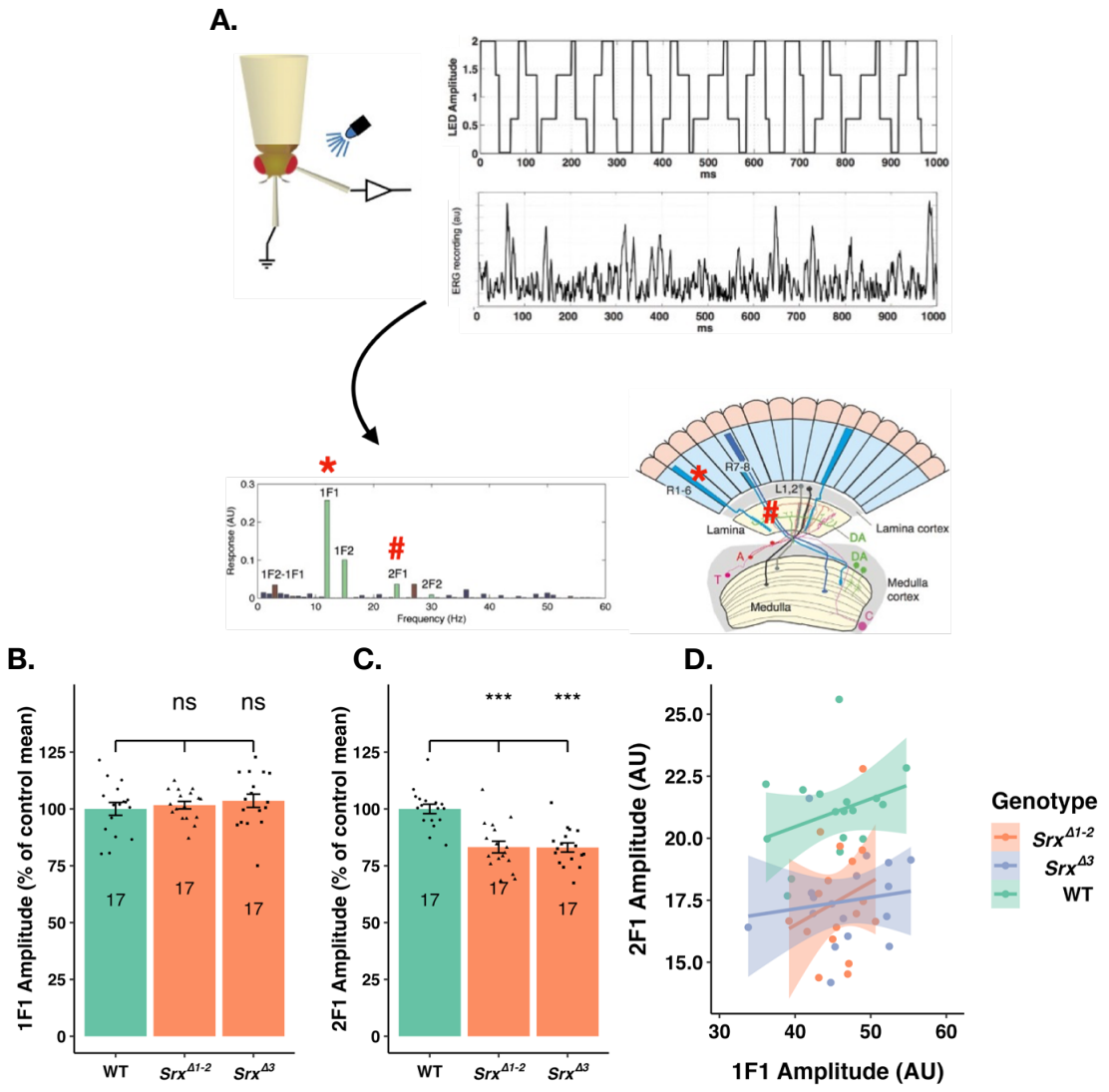

Figure 4.3. Loss of *Srx* perturbs the *Drosophila* visual system response to light stimuli. **A.** Recording and analysing *Drosophila* visual responses with SSVEPs. Harmonic light stimuli are presented to immobilised *Drosophila*. FFT breaks down response traces into individual components that reflect the activity of specific neuron populations in the visual system of flies. **B.** Photoreceptor responses, which correspond to 1F1 peak amplitudes, are unaffected by loss of Srx (one-way ANOVA, df=2, F=0.5, p=0.498, ns). **C.** Lamina neuron responses are diminished in *Srx* mutants, as shown by reduced 2F1 amplitudes (one-way ANOVA: df=2, F=19, p<0.001***, with post-hoc Dunnett's test comparison to WT, p<0.001***). For all of the graphs, sample sizes are presented, and bars represent mean ± SEM. **D.** Comparing the relationship between 1F1 and 2F1 amplitudes did not reveal significantly positive correlations (WT: r=0.197, $Srx^{\Delta 1-2}$: r=0.580, $Srx^{\Delta 3}$: r=0.358), as determined by Pearson's correlation coefficient. Therefore, Fisher's R to Z transformation is not an appropriate form of analysis for this data set.

Comparison of the photoreceptor (1F1) responses revealed that there were no significant differences between WT flies and *Srx* mutants (Figure 4.3.B). $Srx^{\Delta 1\text{-}2}$ and $Srx^{\Delta 3}$ mutants had average amplitudes that were 101.7% (±1.6%) and 103.6% (±2.9%) of the average WT response, respectively. Conversely, lamina neuron response was significantly reduced in the mutants (Figure 4.3.C). $Srx^{\Delta 1\text{-}2}$ and $Srx^{\Delta 3}$ mutants had mean 2F1 amplitudes that were 83.2% (±2.6%) and 83% (±2.0%) of the mean response recorded for WT flies.

Photoreceptors in the *Drosophila* eye synapse onto the second order lamina neurons. Therefore, increased activation of the photoreceptors should correlate with increased lamina neuron activation. Plotting the relationship between the 1F1 and 2F1 amplitudes, which correspond to the activity of these neuron populations, did not reveal significant correlations that were comparable via Fisher's R to Z transformation (Figure 4.3.D). Taken together, this experiment suggests that loss of *Srx* disrupts neurotransmission between first order photoreceptors and second order lamina neurons. Alternatively, the activity of lamina neurons could be selectively perturbed following loss of Srx in *Drosophila*.

4.2.4. Srx does not regulate *Drosophila* circadian rhythms

To see if Srx plays a role in regulating circadian rhythms, the circadian locomotor activity of *Drosophila* was analysed using a locomotor activity monitoring system (TriKinetics). Flies were entrained for 4 days in 12h:12h light:dark (LD) cycles followed by 7 days in constant darkness (DD). The average circadian period, determined from DD data, for both the WT and $Srx^{\Delta 3}$ mutant flies was 23.7 hours (WT: ±0.05 hours, $Srx^{\Delta 3}$: ±0.13 hours) (Figure 4.4.A). This does not demonstrate a significant difference in the ability to maintain circadian rhythmicity after the removal of a zeitgeber. The strength of the circadian rhythms was also not significantly different in $Srx^{\Delta 3}$ mutants (Figure 4.4.B). The average power for WT flies was 1.33 AU (±0.10), but for $Srx^{\Delta 3}$ mutants this was 11.3% lower at 1.18 AU (±0.04).

The average daily crosses in the apparatus was not significantly affected by *Srx* mutations during the LD stage of the experimental paradigm (Figure 4.4.C). The average number of crossings for WT flies was 1238.7 (±88.9), whereas $Srx^{\Delta 3}$ mutants had an average that was 11.8% higher at 1385.0 (±83.6) crossings. The number of crossings during the DD stage of the experiment was similarly unaffected (Figure 4.4.D). The average number of crossings for WT flies was 1093.6 (±97.2), whereas $Srx^{\Delta 3}$ mutants had an average that was 19.5% higher at 1306.6 (±85.5) crossings.

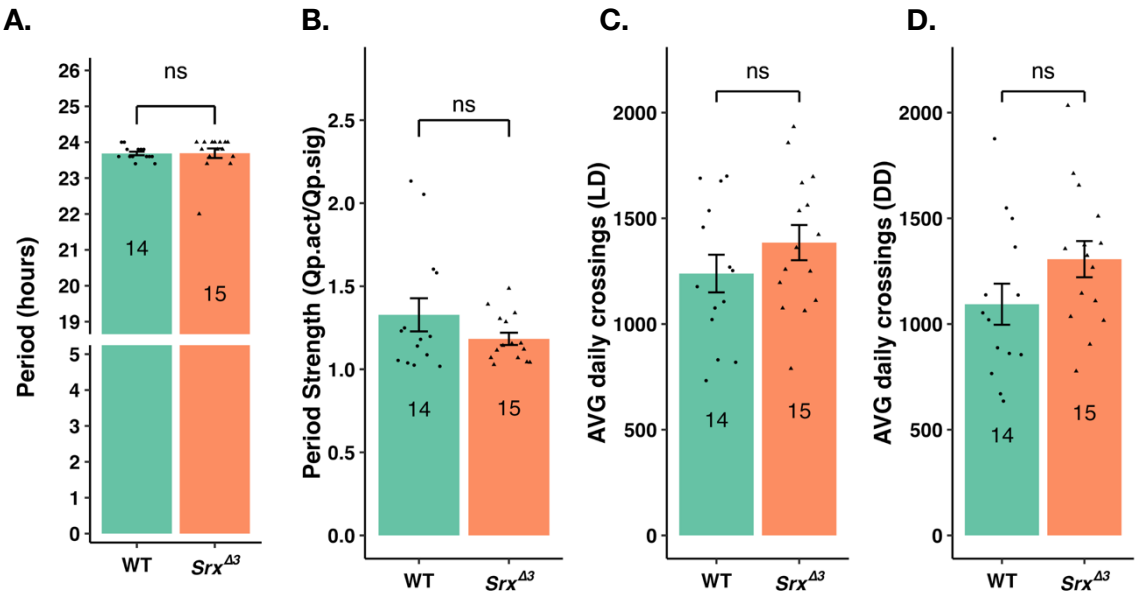
A.
B.
C.
D.
ns
Period (hours)
Period Strength (Qp.act/Qp.sig)
AVG daily crossings (LD)
AVG daily crossings (DD)
14
15
WT
Srx^Δ3

E.

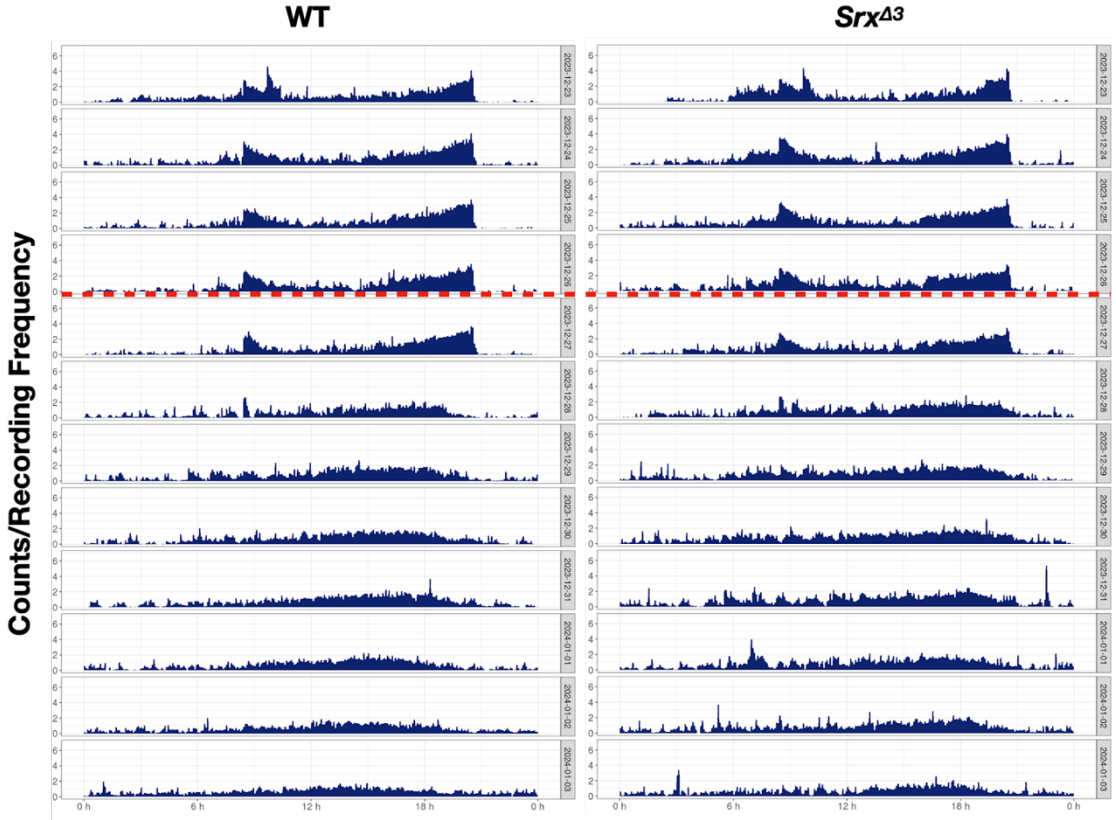
WT
Srx^Δ3
Counts/Recording Frequency
0 h
6 h
12 h
18 h

Figure 4.4. Srx does not regulate *Drosophila* circadian rhythms.
A. *Srx*$^{\Delta 3}$ *Drosophila* do not exhibit a significantly different period in DD, following 4 days of LD conditioning (Wilcoxon rank sum test, W=77, p=0.214, ns). **B.** The strength of these circadian periods is also unaffected by *Srx*$^{\Delta 3}$ mutations (Wilcoxon rank sum test, W=116, p=0.652, ns). **C.** The mean daily crossings through the apparatus did not differ for the LD period (t-test, t=-1.202, df=27, p=0.240, ns). **D.** Similarly, the average number of crossings also did not differ for the DD period (t-test, t=-1.651, df=27, p=0.110, ns). For all the graphs, sample sizes are presented, and bars represent mean ± SEM. **E.** Representative actograms formed from the mean number of crossings for WT and *Srx*$^{\Delta 3}$ mutants at the indicated time points, with crossings grouped into 1-minute bins. The red dashed line indicates the point at which DD began.

4.2.5. Srx regulates *Drosophila* wing size

To determine the relevance of Srx in regulating wing size, a morphological trait controlled by redox-sensitive PTEN signalling, the length of *Drosophila Srx* mutant wings was compared to WT flies. The length between the intersection of longitudinal veins L2 and L3, and the apical end of L3 was measured to record wing size. This research found that *Srx* mutations increased the length of fly wings (Figure 4.5.A). WT flies exhibited an average length of 1.50 mm (±0.005 mm). The mean length of *Srx*$^{\Delta 1\text{-}2}$ mutant *Drosophila* was 8% bigger at 1.62 mm (±0.005 mm). Similarly, average wing lengths for *Srx*$^{\Delta 3}$ mutant *Drosophila* was 7.33% bigger at 1.61 mm (±0.004 mm). Conversely, ectopic expression of Srx, using the *Act5C-Gal4* and *UAS-Srx.FLAG* transgenes, caused a reduction in the size of *Drosophila* wings. Srx over-expression caused the average wing size to decrease by 1.86% from 1.61 mm (±0.008 mm) to 1.58 mm (±0.005 mm) (Figure 4.5.C).

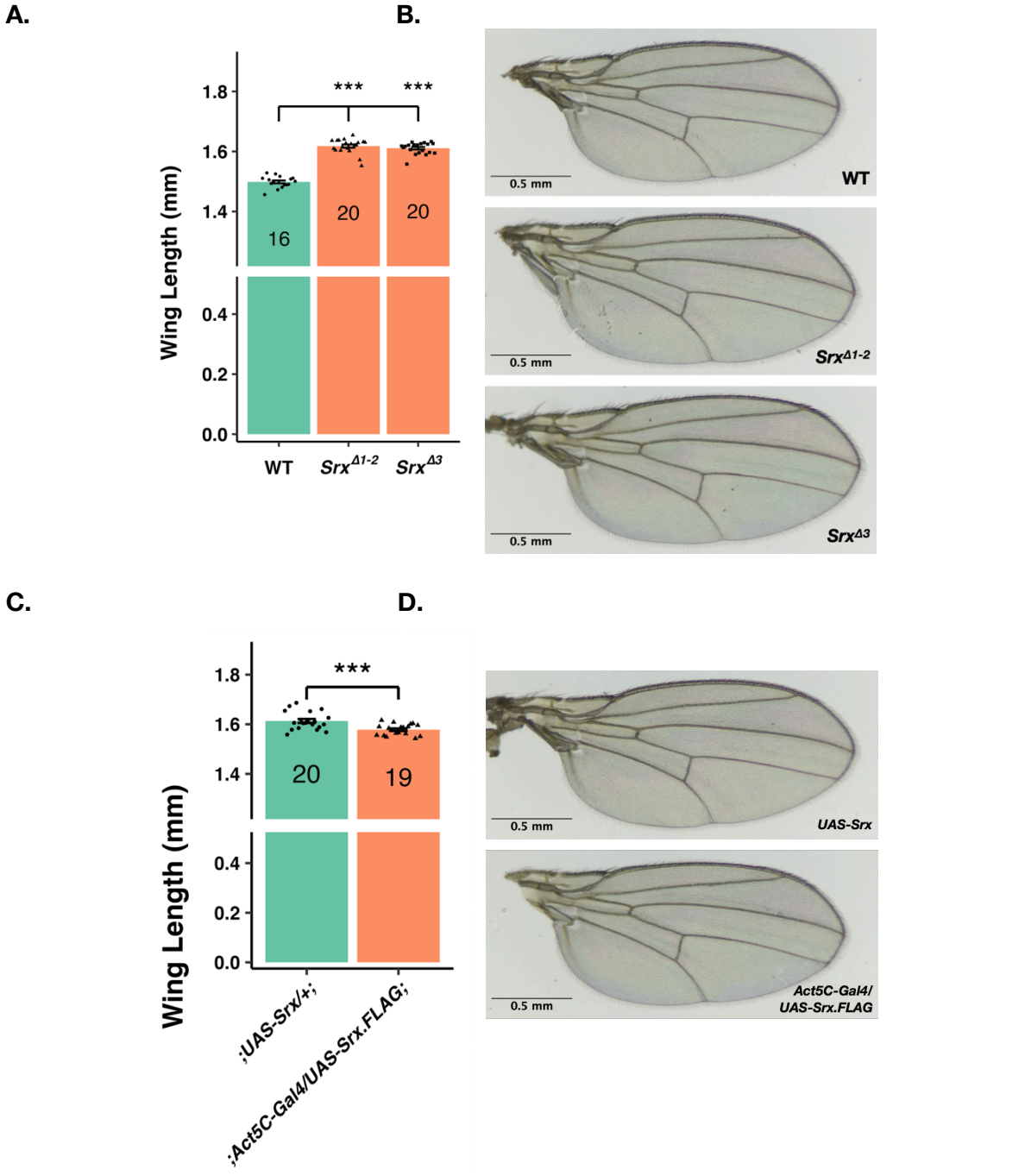

Figure 4.5. Srx regulates *Drosophila* wing size.

A. *Srx* mutations increase wing length (Kruskal Wallis, $\chi^2 = 35$, df =2, p<0.001***, with post-hoc Dunn's test comparison to WT, p<0.001***). **B.** Exemplary images of WT and *Srx* mutant fly wings. **C.** Ectopic overexpression of Srx, using the *Act5c-Gal4* and *UAS-Srx.FLAG* transgenes, decreases the size of *Drosophila* wings (Welch two sample t-test, t=4, df=32, p<0.001***). **D.** Exemplary images of control and Srx-overexpression transgenic flies. For all of the graphs, sample sizes are presented, and bars represent mean ± SEM.

4.3. Discussion

In this chapter I assessed the relevance of Srx to neuron function, using behavioural and electrophysiological assays to screen for neurological abnormalities in *Drosophila Srx* mutants. The *Srx* mutants exhibited an enhanced negative geotaxis response, perturbed neuron activity in the visual system, but unaltered circadian rhythms. Additionally, *Srx* was found to negatively regulate wing size, implicating this antioxidant enzyme in signalling pathways that affect neural development.

4.3.1. *Drosophila Srx* mutants have an altered negative geotaxis response

Here, I have shown that *Srx* mutations enhanced the negative geotaxis response of flies, which was rescued by re-expressing Srx in motor neurons. This suggests that Srx regulates the function of motor neurons. As *Drosophila* motor neurons are glutamatergic, this finding has implications for the function of the mammalian nervous system, as glutamate is the primary excitatory neurotransmitter in the human brain. Interestingly, there is little evidence to suggest that Srx is associated with neuropsychiatric or neurodegenerative diseases. Srx variants are not reported to be associated with any conditions on the NIH Genbank database (NIH, 2025). Future experiments should also determine whether the tissue-specific expression of Gal4 alone affects the climbing performance of flies, to conclusively dispel the notion that they affect this behaviour.

The increased climbing success of *Srx* mutants suggests hyperactivity of the *Drosophila* nervous system. Changes to neuron excitability and ion channel dynamics are commonly associated with seizure-like activity in the flies. Flies with mutations that affect neuron excitability may exhibit ‘bang-sensitivity,’ whereby they undergo temporary paralysis after mechanical agitation and overstimulation of sensory neurons (Ganetzky and Wu, 1982). Similarly, flies with increased neuron excitability can exhibit temporary paralysis following heat-shock at approximately 40°C (Kasbekar et al., 1987). No such phenotype was observed in *Drosophila Srx* mutants (data not shown). To conclusively rule out involvement of Srx in neuron excitability through changes in resting membrane potential, future experiments could use whole cell patch-clamping to see if membrane dynamics are altered in these mutants. Patch-clamping has been successfully performed for large ventrolateral clock neurons in the *Drosophila* brain by Buhl et al. (2016).

An interesting observation of this research was that the enhanced negative geotaxis responses of *Srx* mutant flies did not correlate with enhanced crawling speeds in *Srx* mutant third instar larvae. These contrasting phenotypes may be explained by changes to *Srx* expression in neurons during larval developmental. Srx may be expressed at low levels in neurons of the larval nervous system, whereas it may be expressed to a larger degree in neurons of adult flies. In this scenario, *Srx* mutations may only affect physiology at adult stage and not the larval stage. However, RNA-seq experiments seem to suggest that Srx is maximally expressed during the third instar larval stage at the organismal level (Brown et al., 2014). Future work should address whether there is differential expression of Srx in neurons throughout the lifecycle of *Drosophila*. This can be readily achieved using larval and adult *Drosophila* brain lysates for Western blots, using the antibody generated as part of this study (see Figure 3.5).

Previous research has characterised the role of ROS and redox-sensitive signalling pathways on the locomotion of third instar larvae. Oswald et al. (2018) found that activity-induced ROS caused overgrowths of the glutamatergic neurons at the larval NMJ, which facilitated homeostatic adaptations to the functional output of the locomotor network, as measured by crawling speed. Activity-induced ROS was generated in these assays via changes to the environmental temperature, the expression of temperature-gated ion channels, or the administration of pharmacological agents to induce OS, like DEM. *DJ-1β*$^{\Delta 93}$ mutations prevented OS-induced overgrowths at the larval NMJ, which accordingly blocked the homeostatic adaptations of crawling speed to changes in activity. DJ-1β is consequently proposed to act as a critical sensor of activity-induced ROS to integrate homeostatic changes via PI3K/PTEN signalling.

The mammalian orthologue of *DJ-1β*, DJ-1, is proposed to be a substrate of Srx. The experiments reported in this chapter did not observe changes to larval locomotion following *Srx* mutations under standard conditions. If Srx does reduce DJ-1 to modulate its function, future research should investigate the role of *Srx* mutations on the ability of crawling speed to adapt to changes in locomotor network activation and ROS production. The easiest manner to test this would be to incubate *Srx* mutants at cooler and warmer temperatures to see if crawling is maintained at a constant speed. Additionally, genetic interactions between *Srx* and *DJ-1β* can be investigated in epistasis experiments that combine mutations to both genes. If loss of Srx rescues the resistance to OS-induced changes in NMJ growth and crawling speed associated with *DJ-1β*$^{\Delta 93}$ mutations, this suggests that both proteins act within the same signalling pathways.

4.3.2. *Drosophila Srx* mutants have aberrant visual system responses

Having discovered that changes in *Srx* mutant locomotion originate in motor neurons, I went on to characterise how loss of this Srx affected neuron function using electrophysiological assays. To do so, I used the well-characterised *Drosophila* visual system, which is commonly used to assess neuron excitability and neurotransmission. By performing SSVEPs, I found that visual system function was perturbed in *Srx* mutants. Although photoreceptor function was conserved, the lamina neuron responses of *Srx* mutants were diminished.

This suggests that loss of Srx may impede neurotransmission between the photoreceptors and second-order neurons in the lamina, supplementing the behavioural data that indicated Srx regulates neuron performance. Impaired neurotransmission at motor neurons typically negatively regulates *Drosophila* locomotion (Kratschmer et al., 2021). However, the experiments described in this chapter indicate that loss of Srx leads to impaired lamina neuron function that correlates with increased locomotor response. These seemingly contrasting results may be reconciled by suggesting that Srx has different effects on different neuron types or networks. *Drosophila* photoreceptors are histaminergic and synapse onto lamina neurons (Stuart, 1999; Zhu, 2013), which also receive modulatory dopaminergic inputs (Hindle et al., 2013). Conversely, *Drosophila* motor neurons are predominantly glutamatergic (Broadie and Bate, 1995). Additionally, *Drosophila* compound eyes are continuously exposed to light in their environment, which accounts for 50% of the time under experimental conditions. This substantial period of exposure depolarises photoreceptors and may increase metabolism and ROS production in photoreceptors that is not resolved in *Srx* mutants, leading to dysfunction and diminished lamina neuron responses. Motor neurons may not be exposed to such chronic over-activation and diminished neurotransmission may not occur in the motor neuron network. However, photoreceptor excitotoxicity is likely to also perturb the function of the photoreceptors themselves, which was not observed in *Srx* mutants. The matter could be resolved by repeating the SSVEP experiments for flies reared in complete darkness to avoid chronic photoreceptor activation, rather than rearing them under 12-hour light/dark cycles. If the decreased *Srx* mutant lamina responses persist under dark conditions, this would indicate that lamina neuron function is perturbed in a fashion that is independent of neuron activity or synaptic transmission.

OS-induced, activity-dependent diminishments in neurotransmission have also been observed at the *Drosophila* NMJ. Milton et al. (2011) observed that *spinster* mutants, which demonstrate OS in neurons derived from lysosomal storage dysfunction, exhibit decreased excitatory junction potentials (EJPs) after consecutive stimulations. The expression of a dominant-negative *fos* transgene within neurons rescued this phenotype, indicating that increased OS-induced JNK/AP-1 signalling drives a decrease in neurotransmission (Milton et al., 2011). Crucially, expression of dominant-negative *fos* transgenes in neurons alone did not affect neurotransmission in the absence of *spinster* mutations. It is unlikely that *Srx* mutations diminish neurotransmission between photoreceptors and lamina neurons in a similar manner, via increased AP-1 signalling. My results from Chapter 3.3.3 indicate that loss of Srx attenuates AP-1 signalling.

A weakness of my dataset is that strong, positive correlations were not observed between 1F1 and 2F1 amplitudes for the different experimental groups. Given that lamina neuron activation derives from photoreceptor activation, one might expect to observe such correlations. These unexpected results could be attributed to the white-eyed flies used in this study, which lack the screening pigments that separate individual ommatidia. Eye pigmentation in *Drosophila* is conferred by the *white* gene that encodes a subunit of membrane-bound ATP-binding cassette transporters needed for the uptake of pigment precursors into cells, namely guanine and tryptophan (Mackenzie et al., 1999). Eye pigments function to ensure that only the ommatidia axial to light sources are activated (Stark and Wasserman, 1972). White eyes may promote peripheral photoreceptor activation and exacerbate small differences in the orientation of the flies relative to the light source, or the position of electrodes. In turn, this could affect the correlation between photoreceptor and lamina neuron amplitudes. The possible effects of eye pigmentation on SSVEPs could be addressed in future experiments by expressing a mini-white (w^{+mC}) transgene in the background of the WT or *Srx* mutant flies, to confer expression of the eye screening pigment.

Overall, my electrophysiological experiments show that Srx is important for neuron function in the *Drosophila* visual system. Future experiments should aim to elucidate the specific mechanism underlying this change.

4.3.3. *Drosophila Srx* mutants do not have altered circadian rhythms

The experiments described in this chapter found that circadian period lengths were not significantly affected by *Srx* mutations, nor were the strengths of these periods, which suggests that Srx does not regulate circadian rhythms in the nervous system of flies. Conversely, Srx is known to regulate cellular circadian rhythms in cultured mammalian cells. Antiphasic oscillations between Srx and hyperoxidised Prdx3 in the mitochondria of adrenal cortex cells control the circadian rhythms of steroidogenesis (Kil et al., 2015). It is likely that Srx and Prdx oxidation state is not relevant to circadian function in *Drosophila* neurons, which is supported by the work of McGinnis et al. (2021) who observed low levels of Prdx hyperoxidation in the heads of WT flies, as measured via western blots with antibodies complementary to hyperoxidised Prdx enzymes. However, McGinnis et al. (2021) readily observed hyperoxidation of Prdx enzymes in *Drosophila* bodies, which exhibit a circadian oscillation that is enhanced by *Srx* mutations. Therefore, Srx may regulate circadian rhythms in non-neuronal tissue.

A major caveat of the work of McGinnis et al. (2021) is that it did not resolve whether hyperoxidised Prdx oscillations in *Drosophila* bodies were reflective of changes to the oxidation state of Prdx3 enzymes specifically, as *Drosophila* Prdx1-3 all have the same molecular weight and occupy the same region of western blots. Future research should prove that the mitochondrial Prdx3 exhibits oscillations in oxidation state through the generation of transgenes expressing Prdx3 with a conjugated protein tag that increases its molecular weight to make it distinguishable from Prdx1 and 2 in western blots. If this technique was applied and demonstrated oscillations in Prdx3 oxidation state within *Drosophila* bodies, this may suggest that antiphasic oscillations of Srx and hyperoxidised Prdx3 in mitochondria are conserved across species and relevant to the function of non-neuronal cells.

The potential physiological relevance of oscillations in mitochondrial Srx and hyperoxidised Prdx might be further explored by maintaining Srx as a cytosolic protein in *Drosophila.* Mutating the nucleotides encoding the putative mitochondrial-targeting TOM20 recognition motif at the *Drosophila* Srx N-terminus (see Chapter 3.2.2), would prevent mitochondrial localisation. Molecular cloning techniques could generate pUAST constructs for injection into *Drosophila* embryos, which generate stocks expressing *UAS-Srx* transgenes with missense mutations at the TOM20 recognition motif. The aforementioned transgenes can be expressed in *Srx* mutant flies and compared to *Srx* mutants expressing a non-mutated *UAS-Srx*

transgene to elucidate any physiological processes controlled by Prdx3 oxidation state in mitochondria.

4.3.4. *Drosophila Srx* regulates wing size

The work described in this chapter found that Srx negatively regulates wing size in *Drosophila*. *Srx* mutations increased the size of wings compared to WT flies, whereas ubiquitous over-expression of *Srx* reduced wing size. This phenotype could be attributed to Srx regulating PI3K/AKT signalling, which promotes cell growth and the overall size of *Drosophila* wings. PTEN antagonises PI3K/AKT signalling. PTEN mutations, which promote PI3K/AKT signalling, increase bristle size on *Drosophila* wings, which is rescued by the co-expression of dominant-negative *AKT* transgenes (Gao et al., 2000).

Loss of Srx may alter the redox state in cells to negatively regulate wing size via inhibition of PI3K/AKT signalling. PI3K/AKT signalling is sensitive to redox changes, as intramolecular disulphide bonds can form in PTEN to inhibit its antagonistic effect (Lee et al., 2002). ROS also appears to promote the inhibition of PTEN via DJ-1β oxidation in *Drosophila*, which regulates homeostatic adaptions to OS in neurons (Oswald et al., 2018).

These findings may have implications for the role of Srx on neuron growth and structure. PI3K/AKT/mTOR signalling promotes neuron growth and neurite branching. Inhibiting the PI3K/AKT/mTOR pathway using pharmacological inhibitors targeting PI3K, AKT, and mTOR, decreases the complexity of neurite outgrowths in rat hippocampal neuron cultures. Conversely, expression of constitutively active forms of PI3K and AKT, and knockdown of PTEN via RNAi, promote dendrite branching (Jaworski et al., 2005). As Srx affects morphological features in the fly that are controlled by PI3K/AKT signalling, it suggests that Srx may regulate this pathway and therefore similarly affect the growth of neurons.

There are additional downstream components of PI3K/AKT signalling, such as transcription factors of the FOXO family, which could alternatively be implicated in controlling cell and wing size. AKT-mediated phosphorylation of FOXO transcription factors generates recognition motifs for phospho-binding 14-3-3 proteins, which can promote the nuclear export of FOXO proteins to maintain them in the cytosol and prevent binding to the promoter sequences of target genes (Manning and Toker, 2017). If loss of Srx were to promote PI3K/AKT/FOXO signalling, this is likely to inhibit FOXO-mediated transcription. Ubiquitous over-expression of *Drosophila FoxO* suppresses cell and wing size, giving credence to the notion that Srx may regulate this pathway (Kramer et al., 2003).

My findings could be strengthened by attempting to rescue the increased wing size in *Srx* mutants via epistasis experiments, whereby *Srx* mutations are co-expressed with transgenes or mutations that modify specific components of the PI3K/AKT signalling pathway. This would definitely prove whether Srx modulates PI3K/AKT signalling to control cell size, wing size and potentially neuron growth. One way to address this would be to combine *Srx* and *PI3K* or *Akt* mutations or dominant-negative transgenes. If wing size is returned to the levels observed in WT flies, it would indicate that Srx negatively regulates PI3K/Akt activity. Pharmacological agents could also be used to explore whether downstream mTOR activation drives the larger wing phenotype. *Srx* mutants could be fed food containing the mTOR inhibitor Rapamycin during development to attempt to rescue the increased wing size. Furthermore, if Srx does regulate wing growth, experiments should be performed to deduce whether this is related to a faster rate of overall development. The time taken for *Srx* mutant flies to eclose from their pupal cases should be compared to WT strains.

Overall, the behavioural, electrophysiological, and morphological phenotypes of *Srx* mutant flies described in this chapter provide a platform for further work to understand the cellular role of Srx.

5. Srx modulates neuron morphology

The previous chapter documented organismal and tissue level phenotypes of *Srx* mutant flies. At the cellular level changes in ROS homeostasis manifest as changes in neuronal morphology and this is particularly well-established at the *Drosophila* NMJ. In this chapter I investigated the effects of Srx loss on the morphology of *Drosophila* neurons and rodent hippocampal neurons. I assessed presynaptic structures at the *Drosophila* larval NMJ and overall branching phenotypes of cultured *Drosophila* embryonic neurons. Furthermore, I examined the effects of shRNA-mediated Srx knockdown on dendritic morphology of cultured rodent hippocampal neurons, as well at mitochondrial counts and morphology.

RNAi techniques were preferred in this research to knockout models using CRISPR-Cas9 gene editing, due to RNAi techniques having a less complex, but highly effective workflow. Vectors, which encoded shRNA molecules, were transiently expressed in neurons using cationic lipid-mediated transfection. siRNA duplexes can also be transfected in this manner, which are directly incorporated into RNA-induced silencing complexes (Tseng et al., 2009). However, vectors were preferred because they can also encode markers, such as fluorescent proteins like GFP, that enable transfected cells to be easily identified and imaged. Cationic lipid-mediated transfection was preferred to viral vectors containing RNAi cassettes, as the former exhibits low transfection efficiency in primary cells (Thermo Fisher, 2025). This is beneficial for imaging experiments using neurons. High transfection efficiencies can make it difficult to trace individual neurites, as the neurites from neighbouring cells can extensively overlap.

5.1. Introduction

ROS and redox-sensitive signalling pathways regulate neuron growth, as previously discussed in Chapter 1. In developing rat hippocampal neurons, ROS-generating NOX enzymes at the growth cones modulate axon lengths via Ca^{2+} release from intracellular stores (Wilson et al., 2016, 2015). At the *Drosophila* NMJ, neuron growth is regulated by redox-sensitive JNK/AP-1 signalling, with sources of OS differentially activating JNK/AP-1 signalling components. For instance, jun is dispensable for the increased growth conferred by *spinster*

mutations, whereas both fos and jun are required for growth conferred by *sod2* mutations (Milton et al., 2011).

If Srx modulates neuron morphology, this may underlie the behavioural and electrophysiological phenotypes observed in *Drosophila Srx* mutants (see Chapter 4). My work described in previous chapters has already demonstrated that *Srx* mutations attenuate AP-1 signalling (see Chapter 3.2.8). Milton et al. (2011) observed that the expression of dominant-negative fos and jun isoforms diminished neuron growth at the *Drosophila* larval NMJ, as measured by normalised bouton counts. Therefore, *Srx* mutations that attenuate AP-1 signalling may diminish neuron growth. However, I have shown that *Srx* mutations also increased *Drosophila* wing sizes, which may reflect increased PI3K signalling (see Chapter 4.2.5). PI3K signalling is known to increase the number of boutons with synapses at the *Drosophila* NMJ (Martín-Peña et al., 2006). PI3K/Akt/mTOR signalling also positively regulates dendrite growth and branching in rat hippocampal neurons *in vitro* (Jaworski et al., 2005) and *in vivo* (Tariq et al., 2022). Therefore, *Srx* mutations may enhance neuron growth if this pathway is affected.

In this chapter, I investigated whether loss of Srx alters neuron morphology. I used *Drosophila* third instar larvae to assess the effect of *Srx* mutations on neuron growth at the larval NMJ. Likewise, the effect of *Srx* mutations on the growth of *Drosophila* embryonic neurons was investigated *in vitro*. Furthermore, to investigate for a conserved role of Srx, I used a mammalian system of rat primary neuron cultures. To this end, short hairpin RNA-encoding constructs were generated to suppress Srx expression following cell transfection techniques. Lastly, the morphology of mitochondria in rat primary neurons was observed following Srx knockdown, to determine whether mitochondrial dynamics were altered following loss of this antioxidant enzyme.

5.2. Results

5.2.1. *Srx* mutations enhance neuron growth at the *Drosophila* NMJ

To determine if loss of Srx affected neuron development *in vivo*, third instar larvae were dissected, fixed, underwent immunohistological staining, and were imaged using confocal microscopy. Bouton counts were normalised to muscle surface area (MSA), which were compared between *Srx* mutants and WT larvae. *Srx* mutants exhibited greater numbers of

boutons (Figure 5.1.A). WT larvae exhibited an average count of 51.6 (±2.2), whereas $Srx^{\Delta 1\text{-}2}$ mutants had an average normalised count that was 52.3% greater at 78.6 (±3.3). Similarly, $Srx^{\Delta 3}$ mutants had an average normalised count of 67.2 (±3.5), which was 30.2% greater than the WT average.

The increased normalised bouton counts observed at *Srx* mutant NMJs did not consistently correlate with changes to the surface area of muscles 6/7 at the *Drosophila* NMJ. $Srx^{\Delta 3}$ mutations significantly increased the surface area of muscles compared to WT larvae. $Srx^{\Delta 3}$ mutant larvae exhibited an average muscle surface area of 76855.03 μm^2 (±1116.63 μm^2), which was 6.8% greater than the WT average of 71969.43 μm^2 (±1252.08 μm^2). $Srx^{\Delta 1\text{-}2}$ mutants did not exhibit muscle surface areas that were significantly different from WT larvae.

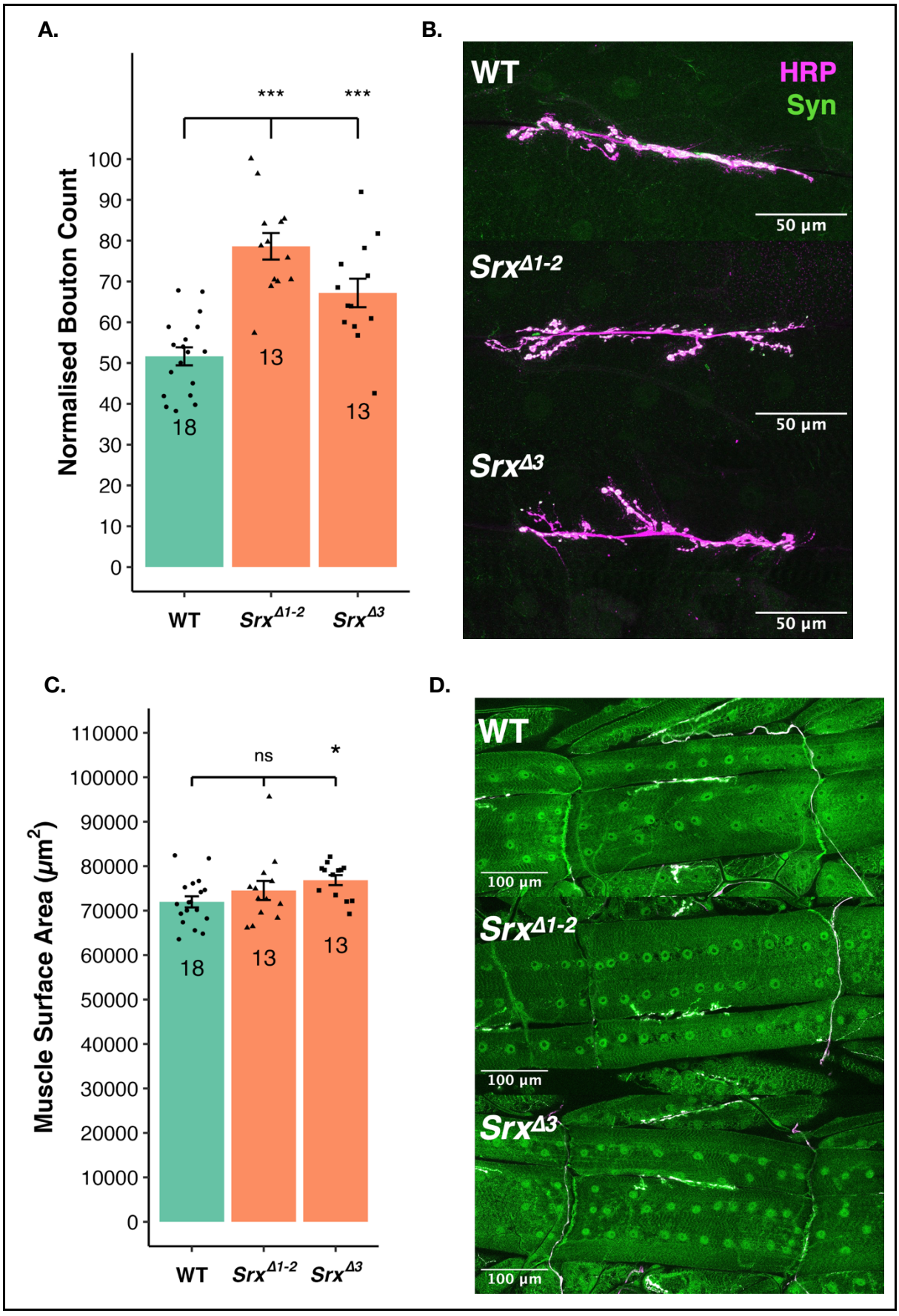
A.
Normalised Bouton Count
***
***
100
90
80
70
60
50
40
30
20
10
0
18
13
13
WT
Srx^Δ1-2
Srx^Δ3
B.
WT
HRP
Syn
50 µm
Srx^Δ1-2
50 µm
Srx^Δ3
50 µm
C.
Muscle Surface Area (µm²)
ns
*
110000
100000
90000
80000
70000
60000
50000
40000
30000
20000
10000
0
18
13
13
WT
Srx^Δ1-2
Srx^Δ3
D.
WT
100 µm
Srx^Δ1-2
100 µm
Srx^Δ3
100 µm

Figure 5.1. *Srx* mutations increase *Drosophila* neuron growth *in vivo*.
A. *Srx* mutations increased neuronal bouton counts at the *Drosophila* third instar larvae NMJ (one-way ANOVA: df=2, F= 22.94, p<0.001***, with post-hoc Dunnett's test comparison to WT, p<0.001***). **B.** Exemplary images of WT and *Srx* mutant larvae NMJs **C.** *Srx* mutations do not consistently alter the surface area of muscle 6/7 in *Drosophila* third instar larvae. $Srx^{\Delta 3}$ mutations increased the surface area of these muscles, whereas $Srx^{\Delta 1\text{-}2}$ mutations did not (Kruskal-Wallis, χ^2=6.40, df=2, p=0.04*, with post-hoc Dunn's test comparison to WT, p<0.05*). **D**. Exemplary images of muscle 6/7 from WT and *Srx* mutant larvae. For all of the graphs, sample sizes are presented, and bars represent mean ± SEM.

5.2.2. *Srx* mutant NMJ overgrowths are not rescued by *Srx* transgene expression or n-acetyl cysteine treatment

To validate that *Srx* mutations are causing the increased NMJ growth observed at the NMJ of *Srx* mutant larvae, *UAS-Srx.FLAG* and *nSyb-Gal4* transgenes were expressed in the background of $Srx^{\Delta 3}$ mutations to attempt to rescue the overgrowth phenotype. These rescue attempts did not bring normalised bouton counts down to the levels observed in WT larvae (Figure 5.2.A). WT larvae, with an *nSyb-Gal4* transgene in the background, exhibited average normalised bouton counts of 56.6 (±3.4). $Srx^{\Delta 3}$ mutations, with an *nSyb-Gal4* transgene in the background, increased these counts by 39.9% to 79.2 boutons (±5.3). Co-expression of the *nSyb-Gal4* and *UAS-Srx.FLAG* transgenes in the $Srx^{\Delta 3}$ mutant background failed to rescue the increased bouton counts, which remained 44.3% higher than WT larvae at 81.7 boutons (±3.9).

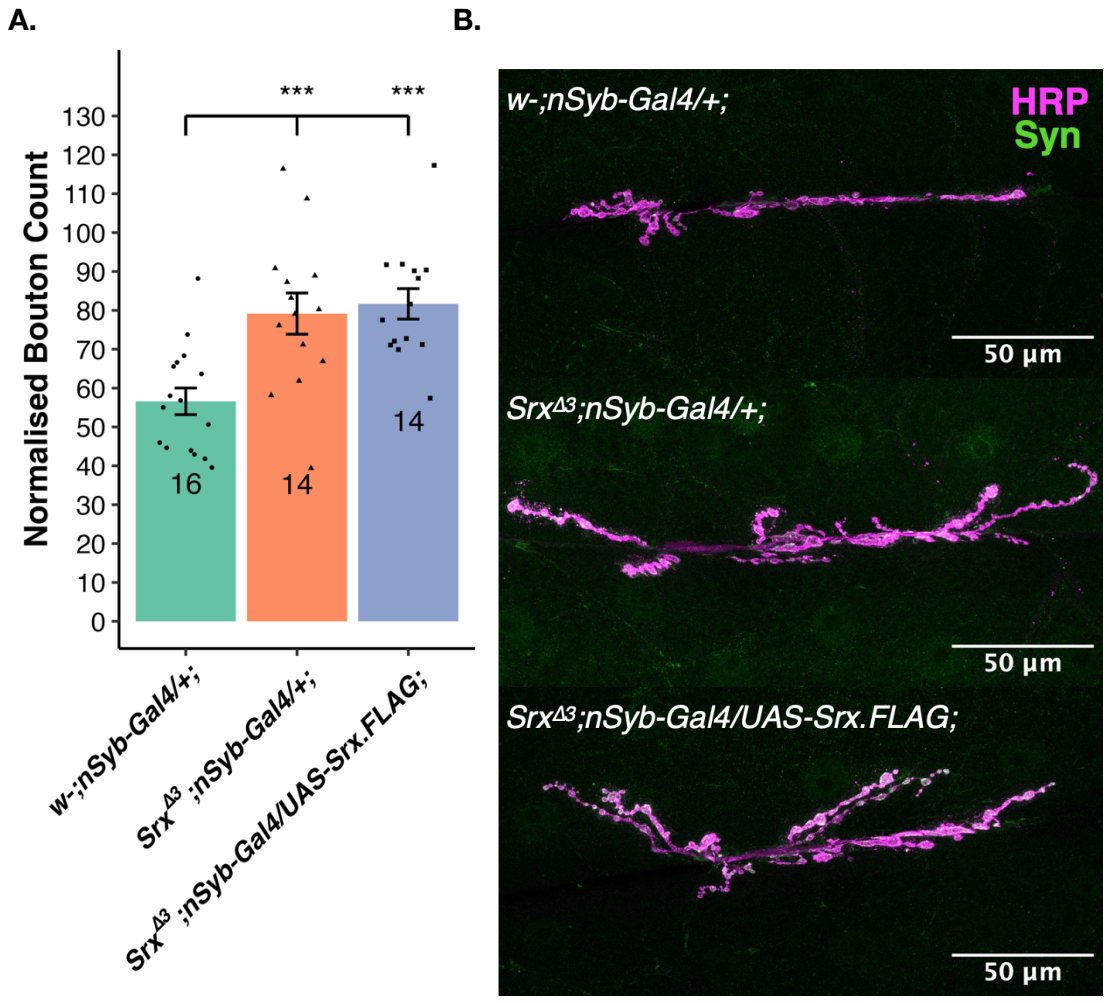

Figure 5.2. Expression of *nSyb-Gal4* and *UAS-Srx.FLAG* transgenes in the *Srx* mutant background do not rescue NMJ overgrowths.

A. NMJ overgrowths are not rescued by the selective expression of Srx in neurons using the Gal4/UAS system (one-way ANOVA: df=2, F= 11.11, $p<0.001$***, with post-hoc Dunnett's test comparison to WT, $p<0.001$***). Sample sizes are presented. Bars represent mean ± SEM. Representative images for this experiment are shown in **B.**

There could be technical reasons for the lack of rescue of the NMJ overgrowth by Srx overexpression, such as the inclusion of the C-terminal FLAG tag in the transgene, which may alter Srx structure and function. I therefore next explored whether the administration of n-acetyl cysteine (NAC) in the food of *Srx* mutant larvae rescued the NMJ overgrowths. If *Srx* mutations lead to the hyperoxidation of substrates, which causes increased neuron growth

at the NMJ, these changes should be ameliorated by the application of antioxidant supplements in the larval food. NAC is thought to exert antioxidant activity via ROS-scavenging, directly reducing thiols, and serving as a cysteine precursor for the rate-limiting synthesis step in glutathione production (Aldini et al., 2018). Therefore, larvae were reared on food containing 0 mM, 5 mM, or 10 mM NAC to see if this rescued the NMJ overgrowth observed in $Srx^{\Delta 3}$ mutants.

The administration of NAC failed to rescue the NMJ overgrowths observed in $Srx^{\Delta 3}$ mutant third instar larvae (Figure 5.3.A-B). When reared on food without NAC, $Srx^{\Delta 3}$ mutants exhibited average bouton counts that were 32.0% greater than those of WT larvae. Similarly, $Srx^{\Delta 3}$ mutants exhibited average bouton counts that were 48.2% greater than those of WT larvae when reared on food made with sucrose-yeast solution containing 10 mM NAC. However, when reared on food made with 5 mM NAC sucrose-yeast solution, $Srx^{\Delta 3}$ mutants no longer demonstrated an overgrowth. This reflected an increase in the average bouton counts between WT larvae reared on food with 0 and 5 mM NAC. Administration of food made with sucrose-yeast solution containing 5 mM NAC significantly increased the average number of boutons in WT larvae by 19.3%. However, significant increases were not observed using NAC concentrations of 10 mM, which were within 1% of the average for WT larvae raised on food without NAC. This suggests that this antioxidant drug is unable to rescue the overgrowth conferred by *Srx* mutations. Overgrowths may be rescued using alternative molecular antioxidants such as the soluble vitamin E variant Trolox.

A.

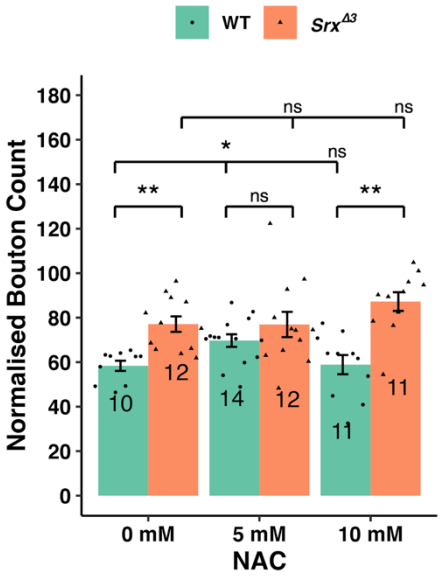

B.

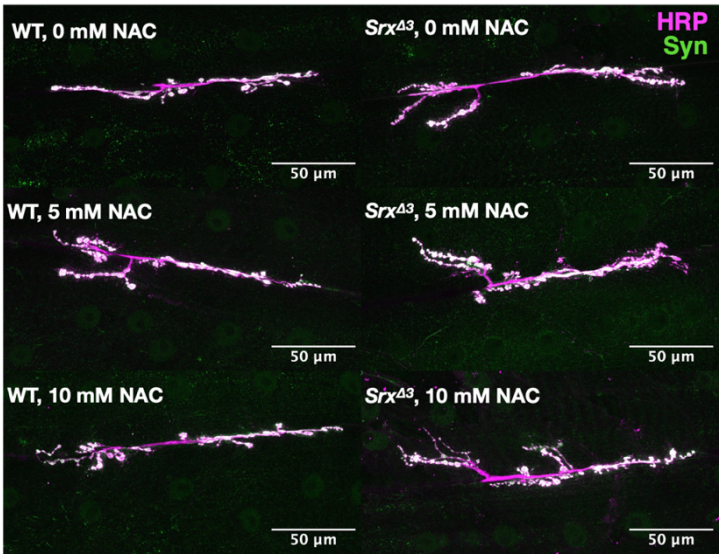

Figure 5.3. *Srx* mutant larval NMJ overgrowths are not rescued by the administration of NAC in food.

A. $Srx^{\Delta 3}$ mutations increased normalised bouton counts (Scheirer-Ray-Hare test, H=19.5, df=1, p<0.001***). NAC administration in the food did not significantly alter bouton counts overall (Scheirer-Ray-Hare test, H=2.10, df=2, p=0.351). A significant interaction term was observed, however (Scheirer-Ray-Hare test, H=6.15, df=2, p=0.0462*). Post-hoc pairwise Wilcoxon rank sum tests with BH correction elucidated the groups that were significantly different from one another (p<0.001***, p<0.01**, p<0.05*). Sample sizes are presented. Bars represent mean ± SEM. **B.** Representative images of neurons from WT and *Srx* mutant larvae reared on 0-10 mM NAC food.

5.2.3. *Srx* mutations enhance *Drosophila* embryonic neuron growth *in vitro*

The discovery that *Srx* mutations increased neuron growth at *Drosophila* third instar larvae NMJs raises the question whether such neuronal overgrowth is generalisable to all neurons. I therefore examined the morphology of *Drosophila* embryonic neurons cultured *in vitro*. Furthermore, I wanted to determine whether loss of *Srx* induced neuron growth because of a loss of its interactions with Prdx enzymes. Therefore, *Srx* mutant embryonic neurons were compared to neurons derived from both WT embryos and embryos with a mutation to the cytosolic typical 2-Cys Prdx enzyme, *Jafrac1*.

Drosophila embryos were homogenised and neurons were cultured *in vitro* to ascertain whether increased growth would be observed in this paradigm as well. Neurons were cultured upon conA-coated coverslips, fixed at 1 DIV, and visualised using a Cy3-conjugated antibody targeting HRP epitopes. Neuron morphology was quantified by measuring the combined length of neurite outgrowths.

I found that neurons from *Srx* mutant embryos had increased combined neurite lengths compared to neurons from WT embryos (Figure 5.4). The average neurite lengths for neurons derived from *Srx* mutant embryos was 139.4 μm (±18.5 μm), a figure that was 62.7% higher than the WT mean of 85.7 μm (±9.3 μm). Conversely, mutations to *Jafrac1* failed to induce a statistically significant increase in neurite lengths.

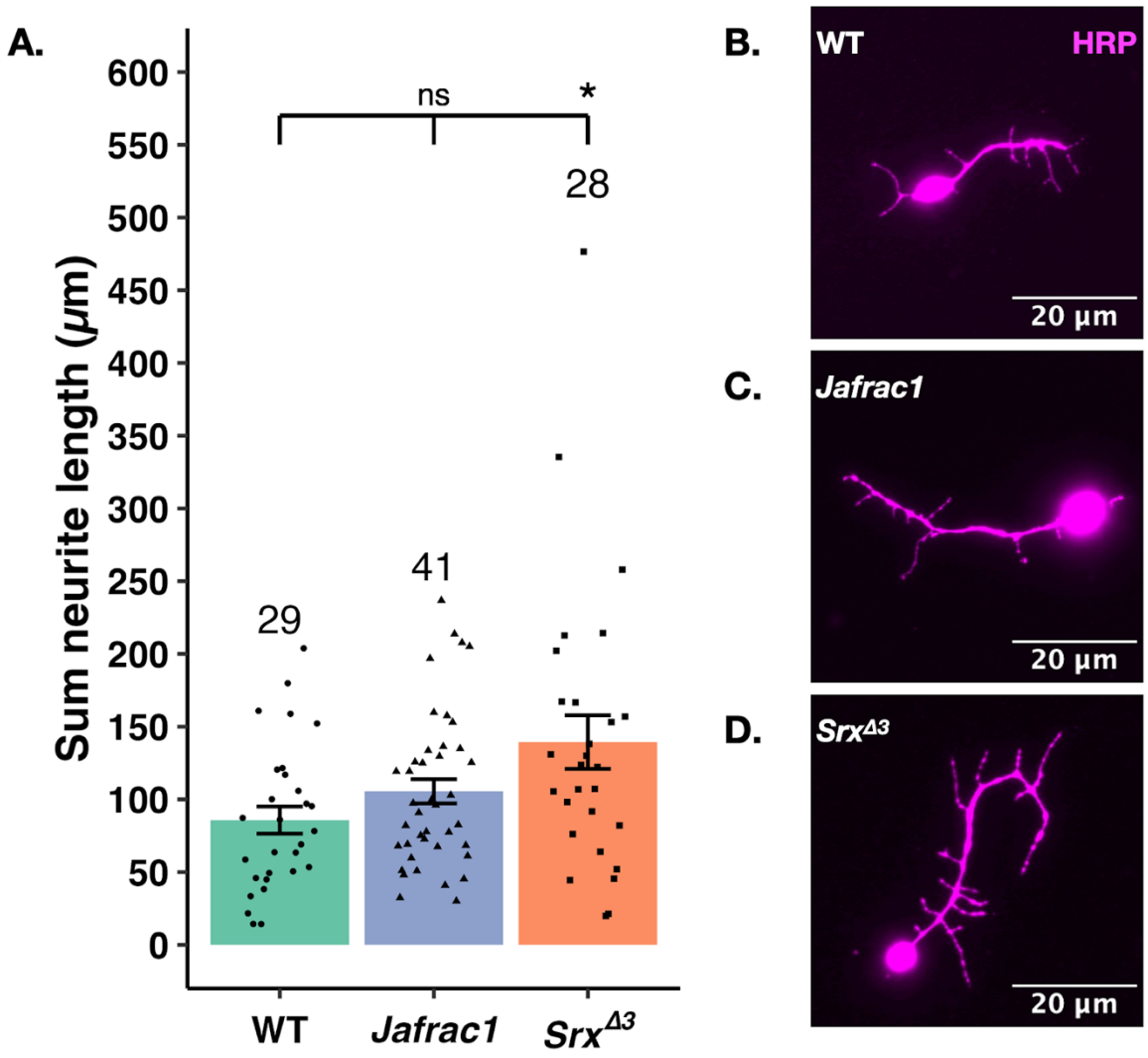

Figure 5.4. *Srx* mutations increase neurite outgrowth lengths of *Drosophila* embryonic neurons.

A. Cultured embryonic neurons from *Drosophila* were fixed at 1 DIV and stained using a Cy3-conjugated, pan-neuronal antibody (targeting HRP epitopes). Increased neurite lengths were observed following *Srx* mutations, but not following mutations to the gene encoding a cytosolic typical 2-Cys Prdx enzyme, *Jafrac1* (Kruskal-Wallis, χ^2=6.92 , df= 2, p=0.031*, with post-hoc Dunn's test comparison to WT, p<0.05*). Sample sizes are presented. Bars represent mean ± SEM. Representative images for this experiment are shown in **B-D.**

5.2.4. Generation of Srx shRNA constructs

To validate the findings made using *Drosophila*, I next manipulated expression of Srx in mammalian cell cultures to investigate whether loss of Srx increases neuron growth in a mammalian model system too. Doing so would allow me to make assertions as to whether the function of Srx, in regulating neuron growth, was conserved across species. To induce knockdown of human and rat Srx, shRNA-encoding plasmids were designed. Oligos encoding shRNA molecules were annealed and ligated into a pSuper.neo+GFP plasmid backbone to be expressed under the control of a H1 promoter sequence. For each species, three constructs were made, with each targeting a distinct 21 nucleotide sequence.

I first validated that the shRNA constructs were effective in inducing Srx knockdown, HEK293t cells were co-transfected with the shRNA constructs and plasmids encoding either the human or rat Srx isoforms with a C-terminal Myc-tag. HEK293t cells have a high transfection efficiency, enabling a large proportion of cells to be transiently transfected with both plasmids. Protein lysates were generated for analysis via western blotting (Figure 5.5.A). Diminished chemiluminescence, following use of antibodies targeting the Myc tag, indicated suppression of Srx translation and effective RNAi.

For the shRNA constructs targeting human Srx, one of the three plasmids generated in this research was effective in suppressing Srx translation, named ‘H1.’ As the only effective construct, this was used for subsequent experiments. For the shRNA constructs targeting rat Srx, all three plasmids generated in this study were effective in suppressing Srx translation, termed ‘R1,’ ‘R2,’ and ‘R3.’ Unless otherwise stated, R2 was used to knockdown Srx in subsequent experiments.

To explore whether loss of Srx knockdown in mammalian cells produced similar phenotypes to *Srx* mutations in *Drosophila*, the Amplex Red assay was performed using HEK293t cells transfected with the H1 plasmid. This failed to show differences in absorbance values, proportional to H_2O_2 concentrations (Figure 5.5.B). Protein lysates derived from HEK293t cells that underwent the transfection protocol used for the Amplex Red assay exhibited decreased Srx expression in HEK293t cells (Appendix Figure 1). This demonstrates that the transfection strategy used, in which approximately 80% of cells are transfected, is still high enough to reduce global Srx levels in the culture.

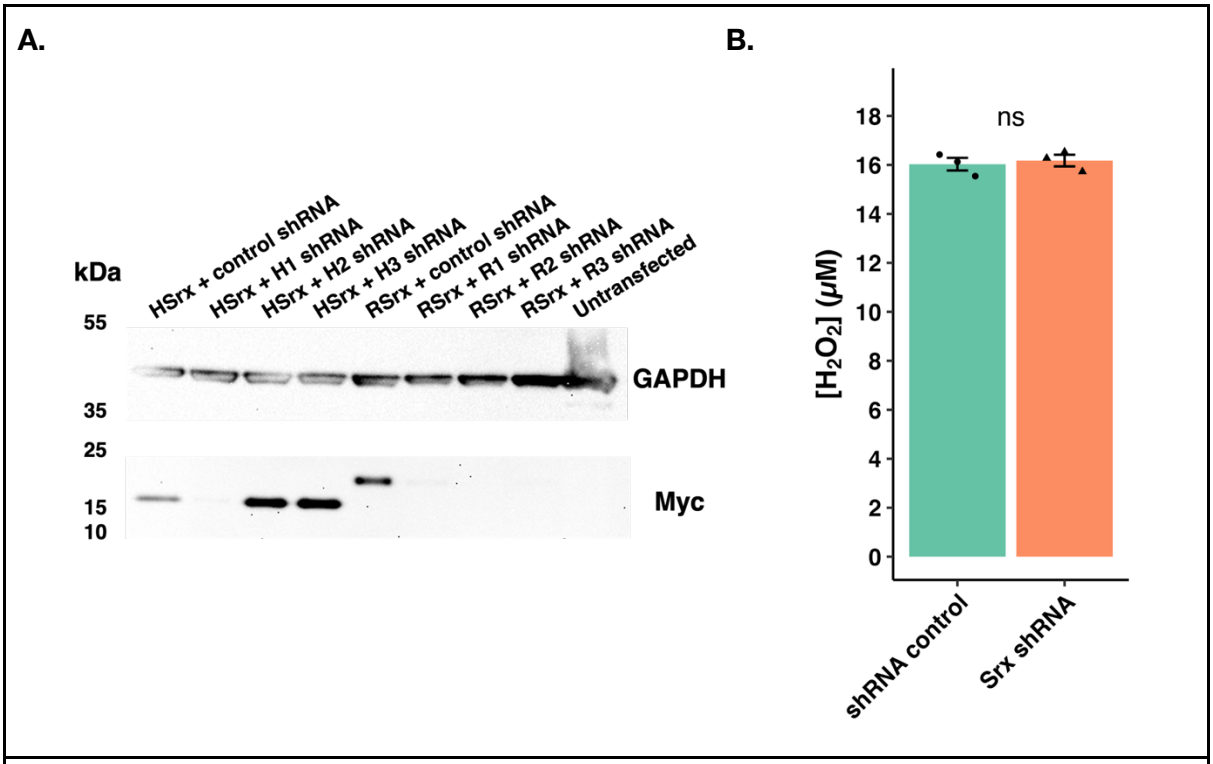

Figure 5.5. Generation of shRNA constructs for Srx knockdown in mammalian cell cultures.

A. Annealed primers were ligated into the pSuper.neo+GFP backbone to generate plasmids that expressed shRNA molecules under the control of a H1 promoter sequence. Knockdown of human and rat Srx mRNA targets was validated by co-transfecting HEK293t cells with constructs encoding the shRNA molecules and Myc-tagged human Srx (hSrx) or rat Srx (rSrx). Protein lysates were generated and western blots were performed. Effective knockdown diminished chemiluminescence observed using antibodies targeting Myc tags. **B.** Similarly to *Drosophila Srx* mutants, use of the effective shRNA construct targeting human Srx failed to alter H_2O_2 production in HEK293t cells (two-sample t-test, df=4, t=-0.417, p=0.698, ns). Bars represent mean ± SEM and n=3 for each group.

5.2.5. Srx knockdown enhances rat primary neuron growth

Having found that *Srx* mutations enhanced neuron growth in *Drosophila*, I next sought to assess whether this phenotype was conserved in a mammalian model. Rat primary hippocampal neurons cultures were used as these neurons are glutamatergic. Neurons were transfected with shRNA constructs targeting Srx at 3-5 DIV, followed by fixation 3 days later. Confocal microscopy was used to image neurons, which were traced and analysed for various morphological parameters indicating growth.

I found that knockdown of Srx enhanced rat primary neuron growth (see Figure 5.6.A for exemplary images). Sholl analysis was conducted, with concentric radii drawn around the soma at 5 μm intervals. Neurite intersections at each radius were counted to assess the growth and branching of neurites derived from the soma. Multiple pairwise comparisons of the cumulative intersections at 50, 100, 150, 200, and 250 μm revealed that Srx knockdown induced increased numbers of intersections at the aforementioned radii (Figure 5.6.B). At 250 μm from the soma, the average number of cumulative intersections following Srx knockdown was 254.8 (±18.36), which was 80.6% greater than the 141.1 (±11.61) average for cells transfected with a control shRNA plasmids. Srx knockdown also caused there to be a greater number of maximum intersections at any given radius (Figure 5.6.C). The average maximum number of intersections for neurons transfected with the control shRNA construct was 7.83 (±0.46), whereas this was 13.1 (±0.70) for neurons transfected with the Srx shRNA construct.

The number of primary neurites also increased following Srx knockdown (Figure 5.6.D). Neurons transfected with control plasmids had an average number of 4.60 primary neurites (±0.23), whereas neurons transfected with Srx shRNA-encoding constructs had an average that was 36.5% higher at 6.28 primary neurites (±0.38). Following Srx knockdown, a larger proportion of neurons also had combined neurite lengths that were at least 1000 μm in length (Figure 5.6.E). Only 37.5% of neurons transfected with control shRNA plasmids produced neurites that reached 1000 μm in sum length, whereas 72.3% of neurons transfected with Srx shRNA constructs produced neurites with sum lengths of 1000 μm.

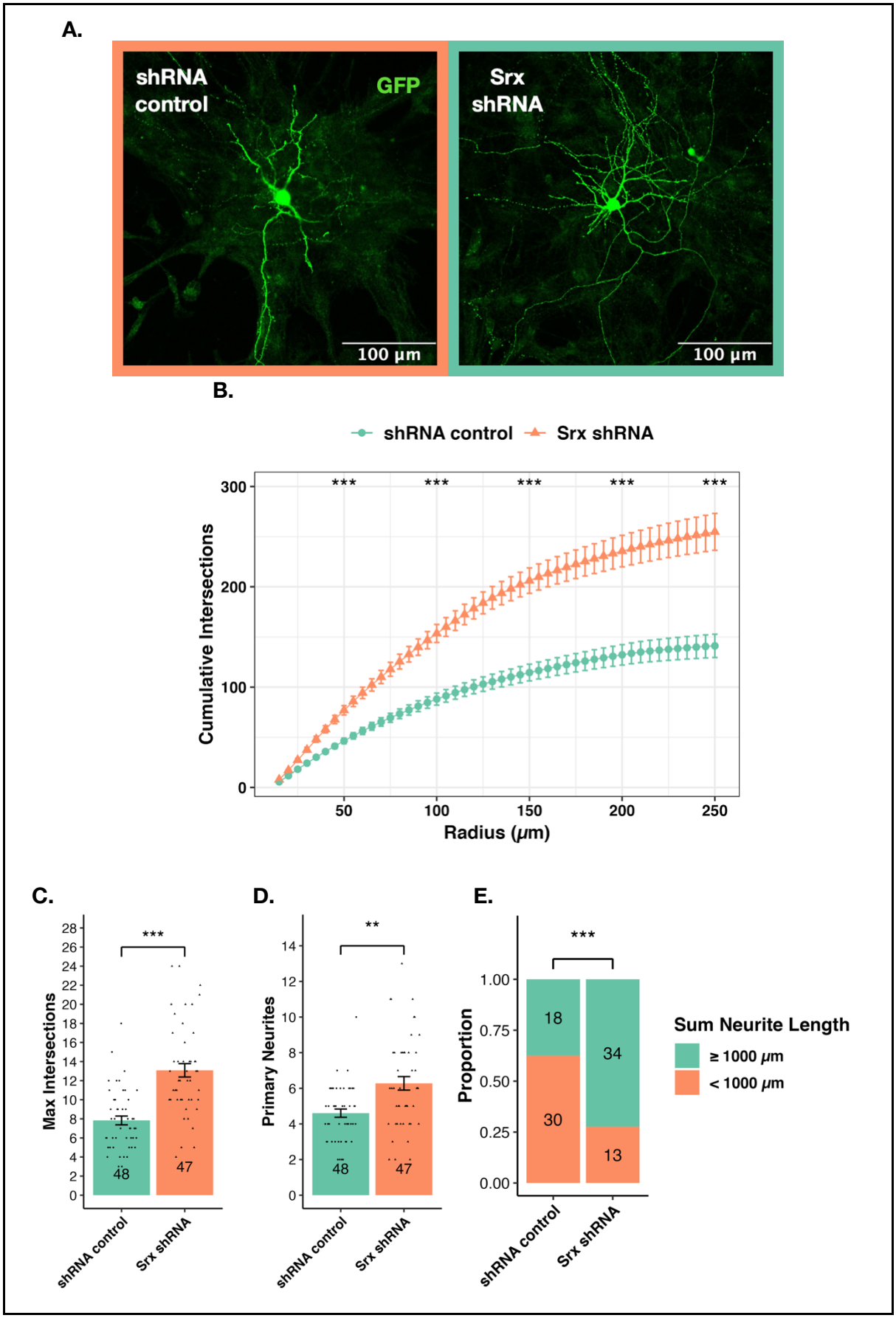
A.
shRNA control
GFP
100 µm
Srx shRNA
100 µm
B.
shRNA control
Srx shRNA
Cumulative Intersections
Radius (µm)
***
C.
Max Intersections
48
47
shRNA control
Srx shRNA
D.
**
Primary Neurites
48
47
shRNA control
Srx shRNA
E.
***
Proportion
18
30
34
13
shRNA control
Srx shRNA
Sum Neurite Length
≥ 1000 µm
< 1000 µm

Figure 5.6. Loss of Srx increases the growth of rat primary hippocampal neurons *in vitro*.

A. Representative images of hippocampal neurons transfected with plasmids encoding non-targeting shRNA molecules and shRNA molecules targeting Srx. **B.** Sholl analysis demonstrates increased dendrite growth and branching following Srx knockdown (multiple two-sample Kolmogorov-Smirnov tests with BH correction, $p<0.0002^{***}$). Points represent mean ± SEM. Sample sizes are identical to those in C and D. **C.** The maximum number of intersections at each of the radii used in the sholl analysis is increased following Srx knockdown (two sample Kolmogorov-Smirnov test, $D=0.559$, $p<0.001^{***}$). **D.** The number of primary neurites is increased following Srx knockdown (two-sample Kolmogorov-Smirnov test, $D=0.342$, $p=0.002^{**}$). For C-D the sample sizes are presented, and bars represent mean ± SEM. **E.** A larger proportion of neurons have combined neurite lengths of at least 1000 µm, indicating increased dendritic growth (Pearson's χ^2 test, $\chi^2=11.635$, $df=1$, $p<0.001^{***}$). The sample sizes are presented.

5.2.6. Loss of Srx does not affect mitochondrial morphology or dynamics

The work presented in this thesis indicates that loss of Srx exerts small but significant effects on redox signalling and redox-related biological processes, such as neuron growth. As mild OS induces mitophagy (Frank et al., 2012), this research hypothesised that mitochondrial dynamics would similarly be affected by loss of Srx. Therefore, this study aimed to investigate whether loss of Srx affected mitochondrial dynamics using rat primary hippocampal neurons that were co-transfected with shRNA constructs to induce Srx RNAi and mito-DsRed plasmids to label mitochondria. Confocal microscopy techniques were used to image the mitochondria within a neurite that was within 150 µm of the neuron soma. Typically, mitochondria were imaged within a stretch of neurite that was approximately 100 µm in length. Images were blinded, thresholded, and analysed as 2D images in Fiji using the 'Mitochondrial Analyzer' plugin (Chaudhry et al., 2020) to investigate whether loss of Srx impacted mitochondrial morphology or dynamics. Where appropriate, the average value for each morphological parameter was calculated and these values were used for statistical analysis.

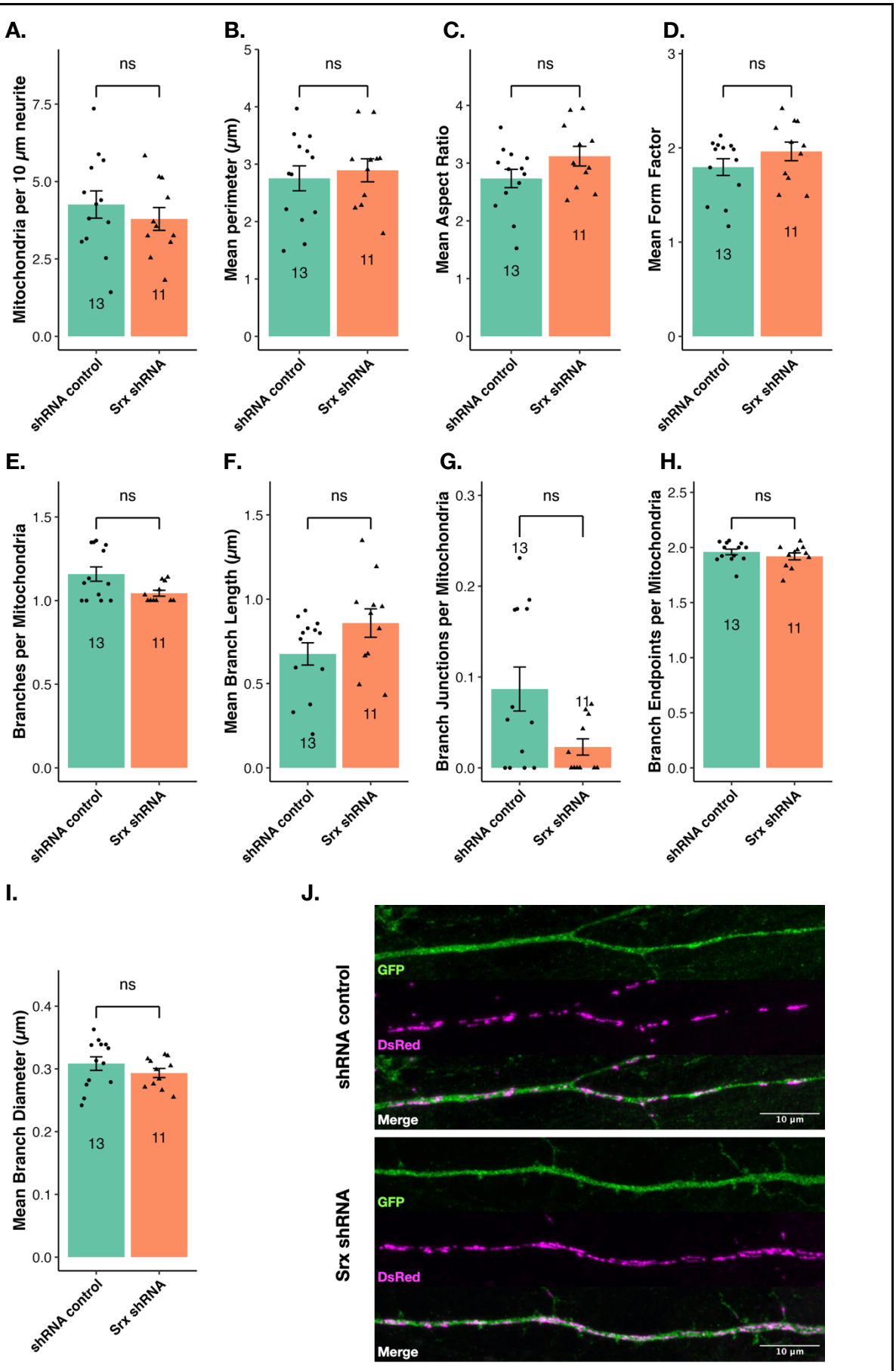
A.
Mitochondria per 10 μm neurite
ns
13
11
shRNA control
Srx shRNA
B.
Mean perimeter (μm)
C.
Mean Aspect Ratio
D.
Mean Form Factor
E.
Branches per Mitochondria
F.
Mean Branch Length (μm)
G.
Branch Junctions per Mitochondria
H.
Branch Endpoints per Mitochondria
I.
Mean Branch Diameter (μm)
J.
shRNA control
Srx shRNA
GFP
DsRed
Merge
10 μm

Figure 5.7. Srx knockdown in rat primary hippocampal neurons does not affect mitochondrial morphology or dynamics.

A. The number of mitochondria per 10 µm of neurite is unaffected by Srx RNAi (two-sample t-test, df=22, t=0.796, p=0.435, ns). **B.** The mean perimeter of mitochondria is unaffected by Srx RNAi (two-sample t-test, df=22, t=-0.467, p=0.645, ns). **C.** The mean aspect ratio of mitochondria is unaffected by Srx RNAi (two-sample t-test, df=22, t=-1.661, p=0.111, ns). **D.** The mean form factor of mitochondria is unaffected by Srx RNAi (Wilcoxon test, W=-50, p=0.228, ns). **E.** The mean number of branches per mitochondria is unaffected by Srx RNAi (two-sample Kolmogorov-Smirnov test, D=0.385, p=0.214, ns). **F.** The mean branch length of mitochondria is unaffected by Srx RNAi (Wilcoxon test, W=41, p=0.082, ns). **G.** The mean number of branch junction per mitochondria is unaffected by Srx RNAi (Kolmogorov-Smirnov test, D=0.385, p=0.214, ns). **H.** The mean mitochondrial branch endpoints is unaffected by Srx RNAi (two-sample t-test, df=22, t=1.003, p=0.327, ns). **I.** The mean mitochondrial branch diameter is unaffected by Srx RNAi (two-sample t-test, df=22, t=1.122, p=0.274, ns). For all of the aforementioned graphs, sample sizes are presented, and bars represent mean ± SEM. **J.** Exemplary images of mito DsRed-positive mitochondria from neurons transfected with the shRNA control and Srx shRNA plasmids.

The number of mitochondria, expressed as mitochondria per 10 µm of neurite, were unaffected by Srx RNAi (Figure 5.7.A). Neurons transfected with a control shRNA plasmid had an average of 4.26 mitochondria per 10 µm of neurite (±0.44 per 10 µm), which did not significantly differ from the 3.79 (±0.37 per 10 µm) average observed in neurons transfected with Srx shRNA plasmids. The mean perimeter of mitochondria was also unaffected by Srx RNAi (Figure 5.7.B). Neurons transfected with shRNA plasmids exhibited mitochondria with average perimeter that were only 5.1% greater than the 2.75 µm (±0.22 µm) average observed for neurons transfected with shRNA control plasmids. The shape of mitochondria was similarly unaffected by Srx knockdown. The mean aspect ratio and the mean form factor of mitochondria were not significantly different in neurons transfected with Srx shRNA plasmids (Figure 5.7.C-D). Similarly, all morphological parameters pertaining to mitochondrial branching were not significantly altered by Srx knockdown (Figure 5.7.E-I).

Given that Srx RNAi failed to induce changes to the quantity of mitochondria in the neurites of rat primary neurons, this suggests that mitophagy is not significantly affected. The morphology of mitochondria was similarly unaffected by Srx knockdown, suggesting that mitochondrial fragmentation and mitophagy were not induced. This evidence collectively suggests that loss of Srx does not induce alter mitophagy, which is known to be induced by mild and strong OS (Frank et al., 2012; Scherz-Shouval et al., 2007).

5.2.7. Srx exhibits broad distribution throughout neurons

I also wanted to determine whether Srx exhibited a high degree of colocalisation with mitochondria, which may suggest that this is primarily a mitochondrial protein (Figure 5.8). Rat primary hippocampal neurons were transfected with hSrx-Myc-DDK and mito-DsRed plasmids and analysed using confocal imaging. Srx exhibited a broad distribution throughout the neurons and did not exclusively colocalise with mitochondria. This suggests that the catalytic activity of Srx is broadly relevant to multiple organelles.

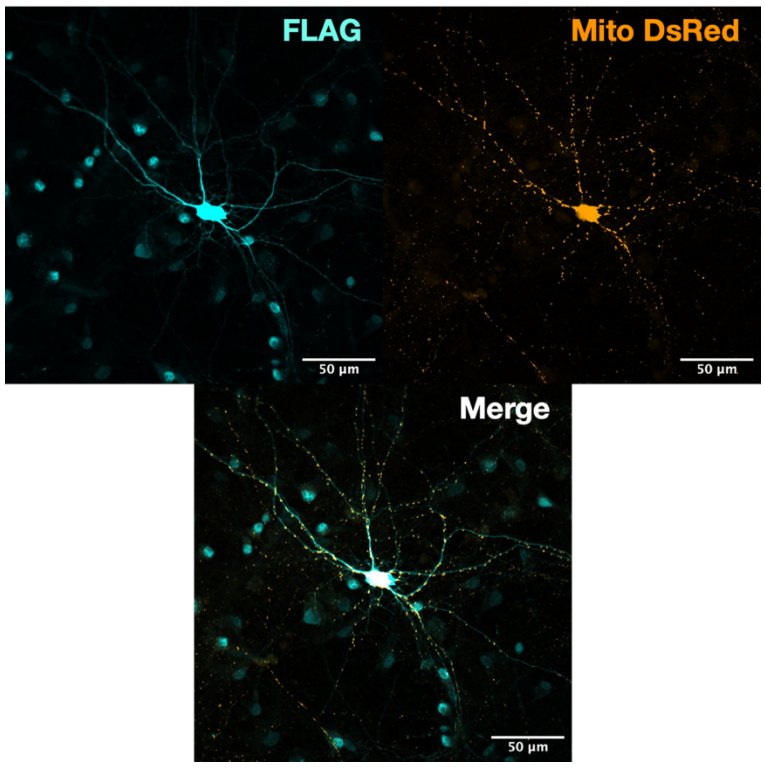

Figure 5.8. Srx is broadly distributed throughout neurons.
Rat primary hippocampal neurons were transfected with hSrx-Myc-DDK and mito-DsRed constructs. Confocal imaging revealed that Srx did not exclusively colocalise with mitochondria and exhibited a broad distribution throughout the neurons.

5.3. Discussion

5.3.1. Loss of Srx enhances *Drosophila* and rat neuron growth

The results of the experiments presented in this chapter show that loss of Srx leads to neuronal overgrowth. *Srx* mutations induced overgrown neurons at the *Drosophila* larval NMJ, as measured by increased numbers of boutons. *Srx* mutations also promoted neuron growth in *Drosophila* embryonic neuron cultures, as measured by cumulative neurite lengths. This finding was found to be conserved in mammalian systems where Srx knockdown in rat primary neuron cultures increased neuron growth as measured by numerous parameters, which include Sholl analysis and analysis of neurite lengths. Collectively, these data suggest that *Srx* mutations may disrupt redox homeostasis to alter the activation of specific signalling pathways that promote neurite outgrowths and synaptogenesis.

Neuron growth at the *Drosophila* NMJ is positively regulated by JNK/AP-1 signalling, which is activated in response to OS (Milton et al., 2011; Papadia et al., 2008; Ugbode et al., 2020). It is unlikely that *Srx* mutations induce increased growth via activation of this pathway, as I found that AP-1 signalling was attenuated in *Srx* mutants (Chapter 3.2.8). Therefore, activation of an alternative redox-sensitive pathway may drive the increased growth observed in *Srx* mutants. PI3K/Akt/mTOR signalling has been shown to increase the numbers of boutons with synapses at the *Drosophila* NMJ (Martín-Peña et al., 2006). The PI3K/Akt/mTOR pathway is susceptible to redox modifications. Intramolecular disulphide bonds in PTEN, which is an upstream negative regulator of PI3K, inhibits the antagonistic effect PTEN exerts over downstream signalling (Lee et al., 2002). Given that I observed increased wing size in *Drosophila* Srx mutants, which is a morphological feature of PTEN mutants (Chapter 3.2.7), this suggests that *Srx* mutations may modulate this signalling pathway to increase neuron growth.

Unlike *Srx* mutations, *Jafrac1* mutations did not increase neurite lengths in *Drosophila* embryonic neurons. Jafrac1 is a cytosolic 2-Cys Prdx enzyme that is important for defence against OS. *Jafrac1* overexpression in *Drosophila* confers increased resistance to OS (Lee et al., 2009), whereas knockdown of *Jafrac1* transcripts shortens *Drosophila* lifespans (McGinnis et al., 2021). As *Jafrac1* mutations did not increase the neurite lengths of embryonic neurons, this suggests that the increased neuron growth conferred by *Srx* mutations may not derive from an inability to recycle cytosolic Prdx enzymes. Instead, this

may stem from an inability to resolve mitochondrial Prdx enzymes, or alternative non-Prdx substrates identified by Akter et al. (2018).

An unexpected finding of the work described here was that expression of the rescue construct in the neurons of *Srx* mutants failed to rescue the overgrown synapses at larval NMJs. A possible reason for the ineffectiveness of the rescue construct in this particular paradigm may be that it is designed to have a FLAG tag conjugated to the C-terminus of the Srx protein. This may interfere with the interaction of Srx with substrates or affect cellular localisation. Future experiments should generate a rescue construct that expresses Srx without a conjugated FLAG tag to resolve this matter.

The administration of NAC in the food of the larvae was also unable to rescue the increased numbers of synaptic boutons observed in *Srx* mutants. This antioxidant is thought to confer protection against OS by acting as a ROS scavenger, reducing disulphide bonds directly, and providing cysteine for increased glutathione synthesis (Aldini et al., 2018). This drug was selected in these experiments for its high solubility in aqueous substances, without the need for solvents in food that may compromise larval health, such as ethanol, which induces oxidative stress (Logan-Garbisch et al., 2014). Concentrations of 5 mM NAC in the food increased bouton numbers in WT larvae, rather than altering bouton numbers in $Srx^{\Delta 3}$ mutants. NAC concentrations of 10 mM did not elicit increased growth in WT larvae. These contrasting results may derive from altered glutathione dynamics. Different concentrations of NAC may promote the differential glutathionylation of cysteine residues of key proteins that facilitate neuron growth.

A strength of this work is that it has used both *Drosophila* and mammalian models to demonstrate that Srx regulates neuron growth. This work may be improved by exploring whether over-expression of Srx negatively regulates neuron growth. While my work has not provided conclusive evidence to suggest that the PI3K/Akt/mTOR signalling pathway is upregulated following loss of Srx it has identified future avenues for investigation. Upregulation of the PI3K/Akt/mTOR pathway increases phosphorylation of Akt, which is readily observable using western blots and antibodies raised against the phosphorylated protein. Future work should investigate for increased phosphorylation of Akt in *Drosophila Srx* mutant lysates or lysates derived from HEK293t cells transfected with shRNA constructs that induce Srx knockdown. However, Akt is also capable of phosphorylating downstream components besides mTOR, such as FOXO (Manning and Toker, 2017). Therefore, to provide definitive proof that loss of Srx activates PI3K/Akt/mTOR signalling, individual components of this signalling pathway should be genetically or pharmacologically silenced to see if this

rescues the increased growth. One way to explore this would be to use Rapamycin, which acts as an acute inhibitor of mTOR complex I (mTORC1) by binding to the non-catalytic domain of the protein to inhibit a subset of functions assumed by mTORC1. Similarly, overexpression of PTEN in the *Srx* mutant background, to antagonise PI3K/Akt/mTOR signalling, could be attempted to see if this rescues overgrowths.

5.3.2. Loss of Srx does not alter mitochondrial counts or morphology in rat hippocampal neurons

Here I found that loss of Srx did not affect the relative quantity of mitochondria in rat hippocampal neuron neurites. Lower mitochondrial counts in cells are indicative of mitophagy, a specific form of macroautophagy in which mitochondria are degraded by lysosomes (Lee et al., 2012). Similarly, the morphology of mitochondria was unaffected by Srx knockdown, which is also thought to reflect the rate of mitophagy and mitochondrial turnover in cells. Increased mitochondrial fragmentation is indicative of mitochondrial fission, whereas long filamentous mitochondria that are indicative of mitochondrial hyperfusion (Picard et al., 2013).

It is widely accepted that OS stimulates mitophagy. Frank et al. (2012) observed that low ROS levels induce mitophagy in a mitochondrial fission-dependent manner that is independent of non-selective autophagy, whereby increased autophagosome formation is not observed and cell viability is unaffected. These changes are assumed to be regulated by redox-sensitive signalling pathways, as modest increases in ROS levels were induced (Frank et al., 2012). My work did not find Srx knockdown to affect baseline mitochondrial counts. However, future experiments should address whether loss of Srx affects mitophagy in cells treated with carbonyl cyanide m-chlorophenylhydrazone (CCCP), which is an uncoupler of mitochondrial oxidative phosphorylation that reduces mitochondrial membrane depolarisation to promote mitophagy. This mitophagy is dependent on PTEN-induced kinase 1 (PINK1) and the E3 ubiquitin ligase Parkin. CCCP damages mitochondria to inhibit PINK1 mitochondrial import, leading to its accumulation on depolarised mitochondrial outer membranes where it phosphorylates ubiquitin and Parkin, with the latter ubiquitinating substrates in the outer mitochondrial membrane that facilitate autophagosome recruitment (Matsuda et al., 2010; Narendra et al., 2008, 2010; Pickrell and Youle, 2015). The use of CCCP has been used to establish that PINK1 and Parkin mutations, which are associated with early-onset Parkinson's disease, disrupt Parkin recruitment to mitochondria and mitophagy

(Matsuda et al., 2010; Narendra et al., 2010). Inducing mitophagy in primary neuron cultures using CCCP might provide a clearer picture as to whether the additional loss of Srx enhances or inhibits this process and may also highlight Srx as a potential therapeutic target for Parkinson's disease intervention.

The findings of this work could be further strengthened by assessing whether the co-localisation of mitochondria with lysosomes is promoted following Srx knockdown. If loss of Srx does not promote colocalisation of mitochondria with lysosomes, this would strengthen the argument that mitophagy is not induced. The broader effect of Srx loss on macroautophagy could be further investigated using SDS-PAGE to see if this increases the proportion of microtubule associated protein light chain 3 (LC3) that is conjugated to phospholipid phosphatidylethanolamine (LC3-II). Lipidation of LC3 in this manner facilitates autophagosome localisation, correlates with autophagosome formation, and can be used as a measure of macroautophagy induction because of the increased molecular weight that is observable through SDS-PAGE (Kuma et al., 2007).

In hepatocellular carcinoma (HCC) cell lines the genetic knockdown and pharmacological inhibition of Srx increases ROS accumulation, activation of Transcriptional Factor EB (TFEB) signalling, and autophagy induction as observed through increased LC3-II levels using SDS-PAGE (Rao et al., 2024). Similarly, overexpression of Srx in HCC cells decreased LC3-II levels (Rao et al., 2024). The function of Srx as a regulator of autophagy may be conserved in neurons, which future experiments should aim to elucidate. Rat hippocampal neurons could be treated with the pharmacological Srx inhibitor J14 (MedChem Express, HY-135008), then protein lysates derived from these cells be analysed using SDS-PAGE to see if LC3-II levels are altered. SDS-PAGE can also be used to investigate the amount of lipidated Atg8a in protein lysates derived from *Drosophila* heads is altered in *Srx* mutants. Atg8a is the *Drosophila* LC3 orthologue and similarly undergoes phosphatidylethanolamine conjugation that correlates with autophagy (Demir and Kacew, 2023).

To conclude, this work has shown that loss of Srx positively regulates neuron growth in *Drosophila* third instar larvae. These changes are not readily reversed by the expression of rescue constructs or the administration of NAC in larval food. However, similar increased growth is observed in *Drosophila* embryonic neuron cultures and rat primary hippocampal neuron cultures. Changes to neuron growth suggest that Srx regulates redox-sensitive signalling pathways during development to affect neuron growth. Such signalling pathways may be distinct from those that are proposed to regulate mitophagy, as my experiments did not observe any differences in mitochondrial morphology or mitochondrial counts that

suggest increased or decreased mitochondrial turnover. Future experiments should aim to further elucidate the mechanisms underpinning the neuron growth phenotype induced by loss of Srx. The functional consequences of neuron overgrowth could also be studied to understand whether the growth altered neuronal excitability and synaptic transmission.

6. Discussion and future research

6.1. Key findings from this research

Sulfiredoxin-1 was discovered over 30 years ago as an oxidoreductase that reduces hyperoxidised peroxiredoxins to aid in neutralising H_2O_2 and thus maintain redox homeostasis. Yet, the relevance of Srx to the function of neurons, cells with high metabolic activity and high sensitivity to OS, remains unclear. In this thesis I addressed this gap through a comprehensive series of experiments. I first generated *Drosophila Srx* mutants to investigate the contribution of Srx to the maintenance of redox homeostasis. I found that *Srx* mutations had a small, but significant effect on the ability of *Drosophila* to survive when fed H_2O_2-supplemented sucrose solution, however levels of H_2O_2 in tissue homogenates were unaffected under physiological conditions.

Redox-sensitive signalling pathways seemed to be differentially affected by loss of Srx in *Drosophila*, as evidenced by reporter transgenes expressed in the *Srx* mutant background. Whilst loss of Srx had no effect on the expression of GFP under the control of *gstD1* promoter sequences, it did significantly diminish the expression of DsRed.T4 under the control *TRE* promoter sequences that AP-1 binds to. This suggests AP-1 signalling is decreased following loss of Srx, possibly due to Prdx hyperoxidation redirecting Trx to alternative substrates (see discussion in Chapter 3.3.3).

I next determined whether the altered signalling had any consequences for *Drosophila* behavioural and physiological traits that reflected perturbed neuron function *in vivo*. A plethora of physiological differences were discovered. Firstly, *Srx* mutants exhibited enhanced negative geotaxis responses, which were rescued via the expression of a *UAS-Srx.FLAG* transgene in the motor neurons of flies. This demonstrates that motor neuron function is perturbed following loss of Srx. Secondly, SSVEPs suggest diminished neurotransmission in the visual system of *Srx* mutants, as evidenced by decreased 2F1 amplitudes in spite of 1F1 amplitudes that did not differ significantly from WT flies. This may reflect activity-induced declines in neuron activity, which future work should resolve by repeating these experiments using flies reared in dark conditions to minimise activation of photoreceptors. Circadian rhythms were unaffected by loss of Srx, suggesting that it does not regulate this process in neurons. This contrasts findings made in mammalian adrenal

cortex cells, whereby there is rhythmic steroidogenesis through antiphasic oscillations between Srx and hyperoxidised Prdx3 in mitochondria (Kil et al., 2015).

Finally, I investigated whether loss of Srx affects neuron morphology in both *Drosophila* and rat primary neuron cultures, which may underlie physiological phenotypes of *Srx* mutant flies. In *Drosophila*, neurons exhibited increased growth *in vivo* and *in vitro*, which suggests changes to the plasticity of neural networks that underlie physiological phenotypes. I validated the discoveries made in *Drosophila* using *in vitro* mammalian cell cultures. HEK293t cells transfected with shRNA molecules targeting Srx did not exhibit differences in H_2O_2 production. Rat primary hippocampal neurons similarly exhibited overgrowths that mirrored the changes observed in *Drosophila Srx* mutants. The similarity in phenotypes observed across rat and *Drosophila* neurons suggests that the function of Srx is conserved across organisms.

6.2. Role of Srx in regulating redox homeostasis

These findings, in which Srx has no significant effect on ROS production and modest effects on tolerance to OS, suggest that Srx does not primarily function to provide defence against ROS. This may reflect genetic redundancy in the *Drosophila* and mammalian genome, whereby this function is primarily served by alternative antioxidant enzymes, such as those that comprise the glutathione system. Notably, the administration of DEM in fly food, to inhibit the glutathione system, reliably increased Nrf2 and AP-1 signalling in *Drosophila* tissue following use of the *gstD1-GFP* and *TRE-DsRed.T4* transgenes, respectively. Srx may provide a modulatory function to control the redox state of proteins within specific cellular processes, locations, and timepoints such as neurodevelopment.

There is contrasting evidence in the literature to support my finding that Srx confers modest protection against OS. McGinnis et al. (2021) found that *Srx* mutations slightly increased *Drosophila* survival when fed H_2O_2-supplemented sucrose solution. Studies in fission yeast have observed that Srx overexpression confers decreased survival under conditions of OS (Day et al., 2012). This is hypothesised to be caused by increased oxidation of Trx by 2-Cys Prdx enzymes, preventing Trx from reducing alternative substrates that are critical for cell survival (see Chapter 3.3.3). Other studies suggest that Srx protects against ROS and promotes cell survival. Knockdown of Srx using short interfering RNAs (siRNAs) increases lipid peroxidation in ischaemic rat brain cortices (Wu et al., 2017), whereas over-expressing

Srx in ischaemic rat spinal cord cultures decreases lipid peroxidation levels and cell apoptosis (Lan et al., 2021). In non-neuronal mammalian cells, similar findings have been made. Human lung carcinoma cells exposed to glucose oxidase, a H_2O_2-generating enzyme, apoptose at a greater rate following loss of Srx (Baek et al., 2012). The contrasting findings, regarding the role of Srx in protecting against OS, may reflect the heterogeneous properties of cells and organisms used in the aforementioned studies and reflect the fact that Srx serves a modulatory role within processes that are differentially carried out in certain cell types.

Future work should resolve the modulatory roles of Srx by conducting unbiased screens that identify proteins with differentially oxidised cysteine residues following loss of Srx. Performing such proteomics screens using multiple organisms and tissues will help to elucidate the role of Srx amongst cells with different functions. The aforementioned experiments could be conducted using protein lysates treated with biotinylated Iodoacetamide (BIAM), a compound that conjugates to nascent free thiols. Proteins labelled with BIAM can be analysed using mass spectrometry to identify those that undergo differential cysteine residue oxidation following loss of Srx (reviewed in Löwe et al., 2019). I investigated the feasibility of this experiment using rat primary hippocampal neurons. Neurons were left untreated or treated with 100 µm DEM or H_2O_2 for 24 hours. Protein lysates derived from these cells were treated with BIAM and analysed using SDS-PAGE and Streptavidin-HRP conjugated antibodies (Figure 6.1). Treatment with DEM or H_2O_2 decreased the chemiluminescence, indicating that there were fewer unoxidised cysteine residues in these protein lysates.

Figure 6.1. OS reduces the proportion of free nascent thiols in primary hippocampal neuron protein lysates.
Neurons treated with 100 µm DEM or 100 µm H_2O_2 exhibit fewer oxidised cysteine residues, as determined by decreased the labelling of free thiols by BIAM as shown by diminished chemiluminescence. Future experiments should aim to combine BIAM labelling with mass-spectrometry to identify the proteins affected by increased cysteine oxidation following loss of Srx in *Drosophila* and mammalian tissues.

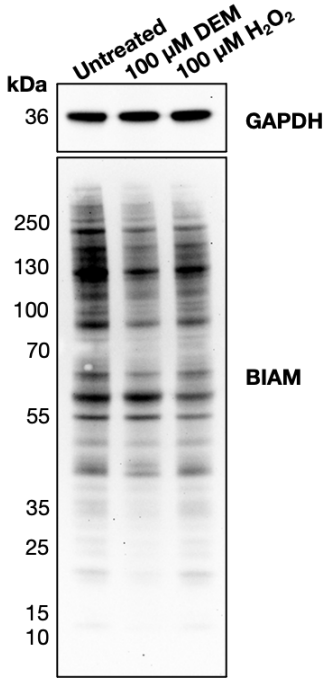

6.3. Srx as a modifier of neuron development

This work found that loss of Srx enhanced neuron growth in *Drosophila*. Increased numbers of synaptic boutons were observed at *Srx* mutant third instar larval NMJs. The expression of a *UAS-Srx.FLAG* transgene in the neurons of *Srx* mutant larvae failed to rescue NMJ overgrowths, which may be attributed to the C-terminal FLAG tag altering the structure and function of Srx. The FLAG tag may impede Srx interactions with specific substrates or prevent it localising to certain organelles. Future work should repeat these experiments using a *UAS-Srx* transgene without a conjugated FLAG tag. It is interesting to note that *UAS-Srx.FLAG* transgene expression in the neurons of *Srx* mutant flies successfully rescued the enhanced negative geotaxis response, suggesting that the loss of Srx interacting with distinct substrates facilitated these phenotypes.

Administration of NAC in the food that larvae were reared in also failed to rescue the increased NMJ growth. This may be because NAC, which is postulated to provide cysteine for the rate-determining step of glutathione synthesis, may alter glutathione dynamics and produce phenotypes of its own. Future work should aim to use alternative antioxidants, like the soluble tocopherol Trolox (Poljšak and Raspor, 2008), to see if this rescues the increased neuron growth at the NMJ.

Despite failed attempts to rescue the NMJ overgrowths observed in *Srx* mutants, the enhanced neuron growth following loss of Srx was validated by performing embryonic neuron cultures. Neurons derived from *Srx* mutant embryos exhibited increased cumulative neurite lengths. Similarly, rat primary hippocampal neurons that underwent Srx knockdown also exhibited enhanced growth as demonstrated by sholl analysis, increased numbers of primary neurites, and increased cumulative neurite lengths.

Future research should aim to elucidate the mechanisms underpinning increased neuron growth following loss of Srx, which may be informed by the BIAM-labelling/mass-spectrometry experiments discussed in Chapter 6.2. Such proteomics screens will identify proteins that have differentially oxidised cysteine residues in response to loss of Srx, which may have well characterised roles in regulating neuron growth. This offers an unbiased, data-driven approach to unravelling the relationship between Srx and neuron growth.

As an alternative to an unbiased screen, a candidate-led experimental approach could be employed to probe the mechanisms underpinning neuron growth following loss of Srx. This study found *Drosophila* wing size, which is a phenotype regulated by PI3K/Akt signalling, to be increased by *Srx* mutations (Gao et al., 2000). PI3K/Akt/mTOR signalling also positively regulates neuron growth at the *Drosophila* NMJ (Martín-Peña et al., 2006) and in rat primary neuron cultures (Jaworski et al., 2005). Therefore, PI3K/Akt signalling may also facilitate the neuron growth enhanced by loss of Srx. Srx knockdown may produce biomarkers of upregulated PI3K/Akt signalling such as increased phosphorylation of Akt, which is readily detected by phospo-Akt specific antibodies (Sun et al., 1999). If the relevant biomarkers suggest that loss of Srx upregulates PI3K/Akt signalling, upstream components of this pathway can be modified to see if this rescues the enhanced neuron growth. Overexpression of PTEN, which antagonises PI3K/Akt signalling, is one strategy that could be employed to try to rescue the neuron overgrowths observed following Srx knockdown.

6.4. Other future directions to explore

This study found that redox-sensitive signalling pathways may be differentially induced by *Srx* mutations (see Chapter 3), with AP-1 signalling seemingly downregulated. The physiological differences observed in Chapter 4 similarly indicated that redox-sensitive signalling pathways may be perturbed following loss of Srx *Drosophila*. This work sought to resolve whether Srx knockdown affected mitochondrial counts or mitochondrial morphology neurons, as redox signalling has important implications for mitophagy.

Loss of Srx in rat primary hippocampal neurons did not affect mitochondrial counts or mitochondrial morphology, which indicates that mitophagy was not induced. Mitophagy is known to be induced by strong and mild OS, with the latter doing so in a manner that is independent of non-selective autophagy and dependent on mitochondrial fission (Frank et al., 2012). Future experiments should address whether loss of Srx affects mitophagy in cells treated with carbonyl cyanide m-chlorophenylhydrazone (CCCP), an uncoupler of mitochondrial oxidative phosphorylation that reduces mitochondrial membrane depolarisation to promote mitophagy. Manipulating Srx activity in combination with CCCP treatment will provide a clearer answer as to how Srx regulates mitophagy (discussed extensively in Chapter 5.3.2).

The relevance of Srx to non-selective macroautophagy and apoptosis as a whole remains to be fully characterised. He et al. (2021) observed that the pharmacological Srx inhibitor J14 enhanced apoptosis in mouse pancreatic acini cells co-treated with cerulein to induce acute pancreatitis (AP). Increased expression of cleaved caspase 3 was used as an indicator of apoptosis induction. Caspase 3 is an 'executioner caspase' that is cleaved from pro-caspase 3 to initiate apoptosis (D'Amelio et al., 2010). He et al. (2021) also found that pharmacological inhibition of PRKR-like endoplasmic reticulum kinase (PERK), a kinase that phosphorylates eukaryotic initiation factor 2 α (eIF2α) to stimulate the integrated stress response, rescued the Srx inhibition-mediated increase in cleaved caspase 3 expression. Conversely, pharmacologically enhancing PERK signalling, using a eIF2α phosphatase inhibitor, potentiated Srx inhibition-mediated increases in cleaved caspase 3 expression. He et al. (2021) also observed that enhancing ER-stress correlated with increased expression of active Cathepsin B and vice versa. Cathepsin B is a cysteine protease released from lysosomes in response to OS that can stimulate caspase-dependent apoptosis (Wang et al., 2023). Collectively these findings suggest Srx protects against AP by maintaining ROS homeostasis in the ER to prevent Cathepsin B activation and caspase-mediated apoptosis.

The work of He et al. (2021) failed to acknowledge that Cathepsin B is predicted to be a substrate of Srx, as identified by Akter et al. (2018). Increased oxidation of Cathepsin B cysteine residues, in the absence of Srx, may modulate apoptosis under specific conditions. Future work should validate whether changes to Cathepsin B activation, expression, localisation, or function are altered following genetic knockdown of Srx in neurons. Interestingly, Cathepsin B inhibition blocks neurite outgrowth in mouse primary cortical neurons *in vitro* due to perturbations of lysosomal trafficking (Jiang et al., 2020). Genetic interactions between Srx and Cathepsin B should be explored to see if modulating Cathepsin B can rescue neuron overgrowths induced by Srx knockdown. Furthermore, lysosomal trafficking and dynamics should be observed in neurons following Srx overexpression or knockdown to see if this recapitulates the changes seen following Cathepsin B inhibition in mouse neurons.

The effect of Srx reducing substrates besides Prdx enzymes is also yet to be fully characterised. Akter et al. (2018) identified 59 additional Srx substrates, including Cathepsin B and DJ-1. Future experiments should combine *Drosophila Srx* mutations with mutations to genes encoding these substrates to see if this potentiates or rescues the physiological phenotypes elucidated in Chapter 4. Any genetic interactions identified can be further characterised with cellular biochemical studies.

I undertook some experiments to explore whether putative Srx substrates were affected by changes to Srx expression in *Drosophila*. Western blots demonstrated that expression of DJ-1β (the neuronal *Drosophila* DJ-1 orthologue) was unperturbed in fly heads following changes to Srx expression (Appendix Figure 2). Protein lysates were derived from flies that had been reared on food containing sucrose-yeast solution with and without 5% H_2O_2 for 48 hours to induce OS, to see if this elucidated differences. However, no difference in DJ-1β levels were observed under either condition. Cellular localisation and function of DJ-1β may be affected by changes to Srx expression instead. Future experiments should apply this technique to other putative Srx substrates, like Cathepsin B, to further unveil the function of Srx.

6.5. Final conclusions

Overall, this work suggests that Srx principally serves a modulatory role in *Drosophila* and mammals to regulate the redox state of specific proteins and cellular processes, rather than conferring widespread defence against OS. *Srx* mutations have pronounced effects on *Drosophila* behaviour and physiology. Similarly, loss of Srx enhances neuron growth in *Drosophila* and in rat primary hippocampal neuron cultures. Future work should strive to elucidate the mechanisms underlying these changes to properly understand how this antioxidant protein regulates neuron morphology and function.

Appendix

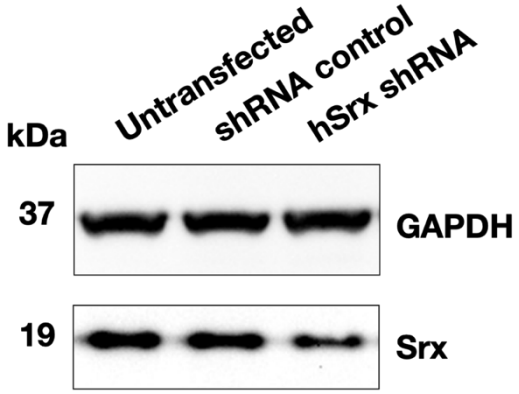

Appendix Figure 1. The transfection techniques used for the Amplex Red assay successfully decreased Srx expression in HEK293t cells.

The transfection techniques used for HEK293t cells produce heterogenous cultures in which most, but not all cells are transfected. Western blots were used to validate that the techniques used for the Amplex Red assay would diminish overall expression.

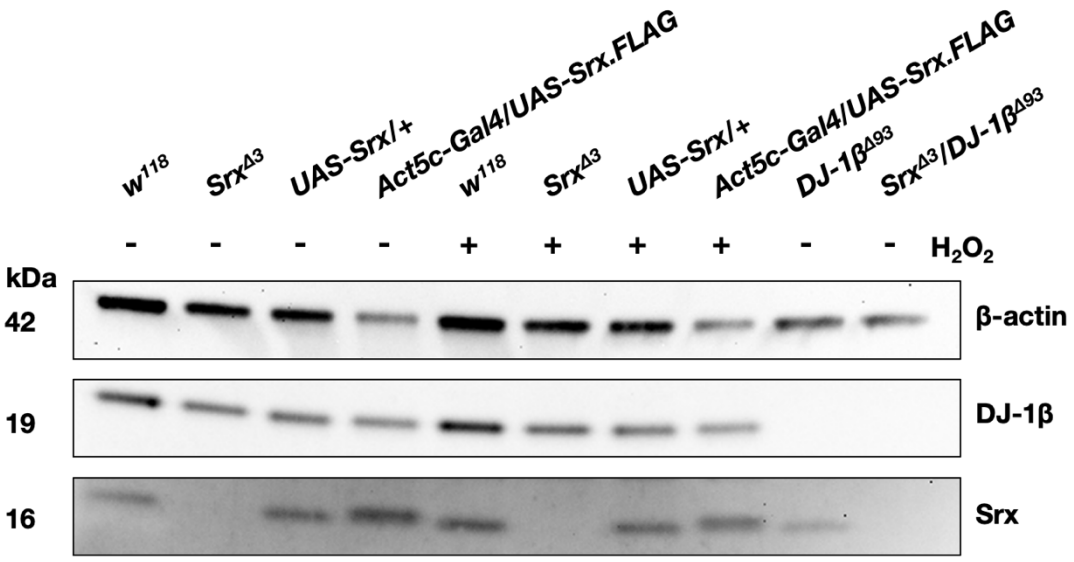

Appendix Figure 2. DJ-1β expression levels are unaffected by *Srx* mutations, or Srx overexpression in *Drosophila* heads.

Flies were reared on the food made from sucrose-yeast solution with and without 5% H_2O_2 to induce OS via feeding. Protein lysates derived from fly heads show that neither condition evoked changes to DJ-1β expression following changes to the expression of Srx. This indicates that, if DJ-1β is in fact a substrate of Srx, Srx does not regulate DJ-1β expression levels.

Abbreviations

AA - Amino acid

Act5c - Actin 5C

ACTH - Adrenocorticotropic hormone

AD - Alzheimer's Disease

ADP - Adenosine diphosphate

ALS - Amyotrophic lateral sclerosis

AMPA - α-amino-3-hydroxy-5-methyl-4-isoxazolepropionic acid

AMS - 4-acetamido-4′-maleimidylstilbene-2,2′-disulfonic acid

ANLS - Astrocyte-neuron lactate shuttle

ANOVA - Analysis of variance

AP-1 - Activator protein 1

ATF - Activating transcription factors

ATP - Adenosine triphosphate

BCA - Bicinchoninic Acid

BIAM - Biotinylated Iodoacetamide

BLAST - Basic local alignment search tool

bp - base pair(s)

Brp - Bruchpilot

BSA - Bovine serum albumin

bZIP - Basic-leucine zipper

CCCP - Carbonyl cyanide m-chlorophenylhydrazone

cDNA - complementary DNA

CDS - Coding sequence

CHO - Chinese hamster ovary (cells)

CNS - Central Nervous System

conA - concanavalin A

CoQ - Coenzyme Q

CRE - cAMP response element

CRY - Cryptochrome

CS - Corticosterone

DAM - *Drosophila* activity monitor

DD - Dark:Dark

DEM - Diethyl maleate

DEPC - Diethyl pyrocarbonate

DIV - days *in vitro*

DM - Dissociation media

DMEM - Dulbecco's modified eagle medium

DNA - Deoxyribonucleic acid

dNTP - Deoxynucleotide triphosphates

Dfz2 - *Drosophila* frizzled 2

DRP1 - Dynamin-related protein 1

EDTA - Ethylenediaminetetraacetic acid (EDTA)

eIF2α - eukaryotic initiation factor 2 α

EJP - Excitatory junction potential

ER - Endoplasmic Reticulum

ERG - Electroretinogram

EST - Expressed sequence tag

ETC - Electron transport chain

EV - Empty vector

FADH2 - Flavin adenine dinucleotide

FFT - Fast fourier transform

FHD - Full high definition

FKBP - FK506-binding protein

FMN - Flavin mononucleotide

FOXO - Forkhead box O

FWRD - Forward (primer)

Gbb - Glass bottom boat

GFP - Green fluorescent protein

GluR - Glutamate receptor

GM - Growth media

GPCR - G protein-coupled receptor

Gpx - Glutathione peroxidase

GSK-3β - Glycogen synthase kinase-3β

GST - Glutathione s-transferase

GTP - Guanosine-5'-triphosphate

HBSS - Hank's balanced salt solution

HCC - Hepatocellular carcinoma (cells)

HEK293t - Human embryonic kidney 293t (cells)

HeLa - Henrietta Lacks (cells)

HEPES - 4-(2-hydroxyethyl)-1-piperazineethanesulfonic acid

HIS - Polyhistidine tag

HMW - High molecular weight

HRP - Horseradish peroxidase

HSP - Heat shock protein

hSrx - Human Sulfiredoxin-1

IP3 - Inositol-1,4,5-triphosphate (IP3)

JNK - c-Jun N-terminal kinase

KD - Kilo Daltons

KEAP1 - Kelch-like ECH-associated protein 1

KY - Kynurenate-Magnesium Solution

LAMP2A - Lysosome-associated membrane protein 2A

LB - Luria-Bertani (media)

LC3 - Light Chain 3

LD - Light:dark

LDH - Lactate dehydrogenase

LED - Light-emitting diode

LOF - Loss-of-function

LTP - Long-term potentiation

MAO - Monoamine oxidase

MAPK - Mitogen-activated protein kinase

MAPKK - Mitogen-activated protein kinase kinase

MAPKKK - Mitogen-activated protein kinase kinase kinase

MBP - Maltose-Binding Protein

MDA - Malondialdehyde

MEF - Mouse embryonic fibroblast (cells)

MHC - Myosin heavy chain

MOPS - 3-Morpholinopropane sulfonic acid (buffer)

MSA - Muscle surface area

mSrx - Mouse Sulfiredoxin-1

mTOR - Mammalian target of rapamycin

mTORC - mTOR complex

NAC - n acetyl cysteine

NAD+ - Nicotinamide adenine dinucleotide (oxidised)

NADH - Nicotinamide adenine dinucleotide (reduced)

NADPH - Nicotinamide adenine dinucleotide phosphate

NMJ - Neuromuscular Junction

NOX - NADPH oxidase

Nrf2 - Nuclear factor erythroid 2-related factor 2

NT - Neurotransmitter

nt - nucleotide(s)

OS - Oxidative stress

PAGE -Polyacrylamide gel electrophoresis

PBS - Phosphate buffer solution

PBT - PBS with 0.05% Triton X-100

PCR - Polymerase chain reaction

PD - Parkinson’s disease

PE - P-Element

PER - Period

PERK - PRKR-like endoplasmic reticulum kinase

PET - Positron emission tomography

PFA - Paraformaldehyde

PI3K - Phosphoinositide 3-kinase

PINK1 - PTEN-induced kinase 1

PIP2 - Phosphatidylinositol-4,5-biphosphate

PIP3 - phosphatidylinositol-3,4,5-triphosphate (PIP3)

PLC - Phospholipase C

PMSF - Phenylmethylsulfonyl fluoride

PPP - Pentose phosphate pathway

Prdx - Peroxiredoxin

PTEN - Phosphatase and tensin homolog

qPCR - quantitative PCR

RCF - Relative centrifugal force

RET - Reverse electron transport

RF - Reading frame

Rh - Rhosopsin

RIPA - Radioimmunoprecipitation assay (buffer)

RISC - RNA-induced silencing complex

RNA - Ribonucleic acid

RNAi - RNA interference

RNS - Reactive Nitrogen species

ROS - Reactive oxygen species

RPM - Revolutions per minute

rSrx - Rat Sulfiredoxin-1

RT-PCR - reverse transcription PCR

RTK - Receptor tyrosine kinase

RVRS - Reverse (primer)

SDS - Sodium dodecyl sulphate

sgg - shaggy

shRNA - short hairpin RNA

siRNA - short interfering RNA

SNc - Substantia nigra pars compacta

SOD - Superoxide dismutase

Srx - Sulfiredoxin-1

SSVEP - Steady state visually-evoked potential

Syn - Synaptotagmin

TAE - Tris-acetate-EDTA buffer

TBS - Tris-buffered saline (buffer)

TBS-T - TBS with 0.1% Tween-20

TH - Tyrosine hydroxylase

TIM - Timeless

TIM - Translocase Of Inner Mitochondrial Membrane

TNPO - Transportin

TOM20 - Translocase Of Outer Mitochondrial Membrane 20

TPA - 12-O-tetradecanoylphorbol 13-acetate

TRE - TPA response element

TRP - Transient receptor potential

Trx - Thioredoxin

TrxR - Thioredoxin Reductase

TTFL - Transcription-translation feedback loop

U2OS - U2 osteosarcoma (cells)

UAS - Upstream activation sequence

UV - Ultraviolet (light)

VMAT2 - Vesicular monoamine transporter 2

wg - wingless

WT - Wild type

Bibliography

Adams, M.D., Celniker, S.E., Holt, R.A., Evans, C.A., Gocayne, J.D., Amanatides, P.G., Scherer, S.E., Li, P.W., Hoskins, R.A., Galle, R.F., George, R.A., Lewis, S.E., Richards, S., Ashburner, M., Henderson, S.N., Sutton, G.G., Wortman, J.R., Yandell, M.D., Zhang, Q., Chen, L.X., Brandon, R.C., Rogers, Y.-H.C., Blazej, R.G., Champe, M., Pfeiffer, B.D., Wan, K.H., Doyle, C., Baxter, E.G., Helt, G., Nelson, C.R., Gabor, G.L., Miklos, Abril, J.F., Agbayani, A., An, H.-J., Andrews-Pfannkoch, C., Baldwin, D., Ballew, R.M., Basu, A., Baxendale, J., Bayraktaroglu, L., Beasley, E.M., Beeson, K.Y., Benos, P.V., Berman, B.P., Bhandari, D., Bolshakov, S., Borkova, D., Botchan, M.R., Bouck, J., Brokstein, P., Brottier, P., Burtis, K.C., Busam, D.A., Butler, H., Cadieu, E., Center, A., Chandra, I., Cherry, J.M., Cawley, S., Dahlke, C., Davenport, L.B., Davies, P., Pablos, B.D., Delcher, A., Deng, Z., Mays, A.D., Dew, I., Dietz, S.M., Dodson, K., Doup, L.E., Downes, M., Dugan-Rocha, S., Dunkov, B.C., Dunn, P., Durbin, K.J., Evangelista, C.C., Ferraz, C., Ferriera, S., Fleischmann, W., Fosler, C., Gabrielian, A.E., Garg, N.S., Gelbart, W.M., Glasser, K., Glodek, A., Gong, F., Gorrell, J.H., Gu, Z., Guan, P., Harris, M., Harris, N.L., Harvey, D., Heiman, T.J., Hernandez, J.R., Houck, J., Hostin, D., Houston, K.A., Howland, T.J., Wei, M.-H., Ibegwam, C., Jalali, M., Kalush, F., Karpen, G.H., Ke, Z., Kennison, J.A., Ketchum, K.A., Kimmel, B.E., Kodira, C.D., Kraft, C., Kravitz, S., Kulp, D., Lai, Z., Lasko, P., Lei, Y., Levitsky, A.A., Li, J., Li, Z., Liang, Y., Lin, X., Liu, X., Mattei, B., McIntosh, T.C., McLeod, M.P., McPherson, D., Merkulov, G., Milshina, N.V., Mobarry, C., Morris, J., Moshrefi, A., Mount, S.M., Moy, M., Murphy, B., Murphy, L., Muzny, D.M., Nelson, D.L., Nelson, D.R., Nelson, K.A., Nixon, K., Nusskern, D.R., Pacleb, J.M., Palazzolo, M., Pittman, G.S., Pan, S., Pollard, J., Puri, V., Reese, M.G., Reinert, K., Remington, K., Saunders, R.D.C., Scheeler, F., Shen, H., Shue, B.C., Sidén-Kiamos, I., Simpson, M., Skupski, M.P., Smith, T., Spier, E., Spradling, A.C., Stapleton, M., Strong, R., Sun, E., Svirskas, R., Tector, C., Turner, R., Venter, E., Wang, A.H., Wang, X., Wang, Z.-Y., Wassarman, D.A., Weinstock, G.M., Weissenbach, J., Williams, S.M., Woodage, T., Worley, K.C., Wu, D., Yang, S., Yao, Q.A., Ye, J., Yeh, R.-F., Zaveri, J.S., Zhan, M., Zhang, G., Zhao, Q., Zheng, L., Zheng, X.H., Zhong, F.N., Zhong, W., Zhou, X., Zhu, S., Zhu, X., Smith, H.O., Gibbs, R.A., Myers, E.W., Rubin, G.M., Venter, J.C., 2000. The Genome Sequence of Drosophila melanogaster. Science 287, 2185–2195. https://doi.org/10.1126/science.287.5461.2185

Afsari, F., Christensen, K.V., Smith, G.P., Hentzer, M., Nippe, O.M., Elliott, C.J.H., Wade, A.R., 2014. Abnormal visual gain control in a Parkinson's disease model. Hum. Mol. Genet. 23, 4465–4478. https://doi.org/10.1093/hmg/ddu159

Akiyama, H., Kamiguchi, H., 2015. Second messenger networks for accurate growth cone guidance. Dev. Neurobiol. 75, 411–422. https://doi.org/10.1002/dneu.22157

Akter, S., Fu, L., Jung, Y., Conte, M.L., Lawson, J.R., Lowther, W.T., Sun, R., Liu, K., Yang, J., Carroll, K.S., 2018. Chemical proteomics reveals new targets of cysteine sulfinic acid reductase. Nat. Chem. Biol. 14, 995–1004. https://doi.org/10.1038/s41589-018-0116-2

Aldini, G., Altomare, A., Baron, G., Vistoli, G., Carini, M., Borsani, L., Sergio, F., 2018. N-Acetylcysteine as an antioxidant and disulphide breaking agent: the reasons why. Free Radic. Res. 52, 751–762. https://doi.org/10.1080/10715762.2018.1468564

Álvarez-Fernández, R., 2013. Chapter One - Explanatory Chapter: PCR Primer Design, in: Methods in Enzymology. Elsevier, pp. 1–21. https://doi.org/10.1016/B978-0-12-418687-3.00001-X

Andres-Mateos, E., Perier, C., Zhang, L., Blanchard-Fillion, B., Greco, T.M., Thomas, B., Ko, H.S., Sasaki, M., Ischiropoulos, H., Przedborski, S., Dawson, T.M., Dawson, V.L., 2007. DJ-1 gene deletion reveals that DJ-1 is an atypical peroxiredoxin-like peroxidase. Proc. Natl. Acad. Sci. U. S. A. 104, 14807–14812. https://doi.org/10.1073/pnas.0703219104

Angel, P., Imagawa, M., Chiu, R., Stein, B., Imbra, R.J., Rahmsdorf, H.J., Jonat, C., Herrlich, P., Karin, M., 1987. Phorbol ester-inducible genes contain a common cis element recognized by a TPA-modulated trans-acting factor. Cell 49, 729–739. https://doi.org/10.1016/0092-8674(87)90611-8

Atwood, H.L., Govind, C.K., Wu, C.F., 1993. Differential ultrastructure of synaptic terminals on ventral longitudinal abdominal muscles in Drosophila larvae. J. Neurobiol. 24, 1008–1024. https://doi.org/10.1002/neu.480240803

Ayala, A., Muñoz, M.F., Argüelles, S., 2014. Lipid Peroxidation: Production, Metabolism, and Signaling Mechanisms of Malondialdehyde and 4-Hydroxy-2-Nonenal. Oxid. Med. Cell. Longev. 2014, 1–31. https://doi.org/10.1155/2014/360438

Baba, S.P., Bhatnagar, A., 2018. Role of thiols in oxidative stress. Curr. Opin. Toxicol. 7, 133–139. https://doi.org/10.1016/j.cotox.2018.03.005

Bachmann, A., Knust, E., 2008. The Use of P-Element Transposons to Generate Transgenic Flies, in: Dahmann, C. (Ed.), Drosophila, Methods in Molecular Biology. Humana Press, Totowa, NJ, pp. 61–77. https://doi.org/10.1007/978-1-59745-583-1_4

Baek, J.Y., Han, S.H., Sung, S.H., Lee, H.E., Kim, Y., Noh, Y.H., Bae, S.H., Rhee, S.G., Chang, T.-S., 2012. Sulfiredoxin Protein Is Critical for Redox Balance and Survival of Cells Exposed to Low Steady-state Levels of H2O2*. J. Biol. Chem. 287, 81–89. https://doi.org/10.1074/jbc.M111.316711

Banerjee, S., Bhat, M.A., 2008. Glial ensheathment of peripheral axons in Drosophila. J. Neurosci. Res. 86, 1189–1198. https://doi.org/10.1002/jnr.21574

Behl, C., 2000. Vitamin E protects neurons against oxidative cell death in vitro more effectively than 17-β estradiol and induces the activity of the transcription factor NF-κB. J. Neural Transm. 107, 393–407. https://doi.org/10.1007/s007020070082

Behrens, A., Sibilia, M., Wagner, E.F., 1999. Amino-terminal phosphorylation of c-Jun regulates stress-induced apoptosis and cellular proliferation. Nat. Genet. 21, 326–329. https://doi.org/10.1038/6854

Bejarano, E., Cuervo, A.M., 2010. Chaperone-Mediated Autophagy. Proc. Am. Thorac. Soc. 7, 29–39. https://doi.org/10.1513/pats.200909-102JS

Bejjani, F., Evanno, E., Zibara, K., Piechaczyk, M., Jariel-Encontre, I., 2019. The AP-1 transcriptional complex: Local switch or remote command? Biochim. Biophys. Acta BBA - Rev. Cancer 1872, 11–23. https://doi.org/10.1016/j.bbcan.2019.04.003

Bell, K.F.S., Al-Mubarak, B., Martel, M.-A., McKay, S., Wheelan, N., Hasel, P., Márkus, N.M., Baxter, P., Deighton, R.F., Serio, A., Bilican, B., Chowdhry, S., Meakin, P.J., Ashford, M.L.J., Wyllie, D.J.A., Scannevin, R.H., Chandran, S., Hayes, J.D., Hardingham, G.E., 2015. Neuronal development is promoted by weakened intrinsic antioxidant defences due to epigenetic repression of Nrf2. Nat. Commun. 6, 7066. https://doi.org/10.1038/ncomms8066

Bellen, H.J., Levis, R.W., He, Y., Carlson, J.W., Evans-Holm, M., Bae, E., Kim, J., Metaxakis, A., Savakis, C., Schulze, K.L., Hoskins, R.A., Spradling, A.C., 2011. The Drosophila Gene Disruption Project: Progress Using Transposons With Distinctive Site Specificities. Genetics 188, 731–743. https://doi.org/10.1534/genetics.111.126995

Bellen, H.J., Levis, R.W., Liao, G., He, Y., Carlson, J.W., Tsang, G., Evans-Holm, M., Hiesinger, P.R., Schulze, K.L., Rubin, G.M., Hoskins, R.A., Spradling, A.C., 2004. The BDGP Gene Disruption Project. Genetics 167, 761–781. https://doi.org/10.1534/genetics.104.026427

Bischof, J., Maeda, R.K., Hediger, M., Karch, F., Basler, K., 2007. An optimized transgenesis system for *Drosophila* using germ-line-specific φC31 integrases. Proc. Natl. Acad. Sci. 104, 3312–3317. https://doi.org/10.1073/pnas.0611511104

Biteau, B., Labarre, J., Toledano, M.B., 2003. ATP-dependent reduction of cysteine–sulphinic acid by S. cerevisiae sulphiredoxin. Nature 425, 980–984. https://doi.org/10.1038/nature02075

Blackinton, J., Lakshminarasimhan, M., Thomas, K.J., Ahmad, R., Greggio, E., Raza, A.S., Cookson, M.R., Wilson, M.A., 2009. Formation of a stabilized cysteine sulfinic acid is critical for the mitochondrial function of the parkinsonism protein DJ-1. J. Biol. Chem. 284, 6476–6485. https://doi.org/10.1074/jbc.M806599200

Bolaños, J.P., Almeida, A., 2010. The pentose-phosphate pathway in neuronal survival against nitrosative stress. IUBMB Life 62, 14–18. https://doi.org/10.1002/iub.280

Bonifati, V., Rizzu, P., Van Baren, M.J., Schaap, O., Breedveld, G.J., Krieger, E., Dekker, M.C.J., Squitieri, F., Ibanez, P., Joosse, M., Van Dongen, J.W., Vanacore, N., Van Swieten, J.C., Brice, A., Meco, G., Van Duijn, C.M., Oostra, B.A., Heutink, P., 2003. Mutations in the DJ-1 Gene Associated with Autosomal Recessive Early-Onset Parkinsonism. Science 299, 256–259. https://doi.org/10.1126/science.1077209

Brand, A.H., Perrimon, N., 1993. Targeted gene expression as a means of altering cell fates and generating dominant phenotypes. Development 118, 401–415. https://doi.org/10.1242/dev.118.2.401

Brawn, K., Fridovich, I., 1981. DNA strand scission by enzymically generated oxygen radicals. Arch. Biochem. Biophys. 206, 414–419. https://doi.org/10.1016/0003-9861(81)90108-9

Broadie, K., Bate, M., 1995. The Drosophila NMJ: a genetic model system for synapse formation and function. Semin. Dev. Biol. 6, 221–231. https://doi.org/10.1016/S1044-5781(06)80031-9

Brown, J.B., Boley, N., Eisman, R., May, G.E., Stoiber, M.H., Duff, M.O., Booth, B.W., Wen, J., Park, S., Suzuki, A.M., Wan, K.H., Yu, C., Zhang, D., Carlson, J.W., Cherbas, L., Eads, B.D., Miller, D., Mockaitis, K., Roberts, J., Davis, C.A., Frise, E., Hammonds, A.S., Olson, S., Shenker, S., Sturgill, D., Samsonova, A.A., Weiszmann, R., Robinson, G., Hernandez, J., Andrews, J., Bickel, P.J., Carninci, P., Cherbas, P., Gingeras, T.R., Hoskins, R.A., Kaufman, T.C., Lai, E.C., Oliver, B., Perrimon, N., Graveley, B.R., Celniker, S.E., 2014. Diversity and dynamics of the Drosophila transcriptome. Nature 512, 393–399. https://doi.org/10.1038/nature12962

Brownawell, A.M., Kops, G.J.P.L., Macara, I.G., Burgering, B.M.T., 2001. Inhibition of Nuclear Import by Protein Kinase B (Akt) Regulates the Subcellular Distribution and Activity of the Forkhead Transcription Factor AFX. Mol. Cell. Biol. 21, 3534–3546. https://doi.org/10.1128/MCB.21.10.3534-3546.2001

Brunet, A., Bonni, A., Zigmond, M.J., Lin, M.Z., Juo, P., Hu, L.S., Anderson, M.J., Arden, K.C., Blenis, J., Greenberg, M.E., 1999. Akt Promotes Cell Survival by Phosphorylating and Inhibiting a Forkhead Transcription Factor. Cell 96, 857–868. https://doi.org/10.1016/S0092-8674(00)80595-4

Brunet, A., Sweeney, L.B., Sturgill, J.F., Chua, K.F., Greer, P.L., Lin, Y., Tran, H., Ross, S.E., Mostoslavsky, R., Cohen, H.Y., Hu, L.S., Cheng, H.-L., Jedrychowski, M.P., Gygi, S.P., Sinclair, D.A., Alt, F.W., Greenberg, M.E., 2004. Stress-Dependent Regulation of FOXO Transcription Factors by the SIRT1 Deacetylase. Science 303, 2011–2015. https://doi.org/10.1126/science.1094637

Buhl, E., Bradlaugh, A., Ogueta, M., Chen, K.-F., Stanewsky, R., Hodge, J.J.L., 2016. Quasimodo mediates daily and acute light effects on Drosophila clock neuron excitability. Proc. Natl. Acad. Sci. 113, 13486–13491. https://doi.org/10.1073/pnas.1606547113

Buul, J.D.V., Fernandez-Borja, M., Anthony, E.C., Hordijk, P.L., 2005. Expression and Localization of NOX2 and NOX4 in Primary Human Endothelial Cells. Antioxid. Redox Signal. 7, 308–317. https://doi.org/10.1089/ars.2005.7.308

Cadenas, E., Boveris, A., Ragan, C.I., Stoppani, A.O.M., 1977. Production of superoxide radicals and hydrogen peroxide by NADH-ubiquinone reductase and ubiquinol-cytochrome c reductase from beef-heart mitochondria. Arch. Biochem. Biophys. 180, 248–257. https://doi.org/10.1016/0003-9861(77)90035-2

Campos-Ortega, J.A., Hartenstein, V., 1997. The Embryonic Development of Drosophila melanogaster. Springer Berlin Heidelberg, Berlin, Heidelberg. https://doi.org/10.1007/978-3-662-22489-2

Canet-Avilés, R.M., Wilson, M.A., Miller, D.W., Ahmad, R., McLendon, C., Bandyopadhyay, S., Baptista, M.J., Ringe, D., Petsko, G.A., Cookson, M.R., 2004. The Parkinson's disease protein DJ-1 is neuroprotective due to cysteine-sulfinic acid-driven mitochondrial localization. Proc. Natl. Acad. Sci. U. S. A. 101, 9103–9108. https://doi.org/10.1073/pnas.0402959101

Cao, J., Schulte, J., Knight, A., Leslie, N.R., Zagozdzon, A., Bronson, R., Manevich, Y., Beeson, C., Neumann, C.A., 2009. Prdx1 inhibits tumorigenesis via regulating PTEN/AKT activity. EMBO J. 28, 1505–1517. https://doi.org/10.1038/emboj.2009.101

Cargnello, M., Roux, P.P., 2011. Activation and function of the MAPKs and their substrates, the MAPK-activated protein kinases. Microbiol. Mol. Biol. Rev. MMBR 75, 50–83. https://doi.org/10.1128/MMBR.00031-10

Castillo, E.A., Ayté, J., Chiva, C., Moldón, A., Carrascal, M., Abián, J., Jones, N., Hidalgo, E., 2002. Diethylmaleate activates the transcription factor Pap1 by covalent modification of critical cysteine residues. Mol. Microbiol. 45, 243–254. https://doi.org/10.1046/j.1365-2958.2002.03020.x

Chacinska, A., Koehler, C.M., Milenkovic, D., Lithgow, T., Pfanner, N., 2009. Importing Mitochondrial Proteins: Machineries and Mechanisms. Cell 138, 628–644. https://doi.org/10.1016/j.cell.2009.08.005

Chae, H.Z., Chung, S.J., Rhee, S.G., 1994a. Thioredoxin-dependent peroxide reductase from yeast. J. Biol. Chem. 269, 27670–27678.

Chae, H.Z., Uhm, T.B., Rhee, S.G., 1994b. Dimerization of thiol-specific antioxidant and the essential role of cysteine 47. Proc. Natl. Acad. Sci. U. S. A. 91, 7022–7026. https://doi.org/10.1073/pnas.91.15.7022

Chance, B., Hollunger, G., 1961. The Interaction of Energy and Electron Transfer Reactions in Mitochondria. J. Biol. Chem. 236, 1534–1543. https://doi.org/10.1016/S0021-9258(18)64210-3

Chang, T.-S., Jeong, W., Woo, H.A., Lee, S.M., Park, S., Rhee, S.G., 2004. Characterization of Mammalian Sulfiredoxin and Its Reactivation of Hyperoxidized Peroxiredoxin through Reduction of Cysteine Sulfinic Acid in the Active Site to Cysteine. J. Biol. Chem. 279, 50994–51001. https://doi.org/10.1074/jbc.M409482200

Chatterjee, N., Bohmann, D., 2012. A Versatile ΦC31 Based Reporter System for Measuring AP-1 and Nrf2 Signaling in Drosophila and in Tissue Culture. PLoS ONE 7, e34063. https://doi.org/10.1371/journal.pone.0034063

Chaudhry, A., Shi, R., Luciani, D.S., 2020. A pipeline for multidimensional confocal analysis of mitochondrial morphology, function, and dynamics in pancreatic β-cells. Am. J. Physiol.-Endocrinol. Metab. 318, E87–E101. https://doi.org/10.1152/ajpendo.00457.2019

Chaudhry, F.A., Edwards, R.H., Fonnum, F., 2008. Vesicular neurotransmitter transporters as targets for endogenous and exogenous toxic substances. Annu. Rev. Pharmacol. Toxicol. 48, 277–301. https://doi.org/10.1146/annurev.pharmtox.46.120604.141146

Chávez, V., Mohri-Shiomi, A., Maadani, A., Vega, L.A., Garsin, D.A., 2007. Oxidative Stress Enzymes Are Required for DAF-16-Mediated Immunity Due to Generation of Reactive

Oxygen Species by Caenorhabditis elegans. Genetics 176, 1567–1577. https://doi.org/10.1534/genetics.107.072587
Chen, D.F., Tonegawa, S., 1998. Why do mature CNS neurons of mammals fail to re-establish connections following injury–functions of Bcl-2. Cell Death Differ. 5, 816–822. https://doi.org/10.1038/sj.cdd.4400431
Chen, K., Featherstone, D.E., 2005. Discs-large (DLG) is clustered by presynaptic innervation and regulates postsynaptic glutamate receptor subunit composition in Drosophila. BMC Biol. 3, 1. https://doi.org/10.1186/1741-7007-3-1
Ciapponi, L., Bohmann, D., 2002. An essential function of AP-1 heterodimers in Drosophila development. Mech. Dev. 115, 35–40. https://doi.org/10.1016/S0925-4773(02)00093-X
Cichewicz, K., Hirsh, J., 2018. ShinyR-DAM: a program analyzing Drosophila activity, sleep and circadian rhythms. Commun. Biol. 1, 25. https://doi.org/10.1038/s42003-018-0031-9
Clark, I.E., Dodson, M.W., Jiang, C., Cao, J.H., Huh, J.R., Seol, J.H., Yoo, S.J., Hay, B.A., Guo, M., 2006. Drosophila pink1 is required for mitochondrial function and interacts genetically with parkin. Nature 441, 1162–1166. https://doi.org/10.1038/nature04779
Cochemé, H.M., Murphy, M.P., 2008. Complex I is the major site of mitochondrial superoxide production by paraquat. J. Biol. Chem. 283, 1786–1798. https://doi.org/10.1074/jbc.M708597200
Collins, C.A., Wairkar, Y.P., Johnson, S.L., DiAntonio, A., 2006. Highwire Restrains Synaptic Growth by Attenuating a MAP Kinase Signal. Neuron 51, 57–69. https://doi.org/10.1016/j.neuron.2006.05.026
Coulombe, P., Meloche, S., 2007. Atypical mitogen-activated protein kinases: Structure, regulation and functions. Biochim. Biophys. Acta BBA - Mol. Cell Res. 1773, 1376–1387. https://doi.org/10.1016/j.bbamcr.2006.11.001
Crapo, J.D., Oury, T., Rabouille, C., Slot, J.W., Chang, L.Y., 1992. Copper,zinc superoxide dismutase is primarily a cytosolic protein in human cells. Proc. Natl. Acad. Sci. 89, 10405–10409. https://doi.org/10.1073/pnas.89.21.10405
Cucos, C.A., Cracana, I., Dobre, M., Popescu, B.O., Tudose, C., Spiru, L., Manda, G., Niculescu, G., Milanesi, E., 2022. Sulfiredoxin-1 blood mRNA expression levels negatively correlate with hippocampal atrophy and cognitive decline. F1000Research 11, 114. https://doi.org/10.12688/f1000research.76191.2
Dalle-Donne, I., 2001. The actin cytoskeleton response to oxidants: from small heat shock protein phosphorylation to changes in the redox state of actin itself. Free Radic. Biol. Med. 31, 1624–1632. https://doi.org/10.1016/S0891-5849(01)00749-3
Dalle-Donne, I., Giustarini, D., Rossi, R., Colombo, R., Milzani, A., 2003. Reversible S-glutathionylation of Cys374 regulates actin filament formation by inducing structural changes in the actin molecule. Free Radic. Biol. Med. 34, 23–32. https://doi.org/10.1016/S0891-5849(02)01182-6
D'Amelio, M., Cavallucci, V., Cecconi, F., 2010. Neuronal caspase-3 signaling: not only cell death. Cell Death Differ. 17, 1104–1114. https://doi.org/10.1038/cdd.2009.180
D'Amico, E., Factor-Litvak, P., Santella, R.M., Mitsumoto, H., 2013. Clinical perspective on oxidative stress in sporadic amyotrophic lateral sclerosis. Free Radic. Biol. Med. 65, 509–527. https://doi.org/10.1016/j.freeradbiomed.2013.06.029
Day, A.M., Brown, J.D., Taylor, S.R., Rand, J.D., Morgan, B.A., Veal, E.A., 2012. Inactivation of a Peroxiredoxin by Hydrogen Peroxide Is Critical for Thioredoxin-Mediated Repair of Oxidized Proteins and Cell Survival. Mol. Cell 45, 398–408. https://doi.org/10.1016/j.molcel.2011.11.027
De Duve, C., Baudhuin, P., 1966. Peroxisomes (microbodies and related particles). Physiol. Rev. 46, 323–357. https://doi.org/10.1152/physrev.1966.46.2.323

De Luca, A., Moroni, N., Serafino, A., Primavera, A., Pastore, A., Pedersen, J.Z., Petruzzelli, R., Farrace, M.G., Pierimarchi, P., Moroni, G., Federici, G., Sinibaldi Vallebona, P., Lo Bello, M., 2011. Treatment of doxorubicin-resistant MCF7/Dx cells with nitric oxide causes histone glutathionylation and reversal of drug resistance. Biochem. J. 440, 175–183. https://doi.org/10.1042/BJ20111333

de Mendiburu, F., 2023. _agricolae: Statistical Procedures for Agricultural Research_.

DeGennaro, M., Hurd, T.R., Siekhaus, D.E., Biteau, B., Jasper, H., Lehmann, R., 2011. Peroxiredoxin Stabilization of DE-Cadherin Promotes Primordial Germ Cell Adhesion. Dev. Cell 20, 233–243. https://doi.org/10.1016/j.devcel.2010.12.007

Deisseroth, A., Dounce, A.L., 1970. Catalase: Physical and chemical properties, mechanism of catalysis, and physiological role. Physiol. Rev. 50, 319–375. https://doi.org/10.1152/physrev.1970.50.3.319

Demir, E., Kacew, S., 2023. Drosophila as a Robust Model System for Assessing Autophagy: A Review. Toxics 11, 682. https://doi.org/10.3390/toxics11080682

Denoncin, K., Nicolaes, V., Cho, S.-H., Leverrier, P., Collet, J.-F., 2013. Protein Disulfide Bond Formation in the Periplasm: Determination of the In Vivo Redox State of Cysteine Residues, in: Delcour, A.H. (Ed.), Bacterial Cell Surfaces, Methods in Molecular Biology. Humana Press, Totowa, NJ, pp. 325–336. https://doi.org/10.1007/978-1-62703-245-2_20

Dias, V., Junn, E., Mouradian, M.M., 2013. The Role of Oxidative Stress in Parkinson's Disease. J. Park. Dis. 3, 461–491. https://doi.org/10.3233/JPD-130230

Donida, B., Jacques, C.E.D., Mescka, C.P., Rodrigues, D.G.B., Marchetti, D.P., Ribas, G., Giugliani, R., Vargas, C.R., 2017. Oxidative damage and redox in Lysosomal Storage Disorders: Biochemical markers. Clin. Chim. Acta 466, 46–53. https://doi.org/10.1016/j.cca.2017.01.007

Dringen, R., 2000. Metabolism and functions of glutathione in brain. Prog. Neurobiol. 62, 649–671. https://doi.org/10.1016/S0301-0082(99)00060-X

Edgar, R.S., Green, E.W., Zhao, Y., Van Ooijen, G., Olmedo, M., Qin, X., Xu, Y., Pan, M., Valekunja, U.K., Feeney, K.A., Maywood, E.S., Hastings, M.H., Baliga, N.S., Merrow, M., Millar, A.J., Johnson, C.H., Kyriacou, C.P., O'Neill, J.S., Reddy, A.B., 2012. Peroxiredoxins are conserved markers of circadian rhythms. Nature 485, 459–464. https://doi.org/10.1038/nature11088

Essers, M.A.G., Weijzen, S., De Vries-Smits, A.M.M., Saarloos, I., De Ruiter, N.D., Bos, J.L., Burgering, B.M.T., 2004. FOXO transcription factor activation by oxidative stress mediated by the small GTPase Ral and JNK. EMBO J. 23, 4802–4812. https://doi.org/10.1038/sj.emboj.7600476

Etminan, M., Gill, S.S., Samii, A., 2005. Intake of vitamin E, vitamin C, and carotenoids and the risk of Parkinson's disease: a meta-analysis. Lancet Neurol. 4, 362–365. https://doi.org/10.1016/S1474-4422(05)70097-1

Fahn, S., Sulzer, D., 2004. Neurodegeneration and neuroprotection in Parkinson disease. NeuroRx J. Am. Soc. Exp. Neurother. 1, 139–154. https://doi.org/10.1602/neurorx.1.1.139

Fellgett, A., Middleton, C.A., Munns, J., Ugbode, C., Jaciuch, D., Wilson, L.G., Chawla, S., Elliott, C.J.H., 2021. Multiple Pathways of LRRK2-G2019S/Rab10 Interaction in Dopaminergic Neurons. J. Park. Dis. 11, 1805–1820. https://doi.org/10.3233/JPD-202421

Fernández-Moreno, M.A., Farr, C.L., Kaguni, L.S., Garesse, R., 2007. Drosophila melanogaster as a model system to study mitochondrial biology. Methods Mol. Biol. Clifton NJ 372, 33–49. https://doi.org/10.1007/978-1-59745-365-3_3

Ferreira, T.A., Blackman, A.V., Oyrer, J., Jayabal, S., Chung, A.J., Watt, A.J., Sjöström, P.J., Van Meyel, D.J., 2014. Neuronal morphometry directly from bitmap images. Nat. Methods 11, 982–984. https://doi.org/10.1038/nmeth.3125

FlyBase, 2024. FlyBase inference based on genome sequence analysis.
Folz, R.J., Crapo, J.D., 1994. Extracellular superoxide dismutase (SOD3): tissue-specific expression, genomic characterization, and computer-assisted sequence analysis of the human EC SOD gene. Genomics 22, 162–171. https://doi.org/10.1006/geno.1994.1357
Forman, H.J., Zhang, H., Rinna, A., 2009. Glutathione: overview of its protective roles, measurement, and biosynthesis. Mol. Aspects Med. 30, 1–12. https://doi.org/10.1016/j.mam.2008.08.006
Fourquet, S., Guerois, R., Biard, D., Toledano, M.B., 2010. Activation of NRF2 by Nitrosative Agents and H2O2 Involves KEAP1 Disulfide Formation. J. Biol. Chem. 285, 8463–8471. https://doi.org/10.1074/jbc.M109.051714
Fowler, J.S., Volkow, N.D., Wang, G.-J., Logan, J., Pappas, N., Shea, C., MacGregor, R., 1997. Age-Related Increases in Brain Monoamine Oxidase B in Living Healthy Human Subjects. Neurobiol. Aging 18, 431–435. https://doi.org/10.1016/S0197-4580(97)00037-7
Fox, J., Weisberg, S., 2019. _An R Companion to Applied Regression_.
Frank, M., Duvezin-Caubet, S., Koob, S., Occhipinti, A., Jagasia, R., Petcherski, A., Ruonala, M.O., Priault, M., Salin, B., Reichert, A.S., 2012. Mitophagy is triggered by mild oxidative stress in a mitochondrial fission dependent manner. Biochim. Biophys. Acta BBA - Mol. Cell Res. 1823, 2297–2310. https://doi.org/10.1016/j.bbamcr.2012.08.007
Fransen, M., Nordgren, M., Wang, B., Apanasets, O., 2012. Role of peroxisomes in ROS/RNS-metabolism: Implications for human disease. Biochim. Biophys. Acta BBA - Mol. Basis Dis. 1822, 1363–1373. https://doi.org/10.1016/j.bbadis.2011.12.001
Fukasawa, Y., Tsuji, J., Fu, S.-C., Tomii, K., Horton, P., Imai, K., 2015. MitoFates: improved prediction of mitochondrial targeting sequences and their cleavage sites. Mol. Cell. Proteomics MCP 14, 1113–1126. https://doi.org/10.1074/mcp.M114.043083
Ganetzky, B., Wu, C.-F., 1982. INDIRECT SUPPRESSION INVOLVING BEHAVIORAL MUTANTS WITH ALTERED NERVE EXCITABILITY IN DROSOPHILA MELANOGASTER. Genetics 100, 597–614. https://doi.org/10.1093/genetics/100.4.597
Gao, X., Neufeld, T.P., Pan, D., 2000. Drosophila PTEN Regulates Cell Growth and Proliferation through PI3K-Dependent and -Independent Pathways. Dev. Biol. 221, 404–418. https://doi.org/10.1006/dbio.2000.9680
Gjerstad, J.K., Lightman, S.L., Spiga, F., 2018. Role of glucocorticoid negative feedback in the regulation of HPA axis pulsatility. Stress 21, 403–416. https://doi.org/10.1080/10253890.2018.1470238
Gourlay, L.J., Bhella, D., Kelly, S.M., Price, N.C., Lindsay, J.G., 2003. Structure-Function Analysis of Recombinant Substrate Protein 22 kDa (SP-22). J. Biol. Chem. 278, 32631–32637. https://doi.org/10.1074/jbc.M303862200
Graham, K.A., Kulawiec, M., Owens, K.M., Li, X., Desouki, M.M., Chandra, D., Singh, K.K., 2010. NADPH oxidase 4 is an oncoprotein localized to mitochondria. Cancer Biol. Ther. 10, 223–231. https://doi.org/10.4161/cbt.10.3.12207
Guo, C., Ma, X., Gao, F., Guo, Y., 2023. Off-target effects in CRISPR/Cas9 gene editing. Front. Bioeng. Biotechnol. 11, 1143157. https://doi.org/10.3389/fbioe.2023.1143157
Haber, F., Weiss, J., 1934. The catalytic decomposition of hydrogen peroxide by iron salts. Proc. R. Soc. Lond. Ser. - Math. Phys. Sci. 147, 332–351. https://doi.org/10.1098/rspa.1934.0221
Halazonetis, T.D., Georgopoulos, K., Greenberg, M.E., Leder, P., 1988. c-Jun dimerizes with itself and with c-Fos, forming complexes of different DNA binding affinities. Cell 55, 917–924. https://doi.org/10.1016/0092-8674(88)90147-X

Hall, A., Karplus, P.A., Poole, L.B., 2009. Typical 2-Cys peroxiredoxins--structures, mechanisms and functions. FEBS J. 276, 2469–2477. https://doi.org/10.1111/j.1742-4658.2009.06985.x

Hall, C.N., Klein-Flugge, M.C., Howarth, C., Attwell, D., 2012. Oxidative Phosphorylation, Not Glycolysis, Powers Presynaptic and Postsynaptic Mechanisms Underlying Brain Information Processing. J. Neurosci. 32, 8940–8951. https://doi.org/10.1523/JNEUROSCI.0026-12.2012

Hayes, J.D., Dinkova-Kostova, A.T., 2014. The Nrf2 regulatory network provides an interface between redox and intermediary metabolism. Trends Biochem. Sci. 39, 199–218. https://doi.org/10.1016/j.tibs.2014.02.002

He, J., Ma, M., Li, D., Wang, K., Wang, Q., Li, Qiuguo, He, H., Zhou, Y., Li, Qinglong, Hou, X., Yang, L., 2021. Sulfiredoxin-1 attenuates injury and inflammation in acute pancreatitis through the ROS/ER stress/Cathepsin B axis. Cell Death Dis. 12, 626. https://doi.org/10.1038/s41419-021-03923-1

Heinz, S., Freyberger, A., Lawrenz, B., Schladt, L., Schmuck, G., Ellinger-Ziegelbauer, H., 2017. Mechanistic Investigations of the Mitochondrial Complex I Inhibitor Rotenone in the Context of Pharmacological and Safety Evaluation. Sci. Rep. 7, 45465. https://doi.org/10.1038/srep45465

Helfrich-Förster, C., Winter, C., Hofbauer, A., Hall, J.C., Stanewsky, R., 2001. The Circadian Clock of Fruit Flies Is Blind after Elimination of All Known Photoreceptors. Neuron 30, 249–261. https://doi.org/10.1016/S0896-6273(01)00277-X

Hemmings, B.A., Restuccia, D.F., 2012. PI3K-PKB/Akt pathway. Cold Spring Harb. Perspect. Biol. 4, a011189. https://doi.org/10.1101/cshperspect.a011189

Herrero-Mendez, A., Almeida, A., Fernández, E., Maestre, C., Moncada, S., Bolaños, J.P., 2009. The bioenergetic and antioxidant status of neurons is controlled by continuous degradation of a key glycolytic enzyme by APC/C–Cdh1. Nat. Cell Biol. 11, 747–752. https://doi.org/10.1038/ncb1881

Hindle, S., Afsari, F., Stark, M., Middleton, C.A., Evans, G.J.O., Sweeney, S.T., Elliott, C.J.H., 2013. Dopaminergic expression of the Parkinsonian gene LRRK2-G2019S leads to non-autonomous visual neurodegeneration, accelerated by increased neural demands for energy. Hum. Mol. Genet. 22, 2129–2140. https://doi.org/10.1093/hmg/ddt061

Hirth, F., Reichert, H., 1999. Conserved genetic programs in insect and mammalian brain development. BioEssays News Rev. Mol. Cell. Dev. Biol. 21, 677–684. https://doi.org/10.1002/(SICI)1521-1878(199908)21:8<677::AID-BIES7>3.0.CO;2-8

Holmström, K.M., Finkel, T., 2014. Cellular mechanisms and physiological consequences of redox-dependent signalling. Nat. Rev. Mol. Cell Biol. 15, 411–421. https://doi.org/10.1038/nrm3801

Hummel, T., Klämbt, C., 2008. P-Element Mutagenesis, in: Dahmann, C. (Ed.), Drosophila, Methods in Molecular Biology. Humana Press, Totowa, NJ, pp. 97–117. https://doi.org/10.1007/978-1-59745-583-1_6

Hutagalung, A.H., Novick, P.J., 2011. Role of Rab GTPases in membrane traffic and cell physiology. Physiol. Rev. 91, 119–149. https://doi.org/10.1152/physrev.00059.2009

Im, J.-Y., Lee, K.-W., Junn, E., Mouradian, M.M., 2010. DJ-1 protects against oxidative damage by regulating the thioredoxin/ASK1 complex. Neurosci. Res. 67, 203–208. https://doi.org/10.1016/j.neures.2010.04.002

Imlach, W., McCabe, B.D., 2009. Electrophysiological methods for recording synaptic potentials from the NMJ of Drosophila larvae. J. Vis. Exp. JoVE 1109. https://doi.org/10.3791/1109

Inden, M., Kitamura, Y., Abe, M., Tamaki, A., Takata, K., Taniguchi, T., 2011. Parkinsonian rotenone mouse model: reevaluation of long-term administration of rotenone in C57BL/6 mice. Biol. Pharm. Bull. 34, 92–96. https://doi.org/10.1248/bpb.34.92

Iwasaki, S., Kobayashi, M., Yoda, M., Sakaguchi, Y., Katsuma, S., Suzuki, T., Tomari, Y., 2010. Hsc70/Hsp90 Chaperone Machinery Mediates ATP-Dependent RISC Loading of Small RNA Duplexes. Mol. Cell 39, 292–299. https://doi.org/10.1016/j.molcel.2010.05.015

Iyer, J., Wang, Q., Le, T., Pizzo, L., Grönke, S., Ambegaokar, S.S., Imai, Y., Srivastava, A., Troisí, B.L., Mardon, G., Artero, R., Jackson, G.R., Isaacs, A.M., Partridge, L., Lu, B., Kumar, J.P., Girirajan, S., 2016. Quantitative Assessment of Eye Phenotypes for Functional Genetic Studies Using Drosophila melanogaster. G3 GenesGenomesGenetics 6, 1427–1437. https://doi.org/10.1534/g3.116.027060

Jacobs, F.M.J., Van Der Heide, L.P., Wijchers, P.J.E.C., Burbach, J.P.H., Hoekman, M.F.M., Smidt, M.P., 2003. FoxO6, a Novel Member of the FoxO Class of Transcription Factors with Distinct Shuttling Dynamics. J. Biol. Chem. 278, 35959–35967. https://doi.org/10.1074/jbc.M302804200

Jaiswal, A., Lorenz, H., 2019. Blind Analysis Tools.

Jan, L.Y., Jan, Y.N., 1982. Antibodies to horseradish peroxidase as specific neuronal markers in Drosophila and in grasshopper embryos. Proc. Natl. Acad. Sci. 79, 2700–2704. https://doi.org/10.1073/pnas.79.8.2700

Jang, H.H., Lee, K.O., Chi, Y.H., Jung, B.G., Park, S.K., Park, J.H., Lee, J.R., Lee, S.S., Moon, J.C., Yun, J.W., Choi, Y.O., Kim, W.Y., Kang, J.S., Cheong, G.-W., Yun, D.-J., Rhee, S.G., Cho, M.J., Lee, S.Y., 2004. Two enzymes in one; two yeast peroxiredoxins display oxidative stress-dependent switching from a peroxidase to a molecular chaperone function. Cell 117, 625–635. https://doi.org/10.1016/j.cell.2004.05.002

Jaworski, J., Spangler, S., Seeburg, D.P., Hoogenraad, C.C., Sheng, M., 2005. Control of dendritic arborization by the phosphoinositide-3'-kinase-Akt-mammalian target of rapamycin pathway. J. Neurosci. Off. J. Soc. Neurosci. 25, 11300–11312. https://doi.org/10.1523/JNEUROSCI.2270-05.2005

Jeibmann, A., Paulus, W., 2009. Drosophila melanogaster as a Model Organism of Brain Diseases. Int. J. Mol. Sci. 10, 407–440. https://doi.org/10.3390/ijms10020407

Jeong, W., Park, S.J., Chang, T.-S., Lee, D.-Y., Rhee, S.G., 2006. Molecular Mechanism of the Reduction of Cysteine Sulfinic Acid of Peroxiredoxin to Cysteine by Mammalian Sulfiredoxin. J. Biol. Chem. 281, 14400–14407. https://doi.org/10.1074/jbc.M511082200

Jiang, M., Meng, J., Zeng, F., Qing, H., Hook, G., Hook, V., Wu, Z., Ni, J., 2020. Cathepsin B inhibition blocks neurite outgrowth in cultured neurons by regulating lysosomal trafficking and remodeling. J. Neurochem. 155, 300–312. https://doi.org/10.1111/jnc.15032

Johansen, J., Halpern, M.E., Johansen, K.M., Keshishian, H., 1989. Stereotypic morphology of glutamatergic synapses on identified muscle cells of Drosophila larvae. J. Neurosci. Off. J. Soc. Neurosci. 9, 710–725. https://doi.org/10.1523/JNEUROSCI.09-02-00710.1989

Johnson, G.L., Nakamura, K., 2007. The c-jun kinase/stress-activated pathway: Regulation, function and role in human disease. Biochim. Biophys. Acta BBA - Mol. Cell Res. 1773, 1341–1348. https://doi.org/10.1016/j.bbamcr.2006.12.009

Jönsson, T.J., Murray, M.S., Johnson, L.C., Poole, L.B., Lowther, W.T., 2005. Structural Basis for the Retroreduction of Inactivated Peroxiredoxins by Human Sulfiredoxin. Biochemistry 44, 8634–8642. https://doi.org/10.1021/bi050131i

Kamsler, A., Segal, M., 2003. Hydrogen Peroxide Modulation of Synaptic Plasticity. J. Neurosci. 23, 269–276. https://doi.org/10.1523/JNEUROSCI.23-01-00269.2003

Karin, M., 1995. The Regulation of AP-1 Activity by Mitogen-activated Protein Kinases. J. Biol. Chem. 270, 16483–16486. https://doi.org/10.1074/jbc.270.28.16483

Kasbekar, D.P., Nelson, J.C., Hall, L.M., 1987. enhancer of seizure : A New Genetic Locus in Drosophila melanogaster Defined by Interactions With Temperature-Sensitive

Paralytic Mutations. Genetics 116, 423–431. https://doi.org/10.1093/genetics/116.3.423
Kassambara, A., 2023. _ggpubr: “ggplot2” Based Publication Ready Plots_.
Kassambara, A., Kosinski, M., Biecek, P., 2021. _survminer: Drawing Survival Curves using ’ggplot2’_.
Kayashima, Y., Yamakawa-Kobayashi, K., 2012. Involvement of Prx3, a Drosophila ortholog of the thiol-dependent peroxidase PRDX3, in age-dependent oxidative stress resistance. Biomed. Res. Tokyo Jpn. 33, 319–322. https://doi.org/10.2220/biomedres.33.319
Keenan, S., Wetherill, S.J., Ugbode, C.I., Chawla, S., Brackenbury, W.J., Evans, G.J.O., 2017. Inhibition of N1-Src kinase by a specific SH3 peptide ligand reveals a role for N1-Src in neurite elongation by L1-CAM. Sci. Rep. 7, 43106. https://doi.org/10.1038/srep43106
Keshishian, H., Broadie, K., Chiba, A., Bate, M., 1996. The drosophila neuromuscular junction: a model system for studying synaptic development and function. Annu. Rev. Neurosci. 19, 545–575. https://doi.org/10.1146/annurev.ne.19.030196.002553
Keyer, K., Imlay, J.A., 1996. Superoxide accelerates DNA damage by elevating free-iron levels. Proc. Natl. Acad. Sci. U. S. A. 93, 13635–13640. https://doi.org/10.1073/pnas.93.24.13635
Khan, S., Jyoti, S., Naz, F., Shakya, B., Rahul, Afzal, M., Siddique, Y.H., 2012. Effect of L-Ascorbic Acid on the Climbing Ability and Protein Levels in the Brain of *Drosophila* Model of Parkinson’s Disease. Int. J. Neurosci. 122, 704–709. https://doi.org/10.3109/00207454.2012.709893
Kil, I.S., Lee, S.K., Ryu, K.W., Woo, H.A., Hu, M.-C., Bae, S.H., Rhee, S.G., 2012. Feedback Control of Adrenal Steroidogenesis via H2O2-Dependent, Reversible Inactivation of Peroxiredoxin III in Mitochondria. Mol. Cell 46, 584–594. https://doi.org/10.1016/j.molcel.2012.05.030
Kil, I.S., Ryu, K.W., Lee, S.K., Kim, J.Y., Chu, S.Y., Kim, J.H., Park, S., Rhee, S.G., 2015. Circadian Oscillation of Sulfiredoxin in the Mitochondria. Mol. Cell 59, 651–663. https://doi.org/10.1016/j.molcel.2015.06.031
Kim, A.H., Khursigara, G., Sun, X., Franke, T.F., Chao, M.V., 2001. Akt phosphorylates and negatively regulates apoptosis signal-regulating kinase 1. Mol. Cell. Biol. 21, 893–901. https://doi.org/10.1128/MCB.21.3.893-901.2001
Kim, R.H., Smith, P.D., Aleyasin, H., Hayley, S., Mount, M.P., Pownall, S., Wakeham, A., You-Ten, A.J., Kalia, S.K., Horne, P., Westaway, D., Lozano, A.M., Anisman, H., Park, D.S., Mak, T.W., 2005. Hypersensitivity of DJ-1-deficient mice to 1-methyl-4-phenyl-1,2,3,6-tetrahydropyrindine (MPTP) and oxidative stress. Proc. Natl. Acad. Sci. U. S. A. 102, 5215–5220. https://doi.org/10.1073/pnas.0501282102
Kittel, R.J., Wichmann, C., Rasse, T.M., Fouquet, W., Schmidt, M., Schmid, A., Wagh, D.A., Pawlu, C., Kellner, R.R., Willig, K.I., Hell, S.W., Buchner, E., Heckmann, M., Sigrist, S.J., 2006. Bruchpilot Promotes Active Zone Assembly, Ca2+ Channel Clustering, and Vesicle Release. Science 312, 1051–1054. https://doi.org/10.1126/science.1126308
Kobayashi, A., Kang, M.-I., Okawa, H., Ohtsuji, M., Zenke, Y., Chiba, T., Igarashi, K., Yamamoto, M., 2004. Oxidative Stress Sensor Keap1 Functions as an Adaptor for Cul3-Based E3 Ligase To Regulate Proteasomal Degradation of Nrf2. Mol. Cell. Biol. 24, 7130–7139. https://doi.org/10.1128/MCB.24.16.7130-7139.2004
Kohsaka, H., 2023. Linking neural circuits to the mechanics of animal behavior in Drosophila larval locomotion. Front. Neural Circuits 17, 1175899. https://doi.org/10.3389/fncir.2023.1175899

Kops, G.J.P.L., Ruiter, N.D.D., De Vries-Smits, A.M.M., Powell, D.R., Bos, J.L., Burgering, B.M.Th., 1999. Direct control of the Forkhead transcription factor AFX by protein kinase B. Nature 398, 630–634. https://doi.org/10.1038/19328

Kramer, J.M., Davidge, J.T., Lockyer, J.M., Staveley, B.E., 2003. Expressionof Drosophila FOXO regulates growth and can phenocopy starvation. BMC Dev. Biol. 3, 5. https://doi.org/10.1186/1471-213X-3-5

Kratschmer, P., Lowe, S.A., Buhl, E., Chen, K., Kullmann, D.M., Pittman, A., Hodge, J.J.L., Jepson, J.E.C., 2021. Impaired Pre-Motor Circuit Activity and Movement in a *Drosophila* Model of *KCNMA1* -Linked Dyskinesia. Mov. Disord. 36, 1158–1169. https://doi.org/10.1002/mds.28479

Kuma, A., Matsui, M., Mizushima, N., 2007. LC3, an Autophagosome Marker, Can be Incorporated into Protein Aggregates Independent of Autophagy: Caution in the Interpretation of LC3 Localization. Autophagy 3, 323–328. https://doi.org/10.4161/auto.4012

Kumar, M.J., Andersen, J.K., 2004. Perspectives on MAO-B in Aging and Neurological Disease: Where Do We Go From Here? Mol. Neurobiol. 30, 077–090. https://doi.org/10.1385/MN:30:1:077

Kurihara, Y., Kanki, T., Aoki, Y., Hirota, Y., Saigusa, T., Uchiumi, T., Kang, D., 2012. Mitophagy Plays an Essential Role in Reducing Mitochondrial Production of Reactive Oxygen Species and Mutation of Mitochondrial DNA by Maintaining Mitochondrial Quantity and Quality in Yeast. J. Biol. Chem. 287, 3265–3272. https://doi.org/10.1074/jbc.M111.280156

Kussmaul, L., Hirst, J., 2006. The mechanism of superoxide production by NADH:ubiquinone oxidoreductase (complex I) from bovine heart mitochondria. Proc. Natl. Acad. Sci. 103, 7607–7612. https://doi.org/10.1073/pnas.0510977103

Lan, W., Lin, J., Liu, W., Wang, F., Xie, Y., 2021. Sulfiredoxin-1 protects spinal cord neurons against oxidative stress in the oxygen-glucose deprivation/reoxygenation model through the bax/cytochrome c/caspase 3 apoptosis pathway. Neurosci. Lett. 744, 135615. https://doi.org/10.1016/j.neulet.2020.135615

Lanciego, J.L., Luquin, N., Obeso, J.A., 2012. Functional neuroanatomy of the basal ganglia. Cold Spring Harb. Perspect. Med. 2, a009621. https://doi.org/10.1101/cshperspect.a009621

Laplante, M., Sabatini, D.M., 2012. mTOR signaling in growth control and disease. Cell 149, 274–293. https://doi.org/10.1016/j.cell.2012.03.017

Lee, J., Giordano, S., Zhang, J., 2012. Autophagy, mitochondria and oxidative stress: cross-talk and redox signalling. Biochem. J. 441, 523–540. https://doi.org/10.1042/BJ20111451

Lee, K.-S., Iijima-Ando, K., Iijima, K., Lee, W.-J., Lee, J.H., Yu, K., Lee, D.-S., 2009. JNK/FOXO-mediated Neuronal Expression of Fly Homologue of Peroxiredoxin II Reduces Oxidative Stress and Extends Life Span. J. Biol. Chem. 284, 29454–29461. https://doi.org/10.1074/jbc.M109.028027

Lee, S.-R., Yang, K.-S., Kwon, J., Lee, C., Jeong, W., Rhee, S.G., 2002. Reversible Inactivation of the Tumor Suppressor PTEN by H2O2. J. Biol. Chem. 277, 20336–20342. https://doi.org/10.1074/jbc.M111899200

Lee, W., Choi, K.-S., Riddell, J., Ip, C., Ghosh, D., Park, J.-H., Park, Y.-M., 2007. Human Peroxiredoxin 1 and 2 Are Not Duplicate Proteins. J. Biol. Chem. 282, 22011–22022. https://doi.org/10.1074/jbc.M610330200

Legakis, J.E., Koepke, J.I., Jedeszko, C., Barlaskar, F., Terlecky, L.J., Edwards, H.J., Walton, P.A., Terlecky, S.R., 2002. Peroxisome Senescence in Human Fibroblasts. Mol. Biol. Cell 13, 4243–4255. https://doi.org/10.1091/mbc.e02-06-0322

Leiserson, W.M., Harkins, E.W., Keshishian, H., 2000. Fray, a Drosophila Serine/Threonine Kinase Homologous to Mammalian PASK, Is Required for Axonal Ensheathment. Neuron 28, 793–806. https://doi.org/10.1016/S0896-6273(00)00154-9

Lemon, J., 2006. Plotrix: a package in the red light district of R. R-News 6, 8–12.

Lesko, S.A., Lorentzen, R.J., Ts'o, P.O.P., 1980. Role of superoxide in deoxyribonucleic acid strand scission. Biochemistry 19, 3023–3028. https://doi.org/10.1021/bi00554a029

Li, H., Guglielmetti, C., Sei, Y.J., Zilberter, M., Le Page, L.M., Shields, L., Yang, J., Nguyen, K., Tiret, B., Gao, X., Bennett, N., Lo, I., Dayton, T.L., Kampmann, M., Huang, Y., Rathmell, J.C., Vander Heiden, M., Chaumeil, M.M., Nakamura, K., 2023. Neurons require glucose uptake and glycolysis in vivo. Cell Rep. 42, 112335. https://doi.org/10.1016/j.celrep.2023.112335

Liu, D., Wen, J., Liu, J., Li, L., 1999. The roles of free radicals in amyotrophic lateral sclerosis: reactive oxygen species and elevated oxidation of protein, DNA, and membrane phospholipids. FASEB J. 13, 2318–2328. https://doi.org/10.1096/fasebj.13.15.2318

Logan-Garbisch, T., Bortolazzo, A., Luu, P., Ford, A., Do, D., Khodabakhshi, P., French, R.L., 2014. Developmental ethanol exposure leads to dysregulation of lipid metabolism and oxidative stress in Drosophila. G3 Bethesda Md 5, 49–59. https://doi.org/10.1534/g3.114.015040

Loschen, G., Flohé, L., 1971. Respiratory chain linked H_2O_2 production in pigeon heart mitochondria. FEBS Lett. 18, 261–264. https://doi.org/10.1016/0014-5793(71)80459-3

Löwe, O., Rezende, F., Heidler, J., Wittig, I., Helfinger, V., Brandes, R.P., Schröder, K., 2019. BIAM switch assay coupled to mass spectrometry identifies novel redox targets of NADPH oxidase 4. Redox Biol. 21, 101125. https://doi.org/10.1016/j.redox.2019.101125

Lucchesi, J.C., Kuroda, M.I., 2015. Dosage compensation in Drosophila. Cold Spring Harb. Perspect. Biol. 7, a019398. https://doi.org/10.1101/cshperspect.a019398

Mackenzie, S.M., Brooker, M.R., Gill, T.R., Cox, G.B., Howells, A.J., Ewart, G.D., 1999. Mutations in the white gene of Drosophila melanogaster affecting ABC transporters that determine eye colouration. Biochim. Biophys. Acta BBA - Biomembr. 1419, 173–185. https://doi.org/10.1016/S0005-2736(99)00064-4

Madabattula, S.T., Strautman, J.C., Bysice, A.M., O'Sullivan, J.A., Androschuk, A., Rosenfelt, C., Doucet, K., Rouleau, G., Bolduc, F., 2015. Quantitative Analysis of Climbing Defects in a Drosophila Model of Neurodegenerative Disorders. J. Vis. Exp. 52741. https://doi.org/10.3791/52741

Madeira, F., Madhusoodanan, N., Lee, J., Eusebi, A., Niewielska, A., Tivey, A.R.N., Lopez, R., Butcher, S., 2024. The EMBL-EBI Job Dispatcher sequence analysis tools framework in 2024. Nucleic Acids Res. 52, W521–W525. https://doi.org/10.1093/nar/gkae241

Mallajosyula, J.K., Kaur, D., Chinta, S.J., Rajagopalan, S., Rane, A., Nicholls, D.G., Di Monte, D.A., Macarthur, H., Andersen, J.K., 2008. MAO-B elevation in mouse brain astrocytes results in Parkinson's pathology. PloS One 3, e1616. https://doi.org/10.1371/journal.pone.0001616

Manning, B.D., Toker, A., 2017. AKT/PKB Signaling: Navigating the Network. Cell 169, 381–405. https://doi.org/10.1016/j.cell.2017.04.001

Marqués, G., 2005. Morphogens and synaptogenesis in Drosophila. J. Neurobiol. 64, 417–434. https://doi.org/10.1002/neu.20165

Martin-Blanco, E., Gampel, A., Ring, J., Virdee, K., Kirov, N., Tolkovsky, A.M., Martinez-Arias, A., 1998. puckered encodes a phosphatase that mediates a feedback loop regulating JNK activity during dorsal closure in Drosophila. Genes Dev. 12, 557–570. https://doi.org/10.1101/gad.12.4.557

Martín-Peña, A., Acebes, A., Rodríguez, J.-R., Sorribes, A., De Polavieja, G.G., Fernández-Fúnez, P., Ferrús, A., 2006. Age-Independent Synaptogenesis by Phosphoinositide 3

Kinase. J. Neurosci. 26, 10199–10208. https://doi.org/10.1523/JNEUROSCI.1223-06.2006
Martín, D., Salinas, M., Fujita, N., Tsuruo, T., Cuadrado, A., 2002. Ceramide and Reactive Oxygen Species Generated by H2O2 Induce Caspase-3-independent Degradation of Akt/Protein Kinase B. J. Biol. Chem. 277, 42943–42952. https://doi.org/10.1074/jbc.M201070200
Masrori, P., Van Damme, P., 2020. Amyotrophic lateral sclerosis: a clinical review. Eur. J. Neurol. 27, 1918–1929. https://doi.org/10.1111/ene.14393
Mathew, D., Ataman, B., Chen, J., Zhang, Y., Cumberledge, S., Budnik, V., 2005. Wingless signaling at synapses is through cleavage and nuclear import of receptor DFrizzled2. Science 310, 1344–1347. https://doi.org/10.1126/science.1117051
Matsuda, N., Sato, S., Shiba, K., Okatsu, K., Saisho, K., Gautier, C.A., Sou, Y., Saiki, S., Kawajiri, S., Sato, F., Kimura, M., Komatsu, M., Hattori, N., Tanaka, K., 2010. PINK1 stabilized by mitochondrial depolarization recruits Parkin to damaged mitochondria and activates latent Parkin for mitophagy. J. Cell Biol. 189, 211–221. https://doi.org/10.1083/jcb.200910140
May, J.M., 2012. Vitamin C Transport and Its Role in the Central Nervous System, in: Stanger, O. (Ed.), Water Soluble Vitamins, Subcellular Biochemistry. Springer Netherlands, Dordrecht, pp. 85–103. https://doi.org/10.1007/978-94-007-2199-9_6
McCormack, A.L., Thiruchelvam, M., Manning-Bog, A.B., Thiffault, C., Langston, J.W., Cory-Slechta, D.A., Di Monte, D.A., 2002. Environmental risk factors and Parkinson's disease: selective degeneration of nigral dopaminergic neurons caused by the herbicide paraquat. Neurobiol. Dis. 10, 119–127. https://doi.org/10.1006/nbdi.2002.0507
McGinnis, A., Klichko, V.I., Orr, W.C., Radyuk, S.N., 2021. Hyperoxidation of Peroxiredoxins and Effects on Physiology of Drosophila. Antioxidants 10, 606. https://doi.org/10.3390/antiox10040606
McGuire, S.E., Mao, Z., Davis, R.L., 2004. Spatiotemporal Gene Expression Targeting with the TARGET and Gene-Switch Systems in Drosophila. Sci. STKE 2004. https://doi.org/10.1126/stke.2202004pl6
Meijering, E., Jacob, M., Sarria, J. -C. F., Steiner, P., Hirling, H., Unser, M., 2004. Design and validation of a tool for neurite tracing and analysis in fluorescence microscopy images. Cytometry A 58A, 167–176. https://doi.org/10.1002/cyto.a.20022
Menon, K.P., Carrillo, R.A., Zinn, K., 2013. Development and plasticity of the Drosophila larval neuromuscular junction. Wiley Interdiscip. Rev. Dev. Biol. 2, 647–670. https://doi.org/10.1002/wdev.108
Meulener, M., Whitworth, A.J., Armstrong-Gold, C.E., Rizzu, P., Heutink, P., Wes, P.D., Pallanck, L.J., Bonini, N.M., 2005. Drosophila DJ-1 mutants are selectively sensitive to environmental toxins associated with Parkinson's disease. Curr. Biol. CB 15, 1572–1577. https://doi.org/10.1016/j.cub.2005.07.064
Meulener, M.C., Xu, K., Thomson, L., Ischiropoulos, H., Bonini, N.M., 2006. Mutational analysis of DJ-1 in Drosophila implicates functional inactivation by oxidative damage and aging. Proc. Natl. Acad. Sci. U. S. A. 103, 12517–12522. https://doi.org/10.1073/pnas.0601891103
Miech, C., Pauer, H.-U., He, X., Schwarz, T.L., 2008. Presynaptic local signaling by a canonical wingless pathway regulates development of the Drosophila neuromuscular junction. J. Neurosci. Off. J. Soc. Neurosci. 28, 10875–10884. https://doi.org/10.1523/JNEUROSCI.0164-08.2008
Miller, D.E., Cook, K.R., Hawley, R.S., 2019. The joy of balancers. PLoS Genet. 15, e1008421. https://doi.org/10.1371/journal.pgen.1008421

Milton, V.J., Jarrett, H.E., Gowers, K., Chalak, S., Briggs, L., Robinson, I.M., Sweeney, S.T., 2011. Oxidative stress induces overgrowth of the *Drosophila* neuromuscular junction. Proc. Natl. Acad. Sci. 108, 17521–17526. https://doi.org/10.1073/pnas.1014511108
Mitra, S., Nguyen, L.N., Akter, M., Park, G., Choi, E.H., Kaushik, N.K., 2019. Impact of ROS Generated by Chemical, Physical, and Plasma Techniques on Cancer Attenuation. Cancers 11, 1030. https://doi.org/10.3390/cancers11071030
Mohanty, J.G., Jaffe, J.S., Schulman, E.S., Raible, D.G., 1997. A highly sensitive fluorescent micro-assay of H2O2 release from activated human leukocytes using a dihydroxyphenoxazine derivative. J. Immunol. Methods 202, 133–141. https://doi.org/10.1016/S0022-1759(96)00244-X
Mól, A.R., Castro, M.S., Fontes, W., 2018. NetWheels: A web application to create high quality peptide helical wheel and net projections. https://doi.org/10.1101/416347
Moon, J.C., Hah, Y.-S., Kim, W.Y., Jung, B.G., Jang, H.H., Lee, J.R., Kim, S.Y., Lee, Y.M., Jeon, M.G., Kim, C.W., Cho, M.J., Lee, S.Y., 2005. Oxidative Stress-dependent Structural and Functional Switching of a Human 2-Cys Peroxiredoxin Isotype II That Enhances HeLa Cell Resistance to H2O2-induced Cell Death. J. Biol. Chem. 280, 28775–28784. https://doi.org/10.1074/jbc.M505362200
Morgan, T.H., 1910. Sex Limited Inheritance in Drosophila. Science 32, 120–122. https://doi.org/10.1126/science.32.812.120
Muñoz, P., Huenchuguala, S., Paris, I., Segura-Aguilar, J., 2012. Dopamine oxidation and autophagy. Park. Dis. 2012, 920953. https://doi.org/10.1155/2012/920953
Narendra, D., Tanaka, A., Suen, D.-F., Youle, R.J., 2008. Parkin is recruited selectively to impaired mitochondria and promotes their autophagy. J. Cell Biol. 183, 795–803. https://doi.org/10.1083/jcb.200809125
Narendra, D.P., Jin, S.M., Tanaka, A., Suen, D.-F., Gautier, C.A., Shen, J., Cookson, M.R., Youle, R.J., 2010. PINK1 Is Selectively Stabilized on Impaired Mitochondria to Activate Parkin. PLoS Biol. 8, e1000298. https://doi.org/10.1371/journal.pbio.1000298
NCBI, 2024. Protein BLAST: search protein databases using a protein query (blastp).
NEB Tm Calculator, 2024.
NEBioCalculator, 2024.
Neuwirth, E., 2014. RColorBrewer: ColorBrewer Palettes. R package version 1.1-2.
Nguyen Huu, T., Park, J., Zhang, Y., Park, I., Yoon, H.J., Woo, H.A., Lee, S.-R., 2021. Redox Regulation of PTEN by Peroxiredoxins. Antioxidants 10, 302. https://doi.org/10.3390/antiox10020302
Nichols, C.D., Becnel, J., Pandey, U.B., 2012. Methods to assay Drosophila behavior. J. Vis. Exp. JoVE 3795. https://doi.org/10.3791/3795
NIH, 2025. Genbank database.
Noh, Y.H., Baek, J.Y., Jeong, W., Rhee, S.G., Chang, T.-S., 2009. Sulfiredoxin Translocation into Mitochondria Plays a Crucial Role in Reducing Hyperoxidized Peroxiredoxin III. J. Biol. Chem. 284, 8470–8477. https://doi.org/10.1074/jbc.M808981200
Noichri, Y., Palais, G., Ruby, V., D'Autreaux, B., Delaunay-Moisan, A., Nyström, T., Molin, M., Toledano, M.B., 2015. In vivo parameters influencing 2-Cys Prx oligomerization: The role of enzyme sulfinylation. Redox Biol. 6, 326–333. https://doi.org/10.1016/j.redox.2015.08.011
Okado-Matsumoto, A., Fridovich, I., 2001. Subcellular Distribution of Superoxide Dismutases (SOD) in Rat Liver. J. Biol. Chem. 276, 38388–38393. https://doi.org/10.1074/jbc.M105395200
Oswald, M.C., Brooks, P.S., Zwart, M.F., Mukherjee, A., West, R.J., Giachello, C.N., Morarach, K., Baines, R.A., Sweeney, S.T., Landgraf, M., 2018. Reactive oxygen species regulate activity-dependent neuronal plasticity in Drosophila. eLife 7, e39393. https://doi.org/10.7554/eLife.39393

Packard, M., Koo, E.S., Gorczyca, M., Sharpe, J., Cumberledge, S., Budnik, V., 2002. The Drosophila Wnt, wingless, provides an essential signal for pre- and postsynaptic differentiation. Cell 111, 319–330. https://doi.org/10.1016/s0092-8674(02)01047-4

Panday, A., Sahoo, M.K., Osorio, D., Batra, S., 2015. NADPH oxidases: an overview from structure to innate immunity-associated pathologies. Cell. Mol. Immunol. 12, 5–23. https://doi.org/10.1038/cmi.2014.89

Papadia, S., Soriano, F.X., Léveillé, F., Martel, M.-A., Dakin, K.A., Hansen, H.H., Kaindl, A., Sifringer, M., Fowler, J., Stefovska, V., McKenzie, G., Craigon, M., Corriveau, R., Ghazal, P., Horsburgh, K., Yankner, B.A., Wyllie, D.J.A., Ikonomidou, C., Hardingham, G.E., 2008. Synaptic NMDA receptor activity boosts intrinsic antioxidant defenses. Nat. Neurosci. 11, 476–487. https://doi.org/10.1038/nn2071

Parakh, S., Spencer, D.M., Halloran, M.A., Soo, K.Y., Atkin, J.D., 2013. Redox regulation in amyotrophic lateral sclerosis. Oxid. Med. Cell. Longev. 2013, 408681. https://doi.org/10.1155/2013/408681

Park, J., Lee, S.B., Lee, S., Kim, Y., Song, S., Kim, S., Bae, E., Kim, J., Shong, M., Kim, J.-M., Chung, J., 2006. Mitochondrial dysfunction in Drosophila PINK1 mutants is complemented by parkin. Nature 441, 1157–1161. https://doi.org/10.1038/nature04788

Pellerin, L., Magistretti, P.J., 2012. Sweet Sixteen for ANLS. J. Cereb. Blood Flow Metab. 32, 1152–1166. https://doi.org/10.1038/jcbfm.2011.149

Pellerin, L., Magistretti, P.J., 1994. Glutamate uptake into astrocytes stimulates aerobic glycolysis: a mechanism coupling neuronal activity to glucose utilization. Proc. Natl. Acad. Sci. 91, 10625–10629. https://doi.org/10.1073/pnas.91.22.10625

Perkins, A., Nelson, K.J., Parsonage, D., Poole, L.B., Karplus, P.A., 2015. Peroxiredoxins: guardians against oxidative stress and modulators of peroxide signaling. Trends Biochem. Sci. 40, 435–445. https://doi.org/10.1016/j.tibs.2015.05.001

Pickrell, A.M., Youle, R.J., 2015. The Roles of PINK1, Parkin, and Mitochondrial Fidelity in Parkinson's Disease. Neuron 85, 257–273. https://doi.org/10.1016/j.neuron.2014.12.007

Planson, A.-G., Palais, G., Abbas, K., Gerard, M., Couvelard, L., Delaunay, A., Baulande, S., Drapier, J.-C., Toledano, M.B., 2011. Sulfiredoxin protects mice from lipopolysaccharide-induced endotoxic shock. Antioxid. Redox Signal. 14, 2071–2080. https://doi.org/10.1089/ars.2010.3552

Poliak, S., Peles, E., 2003. The local differentiation of myelinated axons at nodes of Ranvier. Nat. Rev. Neurosci. 4, 968–980. https://doi.org/10.1038/nrn1253

Poljšak, B., Raspor, P., 2008. The antioxidant and pro-oxidant activity of vitamin C and trolox *in vitro*: a comparative study. J. Appl. Toxicol. 28, 183–188. https://doi.org/10.1002/jat.1264

Putker, M., Madl, T., Vos, H.R., de Ruiter, H., Visscher, M., van den Berg, M.C.W., Kaplan, M., Korswagen, H.C., Boelens, R., Vermeulen, M., Burgering, B.M.T., Dansen, T.B., 2013. Redox-Dependent Control of FOXO/DAF-16 by Transportin-1. Mol. Cell 49, 730–742. https://doi.org/10.1016/j.molcel.2012.12.014

R Core Team, 2022. R: A language and environment for statistical computing.

Rabah, Y., Francés, R., Minatchy, J., Guédon, L., Desnous, C., Plaçais, P.-Y., Preat, T., 2023. Glycolysis-derived alanine from glia fuels neuronal mitochondria for memory in Drosophila. Nat. Metab. 5, 2002–2019. https://doi.org/10.1038/s42255-023-00910-y

Radi, R., Turrens, J.F., Chang, L.Y., Bush, K.M., Crapo, J.D., Freeman, B.A., 1991. Detection of catalase in rat heart mitochondria. J. Biol. Chem. 266, 22028–22034. https://doi.org/10.1016/S0021-9258(18)54740-2

Radyuk, S.N., Klichko, V.I., Spinola, B., Sohal, R.S., Orr, W.C., 2001. The peroxiredoxin gene family in drosophila melanogaster. Free Radic. Biol. Med. 31, 1090–1100. https://doi.org/10.1016/S0891-5849(01)00692-X

Radyuk, S.N., Rebrin, I., Klichko, V.I., Sohal, B.H., Michalak, K., Benes, J., Sohal, R.S., Orr, W.C., 2010. Mitochondrial peroxiredoxins are critical for the maintenance of redox state and the survival of adult Drosophila. Free Radic. Biol. Med. 49, 1892–1902. https://doi.org/10.1016/j.freeradbiomed.2010.09.014

Ranganathan, R., Malicki, D.M., Zuker, C.S., 1995. Signal Transduction in Drosophila Photoreceptors. Annu. Rev. Neurosci. 18, 283–317. https://doi.org/10.1146/annurev.ne.18.030195.001435

Rao, Q., Guo, M., Sun, J., Yang, B., Cao, X., Xia, J., 2024. Sulfiredoxin-1 promotes the growth of hepatocellular carcinoma by inhibiting TFEB-mediated autophagy and lysosome biogenesis. Exp. Cell Res. 441, 114169. https://doi.org/10.1016/j.yexcr.2024.114169

Ray, P.D., Huang, B.-W., Tsuji, Y., 2012. Reactive oxygen species (ROS) homeostasis and redox regulation in cellular signaling. Cell. Signal. 24, 981–990. https://doi.org/10.1016/j.cellsig.2012.01.008

Repici, M., Giorgini, F., 2019. DJ-1 in Parkinson's Disease: Clinical Insights and Therapeutic Perspectives. J. Clin. Med. 8, 1377. https://doi.org/10.3390/jcm8091377

Rey, G., Valekunja, U.K., Feeney, K.A., Wulund, L., Milev, N.B., Stangherlin, A., Ansel-Bollepalli, L., Velagapudi, V., O'Neill, J.S., Reddy, A.B., 2016. The Pentose Phosphate Pathway Regulates the Circadian Clock. Cell Metab. 24, 462–473. https://doi.org/10.1016/j.cmet.2016.07.024

Rhee, S.G., Woo, H.A., Kil, I.S., Bae, S.H., 2012. Peroxiredoxin functions as a peroxidase and a regulator and sensor of local peroxides. J. Biol. Chem. 287, 4403–4410. https://doi.org/10.1074/jbc.R111.283432

Riederer, P., Konradi, C., Schay, V., Kienzl, E., Birkmayer, G., Danielczyk, W., Sofic, E., Youdim, M.B., 1987. Localization of MAO-A and MAO-B in human brain: a step in understanding the therapeutic action of L-deprenyl. Adv. Neurol. 45, 111–118.

Rojo, A.I., Sagarra, M.R.D., Cuadrado, A., 2008. GSK-3β down-regulates the transcription factor Nrf2 after oxidant damage: relevance to exposure of neuronal cells to oxidative stress. J. Neurochem. 105, 192–202. https://doi.org/10.1111/j.1471-4159.2007.05124.x

Roote, J., Prokop, A., 2013. How to design a genetic mating scheme: a basic training package for Drosophila genetics. G3 Bethesda Md 3, 353–358. https://doi.org/10.1534/g3.112.004820

Rosen, D.R., Siddique, T., Patterson, D., Figlewicz, D.A., Sapp, P., Hentati, A., Donaldson, D., Goto, J., O'Regan, J.P., Deng, H.-X., Rahmani, Z., Krizus, A., McKenna-Yasek, D., Cayabyab, A., Gaston, S.M., Berger, R., Tanzi, R.E., Halperin, J.J., Herzfeldt, B., Van Den Bergh, R., Hung, W.-Y., Bird, T., Deng, G., Mulder, D.W., Smyth, C., Laing, N.G., Soriano, E., Pericak–Vance, M.A., Haines, J., Rouleau, G.A., Gusella, J.S., Horvitz, H.R., Brown, R.H., 1993. Mutations in Cu/Zn superoxide dismutase gene are associated with familial amyotrophic lateral sclerosis. Nature 362, 59–62. https://doi.org/10.1038/362059a0

Różanowska, M.B., 2023. Lipofuscin, Its Origin, Properties, and Contribution to Retinal Fluorescence as a Potential Biomarker of Oxidative Damage to the Retina. Antioxidants 12, 2111. https://doi.org/10.3390/antiox12122111

Rubin, G.M., Hong, L., Brokstein, P., Evans-Holm, M., Frise, E., Stapleton, M., Harvey, D.A., 2000. A Drosophila Complementary DNA Resource. Science 287, 2222–2224. https://doi.org/10.1126/science.287.5461.2222

Sagara, J., Miura, K., Bannai, S., 1993. Maintenance of Neuronal Glutathione by Glial Cells. J. Neurochem. 61, 1672–1676. https://doi.org/10.1111/j.1471-4159.1993.tb09802.x

Salazar, M., Rojo, A.I., Velasco, D., De Sagarra, R.M., Cuadrado, A., 2006. Glycogen Synthase Kinase-3β Inhibits the Xenobiotic and Antioxidant Cell Response by Direct Phosphorylation and Nuclear Exclusion of the Transcription Factor Nrf2. J. Biol. Chem. 281, 14841–14851. https://doi.org/10.1074/jbc.M513737200

Santacroce, G., Gentile, A., Soriano, S., Novelli, A., Lenti, M.V., Di Sabatino, A., 2023. Glutathione: Pharmacological aspects and implications for clinical use in non-alcoholic fatty liver disease. Front. Med. 10, 1124275. https://doi.org/10.3389/fmed.2023.1124275

Sanyal, S., Narayanan, R., Consoulas, C., Ramaswami, M., 2003. Evidence for cell autonomous AP1 function in regulation of Drosophila motor-neuron plasticity. BMC Neurosci. 4, 20. https://doi.org/10.1186/1471-2202-4-20

Sanyal, S., Sandstrom, D.J., Hoeffer, C.A., Ramaswami, M., 2002. AP-1 functions upstream of CREB to control synaptic plasticity in Drosophila. Nature 416, 870–874. https://doi.org/10.1038/416870a

Saura, J., Andrés, N., Andrade, C., Ojuel, J., Eriksson, K., Mahy, N., 1997. Biphasic and Region-Specific MAO-B Response to Aging in Normal Human Brain. Neurobiol. Aging 18, 497–507. https://doi.org/10.1016/S0197-4580(97)00113-9

Scherz-Shouval, R., Shvets, E., Fass, E., Shorer, H., Gil, L., Elazar, Z., 2007. Reactive oxygen species are essential for autophagy and specifically regulate the activity of Atg4. EMBO J. 26, 1749–1760. https://doi.org/10.1038/sj.emboj.7601623

Schindelin, J., Arganda-Carreras, I., Frise, E., Kaynig, V., Longair, M., Pietzsch, T., Preibisch, S., Rueden, C., Saalfeld, S., Schmid, B., Tinevez, J.-Y., White, D.J., Hartenstein, V., Eliceiri, K., Tomancak, P., Cardona, A., 2012. Fiji: an open-source platform for biological-image analysis. Nat. Methods 9, 676–682. https://doi.org/10.1038/nmeth.2019

Scialo, F., Sriram, A., Stefanatos, R., Sanz, A., 2016. Practical Recommendations for the Use of the GeneSwitch Gal4 System to Knock-Down Genes in Drosophila melanogaster. PLOS ONE 11, e0161817. https://doi.org/10.1371/journal.pone.0161817

Shaw, P.J., Ince, P.G., Falkous, G., Mantle, D., 1995. Oxidative damage to protein in sporadic motor neuron disease spinal cord. Ann. Neurol. 38, 691–695. https://doi.org/10.1002/ana.410380424

Shibata, N., Nagai, R., Uchida, K., Horiuchi, S., Yamada, S., Hirano, A., Kawaguchi, M., Yamamoto, T., Sasaki, S., Kobayashi, M., 2001. Morphological evidence for lipid peroxidation and protein glycoxidation in spinal cords from sporadic amyotrophic lateral sclerosis patients. Brain Res. 917, 97–104. https://doi.org/10.1016/s0006-8993(01)02926-2

Shih, A.Y., Johnson, D.A., Wong, G., Kraft, A.D., Jiang, L., Erb, H., Johnson, J.A., Murphy, T.H., 2003. Coordinate Regulation of Glutathione Biosynthesis and Release by Nrf2-Expressing Glia Potently Protects Neurons from Oxidative Stress. J. Neurosci. 23, 3394–3406. https://doi.org/10.1523/JNEUROSCI.23-08-03394.2003

Smith, P.K., Krohn, R.I., Hermanson, G.T., Mallia, A.K., Gartner, F.H., Provenzano, M.D., Fujimoto, E.K., Goeke, N.M., Olson, B.J., Klenk, D.C., 1985. Measurement of protein using bicinchoninic acid. Anal. Biochem. 150, 76–85. https://doi.org/10.1016/0003-2697(85)90442-7

Spillantini, M.G., Schmidt, M.L., Lee, V.M.-Y., Trojanowski, J.Q., Jakes, R., Goedert, M., 1997. α-Synuclein in Lewy bodies. Nature 388, 839–840. https://doi.org/10.1038/42166

Stark, W.S., Wasserman, G.S., 1972. Transient and receptor potentials in the electroretinogram of Drosophila. Vision Res. 12, 1771–1775. https://doi.org/10.1016/0042-6989(72)90049-1

Stuart, A.E., 1999. From Fruit Flies to Barnacles, Histamine Is the Neurotransmitter of Arthropod Photoreceptors. Neuron 22, 431–433. https://doi.org/10.1016/S0896-6273(00)80699-6

Sudbery, I., Enright, A.J., Fraser, A.G., Dunham, I., 2010. Systematic analysis of off-target effects in an RNAi screen reveals microRNAs affecting sensitivity to TRAIL-induced apoptosis. BMC Genomics 11, 175. https://doi.org/10.1186/1471-2164-11-175

Suman, R., Smith, G., Hazel, K.E.A., Kasprowicz, R., Coles, M., O'Toole, P., Chawla, S., 2016. Label-free imaging to study phenotypic behavioural traits of cells in complex co-cultures. Sci. Rep. 6, 22032. https://doi.org/10.1038/srep22032

Sun, H., Lesche, R., Li, D.-M., Liliental, J., Zhang, H., Gao, J., Gavrilova, N., Mueller, B., Liu, X., Wu, H., 1999. PTEN modulates cell cycle progression and cell survival by regulating phosphatidylinositol 3,4,5,-trisphosphate and Akt/protein kinase B signaling pathway. Proc. Natl. Acad. Sci. 96, 6199–6204. https://doi.org/10.1073/pnas.96.11.6199

Sun, J., Xu, A.Q., Giraud, J., Poppinga, H., Riemensperger, T., Fiala, A., Birman, S., 2018. Neural Control of Startle-Induced Locomotion by the Mushroom Bodies and Associated Neurons in Drosophila. Front. Syst. Neurosci. 12, 6. https://doi.org/10.3389/fnsys.2018.00006

Sweeney, S.T., Davis, G.W., 2002. Unrestricted Synaptic Growth in spinster—a Late Endosomal Protein Implicated in TGF-β-Mediated Synaptic Growth Regulation. Neuron 36, 403–416. https://doi.org/10.1016/S0896-6273(02)01014-0

Sykiotis, G.P., Bohmann, D., 2008. Keap1/Nrf2 Signaling Regulates Oxidative Stress Tolerance and Lifespan in Drosophila. Dev. Cell 14, 76–85. https://doi.org/10.1016/j.devcel.2007.12.002

Taira, T., Saito, Y., Niki, T., Iguchi-Ariga, S.M.M., Takahashi, K., Ariga, H., 2004. DJ-1 has a role in antioxidative stress to prevent cell death. EMBO Rep. 5, 213–218. https://doi.org/10.1038/sj.embor.7400074

Tanner, C.M., Kamel, F., Ross, G.W., Hoppin, J.A., Goldman, S.M., Korell, M., Marras, C., Bhudhikanok, G.S., Kasten, M., Chade, A.R., Comyns, K., Richards, M.B., Meng, C., Priestley, B., Fernandez, H.H., Cambi, F., Umbach, D.M., Blair, A., Sandler, D.P., Langston, J.W., 2011. Rotenone, paraquat, and Parkinson's disease. Environ. Health Perspect. 119, 866–872. https://doi.org/10.1289/ehp.1002839

Tariq, K., Cullen, E., Getz, S.A., Conching, A.K.S., Goyette, A.R., Prina, M.L., Wang, W., Li, M., Weston, M.C., Luikart, B.W., 2022. Disruption of mTORC1 rescues neuronal overgrowth and synapse function dysregulated by Pten loss. Cell Rep. 41, 111574. https://doi.org/10.1016/j.celrep.2022.111574

Tataroglu, O., Emery, P., 2014. Studying circadian rhythms in Drosophila melanogaster. Methods San Diego Calif 68, 140–150. https://doi.org/10.1016/j.ymeth.2014.01.001

Terman, A., Gustafsson, B., Brunk, U.T., 2006. The lysosomal–mitochondrial axis theory of postmitotic aging and cell death. Chem. Biol. Interact. 163, 29–37. https://doi.org/10.1016/j.cbi.2006.04.013

Thermo Fisher, 2025. Selecting an RNAi Strategy. Tech. Ref. Libr. URL https://www.thermofisher.com/uk/en/home/references/gibco-cell-culture-basics/transfection-basics/guidelines-for-rna-transfection/selecting-an-rnai-strategy.html

Therneau, T., 2023. _A Package for Survival Analysis in R_.

Tseng, Y.-C., Mozumdar, S., Huang, L., 2009. Lipid-based systemic delivery of siRNA. Adv. Drug Deliv. Rev. 61, 721–731. https://doi.org/10.1016/j.addr.2009.03.003

Turrens, J.F., Alexandre, A., Lehninger, A.L., 1985. Ubisemiquinone is the electron donor for superoxide formation by complex III of heart mitochondria. Arch. Biochem. Biophys. 237, 408–414. https://doi.org/10.1016/0003-9861(85)90293-0

Tuxworth, R.I., Chen, H., Vivancos, V., Carvajal, N., Huang, X., Tear, G., 2011. The Batten disease gene CLN3 is required for the response to oxidative stress. Hum. Mol. Genet. 20, 2037–2047. https://doi.org/10.1093/hmg/ddr088

Ugbode, C., Garnham, N., Fort-Aznar, L., Evans, G.J.O., Chawla, S., Sweeney, S.T., 2020. JNK signalling regulates antioxidant responses in neurons. Redox Biol. 37, 101712. https://doi.org/10.1016/j.redox.2020.101712

Ugur, B., Chen, K., Bellen, H.J., 2016. Drosophila tools and assays for the study of human diseases. Dis. Model. Mech. 9, 235–244. https://doi.org/10.1242/dmm.023762
Vannucci, S.J., Maher, F., Simpson, I.A., 1997. Glucose transporter proteins in brain: Delivery of glucose to neurons and glia. Glia 21, 2–21. https://doi.org/10.1002/(SICI)1098-1136(199709)21:1<2::AID-GLIA2>3.0.CO;2-C
Vilinsky, I., Johnson, K.G., 2012. Electroretinograms in Drosophila: a robust and genetically accessible electrophysiological system for the undergraduate laboratory. J. Undergrad. Neurosci. Educ. JUNE Publ. FUN Fac. Undergrad. Neurosci. 11, A149-157.
Vivancos, A.P., Castillo, E.A., Biteau, B., Nicot, C., Ayté, J., Toledano, M.B., Hidalgo, E., 2005. A cysteine-sulfinic acid in peroxiredoxin regulates H2O2 -sensing by the antioxidant Pap1 pathway. Proc. Natl. Acad. Sci. 102, 8875–8880. https://doi.org/10.1073/pnas.0503251102
Voelzmann, A., Sanchez-Soriano, N., 2022. Drosophila Primary Neuronal Cultures as a Useful Cellular Model to Study and Image Axonal Transport, in: Vagnoni, A. (Ed.), Axonal Transport, Methods in Molecular Biology. Springer US, New York, NY, pp. 429–449. https://doi.org/10.1007/978-1-0716-1990-2_23
Volkenhoff, A., Hirrlinger, J., Kappel, J.M., Klämbt, C., Schirmeier, S., 2018. Live imaging using a FRET glucose sensor reveals glucose delivery to all cell types in the Drosophila brain. J. Insect Physiol. 106, 55–64. https://doi.org/10.1016/j.jinsphys.2017.07.010
Volkenhoff, A., Weiler, A., Letzel, M., Stehling, M., Klämbt, C., Schirmeier, S., 2015. Glial Glycolysis Is Essential for Neuronal Survival in Drosophila. Cell Metab. 22, 437–447. https://doi.org/10.1016/j.cmet.2015.07.006
von Heijne, G., 1986. Mitochondrial targeting sequences may form amphiphilic helices. EMBO J. 5, 1335–1342. https://doi.org/10.1002/j.1460-2075.1986.tb04364.x
Waak, J., Weber, S.S., Görner, K., Schall, C., Ichijo, H., Stehle, T., Kahle, P.J., 2009. Oxidizable residues mediating protein stability and cytoprotective interaction of DJ-1 with apoptosis signal-regulating kinase 1. J. Biol. Chem. 284, 14245–14257. https://doi.org/10.1074/jbc.M806902200
Wan, H.I., DiAntonio, A., Fetter, R.D., Bergstrom, K., Strauss, R., Goodman, C.S., 2000. Highwire Regulates Synaptic Growth in Drosophila. Neuron 26, 313–329. https://doi.org/10.1016/S0896-6273(00)81166-6
Wang, J., Zheng, M., Yang, X., Zhou, X., Zhang, S., 2023. The Role of Cathepsin B in Pathophysiologies of Non-tumor and Tumor tissues: A Systematic Review. J. Cancer 14, 2344–2358. https://doi.org/10.7150/jca.86531
Wang, T., Montell, C., 2007. Phototransduction and retinal degeneration in Drosophila. Pflüg. Arch. - Eur. J. Physiol. 454, 821–847. https://doi.org/10.1007/s00424-007-0251-1
Weigmann, K., Klapper, R., Strasser, T., Rickert, C., Technau, G., Jäckle, H., Janning, W., Klämbt, C., 2003. FlyMove – a new way to look at development of Drosophila. Trends Genet. 19, 310–311. https://doi.org/10.1016/S0168-9525(03)00050-7
West, R.J.H., Lu, Y., Marie, B., Gao, F.-B., Sweeney, S.T., 2015. Rab8, POSH, and TAK1 regulate synaptic growth in a *Drosophila* model of frontotemporal dementia. J. Cell Biol. 208, 931–947. https://doi.org/10.1083/jcb.201404066
West, R.J.H., Ugbode, C., Gao, F.-B., Sweeney, S.T., 2018. The pro-apoptotic JNK scaffold POSH/SH3RF1 mediates CHMP2BIntron5-associated toxicity in animal models of frontotemporal dementia. Hum. Mol. Genet. 27, 1382–1395. https://doi.org/10.1093/hmg/ddy048
Wickham, H., 2016. ggplot2: Elegant Graphics for Data Analysis. Springer-Verlag, New York.
Wickham, H., Averick, M., Bryan, J., Chang, W., McGowan, L., François, R., Grolemund, G., Hayes, A., Henry, L., Hester, J., Kuhn, M., Pedersen, T., Miller, E., Bache, S., Müller, K., Ooms, J., Robinson, D., Seidel, D., Spinu, V., Takahashi, K., Vaughan, D., Wilke,

C., Woo, K., Yutani, H., 2019. Welcome to the Tidyverse. J. Open Source Softw. 4, 1686. https://doi.org/10.21105/joss.01686
Wickham, H., François, R., Henry, L., Müller, K., Vaughan, D., 2023. _dplyr: A Grammar of Data Manipulation_.
Willems, P.H.G.M., Rossignol, R., Dieteren, C.E.J., Murphy, M.P., Koopman, W.J.H., 2015. Redox Homeostasis and Mitochondrial Dynamics. Cell Metab. 22, 207–218. https://doi.org/10.1016/j.cmet.2015.06.006
Wilson, C., Muñoz-Palma, E., Henríquez, D.R., Palmisano, I., Núñez, M.T., Di Giovanni, S., González-Billault, C., 2016. A Feed-Forward Mechanism Involving the NOX Complex and RyR-Mediated Ca 2+ Release During Axonal Specification. J. Neurosci. 36, 11107–11119. https://doi.org/10.1523/JNEUROSCI.1455-16.2016
Wilson, C., Núñez, M.T., González-Billault, C., 2015. Contribution of NADPH-oxidase to the establishment of hippocampal neuronal polarity in culture. J. Cell Sci. jcs.168567. https://doi.org/10.1242/jcs.168567
Woo, H.A., Jeong, W., Chang, T.-S., Park, K.J., Park, S.J., Yang, J.S., Rhee, S.G., 2005. Reduction of cysteine sulfinic acid by sulfiredoxin is specific to 2-cys peroxiredoxins. J. Biol. Chem. 280, 3125–3128. https://doi.org/10.1074/jbc.C400496200
Wood, Z.A., Poole, L.B., Hantgan, R.R., Karplus, P.A., 2002. Dimers to doughnuts: redox-sensitive oligomerization of 2-cysteine peroxiredoxins. Biochemistry 41, 5493–5504. https://doi.org/10.1021/bi012173m
Wood, Z.A., Poole, L.B., Karplus, P.A., 2003. Peroxiredoxin evolution and the regulation of hydrogen peroxide signaling. Science 300, 650–653. https://doi.org/10.1126/science.1080405
Wu, J., Chen, Y., Yu, S., Li, L., Zhao, X., Li, Q., Zhao, J., Zhao, Y., 2017. Neuroprotective effects of sulfiredoxin-1 during cerebral ischemia/reperfusion oxidative stress injury in rats. Brain Res. Bull. 132, 99–108. https://doi.org/10.1016/j.brainresbull.2017.05.012
Yang, K.-S., Kang, S.W., Woo, H.A., Hwang, S.C., Chae, H.Z., Kim, K., Rhee, S.G., 2002. Inactivation of Human Peroxiredoxin I during Catalysis as the Result of the Oxidation of the Catalytic Site Cysteine to Cysteine-sulfinic Acid. J. Biol. Chem. 277, 38029–38036. https://doi.org/10.1074/jbc.M206626200
Ye, J., Coulouris, G., Zaretskaya, I., Cutcutache, I., Rozen, S., Madden, T.L., 2012. Primer-BLAST: A tool to design target-specific primers for polymerase chain reaction. BMC Bioinformatics 13, 134. https://doi.org/10.1186/1471-2105-13-134
Yen, K., Narasimhan, S.D., Tissenbaum, H.A., 2011. DAF-16/Forkhead Box O Transcription Factor: Many Paths to a Single Fork(head) in the Road. Antioxid. Redox Signal. 14, 623–634. https://doi.org/10.1089/ars.2010.3490
Yi, Y., Xu, W., Fan, Y., Wang, H.-X., 2021. Drosophila as an emerging model organism for studies of food-derived antioxidants. Food Res. Int. 143, 110307. https://doi.org/10.1016/j.foodres.2021.110307
Yoritaka, A., Hattori, N., Uchida, K., Tanaka, M., Stadtman, E.R., Mizuno, Y., 1996. Immunohistochemical detection of 4-hydroxynonenal protein adducts in Parkinson disease. Proc. Natl. Acad. Sci. 93, 2696–2701. https://doi.org/10.1073/pnas.93.7.2696
Zhang, Y., Park, J., Han, S.-J., Yang, S.Y., Yoon, H.J., Park, I., Woo, H.A., Lee, S.-R., 2020. Redox regulation of tumor suppressor PTEN in cell signaling. Redox Biol. 34, 101553. https://doi.org/10.1016/j.redox.2020.101553
Zhao, R., Jiang, S., Zhang, L., Yu, Z., 2019. Mitochondrial electron transport chain, ROS generation and uncoupling (Review). Int. J. Mol. Med. https://doi.org/10.3892/ijmm.2019.4188
Zhou, Yunchuan, Zhou, Yang, Yu, S., Wu, J., Chen, Y., Zhao, Y., 2015. Sulfiredoxin-1 exerts anti-apoptotic and neuroprotective effects against oxidative stress-induced injury in rat cortical astrocytes following exposure to oxygen-glucose deprivation and

hydrogen peroxide. Int. J. Mol. Med. 36, 43–52. https://doi.org/10.3892/ijmm.2015.2205
Zhu, Y., 2013. The *Drosophila* visual system: From neural circuits to behavior. Cell Adhes. Migr. 7, 333–344. https://doi.org/10.4161/cam.25521